Porous Framework Materials for Gas Separation and Catalysis

A Thesis

Submitted in Partial Fulfilment of the Requirements

for the Degree of

Doctor of Philosophy

By

Debanjan Chakraborty

ID: 20153365

Indian Institute of Science Education and Research (IISER) Pune

Dedicated to

my father

Late Subhas Ranjan Chakraborty

INDIAN INSTITUTE OF SCIENCE EDUCATION AND RESEARCH (IISER), PUNE
(An Autonomous Institution, Ministry of Human Resource Development, Govt. of India)
900 NCL Innovation Park, Dr. Homi Bhabha Rd., Pashan, Pune – 411 008

Dr. R. Vaidhyanathan
Associate Professor, Chemistry

Certificate

This is to certify that the work incorporated in the thesis entitled "*Porous Framework Materials for Gas Separation and Catalysis*" submitted by Debanjan Chakraborty has been carried out by the candidate at the Indian Institute of Science Education and Research (IISER), Pune, under my supervision. The work presented here or any part of it has not been included in any other thesis submitted previously for the award of any degree or diploma from any other University or Institution.

Date:

Place:

Dr. R. Vaidhyanathan
(Research Supervisor)

Tel.: +91-20-2590 8073 Fax: +91-20-2589 9790 E-mail: vaidhya@iiserpune.ac.in

Declaration

I, hereby declare that the thesis entitled "*Porous Framework Materials for Gas Separation and Catalysis*" submitted for the degree of Doctor of Philosophy in Chemistry at Indian Institute of Science Education and Research (IISER), Pune has not been submitted by me to any other University or Institution. This work was carried out at Indian Institute of Science Education and Research (IISER), Pune, India under the supervision of Dr. R. Vaidhyanathan.

Date: Debanjan Chakraborty

Acknowledgements

I would like to express my gratitude to my PhD guide Dr. Ramanathan Vaidhyanathan for his support throughout my journey in IISER Pune. He has introduced me to the real challenges of a researcher and taught how to overcome the hurdles of research life. He has held my hands when I gave up and motivated me to go forward to achieve the triumph. I have not only improved my scientific knowledge under his guidance but also learnt other professional and communication skills of international standards. I feel fortunate to be a part of his esteemed research team and consider it as one of the finest parts of my life. I sincerely thank you for being a wonderful mentor.

I thank my research Advisory Committee (RAC) members, Dr. R. Boomi Shankar and Dr. C. P. Vinod for the scientific inputs during the RAC meetings. I am thankful to our collaborators, Dr. K. Sreekumar (NCL Pune), Dr. P. Thallapally (PNNL USA), Prof. Satish Ogale (IISER Pune), Prof. Tom K. Woo (University of Ottawa, Canada), Dr. Dinesh Kabra (IIT Mumbai), Prof. R. Murugavel (IIT Mumbai) for their valuable inputs in the scientific projects. I am indebted to my lab mates, Dr. Shyamapada Nandi, Dr. Shalini, Dr. Dinesh Mullangi, Dr. Aparna Banerjee, Dr. Kaleeswaran, Dr. Sreenu, Rahul, Sattwick, Rinku, Himan, Pragalbh, Deepak, Shubhangi, Vamshi, Suchit, Hemkalyan, Aksara, Aiswarrya and Krishna for their constant support in the lab. I thank Dr. Rajkumar Misra, Dr. Arunabha Maity, Dr. Santosh K Singh, Mr. Rajith for helping me during various instrumentation and data analysis. I am grateful to all the faculty members and staffs of the department for their support in miscellaneous matters. I would like to thank Dr. Umeshareddy Kacherki (deputy librarian) and Mrs. Anuradha for library support, Mr. Parveen Nasa for technical support, Mr. Mayuresh Kulkarni, Mr. Tushar Kurulkar and Mrs. Sayalee Damble for academic and official support. I am very much thankful to my all batchmates particularly Soumendu, Rajarshi, Rahul, Rahi and Samraj for their irresistible support during the ups and downs. I am grateful to Prof. Jayant B. Udgaonkar, director, Prof. K. N. Ganesh, former director and Prof. H. N. Gopi, chair Chemistry for proving outstanding research facilities in the department. I thank DST-INSPIRE and CSIR for the financial supports. Above all, I feel proud to be a student of Indian Institute of Science Education and Research Pune (IISER Pune).

I take a vow to express my gratitude my teachers who have shaped me for the future endeavour. I would like to thank my teachers, Mr. Shibesh Adhikari, Mr. Ganapati Das, Mr. Samrat Dey, Mr. Jiban Saha, Mr. Krishnendu Roy, Mr. Suvendu Mujherjee, Mr. Tapan Brahma, Dr. Rajesh Das, Prof. Samaresh Bhattacharjee and Dr. Partha Roy. I am really lucky to have friends like

Acknowledgements

Arindam, Mainak, Ranadhir, Puspita, Sandip, Dipanjan, Debashis, Tirtha, Pritam, Sayan and Sudipta for supporting me in every part of my life. I would thank Dr. Bibhuti Bhushan Sow to guide me during my M.Sc. project and motivating me to peruse research in material science. I acknowledge Raiganj Coronation High School and Jadavpur University for providing indigenous knowledge during my student life.

Now, its time to thank my family members who have recognized my potentials and supported me to fulfil my dreams. I am indebted to my mother Mrs. Annapurna Chakraborty to believe in me. I am thankful to Mrs. Chandana Chakraborty, Mrs. Aparna Chakraborty and Mr. Ratan Kumar Chakraborty for their endless support to shape my career. It would have been impossible for me to achieve success without their constant sustenance.

Finally, I would pay tribute to my beloved father Late Subhas Ranjan Chakraborty who had inspired me to be a researcher and work for mankind. His words inspire me in every moment and empower to climb up to new summits of life. Thank you.

Debanjan Chakraborty

Chapter 1: Porous framework materials for Xe/Kr separation and organo-catalysis

Separation of two molecules is always challenging and researchers have come up with novel techniques to achieve these targets. Introduction of porous materials generates a new research topic for such applications. Development of new porous materials as well as modifying the existing ones are the hallmarks of the porous fields. The porous materials are associated with a number of unique properties like high surface area, tunable porosity, high thermal and chemical stability etc. which make them the desired candidate for a diverse range of applications. They are applied for gas separation/storage, catalysis, optics, batteries and supercapacitors etc. Mainly two distinct classes of porous materials exist, metal-based and organic. Zeolites, metal organic frameworks (MOFs), metal organic cages, porous metal oxides belong to this class, whereas porous organic frameworks (POFs), covalent organic frameworks (COFs), organic cages, porous carbon, hydrogen-bonded organic frameworks (HOFs) etc. are the organic porous materials. In this regard, we have systematically studied the synthesis and characterization of MOF, POF, COF and porous carbon. They have been utilized for gas sorption (noble gas) and catalysis (organic and electrocatalysis).

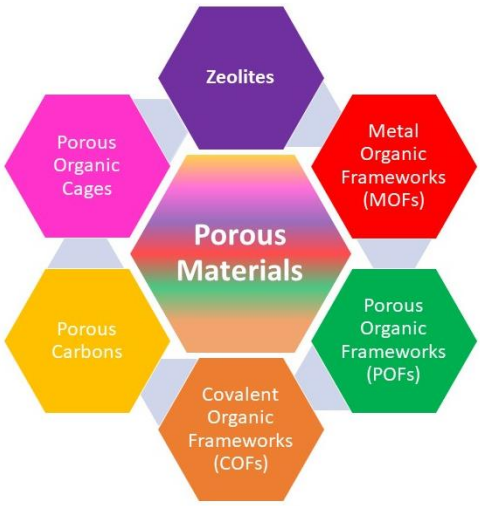

Scheme 1: Different porous materials. MOFs, POFs, COFs and porous carbon are discussed here for their potential application in gas storage and catalysis.

Part 1: Xe/Kr separation using Porous Frameworks.

Chapter 2: Hyper-Crosslinked Porous Organic Frameworks with Ultra-micropores for Selective Xenon Capture

The UNF is associated with humidity, harsh condition and it is desired that the materials would be able to retain their capacity at the harsh condition. However, MOFs face disadvantages in

terms of thermal, chemical stability, purity at large scale preparation, applications at humid atmosphere etc (UNF contains moist air). In this regard, we have investigated hyper-crossed-linked porous polymers for selective Xe capture. The C-C bonding in the polymeric backbone brings exceptional stability to the materials. The polymers are prepared by simple Friedel-Craft reaction between two aromatic moieties. They are extremely stable to thermal and chemical treatments. These polymers have permanent porosity, high BET surface area (645-800 m^2/g) and ultra-microporous networks. The polymers are able to capture Xe selectively over Kr (s(Xe/Kr)) = 6.7, 6.3, 6.3) at 298K and 1 bar pressure. The UNF stream contains an infinitesimally small amount of Xe along with other gases. These polymers can adsorb Xe over N_2 and CO_2 with a high degree of selectivity (Xe/N_2 (s(Xe/N_2)) = 200, 180, 160 at 298K and 1 bar) and Xe/CO_2 selectivity (s(Xe/CO_2)) = 5.6, 7.4, 5.6) for a 1:99 composition of Xe:N_2/Xe:CO_2). The polymers exhibit higher/comparable performance with other benchmark materials like porous carbon and MOFs. Breakthrough experiments are performed to demonstrate the kinetic separation of Xe from the UNF and the polymers show the significant kinetic separation of Xe from the gas mixture. This work exhibits the importance of stable porous polymers for noble gas capture which can withstand the harsh condition of UNF.

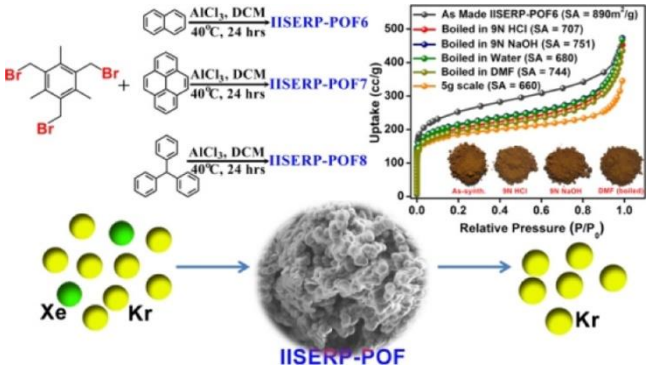

Figure 1: Schematic representation of the preparation of porous polymers. The N_2 isotherms at 77K of the polymers after harsh chemical treatment. The polymers exhibit selective Xe capture from Xe/Kr mixture.

Chapter 3: Ultra-microporous Metal Organic Framework for Exceptional Xe Capacity

Emerging energy demand in the developing world is resulting in the depletion of the conventional fuel sources mainly fossil fuel. The alternate clean energy source is now becoming mandatory for economic development and national security. Along with other alternative energy sources, nuclear energy is considered one of the most effective processes because it has high energy density. However, during nuclear fission process many radioactive

wastes particularly (Xe, Kr) are being released (Used Nuclear Fuel; UNF; 1300 ppm Xe, 130 ppm Kr, 78% N_2, 21% O_2, 0.9% Ar, 0.03% CO_2). The nonradioactive isotope Xe is very useful for different kind of applications in medical, lightening sectors etc. It is very important to selectively capture and store Xe from its analogous noble gas Kr. Currently, cryogenic separation is an industrially opted process for separating Xe/Kr from UNF by utilizing the difference in their boiling points, (Xe = -108.1°C and Kr = -153.2°C) although this is energy demanding as well as explosion hazardous process. Adsorptive separation could be a potential alternate where Xe is adsorbed selectively at ambient temperature and pressure. Solid-state sorbents like porous carbon, zeolites, metal organic frameworks (MOFs), organic cages are being investigated for selective Xe capture. MOFs being crystalline coordination polymers with high surface area and tunable pores serve as a potential candidate for Xe capture. The benchmark MOF for high capacity of Xe is SBMOF-1, but a very low surface area. This provides a room to develop and study MOFs having higher capacity and selectivity. IISERP-MOF2 (Ni-PYC) has been chosen and compared with SBMOF-1. Both of the MOFs have pore size ~4 Å but differ in surface area (SBMOF-1: 145 m^2/g and Ni-PYC: 470 m^2/g). When Ni-PYC is subjected to Xe adsorption, it has been found that the Xe uptake (3.2 mmol/g at 298K and 1 bar) in two times higher than SBMOF-1. Computational modelling is employed to determine the Xe/Kr selectivity as 18.6 which is also better than the SBMOF-1 (16.23). Thus, in this chapter, it has been demonstrated that the surface area of a MOF along with optimal pore size can enhance the Xe capacity significantly.

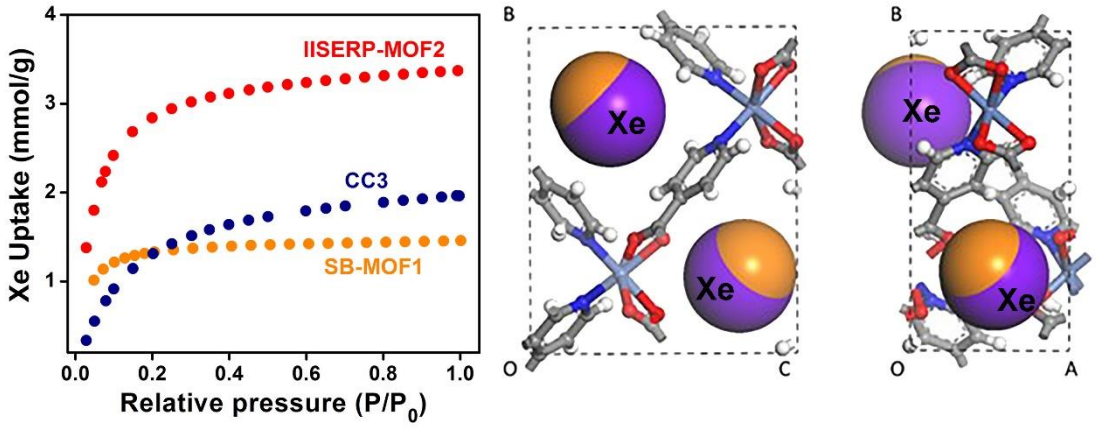

Figure 2: The higher Xe capacity of IISERP-MOF2 compared to other benchmark porous materials which is rationalized by the favourable interaction of Xe with the framework.

Part 2: Organo-catalysis using Porous Framework Supported Nanoclusters.

Chapter 4: Resorcinol-phenylenediamine Based COF for Selective Capture and Chemical Fixation of CO_2

Rising amount of CO_2 in the atmosphere is causing global warming and climate change. The only technology to reduce CO_2 is carbon capture and sequestration (CCS). The liquid amine-based sorbents are industrially used for the CO_2 capture but they are associated with high energy inputs. Solid sorbents like Zeolites, MOFs, porous polymers, COFs are important materials for CO_2 capture and extensive studies have been done on these materials. However, utilization of adsorbed CO_2 could bring novelty into the process of CO_2 sequestration. CO_2 is a small C1 building block for the synthesis a variety of organic molecules, including heterocyclic molecules. But CO_2 is reluctant to react due to its inherent stability and inertness. Developing active catalyst is necessary to react CO_2 generating value-added products like methanol, formic acid, cyclic carbonated etc. Here, a resorcinol-phenylene diamine-based COF is being investigated for the CO_2 capture and fixation study. The COF possesses high BET and Langmuir surface area (BET SA: 1230 m^2/g and Langmuir SA: 1540 m^2/g) with a micropore of 12 Å. The pore wall of the COF is decorated with heteroatoms which can interact with the guest within the pore. The COF shows quite significant CO_2 uptake of 2.5 mmol/g at 298K, 1 bar with a saturation uptake of 15 mmol/g at 195K. The heat of adsorption (HOA) at zero coverage is calculated as 32 kJ/mol which is optimal for the facile regeneration of CO_2. The value of HOA suggests that there is a dipole-quadrupolar interaction between CO_2 and the framework heteroatoms. Ideal Adsorption Solution Theory (IAST) has predicted the CO_2/N_2 (15:85) and CO_2/CH_4 (50:50) selectivities as 65 and 9.3 at 298K, 1 bar which is better than other COF based materials. The breakthrough separation data reveals that the COF has the ability to selectively capture CO_2 under dynamic condition. The COF can accommodate small-sized Ag nanoparticles. This is due to the presence of heteroatoms in the pore that hold the nps tightly without leaching out from the framework. This composite is utilized for the CO_2 fixation into cyclic carbonates with propargyl alcohols. The Ag nps interacts with the propargyl alcohols and the COF adsorbs CO_2, thus the composite is able to fix CO_2 with a yield of >90%. Recyclability of the catalyst has been demonstrated with five consecutive cycles and the integrity of the catalyst has been proven by several analytical techniques. This chapter shows the importance of the ordered porous structure of a COF for favourable host-guest interaction.

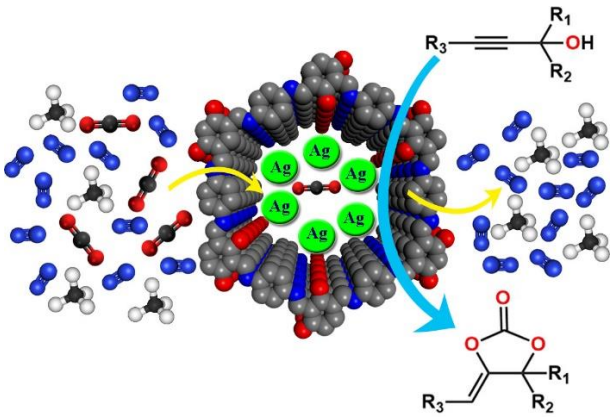

Figure 3: Selective CO_2 capture by resorcinol-phenylene diamine-based COF. Silver nanoparticle supported COF catalyses the chemical fixation of CO_2 with propargyl alcohols.

Chapter 5: Cu/Cu$_2$O Nanoparticles Supported on a COF for heterogeneous Glaser-Hay Hetero Coupling

In the previous chapter, it has been documented that the COFs are suitable candidates for the growth of small-sized active nanoparticles. The abundance of heteroatoms in the ordered pore is the driving force for favourable host-guest interaction. In this chapter, we have explored the ability of a COF to host small Cu/Cu_2O nps and catalyse the challenging Glaser-Hay coupling yielding hetero-coupled product selectively. The COF has a high surface area (1171 m^2/g) and micropores (13Å). The presence of phenolic -OH group brings exceptional stability in the framework by keto-enol tautomerism as well as microporosity. The COF is able to support small-sized Cu nps (av. 3 nm) on it. The composite is studied for the Glaser-Hay (GH) hetero coupling. GH reaction is the C-C coupling between two unactivated alkynes catalysed by metals. Most importantly, the hetero-coupled core is present in various medicinal and natural products. Despite their broad successes in homo-coupled products, preparation of unsymmetrical 1,3-diynes is challenging due to poor selectivity. Here, our COF composite provides a novel approach to perform the GH hetero coupling with high yields (>70%; reaction between aromatic alkynes and the propargyl alcohols). The TOFs and TONs of the catalytic reaction are quite high and a detailed substrate scope is studied with different substitution in the aromatic alkynes and propargylic part. The redox mechanism of the coupling is established from XPS studies of the frozen catalysts at different time segments of the reaction. The prominent change in the satellite peak during the course of the reaction establishes the redox pathway. The coupling proceeds via oxidative addition and reductive elimination of the Cu centre in presence of terminal alkynes. Further, theoretical calculations (DFT) reveal that there is a hydrogen bonding interaction between the propargyl alcohol and the -OH groups of the

COF. This interaction stabilizes the hetero configuration within the COF pore and results in hetero-coupled product. The cyclability and the post catalysis integrity is studied. This work presents the ability of the COF to provide an optimal environment for the challenging reaction through its pore architecture.

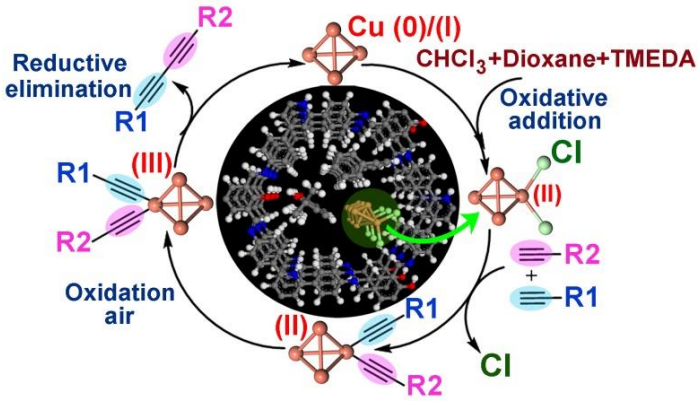

Figure 4: Catalytic transformation involving oxidative addition and reductive elimination of the Cu cluster supported by COF.

List of Acronyms

1. MOF: Metal Organic Frameworks
2. POF: Porous Organic Frameworks
3. COF: Covalent Organic Frameworks
4. ZIF: Zeolite Imidazole Frameworks
5. PAF: Polymeric Aromatic Framework
6. NLDFT: Non Local Density Functional Theory
7. TGA: Thermogravimetric Analysis
8. PXRD: Powder X-Ray Diffraction
9. DMF: N, N-Dimethyl formamide
10. DMSO-D6: Dimethyl Sulphoxide -duterated
11. $CDCl_3$: Deuterated Chloroform
12. O-DBC: Ortho-Dichlorobenzene
13. FE-SEM: Field Emission-Scanning Electron Microscopy
14. FT-IR: Fourier Transform Infra-red-spectra
15. NMR: Nuclear Magnetic Resonance
16. MAS: Magic Angle Spinning
17. AFM: Atomic Force Microscopy
18. XPS: X-ray Photoelectron Spectroscopy
19. BET: Brunauer Emmett Teller
20. IAST: Ideal Adsorption Solution Theory
21. HOA: Heat of Adsorption
22. ACN: Acetonitrile
23. FE-TEM: Field Emission-Transmission Electron Microscopy
24. HR-TEM: High Resolution-Transmission Electron Microscopy
25. mol: moles
26. PSD: Particle Size Distribution
27. np: Nano particles
28. K: Kelvin
29. °C: Degree Celsius
30. mmol: Milli moles
31. nm: nanometer
32. TOF: Turnover Frequency
33. TON: Turnover Number
34. mL: Milliliter
35. MHz: Megahertz
36. Å: Angstrom
37. AcOH: Acetic acid
38. MHz: Megahertz
39. BE: Binding Energy
40. BTC: Breakthrough Curve
41. GCMC: Grand Canonical Monte-Carlo
42. UFF: Universal Force Field
43. DFT: Density Functional Theory

List of Publications

Included in the thesis

1. ***Debanjan Chakraborty***, *Shyamapada Nandi, Michael A. Sinnwell, Jian. Liu, Rinku Kushwaha, Praveen K. Thallapally and Ramanathan Vaidhyanathan*. Hyper-Cross-linked Porous Organic Frameworks with Ultramicropores for Selective Xenon Capture. *ACS Appl. Mater. Interfaces* **2019**, *11*, 13279-13284.
2. ***Debanjan Chakraborty***, *Shyamapada Nandi, Michael Sinnwell, Rahul Maity, Radha Kishan Mot-kuri, Han Kee Sung, Sean Collins, Tom K. Woo, Ramanathan Vaidhyanathan and Praveen K. Thallapally.* An Ultra-microporous Metal Organic Framework with Exceptional Xe Capacity. *Manuscript submitted*.
3. ***Debanjan Chakraborty***, *Pragalbh Shekhar, Himan Dev Singh, Rinku Kushwaha, C. P. Vinod and Ramanathan Vaidhyanathan.* Ag Nanoparticles Supported on a Resorcinol-PhenylenediamineBased Covalent Organic Framework for Chemical Fixation of CO_2. *Chem. Asian J.* **2019**, *14*, 4767-4773.
4. ***Debanjan Chakraborty***, *Shyamapada Nandi, Dinesh Mullangi, Sattwick Haldar, C. P. Vinod and Ramanathan Vaidhyanathan.* Cu/Cu_2O Nanoparticles Supported on a Phenol–Pyridyl COF as a Heterogeneous Catalyst for the Synthesis of Unsymmetrical Diynes via Glaser–Hay Coupling. *ACS Appl. Mater. Interfaces* **2019**, 11, 15670−15679.

Not included in the thesis

5. ***Debanjan Chakraborty***, *Shyamapada Nandi, Rajith Illathvalappil, Dinesh Mullangi, Rahul Maity, Santosh K. Singh, Sattwick Haldar, C. P. Vinod, Sreekumar Kurungot and Ramanathan Vaidhyanathan*. Carbon Derived from Soft Pyrolysis of COF as a Support for Small-Sized RuO_2 Showing Exceptionally Low-Overpotential for OER. *ACS Omega* **2019**, *4*, 13465-13473. **(equal contribution with SN)**
6. *Sattwick. Haldar,* ***Debanjan Chakraborty****, Bibhisan Roy, Gangadhar Banappanavar, Kushwaha Rinku, Dinesh Mullangi, Partha Hazra, Dinesh Kabra and Ramanathan Vaidhyanathan*. Anthracene-Resorcinol Derived Covalent Organic Framework as Flexible White Light Emitter. *J. Am. Chem. Soc*. **2018**, *140*, 13367-13374. **(equal contribution with SH)**
7. *Shyamapada Nandi, Phil De Luna, Rahul Maity,* ***Debanjan Chakraborty****, Thomas Daff, Thomas Burns, Tom K. Woo and Ramanathan Vaidhyanathan*. Imparting Gas Selective and Pressure Dependent Porosity into a Non-Porous Solid via Coordination Flexibility. *Mater. Horiz*. **2019**, *6*, 1883-1891.
8. *Gulzar A Bhat, Sattwick Haldar, Sonam Verma,* ***Debanjan Chakraborty****, Ramanathan Vaidhyanathan, Ramaswamy Murugavel.* Facile Exfoliation of Single-Crystalline Copper Alkylphosphates to Single-Layer Nanosheets and Enhanced Super capacitance. *Angew. Chem. Int. Ed.* **2019**, *58*, 16844-16849.
9. *Rahul Maity, Himan Dev Singh, Ankit Kumar Yadav,* ***Debanjan Chakraborty****, Ramanathan Vaidhyanathan.* Water-stable Adenine-based MOFs with Polar Pores for Selective CO_2 Capture. *Chem. Asian J.* **2019**, *14*, 3736-3741.
10. *Rahul Maity,* ***Debanjan Chakraborty****, Shyamapada Nandi, Ankit Kumar Yadav, Dinesh Mullangi, C P Vinod, Ramanathan Vaidhyanathan*. Aqueous-Phase Differentiation and Speciation of Fe^{3+} and Fe^{2+} Using Water-Stable Photoluminescent Lanthanide-Based Metal–Organic Framework. *ACS Appl. Nano Mater.* **2019**, *2*, 5169-5178.
11. *Dinesh Mullangi,* ***Debanjan Chakraborty****, Anu Pradeep, Vijay Koshti, C. P. Vinod, Soumendranath Panja, Sunil Nair and Ramanathan Vaidhyanathan*. Highly Stable COF-

Supported Co/$Co(OH)_2$ Nanoparticles Heterogeneous Catalyst for Reduction of Nitrile/Nitro Compounds under Mild Conditions. *Small* **2018**, *14*,1801233-1801251.

12. *Shyamapada Nandi, Rahul Maity,* ***Debanjan Chakraborty****, Hemkalyan Ballav and Ramanathan Vaidhyanathan*. Preferential Adsorption of CO_2 in an Ultramicroporous MOF with Cavities Lined by Basic Groups and Open-Metal Sites. *Inorg. Chem*. **2018**, *57*, 5267-5272.
13. *Sattwick Haldar, Kingshuk Roy, Shyamapada Nandi,* ***Debanjan Chakraborty****, Dhanya Puthusseri, Yogesh Gawli, Satishchandra Ogale and Ramanathan Vaidhyanathan*. High and Reversible Lithium Ion Storage in Self-Exfoliated Triazole-Triformyl Phloroglucinol-Based Covalent Organic Nanosheets. *Adv. Energy Mater*. **2018**, *8*,1702170-1702181.
14. *Remya Narayanan, Anweshi Dewan and* ***Debanjan Chakraborty***. Complimentary Effects of Annealing Temperature on Optimal Tuning Of Functionalized Carbon–V_2O_5 Hybrid Nanobelts for Targeted Dual Applications in Electrochromic and Supercapacitor Devices. *RSC Adv*. **2018**, 8, 8596-8606.
15. *Rahul Maity,* ***Debanjan Chakraborty****, Shyamapada Nandi, Kushwaha Rinku and Ramanathan Vaidhyanathan*. Microporous Mixed-Metal Mixed-Ligand Metal Organic Framework for Selective CO_2 Capture. *CrystEngComm* **2018**, *20*,6088-6093.
16. *Aparna Banerjee,* ***Debanjan Chakraborty*** *and Ramanathan Vaidhyanathan*. Ultra-microporous Metal–Organic Framework Built from Rigid Linkers Showing Structural Flexibility Resulting in a Marked Change in Carbon Dioxide Capacity. *Eur. J. Inorg. Chem.* **2017**, *18*, 2464-2468.
17. *Shyamapada Nandi, Sean Collins,* ***Debanjan Chakraborty****, Debasis Banerjee, Praveen K Thallapally, Tom K. Woo and Ramanathan Vaidhyanathan*. Ultralow Parasitic Energy for Postcombustion CO_2 Capture Realized in a Nickel Isonicotinate Metal–Organic Framework with Excellent Moisture Stability. *J. Am. Chem. Soc*. **2017**, 139,1734-1737.
18. *Shyamapada Nandi, Jens Rother,* ***Debanjan Chakraborty****, Rahul Maity, Ulrike Werner-Zwanziger and Ramanathan Vaidhyanathan*. Exceptionally Stable Bakelite-Type Polymers for Efficient Pre-Combustion CO_2 Capture and H_2 Purification. *J. Mater. Chem. A* **2017**, 5, 8431-8439.
19. *Shyamapada Nandi, Sattwick Haldar,* ***Debanjan Chakraborty*** *and Ramanathan Vaidhyanathan*. Strategically Designed Azolyl-Carboxylate Mofs for Potential Humid CO_2 Capture. *J. Mater. Chem. A* **2017**, *5*, 535-543.
20. *Shyamapada Nandi,* ***Debanjan Chakraborty*** *and Ramanathan Vaidhyanathan*. A Permanently Porous Single Molecule H-Bonded Organic Framework for Selective CO_2 Capture. *Chem. Commun*. **2016**, *52*, 7249-7252.

Table of Contents

Chapter 1

Introduction to Porous Materials for Gas Separation and Catalysis

1. Introduction:

Porous materials have been an emerging topic of research for the last few decades. Their modular pore architecture, accessible design strategies and diverse applications lead to a revolution in the development of target-specific porous solids.[1] Several aspects of porous materials such as the kinetics and thermodynamics of gas adsorptions within their pores, the diffusion kinetics of different gases have been investigated in-depth using a variety of experimental and theoretical approaches. However, the fact that these parameters still are significantly different for every new designed porous solid, there is a lot of room for understanding new gas sorption phenomenon in them, which provide insights for further material developments. Thus, there is a huge scope of development of porous solids in terms of advanced application and commercialization. Porous materials carry several advantages.[2-4] They possess high surface area, nano-porous to macroporous architecture which can be controlled by synthetic strategies. These porous networks exert high thermal and chemical stabilities depending on their covalent linking and architectures.[5-11] They are capable of hosting different guests into their functional pores which provide room for diverse applications starting from gas capture/storage and purification,[12-18] catalysis,[19-23] optics,[24-37] energy[38-48] to the biological regime.[49] Porous materials can be divided into two distinct classes – (i) porous materials having inorganic backbones and (ii) porous materials with pure organic backbones. The former one includes zeolites, porous metal oxides/nitrides, porous silica and inorganic-organic hybrid materials namely Metal-Organic Frameworks (MOFs) (Scheme 1.1).[50-63] On the other hand, organic materials comprise of porous polymers (POFs),[7-12,18] Covalent Organic Frameworks (COFs),[19,20] Hydrogen-Bonded Frameworks (HOFs),[64-66] porous organic cages[14,18] etc.

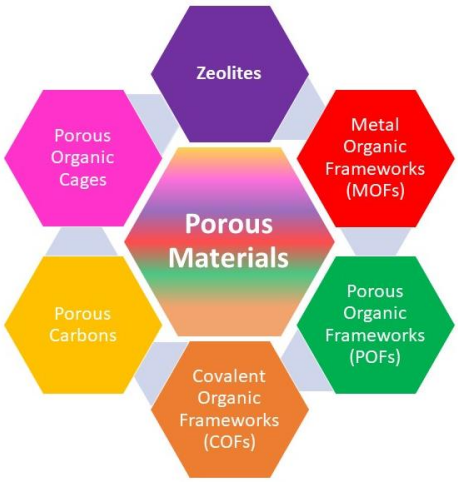

Scheme 1.1. Different classes of porous materials.

Porous organic materials are typically constructed by covalent linking of small organic building blocks. The most important feature of the porous organic materials is the absence of metal ions in the backbone. The covalently bonded network provides extreme chemical and thermal stability. The organic framework can be tuned to have lowered affinity to humidity or water, which are known to attack these materials, a well-established drawback of the inorganic porous materials like zeolites. Judicious choice of building blocks renders into different structures with a range of pores (micro to mesoporous structures). Their intrinsic pores can be functionalized to render favourable interactions with the guests. Depending upon the building block selection and reaction conditions, the organic materials could be amorphous or crystalline in nature. Crystallinity helps study the structure-property relationship of the porous materials in detail using a range of diffraction experiments and computational modelling. The porous organic materials are used in gas separation, storage[67-72] catalysis,[19-23,72-80] energy storage,[38-42, 81-87] fuel cell application,[47,48] photo-catalysis,[88-95] drug delivery,[49] solar cells[96] etc.

Metal-Organic Frameworks (MOFs) are built from the self-assembly of metal ion/cluster with organic building units.[97-99] This imparts an extraordinary degree of crystallinity, high surface area, tunable pore architecture, and flexibility into the backbone. Depending on the pore dimensions, MOFs are being classified into three types, Ultra-microporous: pore size < 6 Å; Microporous: pore size 6-20 Å; Mesoporous: pore size > 20 Å.[101-103] Ultra-microporous MOFs are suitable candidates for gas separation and capture.[104-111] However, gas storage,[112-115] catalysis,[116-120] photoluminescence,[121-123] sensing,[124-125] proton conductivity,[126-128] and energy storage & conversion[129-131] are the widely studied applications using MOFs.

In this chapter, different porous materials such as Hyper-Cross-Linked polymers (HCPs)[87,132-135] Metal-Organic Frameworks (MOF) and Covalent Organic Frameworks (COFs), [136-142] are briefly discussed. They are conferred with seminal examples where the materials are investigated for gas separation and catalysis.

1.1. Hyper-Cross-Linked Polymers (HCPs):

Hallmark of HCPs is their high degree of cross-linking and stability towards chemical and thermal treatment. The cross-linked polymeric structure results in the robustness and high surface area, micro-porosity and the all-organic framework confers low density. Typically, they are amorphous in nature. Many HCP are prepared by Friedel-Craft reactions which enable cost-

effective multigram scale synthesis. The main three approaches to prepare HCPs are direct polycondensation of monomers, post-cross-linking of polymeric species and use of external crosslinkers.[133] The direct polycondensation is executed by the condensation of the monomeric units into the polymer in a suitable solvent.[134] In post-cross-linking technique, the polymeric chains are immersed in solvents and further crosslinked. The spaces occupied by the solvents are then stabilized by the crosslinking and thus it generates the porous networks.[135] The use of external cross-linker was first shown by Tan and co-workers, where an external linker was employed for knitting the aromatic framework to develop special functionality and desired morphology for an application.

1.1.1. Tetraphenylethylene based HCP for CO_2 capture:

The HCPs were prepared via Friedel Craft reaction of Tetraphenylethylene (TPE)/ 1,1,2,2-tetraphenylethane-1,2-diol (TDP) with formaldehyde dimethyl acetal and $FeCl_3$ as catalyst.[143] The building blocks were mixed in a particular molar ratio to obtain the ideal material for post-combustion CO_2 capture application (Figure 1.1). The polymers were not soluble in the traditional organic solvents and they exhibited thermal stability up to 250°C under N_2 atmosphere. The presence of methylinic linkage in the framework reduced the thermal stability compared to the pure aromatic porous frameworks. FT IR spectra provided the evidence of the cross-linking where the -C-H stretching vibration occurs at 2920 cm^{-1}. The polymers were highly porous in nature and possess a high BET surface area. However, a trend had been observed in the surface area of the mixed linker-based polymers. The polymer having TPE exhibited the highest BET surface area of 1980 m^2/g, but the value dropped with the increasing ratio of TDP. The polymer with 100% TDP displayed a BET surface area of 618 m^2/g.[143] The pore size distribution was also affected by the relative composition ratio of the two linkers. In general, all the networks had microporous structure (11 to 16 Å), however, a significant amount of mesopores were present in the structure. On increasing the TDP concentration, the mesoporous nature was condensed, and the polymer made of 100% TDP didn't have any mesoporous contribution in its structure. The reason behind the modulation of the surface area and pore size remains in the chemical bondings of the monomers. TPE had a double bond, whereas TDP carried a single bond, which imposes flexibility in the framework leading to the lowered surface area. However, the hydroxyl groups of TDP linker occupy a fraction of the pore, minimizing the formation of mesopores. The CO_2 separation capabilities of these HCPs

have been investigated. As expected, the network-1 (with 100% TPE) had the highest CO_2 capacity (3.63 mmol/g at 1 bar at 273K) compared to the other networks.[143] The network-7

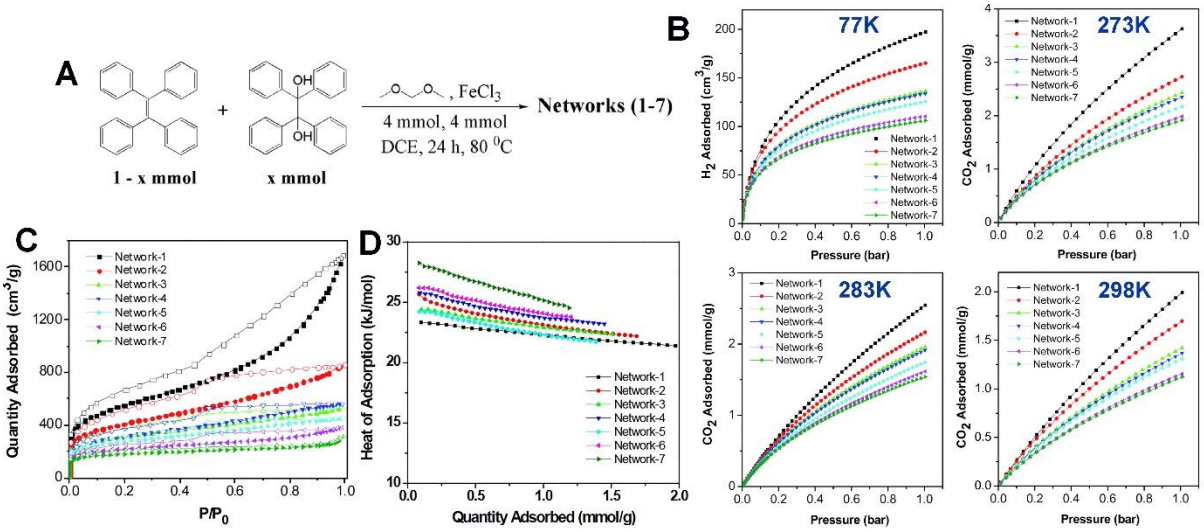

Figure 1.1. (A) Synthetic scheme. (B) H_2 and CO_2 adsorption isotherms collected at different temperatures. (C) N_2 77K isotherms of the polymer, which shows that the effect of mixed linker strategy on the porous architecture. (D) The heat of Adsorption (HOA) for the polymers, network-7 is having the highest HOA due to microporous nature. *(Adopted from ref. 143 from the Royal Society of Chemistry with permission).*

(with 100% TDP) exhibited the lowest CO_2 uptake (1.92 mmol/g at 1 bar at 273 K) (Figure 1.1). This trend observed in the CO2 uptakes correlated with the trend of surface area and pore volume of the polymeric networks. Ideal Adsorption Solution Theory (IAST) was employed to calculate the CO_2/N_2 selectivity (0.15 CO_2/ 0.85 N_2). The network-1 showed a selectivity of 33 whereas, network-7 showed 119 at 1 bar at 273K. The heat of adsorption has been evaluated from Virial model where 28.2 and 23.3 kJ/mol HOA are obtained for network-1 and network-7, respectively, which corroborated with the observed selectivities of the networks (Figure 1.1). The network-7 has -OH groups which have a favourable interaction with polarizable CO_2 molecules giving rise to relatively higher HOA values.[143] Thus, the chemical modulation in the monomeric unit can modify the CO_2 capture ability of these porous networks.

1.1.2. Effect of crosslinking in HCPs on selective CO_2 capture:

The extent of cross-linking and the cross-linker length play a significant role in gas separation and storage. To express this, Sun and co-workers have prepared three different HCPs by the Friedel Craft condensation of 2,4,6-Tris(chloromethyl)-mesitylene (TCM), p-dichloroxylene (DCX) and 4,40-bis(chloromethyl)-1,10-biphenyl (BCB). The three polymers involved in this

study were named as follows, NUT-5: self-condensation of TCM, NUT-6: polymerisation of TCM with DCX and NUT-7: polymerisation of TCM with BCB. All three polymers showed

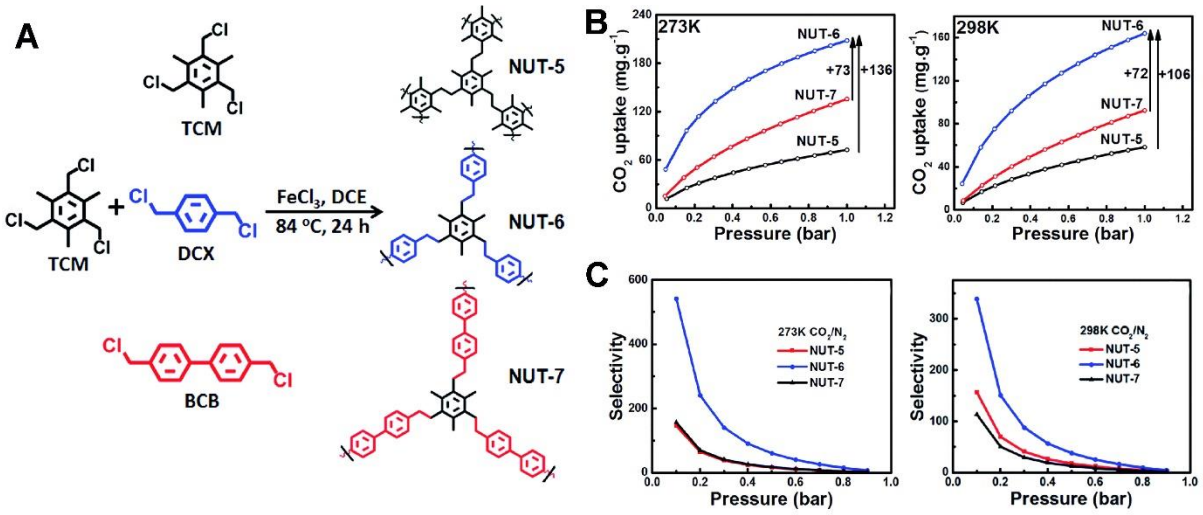

Figure 1.2. (A) Facile synthetic routes of the polymers. (B) CO_2 adsorption isotherm of the polymers at two different temperatures, 273K and 298K. (D) IAST selectivity for $15CO_2/85N_2$ mixture at 273K and 298K. (*Adopted from ref. 144 from the Royal Society of Chemistry with permission).*

micro porosity, but their surface area followed the order: NUT-6 > NUT-7 > NUT-5 (BET surface area: 1137, 987, 771 m^2/g, respectively) (Figure 1.2).[144] The main reason behind this surface area trend remained in the extent of cross-linking and the linker length. NUT-5 having no crosslinking exhibit diminished porosities compared to the other polymers, this was despite they having very similar pore size distribution. The pore volumes for the NUT-5, 6 and & are 0.4, 0.7, 0.6 cm^3/g. CO_2, CH_4 and N_2 adsorption studies were carried out with these microporous polymers at different temperature (273 and 298K) (Figure 1.2). The polymers possessed significant CO_2 uptakes. But they did not adsorb CH_4 or N_2 at room temperature (CO_2 uptake: 58.2, 164.1, and 92.4 m^2/g at 1 bar at 298K).[144] It was evidenced from the CO_2 uptakes of the polymers that a balance between the surface area and pore volumes was an important parameter. NUT-6 was optimized with a cross-linker of right length which yielded a pore environment highly suited for CO_2 sorption, particularly in comparison to the other NUTs. IAST selectivities were also influenced by the crosslinker modification (Figure 1.2). The IAST selectivities for CO_2/N_2 and CO_2/CH_4 for the NUT-6 are 541.4 and 48, respectively, at low pressure and 273K which was much higher than the NUT-5 and NUT-7. This selectivity corroborated well with previous observations. The isosteric heat of adsorptions followed the same order as the surface area i. e. NUT-6 > NUT-7 > NUT-5 (14.4, 21.8, and 19.0 kJ/mol) (Figure 1.2).[144] The design and choice of the cross-linking moieties played a significant role in

polymer preparation. When TCM had been crossed-linked with a small linker DCX, the resulting polymer had more surface area and pore volume than the self-condensed TCM polymer. When the length of cross-linker had been increased, it forms longer chains in the polymeric backbone which affected the textual properties of the polymers. Whereas, NUT-6 had an optimal surface area, pore volume and textual characteristics enabling the best performances among the three polymers. Further, excellent CO_2 cyclic performance had been demonstrated by NUT-6 in this report.[144]

1.1.3. Heteroatom incorporated in HCPs for selective CO_2 capture:

CO_2 can have favourable interactions with the polarising moieties in the frameworks. The aromatic groups present in the HCPs are known to interact well with CO_2 which reflect in their selectivity and heat of adsorption values. In this example, the micropores of the HCPs have been decorated with heteroatoms to gain improved CO_2 adsorption characteristics. Three polymers are prepared via the condensation of 2,4,6-tri(thiophene-2-yl)-1,3,5-triazine (TTPT) and thiophene in different ratio with $FeCl_3$ (1:1 for HMC-1, 1:2 for HMC-2, and 2:1 for HMC-3) (Figure 1.3). The two-step reaction (first reflux in chloroform and then solvothermal at 150°C) led to the formation of amorphous polymers which are microporous in nature.[145] The BET surface area for HMC-1, 2 and 3 were 855, 425, and 566 m^2/g, respectively. The TTPT did not produce a polymer with a high surface area as the thiophene ring is reluctant to crosslink with the electron-deficient triazine ring. The two-step condensation seems critical to generate sufficiently high surface area polymers. Here, chloroform is templating and co-polymerising the monomers to render better cross-linking hence better surface area. 1:1 ratio favours the co-polymer formation and yields the polymer with the highest surface area. NLDFT model yielded a pore size of ~ 15 Å and the pore volumes are 0.2968, 0.1920, and 0.1618 cc/g for HMC-1, 2 and 3, respectively.[145] Microscopic studies revealed that the polymers possessed a ribbon-like morphology due to cross-linking. The presence of a peak at 50.9 ppm in the solid-state ^{13}C NMR spectra revealed that $CHCl_3$ also takes place in the polymerisation. The polymers exhibited high thermal and chemical stability due to C-C linkages. The polymers exhibited quite satisfactory CO_2 uptakes ranging from 10.5 to 14.2 mmol/g and 1.9 to 2.6 mmol/g at 273 and 298K (Figure 1.3). HMC-2 exhibited the highest CO_2 capacity among the polymers. The isosteric heat of adsorption for the polymers was remarkably high, for example, HMC-2 has HOA value ~60 kJ/mol which indicated that the nitrogen atoms in the triazine groups and the sulphur atoms from the thiophene groups were having a significant polarising effect on CO_2.

HMC-3 exhibited the highest CO_2 capacity which has been attributed to the higher sulphur content of the polymer than the other two.[145] CO_2 cycling experiments up to five cycles confirmed the reproducible physisorptive capacity of the polymers. The CO_2/N_2 selectivity values have been calculated at 273K from the initial slope method. The values were recorded as 72:1, 70:1, 23:1 for HMC-1, 2, 3, respectively. Thus, it has been observed that there would

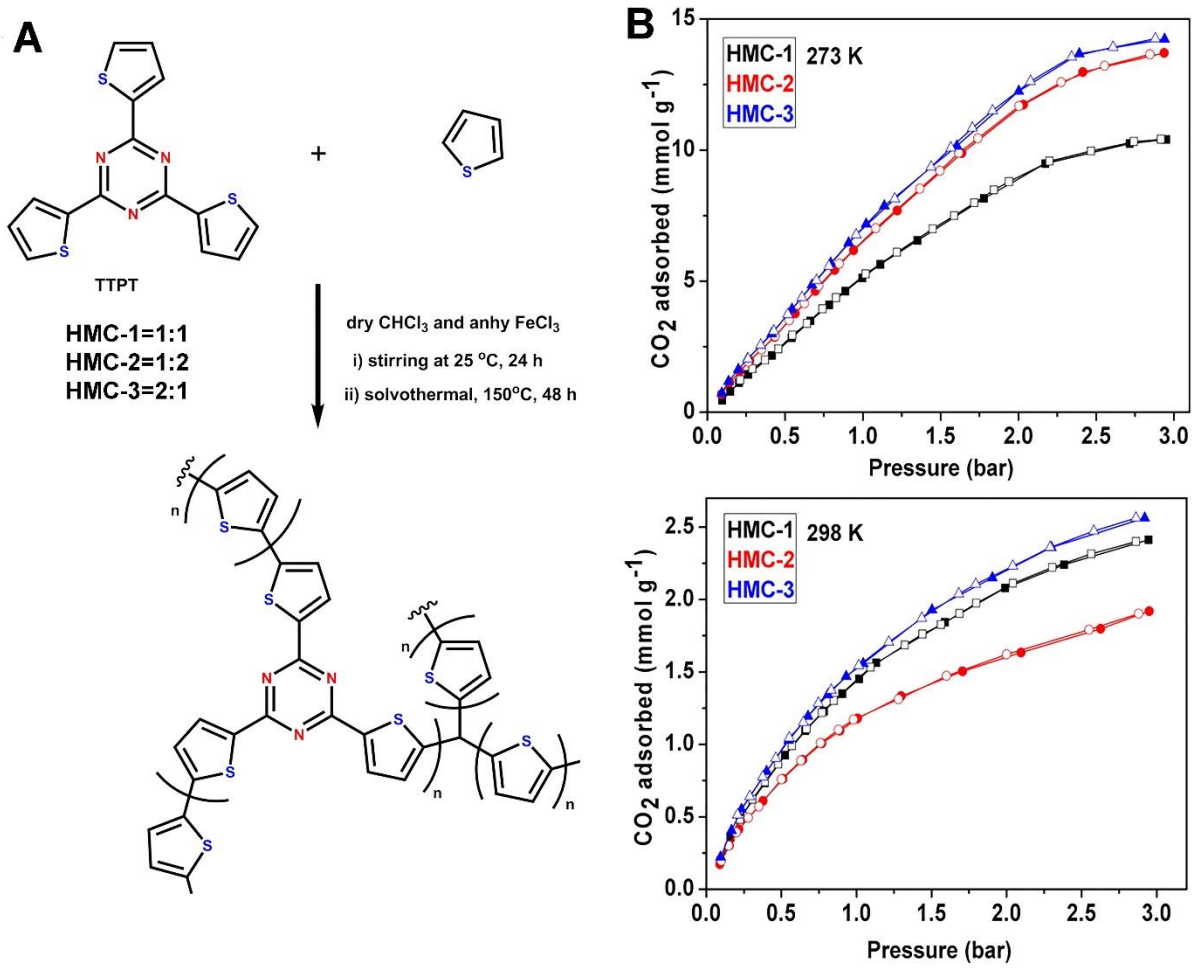

Figure 1.3. (A) Synthesis of heteroatom incorporated polymers. (B) CO_2 adsorption isotherms of the polymers recorded at 273K and 298K up to 3 bar. *(Adopted from ref. 145 from the American Chemical Society with permission).*

be a serious implication if the heteroatoms are doped in the hyper-crossed-linked polymers with a judicial selection of the building blocks.[145]

1.1.4. Microporous HCP for methane storage:

Methane is a natural fuel which provides a cleaner combustion route. The practical use of methane is limited by the safer storage of the gas at high pressure (30-40 bar). Physisorption

processes are employed to store methane. MOFs and activated carbons have been used for the same purpose, but they face real-life challenges, such as less volumetric capacity due to low packing density of the materials, stability issue of the MOFs. Activated carbons show quite satisfactory performance, but the reproducibility is a concern. To overcome the challenges, Cooper and co-workers reported microporous polymers for methane storage. The polymers were prepared in the monolithic form to reduce the volumetric storage issues. The Friedel Craft condensation of monomers dichloroxylene (DCX), and 4,4′-bis(chloromethyl)-1,10-biphenyl (BCMBP) led to the formation of microporous polymers (Figure 1.4). The relative ratio of the monomers has been varied to generate a set of networks with different surface area and pore volumes. Self-condensation of pure DCX and BCMBP formed the networks with higher surface area, pore volume and densities. The polymers were amorphous in nature and they had a hierarchical porosity. The optimal pore size for methane was considered to be 7.6 Å.[146] It has been observed that there was a significant difference in the adsorption of powdered polymers to that of monolithic phases. The monolithic polymer samples exhibited type-I N_2 isotherm at 77K, while the powdered samples had mesoporous characters with a pore-filling at higher pressures. This indicated that the monolithic polymers were a better contender for gas storage due to their enhanced microporous volumes. The BCMP polymer showed the highest CH_4 uptake (5.2 mmol/g) at 20 bar at room temperature which was correlated to the highest surface area of the polymer (1904 m^2/g).[146] The monolithic polymer exhibited 4.3 mmol/g methane uptake at 15 bar which is similar to the BCMP powder (4.4 mmol/g) (Figure 1.4). Although the surface area of the monolithic polymer (1366 m^2/g) was lower than that of BCMP powdered polymer the pore volumes were similar resulting into the similar methane uptakes for both forms (0.55 and 0.54 cm^3/g respectively). A rigorous theoretical simulation study had been employed to understand the methane storage of the polymers and the isosteric heat of adsorption was calculated for the modelled structures. It was in good agreement with the experimentally determined isosteric heat of adsorption (Modelling: 22 kJ/mol vs experimental: 20.8 kJ/mol). This heat of adsorption value was much greater than the MOFs and activated carbons (~16 kJ/mol) due to their improved pore-confinement and larger surface areas. Also, high HOA rationalized the storage capacity of the polymers and this could be improved by simply changing the pore volume/surface area. The polymers were remarkably stable, could be synthesized in multigram scale as monolithic blocks. These features made them promising candidates for selected industrial application over MOFs and activated porous carbons.[147]

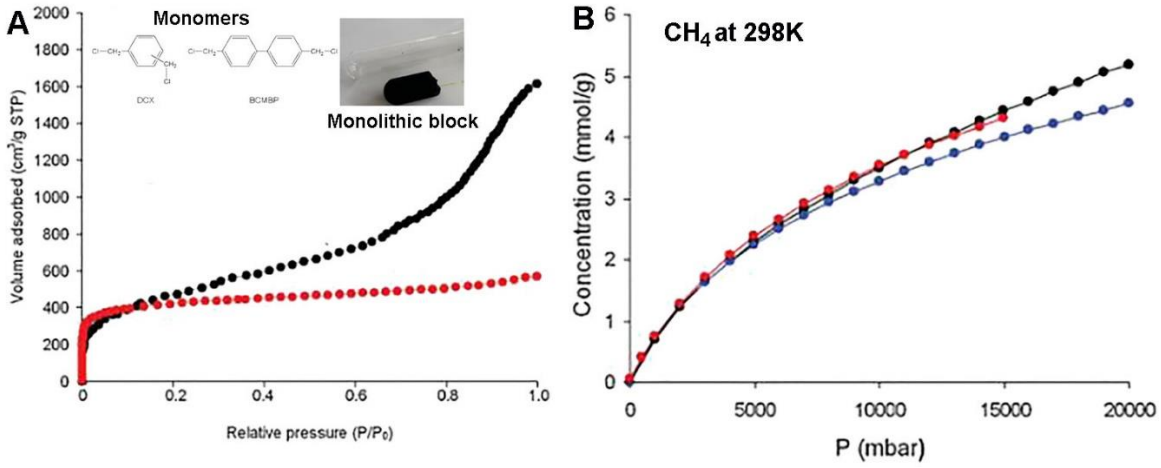

Figure 1.4. (A) N_2 isotherm at 77K of BCMBP polymer (Black curve is for powder and the red curve is for monolithic block). Inset shows the monomers and visual image of the monolithic polymer. (B) CH_4 storage isotherms of the polymers at 298K (Blue: *p*-DCX, Red: monolithic BCMBP, Black: BCMBP/ *p*-DCX). *(Adopted from ref. 147 from the Wiley Online Library with permission).*

1.1.5. Hydrogen adsorption and storage by microporous HCP:

Hydrogen is an important clean-burning fuel with the highest gravimetric energy density. But the usage of hydrogen as a fuel is limited by its safer storage and transportation. In recent years, different porous materials are being used for storing hydrogen via adsorption-based techniques. Some of these porous materials include zeolites,[148] porous carbons,[149] MOFs.[150-152] But these materials do not simultaneously meet the criteria of safe storage, cost, optimal pore-size for high capacity and selectivity, and regeneration kinetics. This opens up a new window for the researchers to develop tailor-made materials for hydrogen storage. In the porous polymer family, initially, the polymers with intrinsic microporosity (PIMs) were investigated for

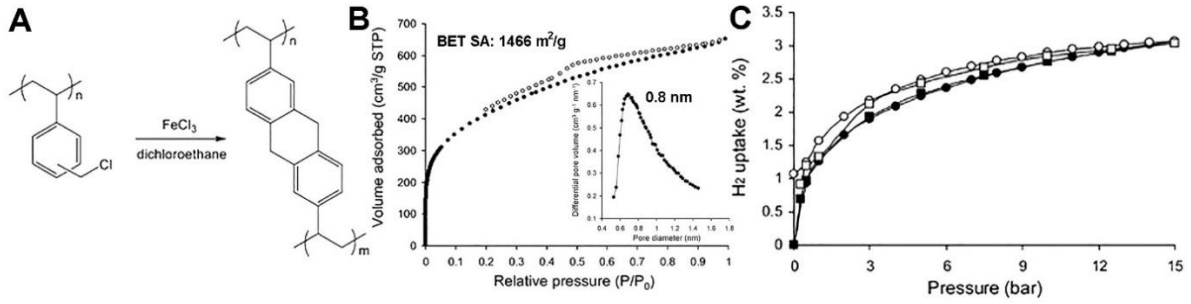

Figure 1.5. (A) The synthetic strategy of the polymer. (B) Permanent porosity of the polymer is observed from N_2 isotherm at 77K. Inset shows the pore size distribution, the polymer has an average pore of 0.8 nm. (C) H_2 adsorption isotherm at 77K. *(Adopted from ref. 155 from the Royal Society of Chemistry with permission).*

hydrogen storage. However, they were ruled out because the storage capacity was a mere ~1.7 weight % at 77 K and 10 bar (US DOE target is 6.5 wt%). The surface area of the PIMs was low which explained the low storage capacity. HCPs could be the ideal candidate to deliver a high surface area and pore volume to serve this purpose. The HCP was prepared via Friedel post-cross-linking of polymerized vinyl benzene chloride using dichloromethane as solvent and $FeCl_3$ as the catalyst (Figure 1.5). The permanent porosity of the polymer was confirmed by the N_2 isotherm at 77K and the BET surface area was found to be 1466 m^2/g. The polymer possessed micropores in its structure. The pore diameter and the pore volume were 8 Å and 0.48 cc/g (Figure 1.5). The hydrogen storage was studied at 77K, 15 bar pressure and it was found that the material can adsorb 3.04% of hydrogen at 15 bar. The adsorption was repeated several times to ensure the reproducibility. Interestingly, the HCP had higher H_2 capacity compared to the other congener of the polymer family (PIMs) at a pressure >5 bar. However, the capacity was almost similar to PIMs at 1 bar. The H_2 adsorption at 77K showed a small hysteresis, which was occurring due to the distribution of pore size in case of the polymers. Also, the hydrogen capacity was comparable and better than some of the MOFs and activated carbons.[153-154] For instances, IRMOF-13 showed an H_2 capacity of 2.75 wt% having a similar surface area of the HCP (1551 m^2/g), but MOFs were not chemically and thermally stable (Figure 1.5). The problem associated with porous carbon was the reproducibility of the material. In this aspect, polymers particularly HCPs were ahead of MOFs and carbons regarding reproducibility in multigram scale synthesis and chemical/thermal stability. In this example, the polymer has been proven to be a promising candidate for the hydrogen storage application.[155]

1.1.6. HCP for catalysis, CO_2 fixation:

CO_2 fixation is a very important chemical process to produce value-added chemicals. CO_2 is the abundant source of C1 building block.[156] In this example, it has been shown that the CO_2 has been fixed through the formylation of amines. Formylation of the amine has been chosen as a model reaction as the N-formylated compounds are the useful intermediates for several drugs, dyes and agrochemicals.[157,158] In order to demonstrate the ability of the HCP to fix CO_2, small-sized Pd nanoparticles have been grown on the HCP and the composite serves as the efficient heterogeneous catalysis for the formylation of amines.[159] The polymer was prepared by the Friedel-Craft reaction between dibromo-p-xylene and carbazole with $FeCl_3$ in dichloroethane under reflux conditions (Figure 1.6). The Pd nanoparticles were grown on the

HCP in a simple fashion: Mixture of $PdCl_2$ and HCP were stirred in the water at 100℃ for 1 hour, followed by addition of ethylene glycol and heating at 160℃ for 5 hours. Atomic absorption spectroscopy (AAS) revealed a 4.52 wt% of Pd loading in the HCP framework. The powder X-ray diffraction pattern of Pd@HMP-1 showed the characteristics reflections for the Pd(0) nanoparticles. The N_2 isotherm at 77 K revealed that the composite (Pd@HMP-1) has a microporous-mesoporous framework. The mesoporosity was obtained from the interparticle spaces present in the polymer. The BET surface area was 384 m^2/g and the Pd@HMP-1 composite had a hierarchical porous network (6, 11 and 19 Å). The neat polymer had a pore of 16 Å which was reduced due to the incorporation of Pd nanoparticles in the framework. Transmission Electron Microscopic (TEM) studies revealed the spherical morphology of the polymers and the Pd nanoparticles had been dispersed on the polymer matrix with an average diameter of 10 to 15 nm. The X-Ray Photoelectron Spectroscopy (XPS) gave an idea of the oxidation state of the Pd nanoparticles and the peaks at 334.8 eV and 340.5 eV corresponding to the $3d_{5/2}$ and $3d_{3/2}$ levels of the metallic Pd nanoparticles (Figure 1.6). The nitrogen atom of the carbazole moiety had an interaction with the Pd nanoparticles and this was evidenced from the N1s XPS spectra with a peak at 399.3 eV. This Pd@HMP-1 catalyst has been used for the formylation of amines. To optimize the reaction conditions, N-methyl aniline had been chosen and diphenylmethylsilane as the reducing agent. The optimum condition of the reaction

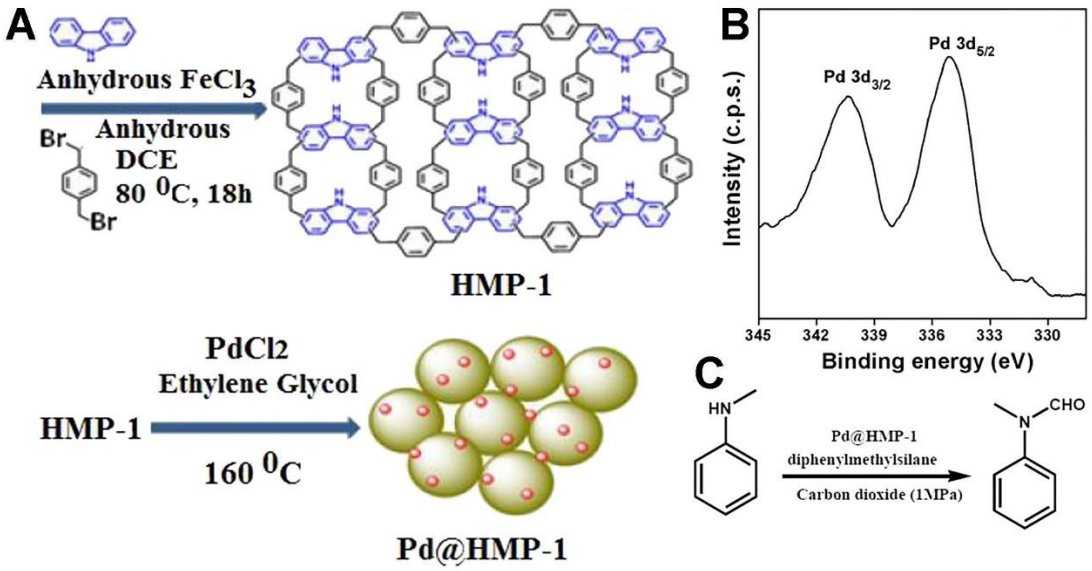

Figure 1.6. (A) Design and Pd nanoparticle loading on HMP-1 (B) Pd 3d XPS spectrum depicting that Pd is at zero oxidation state. (C) The catalytic reaction of CO_2 fixation using Pd@HMP-1 as the catalyst. *(Adopted from ref. 159 from the Wiley Online Library with permission).*

included 50 mg of catalyst, dioxane/water mixed solvent at 60°C temperature for 15 hours (Figure 1.6). The yield of the reaction was influenced by CO_2 pressure. At an optimal CO_2 pressure of 1 MPa approximately 90% conversion was obtained. In absence of the Pd nanoparticles, the polymer itself was able to catalyse the reaction, but to a yield of only 22%. This has been due to the presence of basic nitrogen groups in the polymer which has an interaction with the reactant promoting favourable sites for the reaction. A detailed substrate scope bearing diverse functional group had been studied and the catalytic recyclability was demonstrated for five consecutive cycles. Thus, the polymer acts as good support for the Pd nanoparticles and the reactants for the catalytic reaction and also provides future scope to develop new heterogeneous active catalysts.[159]

1.2. Metal-Organic Frameworks (MOFs):

In the last two decades, metal-organic frameworks have emerged as a unique class of porous coordination polymers that can replace zeolites in many aspects.[97-99] It has crystalline nature, ordered pores ranging from microporous to the mesoporous region (Ultra-microporous: pore size < 6 Å; Microporous: pore size 6-20 Å; Mesoporous: pore size > 20 Å), high surface area and modularity of the pore by different ligands.[101-103] MOFs have emerged as superior over zeolites due to their enhanced stability and applicability in gaseous as well as liquid phase reactions and catalysis. Their ability is well established in gas storage, separation, catalysis, sensing, proton conductivity, energy storage and conversion etc.[104-131] Here, we have discussed selective CO_2 capture by ultra-microporous MOFs.

1.2.1. Zeolitic Imidazole Frameworks (ZIFs):

Such an example is Zeolitic Imidazole Frameworks (ZIFs). ZIFs were prepared by linking imidazolium linkers with metal ions to develop thermally and chemically stable porous frameworks. The structure of the ZIFs resembled that of the aluminosilicates, interestingly, they exhibited wider application compared to zeolites. Yaghi and co-workers reported a family of ZIFs which could be prepared in a convenient way at a large scale. The ZIFs were having open framework structure, hetero linking as well as pore size > 10 Å.[160] The hetero linked ZIFs were of particularly more interesting because they had been found to possess better CO_2 selectivity and storage capacity (Figure 1.7). But the most important feature of the ZIFs was the thermal and chemical stability which was questionable in case of zeolites. ZIF-68 to ZIF-70 were having the same topology as zeolites (gme) whereas ZIF-4, ZIF-23, ZIF-73 had

tetrahedral topologies unlike zeolites (cag, dia, frl) (Figure 1.7). Thus, ZIFs provided an extendable metal-organic structure which was directly related to zeolites, but with modified properties. Deriving the structure of a ZIF from zeolite, if the tetrahedral atom of the zeolite was replaced by transition metal ions like Zn^{2+}, Co^{2+} etc. and the oxide was replaced by imidazolium, one can end up with ZIFs.[160]

Recently, Li and co-workers found that ZIF-7 membrane possessed optimal pore size to selectivity towards hydrogen with an enhanced separation factor.[161] Hydrophobic pockets of ZIF-8 with a pore diameter of 3.4 Å enabled the H_2 separation over other heavier gases like methane.[162] The separation factor for ZIF-8 membrane reported by Bux et al. was 11.2 which was desirable for practical applications. ZIF-8 membrane was also being used for hydrocarbon separation such as ethane–propane, ethylene-propylene and ethylene–propane mixtures.[163] Often ZIFs were blended with organic linkers to enhance the compatibility of the membrane formation. Such ZIFs exhibited higher gas separation ability.[164,165] Not only gas separation, but ZIFs were also very important candidates for vapour sorption. ZIF-8, ZIF-71, ZIF-90 had been used to separate alcohols (methanol, ethanol, 1-propanol, 2-propanol) from water vapour with enhanced ease.[166] Thus, ZIFs exhibited promising application in biofuel recovery. Having a high surface area, stable framework structure and molecular confinement effect, ZIFs catalysed several organic reactions. ZIF-8, 9, and 10 has been used as a heterogeneous catalyst for Knoevenagel condensation to prepare benzylidene malononitrile.[167-168] A trace amount of ZIF-8 catalysed the Friedel Craft acylation of anisole with benzoyl chloride at the ambient condition with high yield.[169] Owing to the high surface area and ordered pore ZIFs could encapsulate highly active metal nanoparticles for different catalytic transformations. This provided a capping agent-free growth of nps with high catalytic activity. Several catalytic cycles had been performed with the composites and the catalytic activity was retained. Catalytic CO oxidation reaction had been performed with Au, Ag, Pt encapsulated ZIF-8.[170] TiO_2 incorporated Pt/ZIF-8 composite exhibited photocatalytic degradation of phenol.[171] Thus, ZIFs and their composites were widely used for catalytic reactions. Although ZIFs are being used mainly for gas separation and catalysis, there are seminal examples where they have been utilized for sensors, electronics and biomedical applications. Hupp and co-workers reported ZIF-8 composites for selective sensing of vapours and gases.[172] Branched polyethyleneimine-capped carbon quantum dots/ZIF-8 composite served as the sensor for the detection of Cu^{2+} ions in the environmental water.[173] Electronic devices, chips are manufactured using ZIFs. ZIF-8 membranes deposited on silicon wafers are used as chips for microelectronics.[174] ZIF-8 is

unstable in an acidic condition which has been utilized for delivering anticancer drugs in cells with acidic pH. Thus ZIF-8 has been demonstrated a promising candidate for the biomedical application where the pH response is utilized for sacrificial delivery of the drug.[175] In this discussion, it has been established that researchers have come forward from traditional zeolites to ZIFs and has been successful to demonstrate enhanced stability and catalytic activity of the materials compared to zeolites.

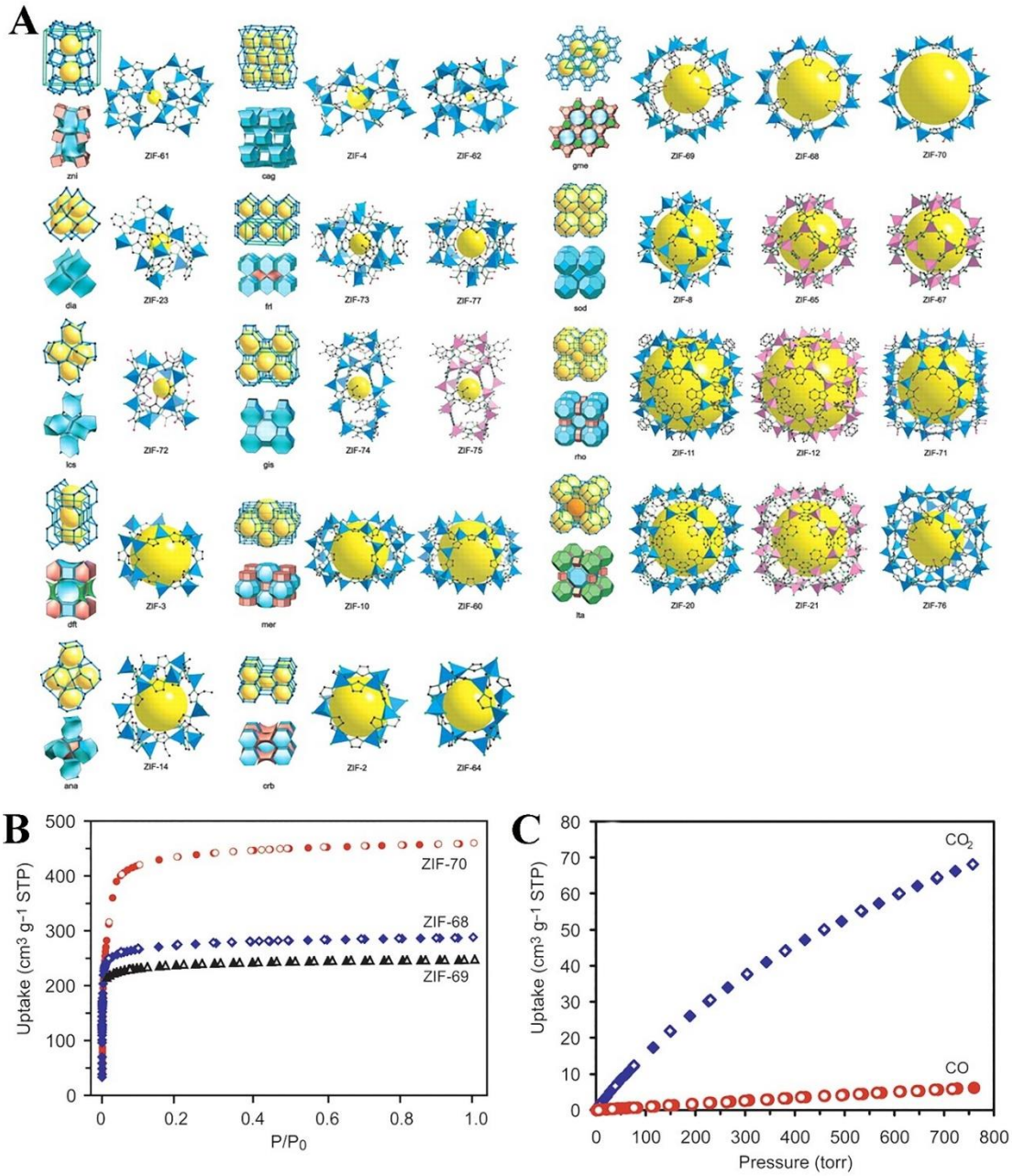

Figure 1.7. (A) Design topology of different ZIF crystals. (B) N_2 adsorption isotherms at 77K of heterolinked ZIF-68, 69 and 70. (C) CO_2 and CO adsorption isotherms of ZIF-69 at 273K. *(Adopted from ref. 160 from the American Association for the Advancement of Science with permission).*

1.2.2. Amine functionalized ultra-microporous MOF for CO_2 capture:

Incorporation of CO_2 binding sites in the MOF pore enhances the affinity of CO_2 over other gases.[176] Recently Simizu and co-workers reported an ultra-microporous MOF constructed by Zn^{2+}, oxalic acid and amino triazole linkers. The Zn-ATZ layers were pillared by oxalate linker (Figure 1.8). There were free amine groups present in the structure which are oriented towards

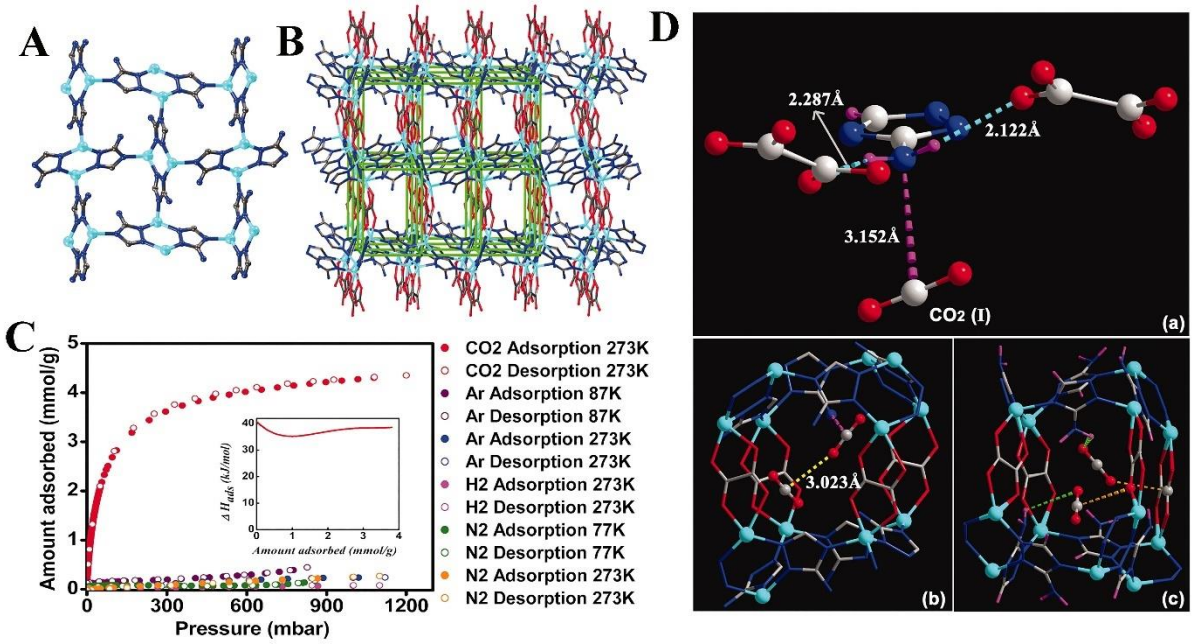

Figure 1.8. (A) Structure of Zn Amino triazole layer. (B) Three-dimensional structure of the MOF, Zn-ATZ layers pillared by oxalate linkers. (C) Different gas adsorption isotherms of the MOF at 273K. Inset shows the Heat of Adsorption curve obtained from Virial method. (D) X-ray crystallographic structure of the CO_2 loaded MOF showing the CO_2 binding sites and CO_2…CO_2 cooperative interaction. *(Adopted from ref. 176 from the American Association for the Advancement of Science with permission).*

the pore. When the MOF was subjected to CO_2 adsorption study, it had been found that it had sharp CO_2 uptake at low partial pressure with high CO_2 capacity at room temperature (3.8 mmol/g at 1 bar). However, the MOF didn't have any affinity towards other gases such as N_2, H_2, Ar etc. The heat of adsorption was calculated using the Virial method and it was found to be 40 kJ/mol. Such high HOA was indicative of framework-CO_2 interaction. However, there was an unusual trend of HOA plot, a constant value over a wide CO_2 loading range, which was attributed to CO_2-NH_2 interactions and the cooperative CO_2-CO_2 interactions of comparable strength. Further, the claim was established by locating the CO_2 interacting sites within a single crystal of the MOF which was also supported by theoretical calculations (Figure 1.8).[176] Similarly Nickel isonictotinate MOFs with exceptional CO_2/H_2 separation capability marked

by large working capacities for pre-combustion and hydrogen purification mixtures have been demonstrated. In another embodiment, a different nickel isonicatinate MOF was developed by the same group of researchers (Nandi et al.) which showed record-low parasitic energy for CO_2/N_2 separation from flue gas mimics.[59]

1.2.3. SiF_6 based ultra-microporous MOFs for CO_2 capture:

An important class of ultra-microporous MOF was reported by Zaworotko and co-workers.[177] The MOFs were prepared via room temperature diffusion of a solution containing the metal hexafluoro silicates (MSiF6, M: Cu/Zn) with a neutral N-donor ligand (such as 4, 4′-dipyridylacetylene; dpa / Pyrazene) into a solution of $MSiF_6$ (where, M=Cu/Zn). SIFSIX-2-Cu and SIFSIX-2-Cu-i had been prepared by the reaction of $CuSiF_6$ with dpa, but in different solvents. SIFSIX-2-Cu had a pore dimension of 13.05 Å whereas, SIFSIX-2-Cu-i provided a 2-fold interpenetrated network with a 5.15 Å pore width. SIFSIX-3-Zn had a cubic channel

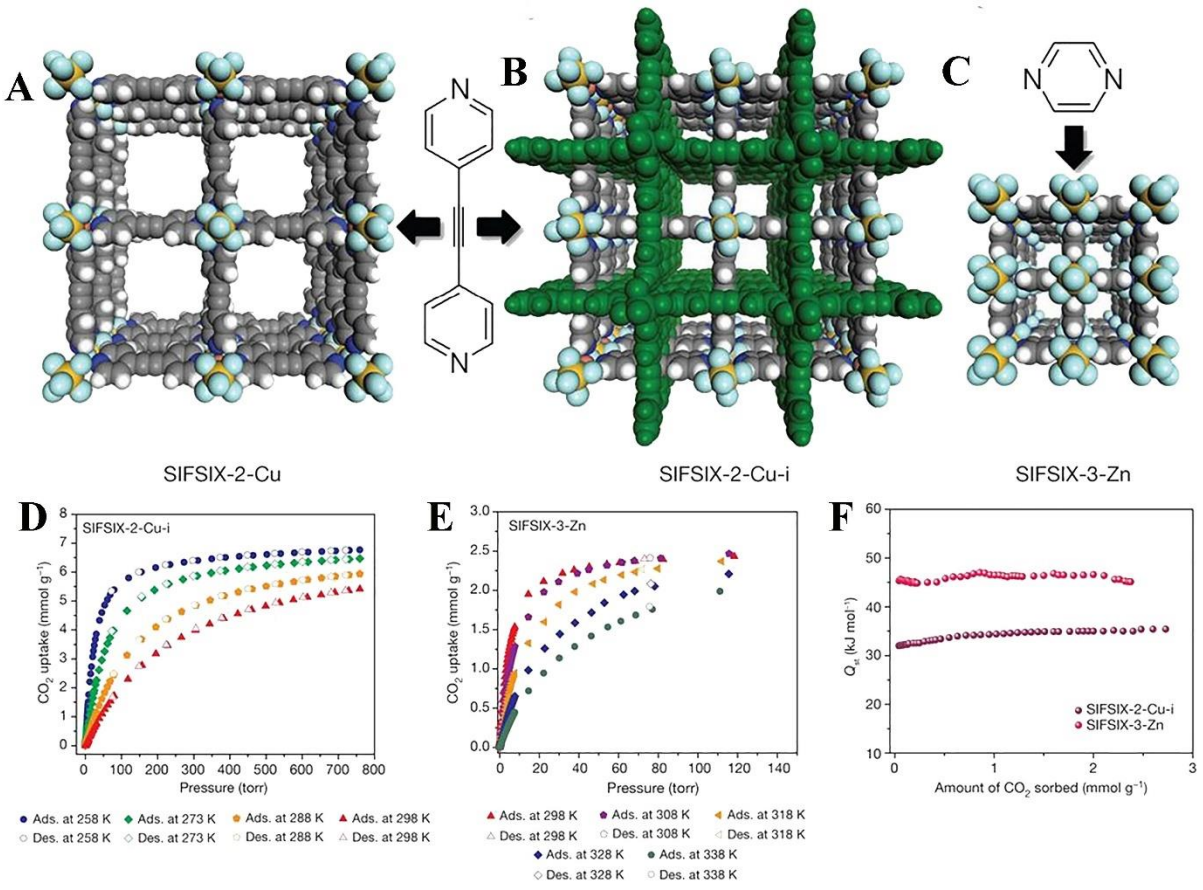

Figure 1.9. (A, B, C) Design strategies to obtain a systematic reduction in pore sizes by choosing appropriate linkers. (D, E) CO_2 adsorption isotherms of SIFSIX-2-Cu-i and SIFSIX-3-Zn at different temperatures. (F) The heat of adsorption for these two MOFs. SIFSIX-3-Zn has higher zero loading

HOA value indicating strong framework CO_2 interaction. *(Adopted from ref. 177 from the Nature Publishing Group with permission).*

with a pore dimension of 3.84 Å (Figure 1.9). N_2 isotherms at 77K provided the BET surface areas for the MOFs (3,140 and 735 m^2/g for SIFSIX-2-Cu and SIFSIX-2-Cu-i, SIFSIX-3-Zn didn't adsorb N_2 gas at 77K). When the MOFs were subjected to CO_2 adsorption, it had been observed that SIFSIX-2-Cu had 1.84 mmol/g at 298 K and 1 bar. But SIFSIX-2-Cu-i possessed a very high CO_2 capacity, 5.41 mol/g at 298K and 1 bar with a high uptake at low pressure. The IAST CO_2/N_2 selectivities were 13.7 and 140 at 298K, 1 bar for SIFSIX-2-Cu and SIFSIX-2-Cu-I, respectively. This observation was corroborated with the reduction of pore sizes from SIFSIX-2-Cu to SIFSIX-2-Cu-i as the ultra-microporous MOFs were better CO_2 selective than the other ones. SIFSIX-3-Zn also showed very high CO_2 uptake which was comparable to the Mg-MOF-74 (Figure 1.9).[178]

1.2.4. Fluorinated MOF for a trace amount of CO_2 capture:

To remove the trace amount of CO_2 (400 ppm) from the air is a challenging task. This study provides an example of hydrolytically stable fluorinated MOF (NbOFFIVE-1-Ni) for the above-mentioned application.[179] Here, the MOF was quite comparable with the SIFSIX-3-M series where SiF_6 is deliberately replaced by the $NbOF_5^{2-}$.

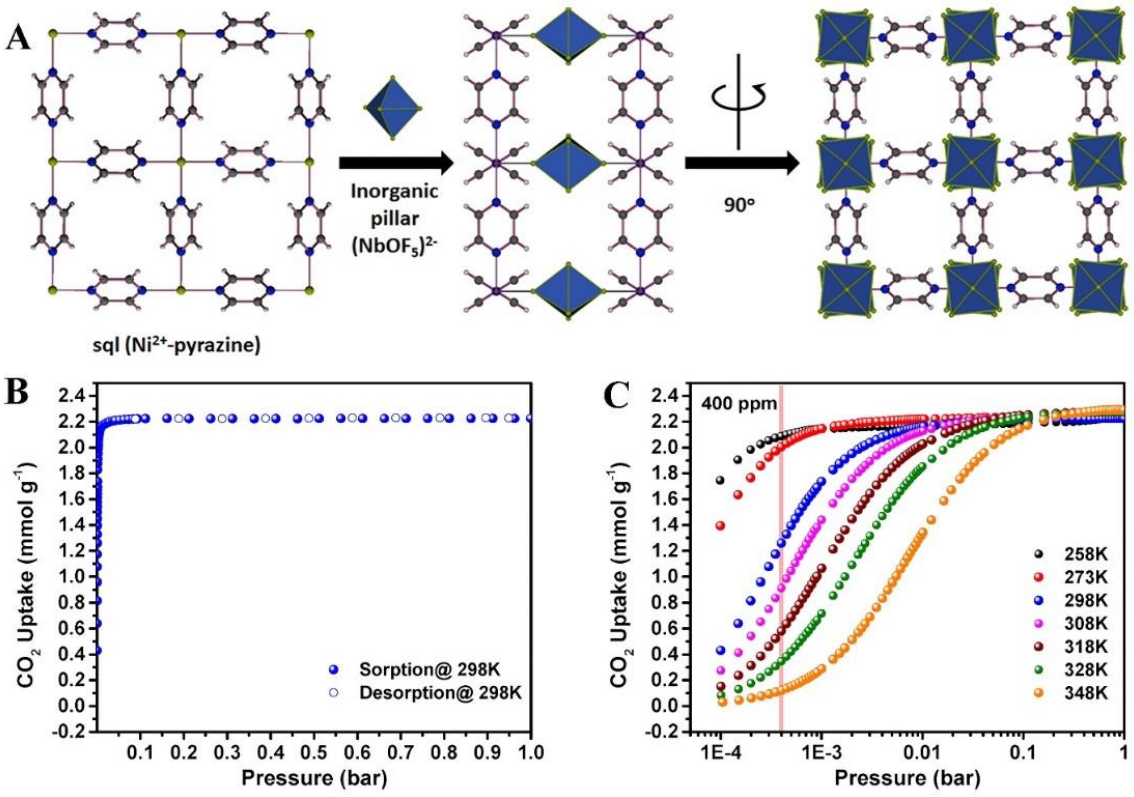

Figure 1.10. (A) Schematic representation of the synthesis of NbOFFIVE-1-Ni (B) CO_2 adsorption isotherm at 298K. (C) CO_2 adsorption isotherms of NbOFFIVE-1-Ni at different temperatures and low pressures. *(Adopted from ref. 179 from the American Chemical Society with permission).*

$NbOF_5^{2-}$ being more nucleophilic in nature, provided stronger coordination and hydrolytic stability (Figure 1.10). The size of the Nb^{5+} reduced the proximal distance of the F atoms in the pore. The MOF crystallized in a tetragonal space group (*I*4/*mcm*) with a pore aperture of 3.2 Å. The MOF had a BET surface area of 280 m^2/g which was evaluated from CO_2 adsorption isotherm at 273K. The CO_2 adsorption isotherms showed a stiff increase at low pressure indicating very high CO_2 framework interaction present in the MOF. Importantly, the MOF showed enhanced volumetric CO_2 uptake at 400 ppm compared to the SIFSIX-3-Cu (51.4 cm^3/cm^3 for NbOFFIVE-1-Ni vs 44.6 cm^3/cm^3 for SIFSIX-3-Cu). Thus, the MOF proves to be the best adsorbate for a trace amount of CO_2 capture both volumetrically and gravimetrically by physisorptive process.

1.3. Porous polymers for gas capture under humid conditions:

An alternate approach to developing porous solids for humid gas capture would be to utilize metal-free organic polymers. Previously from our group, we have demonstrated the pre-combustion and post-combustion CO_2 capture performances by porous Bakelite based polymers and ultra-microporous MOFs. These materials are stable, reproducible and high performing toward CO_2 capture. Owing to these phenomenal properties, these materials could be screened for noble gas capture.

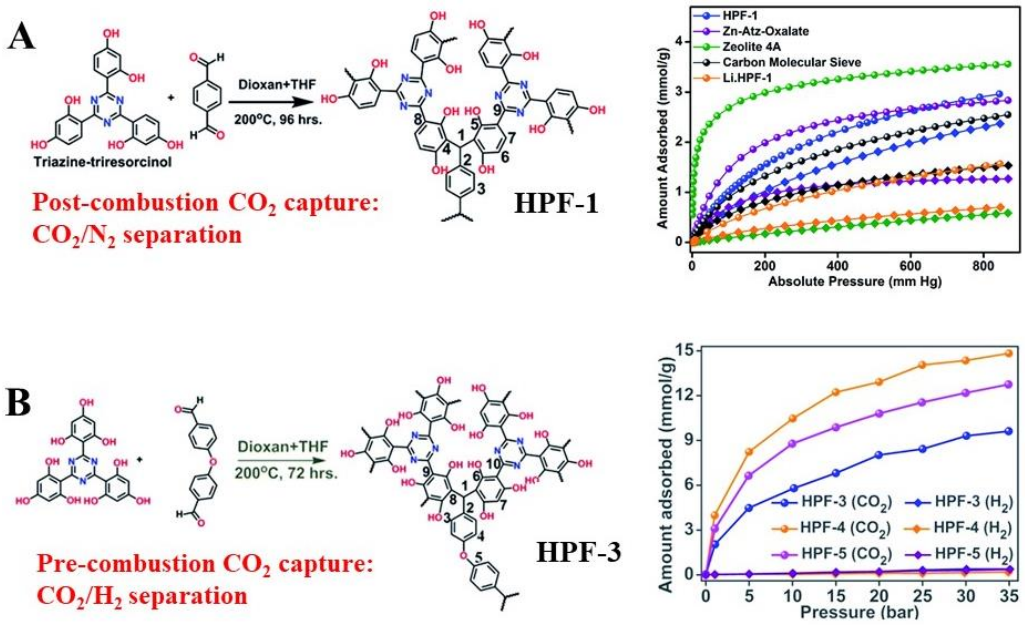

Figure 1.11. (A) Stable HCP for CO_2/N_2 separation under humid condition. (B) Pre-combustion CO_2 capture has been demonstrated using humidity stable porous polymers. *(Adopted from refs. 181 and 182 from the Royal Society of Chemistry).*

1.3.1. Hydrophobic polar frameworks (HPFs) for post-combustion CO_2 capture:

In post-combustion CO_2 capture, the stream of flue gas contains 85% N_2: 15% CO_2 along with SO_x, NO_x and water vapour. The adsorbent materials for the flue gas must be designed in such a way that the materials can adsorb CO_2 at low pressure selectively over the other components. The materials desire an obvious requirement of humid stability. HCPs are proven to exhibit good capacity and selectivity for the same but the lack of functionality affects the CO_2 adsorption property. To address that the HPFs were synthesized by the Bakelite chemistry. Triazine–tri resorcinol is being reacted with terephthaldehyde at the solvothermal condition. The resulting polymer was amorphous in nature and the characteristics C-C bond formation is monitored by the solid-state NMR and IR spectroscopic data. The microscopic study revealed that the polymer had homogeneously distributed spherical morphology (Figure 1.11 A). The polymer exhibited high thermal and chemical stability due to the presence of C-C bondings in the backbone. It had a moderate BET surface area of 576 m^2/g and a pore diameter of 5.5 Å. The CO_2 adsorption isotherms were measured at different temperatures and it was found that the polymer exhibited 9.35 mmol/g at 195K and 2.8 mmol/g at 303K. There was no N_2 uptake at room temperature. The IAST selectivity was calculated for the polymer at a composition of 85% N_2: 15% CO_2 at 303K at 1 bar and the selectivity was found to be 120. To demonstrate the chemical stability and the retention of activity of the polymer in flue gas condition, it was exposed to the acidic vapour (solution containing sulphur trioxide, $SO_3(g)$ + conc. HNO_3+H_2O heated for about 48 h and exposed to the polymer). Further, the polymer was dispersed and boiled in DMF, DMSO, water and their mixtures. In all the cases, the CO_2 uptake of it was retained. This confirmed the chemical stability and structural integrity of the polymer which made this a promising candidate for post-combustion CO_2 capture. To demonstrate the hydrophobicity, vapour adsorption had been performed with toluene and water. The water adsorption isotherm was of type-III and the heat of adsorption calculated is 43 kJ/mol which was much lower than the hydrophilic materials.[180] However, toluene showed a type-I adsorption isotherm and a zero loading HOA of 35 kJ/mol which subsequently increased to 65 kJ/mol with higher loading. This was explained as the toluene finds proper interaction with the aromatic groups. The contact angle of the polymer was 153° which had indicated the hydrophobic nature of the polymer. The spherical morphology corroborated the hydrophobic

surface of the polymer. The zero loading HOA was found to be 25 kJ/mol obtained from the Virial method which was optimal for the facile regeneration of CO_2. The polymer still had appreciable water uptake that could hamper the CO_2 capacity at the practical condition. To test that, the polymer was subjected to the humid N_2 stream (passing N_2 through saturated NaCl solution which generates a relative humidity of 75%) for 24 hours and after that, the CO_2 adsorption was measured without activating the sample. The CO_2 capacity was dropped by 20% which is much better than the other porous materials like ZnATZOx MOF which lose 55% of its capacity. The CO_2/N_2 selectivity is obtained to be 90 at 303K at 1 bar. This was a very important observation depicting the superiority of the polymer for humid CO_2 capture application (Figure 1.11 A). The CO_2 binding sites were studied with the help of theoretical modelling which revealed that the polar groups provided favourable interaction for the CO_2 molecules while providing an optimal hydrophobic-hydrophilic balance in the pore. Thus, this exemplified that the hydrophobic polar frameworks had the magic composition for humid CO_2 capture application.[181]

1.3.2. HPFs for pre-combustion CO_2 capture and hydrogen purification:

Generation of CO_2 from fossil fuel burning and steam reforming process is associated with a mixture of hydrogen at high pressure and temperature. The pre-combustion CO_2 capture is an important process which can generate clean-burning fuel (H_2). However, sorbent material should have all the characteristics properties to withstand the harsh condition. The HPFs could have been promising candidates as their inherent stability and microporous nature. Here three HPFs were prepared namely HPF-3, HPF-4 and HPF-5 using the phenol-formaldehyde bakelite chemistry between different aldehyde and phenolic moieties (Figure 1.11 B). The polymers were thermally stable up to 380 ℃ and had homogeneous spherical morphologies. HPF-4 showed 4.03 mmol/g CO_2 uptake at 1 bar at 303K. The polymers didn't adsorb hydrogen at room temperature and the IAST selectivities were calculated in the composition of pre-combustion (60 H_2/40 CO_2) and hydrogen purification composition (80 H_2/20 CO_2) at 303K and 1 bar. It showed quite high selectivities over hydrogen in both of the conditions (~300 and 600). The isosteric heat of adsorption had been in the order of 27 to 32 kJ/mol for the three polymers, respectively, which was optimal for the facile regeneration of CO_2. Pre-combustion CO_2 capture involved high-pressure systems (30-40 bars). The polymers showed promising CO_2 uptake at high-pressure measurements (HPF-4: 14.7 mmol/g, HPF-5: 12.5 mmol/g and HPF-3: 9.6 mmol/ g) at 298K and 35 bar which was comparable to their saturation CO_2 uptake

at 195K at 1 bar. IAST selectivity was calculated for the high-pressure measurements and HPF-4 is having the highest selectivity at 298K (191, 289 and 238 respectively at 10 bar and 98, 145 and 104 at 35 bar for HPF-3, 4, 5 respectively).[182] Thus, the high-pressure adsorption isotherms suggested that the HCPs are promising candidates for the pre-combustion CO_2 capture. The working capacities of CO_2 of the polymers in a pressure swing of 10 to 1 bar were found to be 4.42, 6.70 and 6.78 mmol/g which was quite remarkable for the microporous polymers. The polymers exhibited contact angles greater than 150° and the hydrophobicity was further confirmed by the preferential toluene adsorption over water. Humid CO_2 isotherm studies yield only 15 to 20% loss in the overall capacity. The dynamic breakthrough studies were performed with HPF-4 to study the pre-combustion (60 H_2/40 CO_2) and hydrogen purification composition (80 H_2/20 CO_2) at 298K, 1 bar and it was found that the polymer had CO_2 uptake of 3.52 and 2.42 mmol/g for the two conditions, respectively (Figure 1.11 B). The polymers exert outstanding stability in acidic and basic conditions, and these have emerged as the challenging contender for the pre-combustion CO_2 capture and hydrogen purification.[182]

In the present decade, capturing and separating precious noble gases have become a challenge to be addressed. Some of the largest sources of Xe include nuclear waste, which involves separating Xe from humid gas mixtures. Hence the design aspects used in these humid CO_2 capture materials could come handy for Xe separators. Here, a brief introduction to the noble gas capture (mainly Xe) is presented in the following section.

1.4. Introduction to Xe/Kr capture:

The emerging demand for energy in the 21st century is associated with rapid global urbanization and economic development. The United States Department of Energy (DOE) estimates an average ~28% enhancement in the electric demand by 2040. It is high time to seek new renewable energy sources to meet the demand of the requirement. Nuclear energy is the most effective alternative energy sources for the present decade, but the power generation through nuclear energy sources is accompanied by a number of challenges.[183] The researchers are revisiting nuclear safety practices prior to the Chernobyl and Fukushima disaster. The nuclear energy production yields Used Nuclear Fuel (UNF) which is high-level solid, low-level liquid and gaseous radioactive wastes. These wastes may take a thousand years to decay. Some of the countries like France, Japan, Russia reprocess the UNF to extract valuable materials like plutonium, uranium. But the gaseous radioactive nuclei (isotopes of Xe, Kr, I, C etc.) are released into the environment through off-gas stream which is hazardous to the living entities.

Aqueous reprocessing includes the capture of radioactive Iodine and Tritiated water, but CO_2, Xe, Kr are not separated from the stream. Xe is an important component for many applications in our daily lives ranging from lighting, lasers, space technologies to medical applications.[184] But, the concentration of Xe present in the atmosphere is very low (0.09 and 1.1 ppm for Xe and Kr). The present technology for obtaining the gases from the air is the cryogenic distillation which is performed based on the difference of their boiling points (−108.12 and−153.22°C for Xe and Kr, respectively). But this is an energy-demanding process and associated with hazardous ozone formation.[184] In order to avoid this approach, researchers are seeking materials to separate the gases in the off-gas stream itself which may lead to greater Xe production. The half-life of Xe is much lower than Kr (36.3 days for Xe and 110 years for Kr). In other words, successful removal of Xe and subsequent sequestration of the Kr may lead to the economically viable processing of the UNF. Selective adsorption and separation of these gases are achieved by two processes, liquid phase dissolution and physisorptive separation. A suitable solvent is used to dissolve the gases as a function of pressure and temperature for the case of liquid extraction. But this process is somewhat comparable to the cryogenic distillation and lacks in the selectivity of the two gases. Porous materials provide an effective alternative platform for the noble gas capture due to their high surface area.[184] Microporous materials such as Zeolites, activated carbons are the promising candidates for the selective Xe capture, however, zeolites face serious structural effects in the off-gas condition. The presence of NO_x in the off-gas stream creates fire hazards when exposed to activated charcoal. Thus, researchers are investigating the potentials of MOFs and other porous materials for this important application. Here, we present two seminal examples of porous materials for the selective Xe capture.[184]

1.4.1. Optimal MOF for selective Xe capture and separation:

Thallapally and co-workers screened a database (125,000 MOF structures at UNF processing conditions) of MOFs for the optimal Xe/Kr selectivity based on their structural aspects.[185] They identified and synthesized SBMOF-1 to experimentally verify the outputs from the theoretical calculations. SBMOF-1 was a Calcium based MOF which had 4,4 -sulfonyldibenzoate as the linker (Figure 1.12). The SBMOF-1 had been subjected to Xe adsorption, but the Xe uptake didn't meet the theoretical prediction. However, at low pressure, the MOF attained saturated Xe uptake, which was important for a material to be able to work under the UNF processing condition. The Kr isotherm had a smaller slope and didn't attain the saturation at 1 bar. This

indicates that the MOF had a greater affinity for Xe compared to Kr. The henry coefficient analysis yielded a Xe/Kr selectivity of 16 at dilute condition (Figure 1.12). The selectivity is

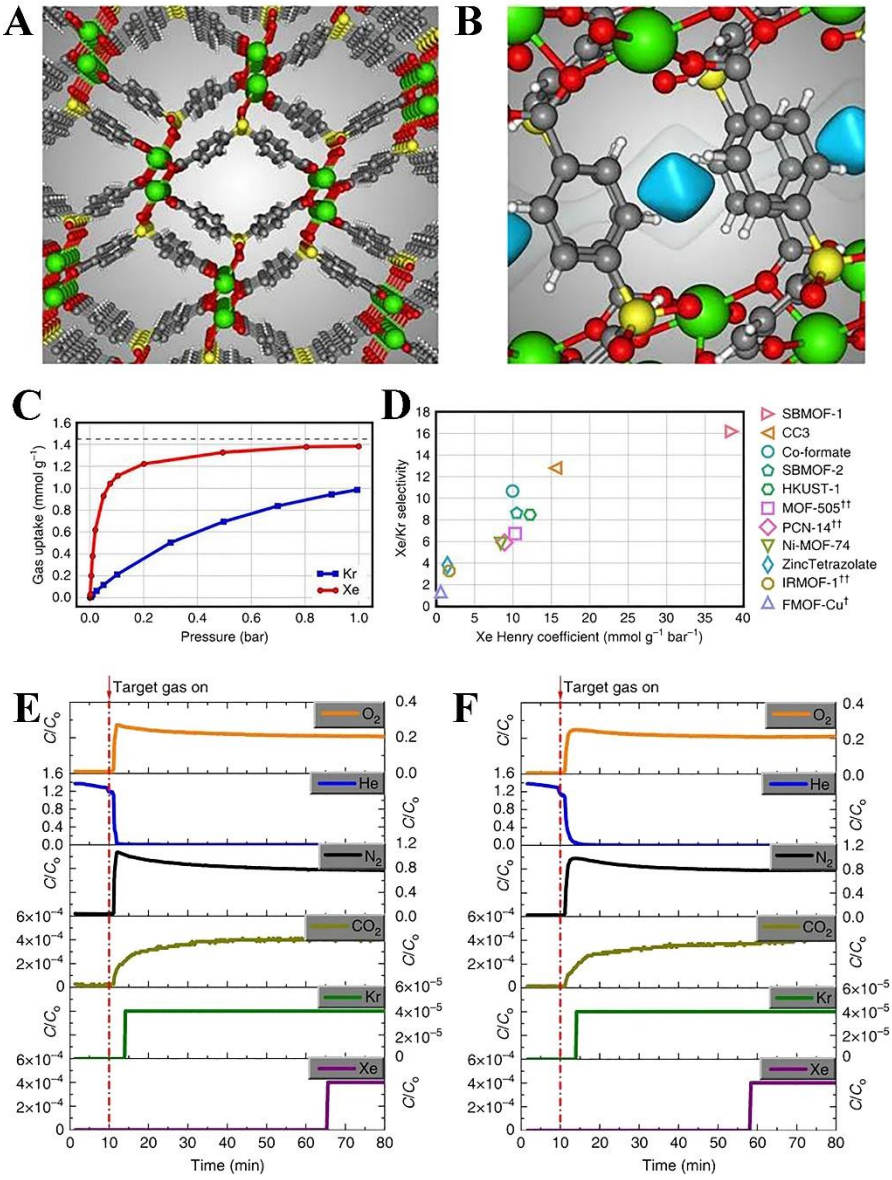

Figure 1.12. (A) Structure of SBMOF-1. (B) The blue structure indicates the position of Xe in the MOF crystal. (C) Xe and Kr adsorption isotherms at 298K and 1 bar. (D) Xe/Kr selectivity of SBMOF-1 compared with the existing benchmark materials. (E) The breakthrough experiment performed with 400 ppm Xe and 40 ppm Kr mixture balanced with air. (F) The breakthrough experiment performed in the presence of humidity. *(Adopted from ref. 185 from the Nature Publishing Group with permission).*

the highest compared to the other benchmark materials like Co-formate,[186,187] HKUST-1,[188] SBMOF-2,[189] Ni-MOF-74[190] etc. The low-pressure uptake was a key feature for UNF processing condition as the concentration of Xe was quite low at that fuel (400 ppm). In this regards, SBMOF-1 beats other materials. However, the saturation capacity was not very high

because of the low surface area of SBMOF-1 (145 m^2/g). SBMOF-1 exhibits fast kinetics for the Xe capture and cyclability of adsorption over 10 cycles was also achieved. To confirm the practical use, a single column breakthrough experiment was performed. In this experiment a column of SBMOF-1 was passed with the gas mixture of desired composition (400 p.p.m. Xe, 40 p.p.m. Kr, 78.1% N_2, 20.9% O_2, 0.03% $CO_2$and 0.9% Ar)) and the breakthrough was monitored with a mass spectrometer. It had been observed that the Xe was retained in the column for a significant time and other gases were coming out of the column. SBMOF-1 could adsorb13.2 mmol/kg Xe at the UNF condition (Figure 1.12).[185] Thus, this was concluded to be a promising contender for this application. In presence of humidity, the uptake was 11.5 mmol/kg, retention of the activity was observed even in wet condition. The outstanding stability was observed due to the absence of open metal sites in the framework. The interaction site of the Xe within the MOF was obtained by single-crystal X-Ray analysis of the Xe loaded MOF. It had been found that the Xe was located at the midpoint of the channel and it had van der Waals interaction with the aromatic groups in the framework. The theoretical calculation revealed that the optimal Xe adsorbing material should have a pore aperture slightly greater than the kinetic diameter of Xe (4.1 Å). The pore diameter for SBMOF-1 is 4.2 Å which met the criteria perfectly thus exhibiting outstanding Xe/Kr selectivity at low pressure.[185]

1.4.2. Porous organic cage for selective Xe capture:

Cooper and co-workers studied the selective Xe capture ability of a porous organic cage. The cavity size of the cage was 4.4 Å which perfectly matches the kinetic diameter of Xe (4.10 Å). But the window size of the cage was 3.6 Å, slightly lesser than the kinetic diameter of Kr (3.69 Å). The cage had a Xe uptake of 2.69 mol/kg at 1 bar with saturation which corresponds to the three Xe molecules per cage. Kr isotherm did not meet the saturation at 1 bar indicating the strong interaction with Xe of the cage. The heat of adsorption corroborated the strong Xe interaction (Figure 1.13).[191] The zero loading HOA for Xe and Kr were 31.3 and 23.1 kJ/mol. Powder X-Ray diffraction at higher Xe pressure had been collected to determine the structure of CC3 cage in the presence of Xe. It has been found form the structural analysis that all the cage cavities were occupied by Xe atoms and 88~% of the window cavity was occupied by the Xe. Thus, the unit cell contained 2.86 molecules (1.86 mmol/kg, 25 wt%) of Xe which agreed with the experimentally observed Xe capacity. On the other hand, the in situ PXRD of Kr loaded sample resulted in 2 molecules of Kr per unit cell of the cage (1.63 mmol/kg, 13 wt%).

To demonstrate the practical Xe selectivity of the cage, a mixture of 400 ppm Xe and 40 ppm Kr balanced by the other gases (N_2, CO_2, Ar) was passed through a column. The Xe was

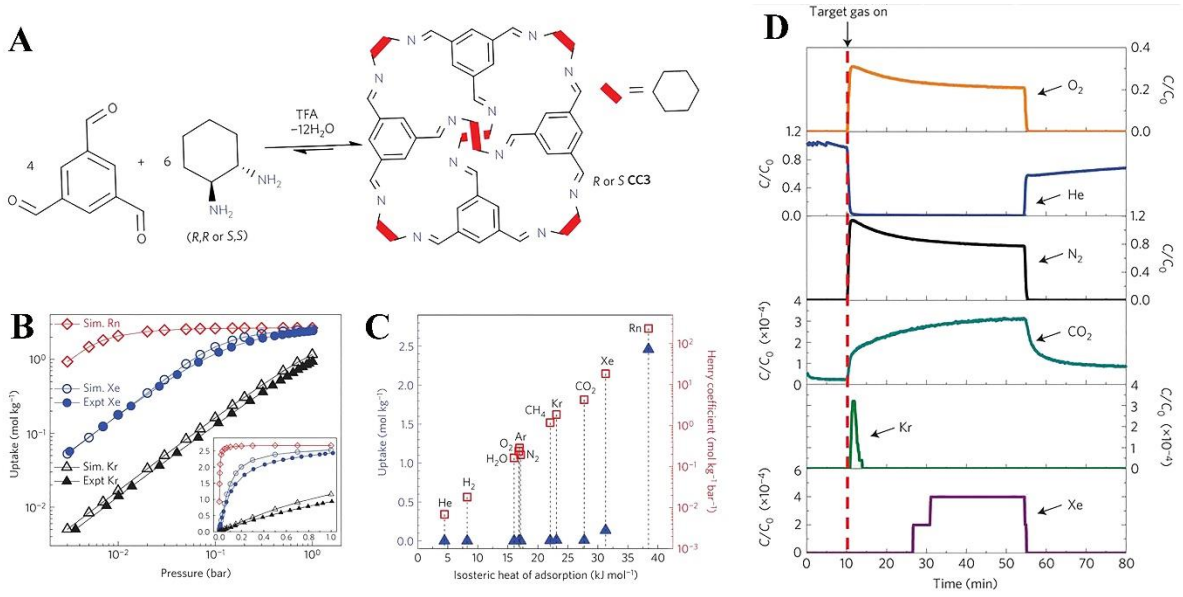

Figure 1.13. (A) Synthetic scheme of the cage (B) Noble gas adsorption isotherms obtained experimentally and comparable simulated isotherms (C) HOA and Henry coefficients depicting that Xe has greater interaction with the framework. (B) The breakthrough experiment performed with 400 ppm Xe and 40 ppm Kr mixture balanced with air. *(Adopted from ref. 191 from the Nature Publishing Group with permission).*

retained in the column for ~15 mins, but the other gases broke through immediately (Figure 1.13). The kinetics measurements of pure component Xe and Kr gases reveals that the kinetics was fast enough to execute the real separation. Although the window cavity was smaller than the kinetic diameter of Xe, still the material showed exceptional Xe capacity and selectivity. Molecular dynamics simulation studies revealed that the pore window opens 7% of the simulation time for Xe. This was enough to initiate the hopping motion of Xe into the cage cavity. This is a unique example of a material which has very high Xe capacity and selectivity at the dilute condition. This material was identified to be a promising candidate for Xe sorbents at UNF condition.[191]

In recent years, researchers have developed crystalline organic polymers by adopting simple chemistry and the meticulous choice of building blocks. COFs can be considered as ordered heteroatom doped graphene. But, owing to their crystallinity, COFs can be easily modulated and studied to molecular precision. The pore is highly functionalized to render favourable host-

guest interactions. In the following section, we have discussed the CO_2 capture and catalytic application with imine bonded COFs.

1.5. Covalent Organic Frameworks (COFs):

Covalent organic frameworks are the porous organic materials which are crystalline in nature. Cote et al. first introduced this class of materials and the potential of COF was realized.[192] COF are simply polymers formed by involving symmetrically well-defined rigid cross-linking monomers in its construct. Such cross-linking monomers can be combined with rigid linear linkers or other cross-linking monomers. This generates ordered polymeric structures extending in two or three-dimensions with well-defined pores. The geometry of the cross-linking nodes and the linkers results in the formation of two-dimensional (2D) and three-dimensional (3D) network. The 2D COFs have interlayer π-π interaction which stabilizes and crystalizes the network, whereas 3D COFs are three-dimensionally connected (containing

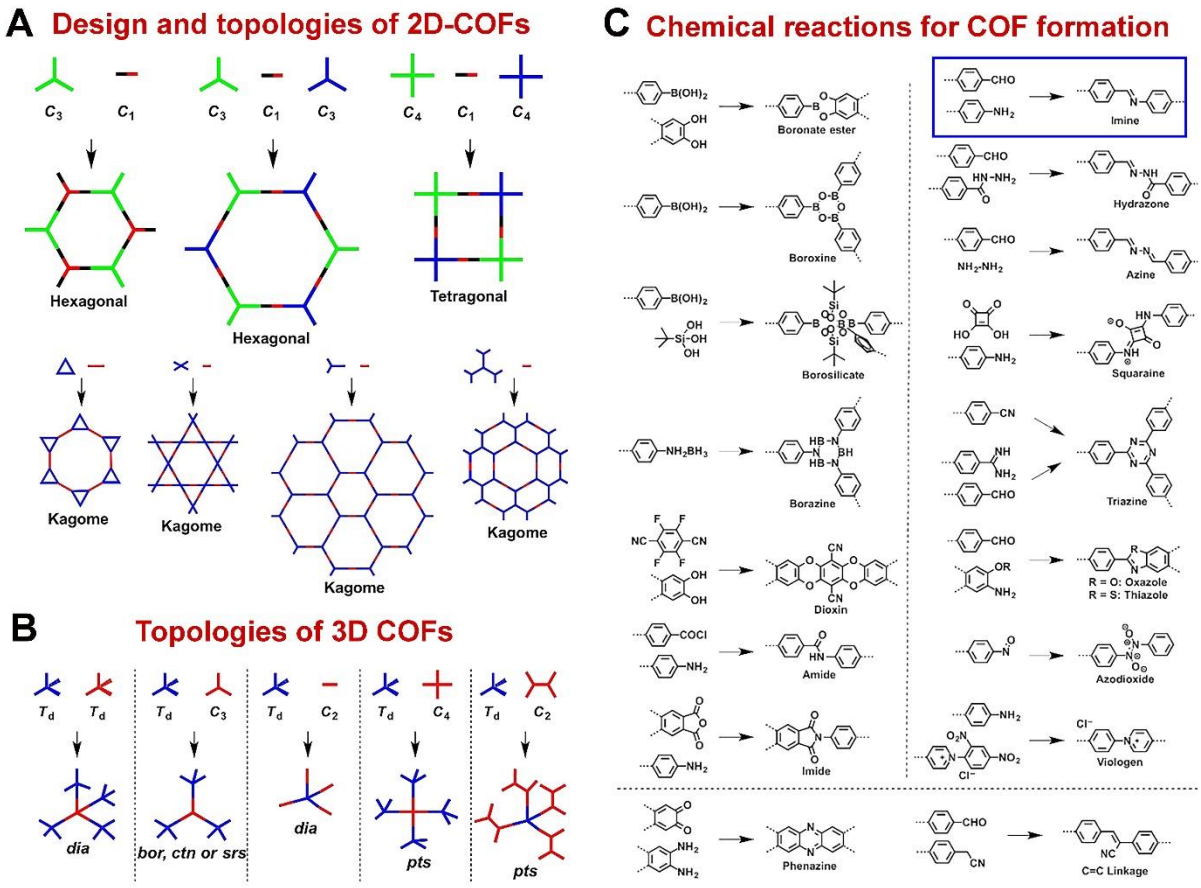

Figure 1.14. (A, B) Design and topological description of 2d and 3D COFs. (B) Chemical reactions involved in the COF formation. *(Adopted from ref. 194 from the Royal Society of Chemistry with permission).*

tetrahedral linkers, different topologies like gra, bnn, ctn etc.) to provide a stable network (Figure 1.14).[193] The high surface area, ordered porous network and crystalline nature make the COFs a valuable contender for different application in the porous materials field of research.[194] Diverse chemistries are being employed to develop novel COFs with different functionalities, topology and stabilities. The most common is the Schiff's base formation between aldehydes and amines because a huge library of aldehydes and amine are available in the literature (Figure 1.14). The crystallization of the organic building blocks renders periodicity into the framework and often 2D COFs are compared with ordered heteroatom doped graphene sheets.[194] The strong covalent bonds are responsible for high thermal and chemical stability. The crystalline nature of the COFs is helpful to elucidate the structural insights and the properties which are related to the structural aspects. A most important feature of COFs is the hetero atom rich pores, which enables to a favourable host-guest interaction. In this aspect, here some seminal examples of COFs (imine bonded) are discussed for selective gas capture and separation and catalysis.

1.5.1. Triformyl Phloroglucinol based COFs for selective CO_2 capture:

The Trifolmyl Phloroglucinol (Tp) based COFs have unique features compared to other imine bonded COFs. Imine bond is not stable and can be broken in the presence of acids, bases, even in boiling water. But TP group introduces keto-enol tautomerism in the framework which forms an intramolecular hydrogen bonding with the imine groups and exerts stability towards

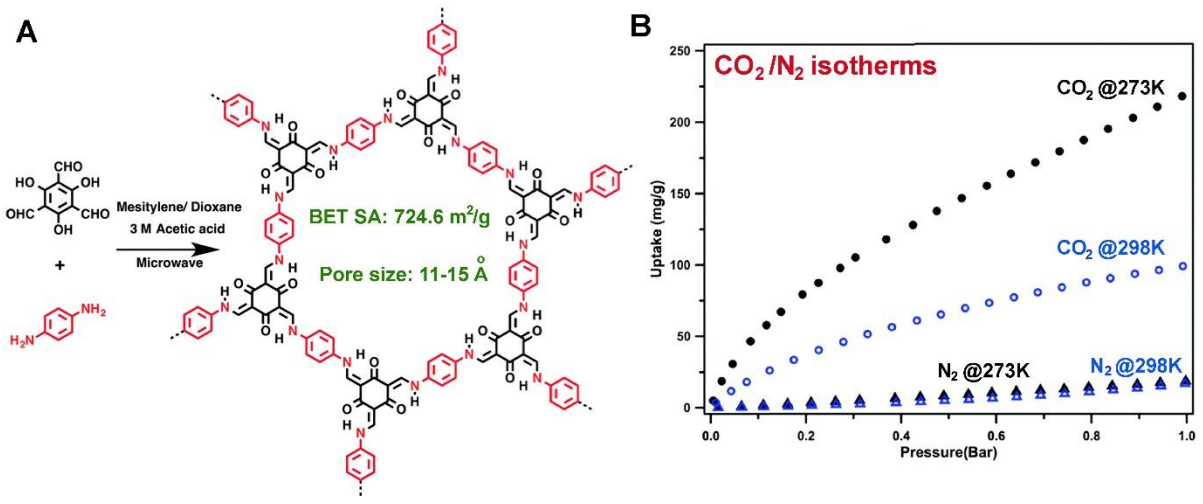

Figure 1.15. (A) The design strategy of TpPa-COF. (C) CO_2 and N_2 isotherms of the COF showing CO_2 selectivity over N_2 at 273K and 298K. *(Adopted from ref. 197 from the Royal Society of Chemistry with permission).*

hydrolysis.[195,196] The TpPa-COF has been prepared in microwave technique to avoid high temperature and time consuming solvothermal process (Figure 1.15). The disappearance of the -N-H vibrational peaks (~3200 cm^{-1}) and the presence of the -C=N (1253 cm^{-1}) indicated the imine bond formation in the COF. The COF existed in keto form under ambient conditions. The powder X-Ray diffraction pattern showed sharp low angle peaks confirming the crystalline nature of the COF and the intensity of the (100) peak was higher for the microwave synthesized sample compared to the solvothermally synthesized COF. This was attributed to the fact that the layers are well-organized and stacked in the 2D fashion for microwave synthesized phases. The TpPa-COF (MW) showed a BET surface area of 724.6 m^2/g and the NLDFT fitting yielded a pore size of 11-15 Å. Encouraged by the microporous nature, the CO_2 adsorption has been carried out at two different temperatures (273K and 298K) and it adsorbed 21.8 wt% at 273K, 1 bar. The isosteric heat of adsorption has been obtained to be 34.1 kJ/mol at zero loading of CO_2 which indicated that CO_2 molecules potentially interact with the heteroatoms present within the pore wall of the COF (Figure 1.15). Further, the CO_2/N_2 selectivity at post-combustion ration had yielded 32 at 273K at the initial slopes of the isotherms. The optimal HOA value and the CO_2 selectivity suggested that the TpPa-COF (MW) could be an important candidate for selective CO_2 capture.[197]

1.5.2. 2D mesoporous COF for gas storage:

The mesoporous COF (ILCOF-1) has been prepared by the reaction of 1,3,6,8-tetrakis(p-formylphenyl) pyrene with phenylene diamine under solvothermal conditions (Figure 1.16). The resulting COF was thermally stable up to 400°C. The presence of -C=N peak in solid-state ^{13}C NMR (156 ppm) spectra and -C=N stretching band at 1617 cm^{-1} in the IR spectrum confirmed the formation of the COF. PXRD of the COF revealed a highly crystalline nature and the structure was modelled to an orthorhombic space group with an eclipsed conformation. Argon adsorption study at 87 K yielded a BET surface area of 2723 m^2/g and a major pore of size 23 Å with some minor pores of size 10 to 17 Å. The total pore volume at 0.96 P/P_0 was 1.21 cc/g. This high pore volume and surface area of the COF could be of interest to gas storage application. The storage of H_2, CH_4 and CO_2 has been studied at high pressure as the COF possesses significant physicochemical stability. The storage capacity of H_2, CH_4 and CO_2 were 1.3 wt.% at 77 K, 0.9 wt.% at 273 K and 6.0 wt.% at 273 K, respectively, all measurements were at 1 bar (Figure 1.16). The low capacities of the gases had been attributed to the mesoporous nature of the COF. The heat of adsorption has been calculated for all the gases

using Clausius–Clapeyron equation a Virial analysis and was reported as 5.9, 13.7, and 18.3 kJ/mol for H_2, CH_4 and CO_2 respectively. The saturation had not been achieved in case of low-pressure adsorption and hence high-pressure data was collected for all of these gases. H_2 isotherm had a saturation at 35 bar with the uptake of 4.7 wt% at 77K at 40 bar. Interestingly, the CO_2 uptake was 29.3 mmol/g at 298K, 40 bar which is superior to most of the hyper-crossed-linked polymers (HCPs), porous aromatic frameworks (PAFs).[198,199] This has been attributed to the presence of heteroatoms in the mesopores of the ILCOF-1 which provides an

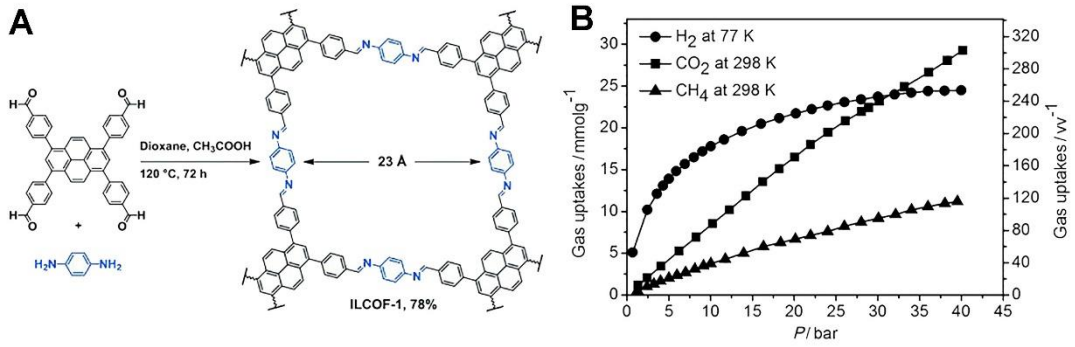

Figure 1.16. (A) Schematic representation of COF. (C) High pressure isotherms collected for CO_2, CH_4 and H_2 for the COF. *(Adopted from ref. 200 from the Wiley Online Library with permission).*

interaction site for CO_2. The CH_4 uptake was 11.2 mmol/g which is significantly higher than some of the COFs. Thus, it has been demonstrated through this example that the mesoporous COFs are potential candidates for gas storage and opens up new paths for the development of functionalized COFs for such applications.[200]

1.5.3. Nitrogen-rich 2D COFs for CO_2 capture:

In this example, three COFs are introduced with varied pore sizes (TPA-COF-1, 2, 3 and TPT-4, 5, 6). Tris(4-aminophenyl)amine (TPA) was the amine part in the first three COFs and,4,6-tris(4-aminophenyl)triazine was the common amine part in other three COFs. TPA brought sp^3 nitrogen into the frameworks, whereas TPT provided triazine core into the networks. The sp^3 core would introduce flexibility and effect the planarity in the 2D COF structure (Figure 1.17). All the COFs contained hexagonal porous structure and they were quite thermally stable (~350°C). The N_2 77K isotherm analysis showed a significant correlation of the planarity to the BET surface area. The most planar COF containing two symmetrical monomers exhibited the highest surface area (TPT-COF-5, 1747 m^2/g) whereas the TPA-COF-2 had only 478 m^2/g surface area. Thus, the symmetry and the planarity play an important role in the surface area of

the COFs. Lowering the symmetry as well as planarity leads to a reduction of the surface area. The NLDFT model yielded the pore sizes of the COFs, 1.93, 1.80, and 2.01 nm for TPA-COF-1, 2, 3 and 2.13, 2.50 and 2.55 nm for TPT-4, 5, 6, respectively (Figure 1.17). In TPA series, the TPA-COF-3 had the highest CO_2 uptake of 63.94 and 91.15 mg/g at 298 and 273K all at 1 bar (Figure 1.17). The TPA-COF-1 ad TPA-COF-2 (45.8 mg/g and 37.5 mg/g for TPA-COF-2 and TPA-COF-1 at 298K, 1 bar) had lower uptake than the third one and this was directly related to the nitrogen functionalities present in the unit cell/monomers. As the steric hindrance

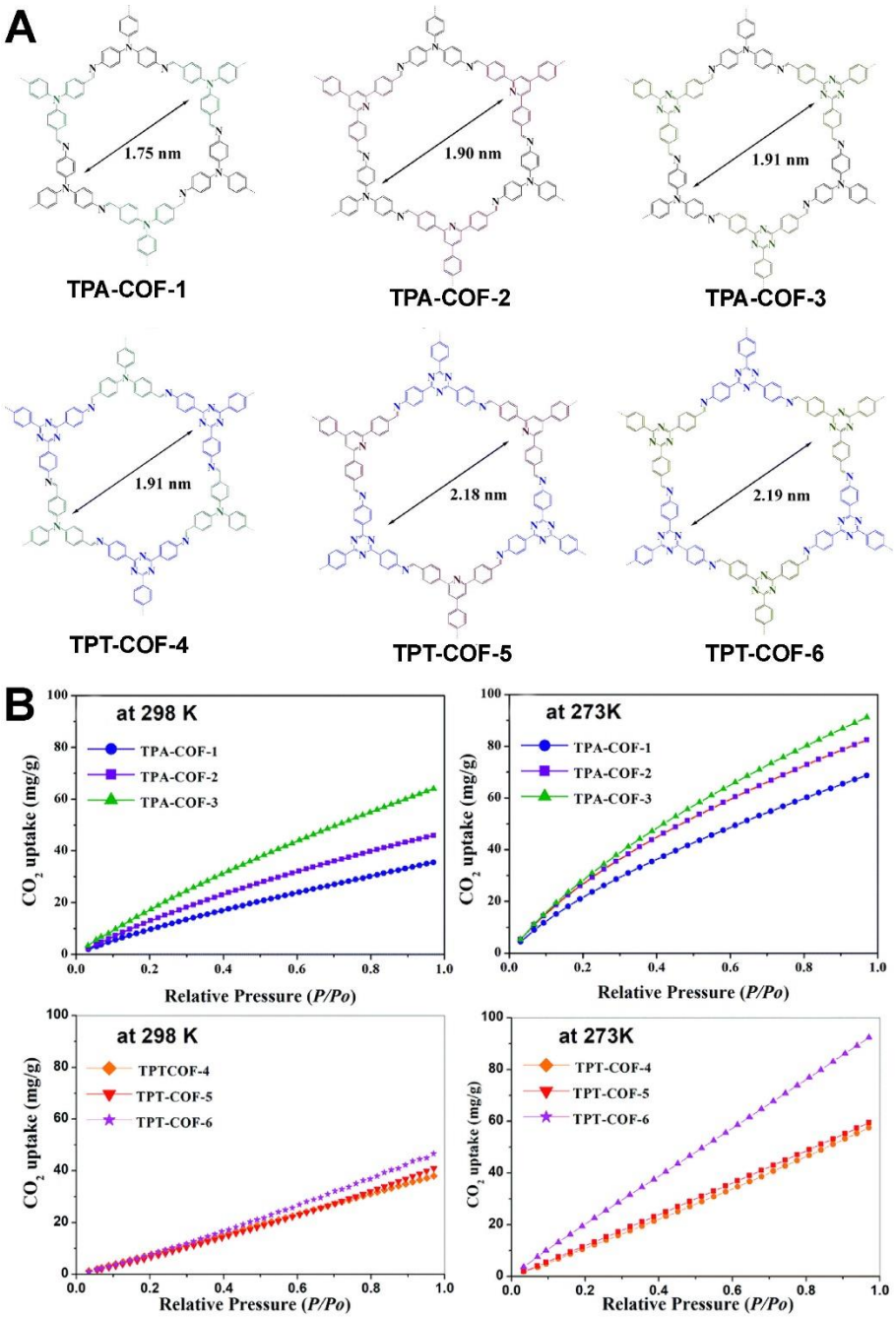

Figure 1.17. (A) Representation of six COFs prepared by the combination of the different nitrogen-rich aldehydes and amines. (C) CO_2 adsorption isotherm of the COFs at 298K and 273K. *(Adopted from ref. 201 from the Royal Society of Chemistry with permission).*

around the sp^3 N atom increased, the polarizing effect of the nitrogen atoms was reduced giving rise to less favourable interaction with CO_2 molecules (e. g. TPA-COF-1 is prepared by two sp^3 N containing monomers).[201] Similar trend had been observed in the case of TPT series, where TPT-COF-6 exhibited the highest CO_2 uptake and TPT-COF-4 had the lowest capacity in the series (65, 41, 37 mg/g for COF-6, 5 and 4 respectively) (Figure 1.17). Further, the isosteric heat of adsorption values of the COFs was significant in terms of CO_2 capture. The values were as follows: TPA-COF-1, TPA-COF-2, and TPA-COF-3 had Q_{st} values of 15.92, 25.88, and 28.11 kJ/mol and TPT-COF-4, TPT-COF-5 and TPT-COF-6 possessed 9.70, 16.97, and30.59 kJ/mol. This trend of HOA was corroborated to the higher nitrogen contents in the COF by the incorporation of more triazine units thus it improved the quadrupolar interaction with CO_2 enhancing the CO_2 capacity.[201] Few 2D COFs have been modified via post-synthesis approach to gain enhanced CO_2 capture properties. [202] [203,204] CO_2 capture in COF has been modulated also by varying the solvent of choice.[205]

1.5.4. Nitrogen-rich COF for selective CO_2 capture and conversion:

A nitrogen-rich triazine-based benz-bis(imidazole)-bridged COF (TBICOF) was reported by Mandal and co-workers which is a good candidate for selective CO_2 capture and benzene/cyclohexane separation. The COF has been prepared by the polycondensation of tri(4-formylphenoxy) cyanurate (TFPC) and 1,2,4,5-tetramino-benzene (TAB) under solvothermal condition. Imidazole is a basic catalyst to promote the ring-closing reaction during the COF formation (Figure 1.18). Wide-angle X-ray pattern (WAX) and maps showed the crystalline nature of the COF. The COF had significant thermal and chemical stability (examined by soaking the COF at 3N HCl and 3N NaOH). The COF had a surface area of 1702 m^2/g obtained from N_2 at 77K isotherm and the average pore diameter was 2.5 Å. CO_2 sorption studies were performed at four different temperatures and the COF showed 24 and 39 cc/g CO_2 uptakes at 313K and 298K at 1 bar (Figure 1.18). Interestingly, there was significant CO_2 uptake at low pressure, which was attributed to the dipole-quadrupolar interaction between the CO_2 molecules and the heteroatoms of the framework. On the other hand, CH_4 and N_2 uptakes at 313/298K were very low. The heat of adsorption values for CO_2, CH_4 and N_2 were 42.8, 21.3, and 16.2 kJ/mol, respectively at zero loadings, indicating the favourable interaction of CO_2

with the framework. IAST was applied to calculate the selectivity of the binary mixture of gas at different compositions and the COF had significant CO_2/N_2 ($15CO_2/85N_2$: 44.03 at 313K, 1 atm) and CO_2/CH_4 ($50CO_2/50CH_4$: 5.96 at 313K at 1 atm) (Figure 1.18). Thus, it is evidenced from the above experiments that the COF is highly selective toward CO_2 capture. To demonstrate the superior CO_2 capacity, Grand Canonical Monte Carlo approach was adopted which yielded the binding energies of CO_2, CH_4 and N_2 to be -35.6, -8 and -8.7 kJ/mol. DFT calculation revealed that there was an interaction of CO_2 with the phenyl ring of the central imidazole and the phenyl ring attached to the triazine moiety along with the CO_2-CO_2

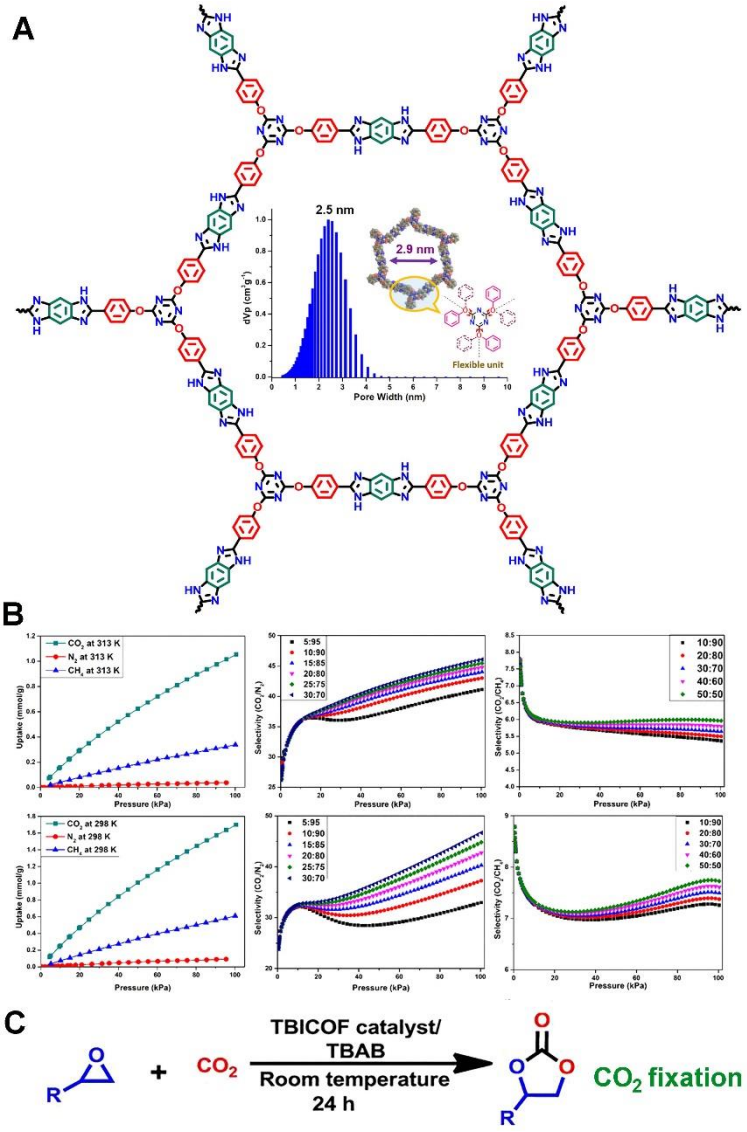

Figure 1.18. (A) Chemical structure of the COF. Inset is the pore size distribution obtained from the N_2 isotherm at 77K. (B) CO_2/N_2 and CO_2/CH_4 selectivity at different temperature and compositions. (C) Schematic representation of the CO_2 fixation reaction with an epoxide. *(Adopted from ref. 206 from the American Chemical Society with permission).*

cooperative interaction. These simulations corroborated the observed ISAT selectivity and high isosteric heat of adsorption for CO_2. Further, chemical fixation of CO_2 was performed using an epoxide which formed cyclic carbonates with CO_2. The reaction was performed at ambient temperature with a 0.5 mol% catalyst loading with a CO_2 balloon (Figure 1.18). The reaction attended high yields, substrate scope, high turnover number (TON) and recyclability of the catalyst. The COF was a selective sorbent of benzene (Bz) over cyclohexane (Cy). It adsorbed 642 and 186 cc/g Bz and Cy respectively at 298K and 1 bar. Benzene adsorption selectivity was >44 (IAST) which had been attributed to the interaction of π-electro rich benzene to the electron-deficient triazine and bis-imidazole rings. Thus, this work presents an interesting example of COF which is able to separate CO_2 as well as benzene from their congeners selectively.[206]

1.5.5. COF as an active catalyst for C-C coupling reactions:

Imine-bonded COFs are able to bind to the catalytically active metal ions. In this work, Pd^{2+} has been anchored in an imine-bonded COF.[207] The COF (COF-LZU1) was prepared using 1,3,5-Triformylbenzene and p-phenylene diamine in solvothermal condition (Figure 1.19). The appearance of -C=N stretching vibration at 1618 cm^{-1} confirmed the imine bond formation. The COF was highly crystalline in nature evidenced from PXRD pattern. Pd^{2+} was loaded in the COF by dispersing the COF at $Pd(OAc)_2$ solution (Figure 1.19). The PXRD of Pd/COF-LZU1 and the pristine COF were identical indicating the structural integrity upon loading of Pd^{2+}. The appearance of new peaks at solid-state ^{13}C NMR spectra at 176 and 23 ppm was due to the carbonyl group and the methyl group of acetate. The high resolution TEM image, EDX showed a homogeneous distribution of Pd in the matrix. The proof of the bonding between the imine group and the Pd^{2+} was further confirmed by XPS analysis. The Pd $3d_{5/2}$ appeared at 337.7 eV which was shifted from $Pd(OAc)_2$ sample (Pd $3d_{5/2}$ at 338.4 eV) (Figure 1.19). Further, a model compound of Pd was prepared with 1,10-phenanthroline (Pd/Phen) which had Pd $3d_{5/2}$ at 337.8 eV.[207] This observation confirmed the formation of Pd-N bond in the framework. The BET surface areas and the pore volume were 410 and 146 m^2/g & 0.54 and 0.19 cc/g for the COF-LZU1 and Pd/COF-LZU1 respectively. COF-LZU1 had a pore size of 12 Å which was retained on Pd loading, only the pore volume was decreased. This catalyst was used to perform heterogeneous Suzuki–Miyaura cross-coupling reaction. 0.5 mol% Pd/COF-LZU1 catalysed the reaction of substituted aryl iodides (electron-withdrawing/electron-donating groups) with phenylboronic acid at 150°C for 2.5 to 4 hours with excellent yields (90-

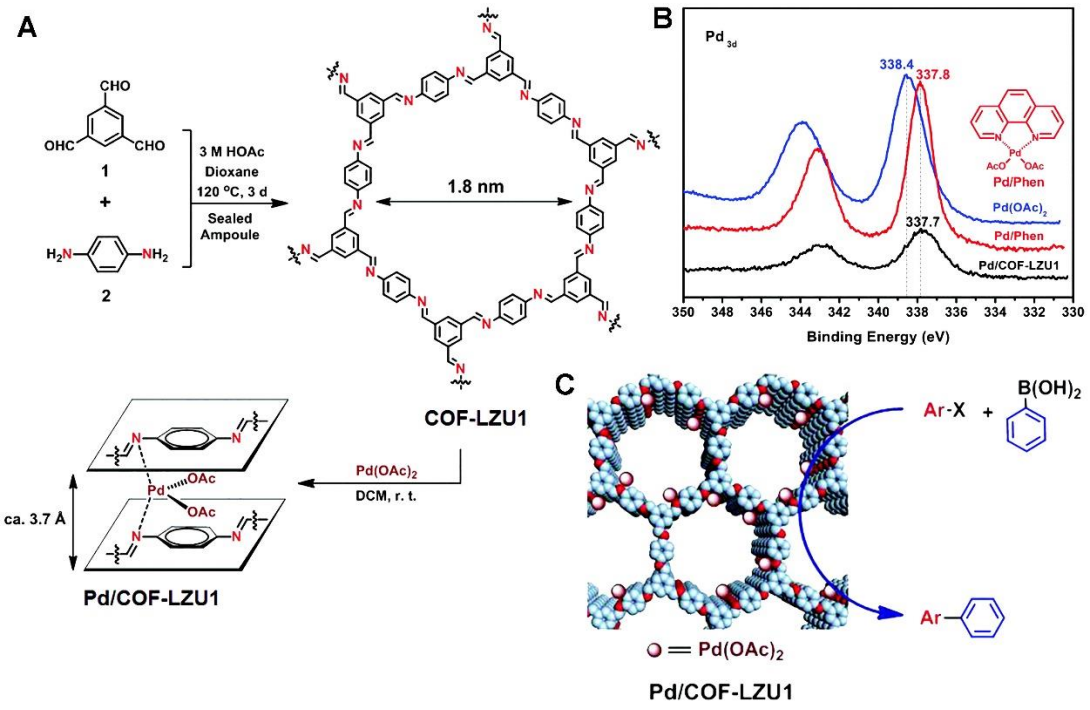

Figure 1.19. (A) Schematic representation of COF/catalyst preparation. (B) The Pd 3d XPS spectrum showing the interaction between the nitrogen and Pd^{2+}. (C) Pd/COF-LZU1 as a heterogeneous catalyst for Suzuki–Miyaura cross-coupling reaction *(Adopted from ref. 207 from the American Chemical Society with permission).*

96%) (Figure 1.19). The reaction times were longer when the catalyst loadings were low (for 0.1 mol% catalyst reaction time is 5 hours). The leaching test had been carried out to demonstrate that $Pd(OAc)_2$ was strongly coordinated to the imine bond. The catalytic reaction was performed in p-xylene and sodium carbonate and when the supernatant solution was analysed by ICP at 50% of the reaction, no trace of Pd was found confirming that the Pd species were well-anchored. Further, the recyclability of the catalyst over five consecutive cycles was carried out and the integrity of the post-catalyst sample was confirmed from several analytical characterizations .[207]

1.5.6. Pd@COF for Suzuki-Miyaura coupling:

This example presents a facile route to perform heterogeneous Suzuki–Miyaura cross-coupling reaction by a composite catalyst made of Pd nanoparticles incorporated on a COF. Two COFs had been prepared by the Imine bond formation between 1,3,5-tris-(4'-aminophenyl)-triazine (TAT, amine), triformyl phloroglucinol (TFP) and 2,5-dihydroxybenzene-1,4-dicarboxaldehyde (DHBD) (TAT-TFP and TAT-DHBD) (Figure 1.20). TAT-TFP exhibited -C=O and C=C vibrations due to the existence of keto form. A similar observation was obtained

in case of solid-state ^{13}C NMR spectra where chemical shift at 183 ppm was due to the keto group in TAT-TFP. The COFs were thermally and chemically stable. The PXRD was indexed and refined with Pawley methods. Both COFs were stabilized via interlayer π-π interactions. However, the COFs were energetically stable in slipped arrangements which could likely be due to improved packing. N_2 at 77K isotherm yielded the BET surface areas for the COFs as 750 and 464 m^2/g for TAT-DHBD and TAT-TFP, respectively.[208] TAT-TFP had a pore size of 11.7 Å, whereas, TAT-DHBD had a distribution of pore sizes as evidenced from NLDFT method. Both the COFs were quite functionalized and had a high surface area. The COFs were

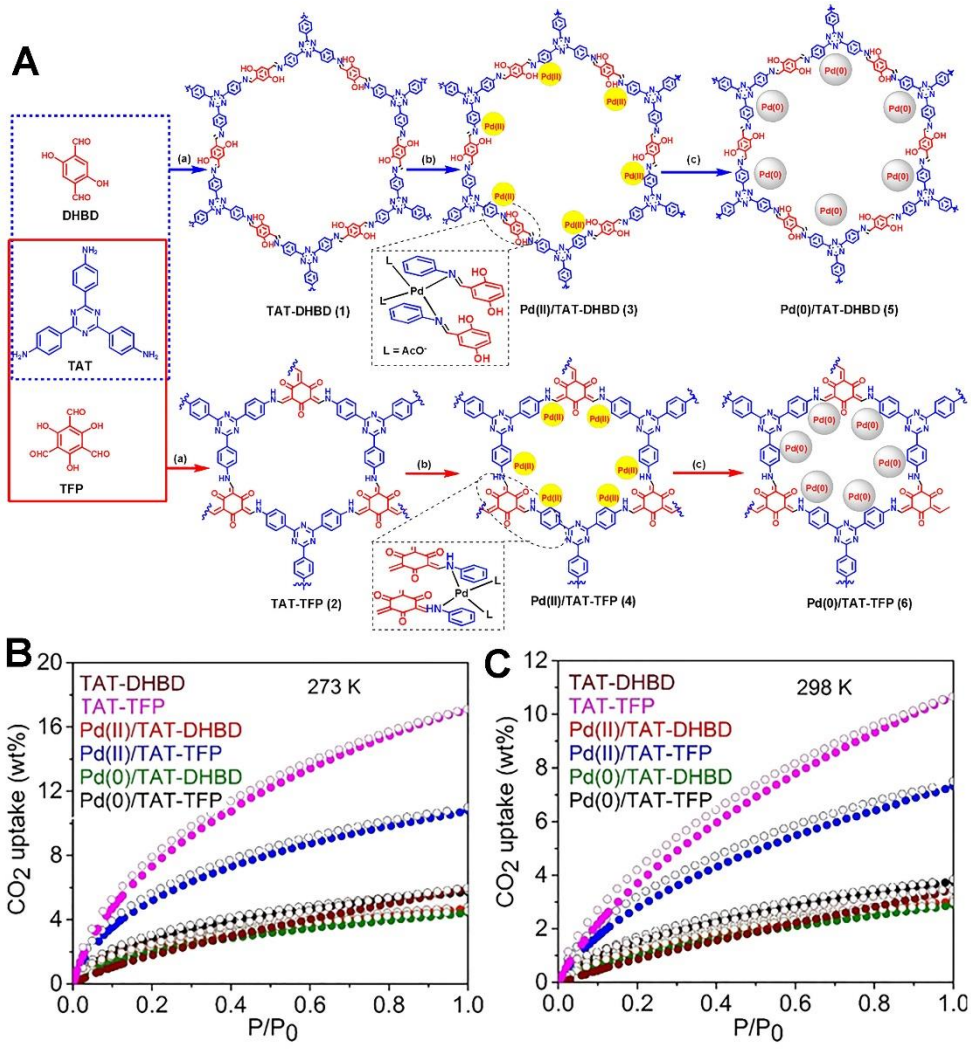

Figure 1.20. (A) Details of the COF synthesis and Pd np loading. (B, C) CO_2 adsorption isotherms of the COF and composites. *(Adopted from ref. 208 from the Wiley Online Library with permission).*

then used for supporting Pd nanoparticles. $Pd(OAc)_2$ was loaded in the COFs and subsequently reduced by $NaBH_4$ in methanolic solution which reduced Pd^{2+} to Pd(0) (Figure 1.20). The peaks at 40° and 47.5°C in PXRD appeared due to the incorporation of Pd nps in the COFs. The

particle size distribution was found to be <5 nm from field emission TEM. The oxidation state had been confirmed from XPS study, Pd $3d_{5/2}$ appears at 335.5 and 335.8 eV, whereas Pd $3d_{3/2}$ appeared at 340.7and 341.1eV, respectively, which corresponds to their metallic state. The shift in the binding energy of the -C=N indicated the interaction of Pd nps with the nitrogens present in the frameworks. This held the Pd nps strongly and prevented leaching of the metal. The composites were tested as catalysts in the Suzuki–Miyaura cross-coupling. The reaction condition was optimized with Phenylboronic acid, bromobenzene in dimethyl formamide at 100℃ for 24 hours. The reaction yielded more than 80% cross-coupled product. Effect of the substitution was also studied and it was found that the reaction was facile for electron-withdrawing groups such as -CN, with ~100% conversion. The activity of the catalyst was retained after multiple cycles. The CO_2 uptake of the COFs and the composites were moderate. The TAT-TFP COF had the highest CO_2 uptake of 10.66 wt% at 298K t 1 bar, but the capacity reduced with Pd doping in the COF. The Heat of adsorption values were ranged between 27 to 38 kJ/mol which is optimal for the regeneration of CO_2 (Figure 1.20).[208]

1.5.7. Ultrafine metal nanoparticles on COF for nitrophenol reduction:

The ability of the COF to grow small-sized nanoparticles has been demonstrated in this work. The COF is decorated with thioether groups in the pore to demonstrate the effect of crystallinity and the optimal interaction sites for the nanoparticle growth. Triformyl phloroglucinol and thioether containing di amine were used to prepare the COF. The COF existed in β-keto-enamine form under ambient conditions and the elemental mapping showed homogeneous distribution of sulphur in the network (Figure 1.21).[209] The hexagonal layered structure of the COF adopted a AAA… stacking. Even in this eclipsed configuration, the COF possessed a significantly low BET surface area (50 m^2/g) as the pore was filled with the alkyl groups from the thioether moieties. Pt and Pd nanoparticles were grown in the COF and the nps had favourable interaction. K_2PtCl_4 was impregnated in the COF and then reduced with $NaBH_4$. High resolution TEM images exhibited ultra-small nanoparticle distribution in the COF matrix. Pt nanoparticles had an average size of 1.7 nm which was remarkably small and depicted the ability of COFs to host active small nps (Figure 1.21). The High-Angle Annular Dark-Field Scanning Transmission Electron Microscopy (HAADF-STEM) image of the PtNPs@COF revealed that the Pt nps were well dispersed in the COF and no signature of agglomeration or unsupported nps were observed (Figure 1.21). The lattice fringes were indexed to 0.23 nm corresponding to the active facets of the fcc Pt lattice. Pt $4f_{7/2}$ and $4f_{5/2}$ appeared at 71.3 and

74.8 eV respectively which indicated the presence of Pt(0).[209] However, evidence of Pt(II) was also observed, which was due to the surface oxidation of the nps. The Pt/S ratio was quite low in XPS (1.38) compared to the ratio obtained in EDX (5.13). This proves that the Pt nanoparticles are residing within the pore of the COF. A series of control studies using thioether containing porous polymers and other COFs confirmed the role of thioether groups and the crystallinity in encapsulating ultra-small-sized nanoparticles. The PtNPs@COF composite had a high catalytic activity which was evidenced by the reduction of 4-nitrophenol in the presence of $NaBH_4$. 50 mg/ml catalyst was able to fully reduce the nitrophenol in less than 8 mins,

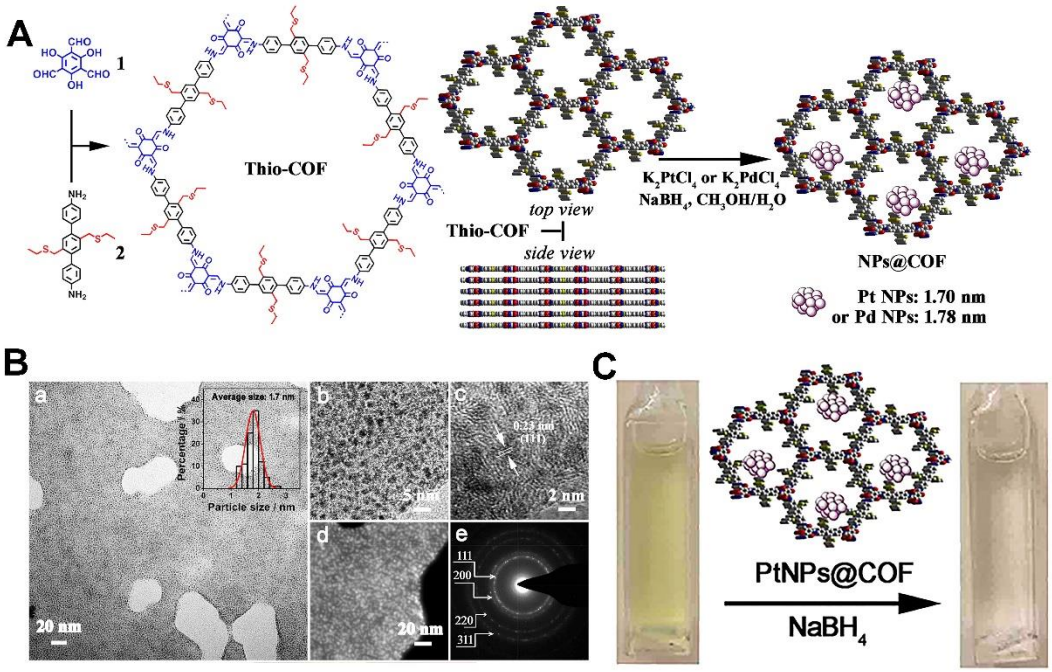

Figure 1.21. (A) Schematic representation of COF preparation and nanoparticle encapsulation. (B) TEM images showing homogeneous dispersion of Pt nanoparticles with an average diameter of 1.7 nm. (C) Visible representation of the catalytic conversion of p-nitrophenol by the catalyst. *(Adopted from ref. 209 from the American Chemical Society with permission).*

whereas unsupported Pt nps performed the same reaction in 50mins (Figure 1.21). The catalyst had excellent recyclability and reusability for the catalytic reaction. Further, to generalize the idea, Pd nanoparticles were chosen to grow within the COF network. Similar synthetic strategy (growth of Pt nps) was adopted to grow the Pd nps on COF and HRTEM analysis yielded an average particle size distribution of 1.78 nm. Lattice fringes of 0.23 nm appeared due to the exposed facets of fcc Pd. The XPS revealed the oxidation state of Pd to be zero, however, due to the surface oxidation evidence of Pd-O species was also observed. This catalyst was highly active towards Suzuki−Miyaura cross-coupling reaction where 0.1 mol% of PdNPs@COF was used in DMF/H_2O mix solvents at 50°C. The reaction proceeded with an elevated rate

compared to the unsupported nanoparticles and with an excellent yield >99%. Thus, the pore architecture supports the growth of ultra-fine metal nanoparticles which are extremely active. The well-defined pores of the COF provide constructive interaction sites with the nps and favourable mass transfer.[209] Similar nitrophenol reduction has been achieved from a COF-derived catalyst made by embedding Au nanoparticles into the COF via an in-situ growth procedure.; Au nanoparticles were suspended in the COF's synthesis medium.[210]

1.5.8. $Co/Co(OH)_2$ np supported on exceptionally stable methoxy-functionalized COF for tandem hydrogen generation and nitrile to amine reduction:

In this example, it has been shown that a highly stable COF is able to host $Co/Co(OH)_2$ nanoparticles which are active for catalytic reduction of nitro/nitrile compounds to the corresponding amines. IISERP-COF5 was prepared by the conventional Schiff base formation during the solvothermal reaction of a triazine triamine and 2,5-dimethoxy terephthaldehyde (Figure 1.22). The COF displayed a BET surface area of 1036 m^2/g and pore size of ~36Å (Figure 1.22). A noticeable feature in the COF construction was the utilization of the methoxy groups. They increased the stability of the imine bonds through their electron-donating effect.[211] Such stabilized imine bonds made the COF stable in various solvents like DMF, DMSO, benzene, even at 3M HCl, 3M NaOH and boiling water. Cobalt nanoparticles were grown on the COF using a double-solvent method employing $NaBH_4$ as the reducing agent. HRTEM analysis of the Co@COF revealed the homogeneous dispersion of the nPs in the COF, which had an average dia. of 3-5 nm. From the HRTEM, the d-spacing of the nanoparticles was calculated to be 0.21 nm, which corresponds to Co metal. However, in the XPS, Co $2p_{3/2}$ peak appears at 781.1 eV, which suggests $Co(OH)_2$. The phase of the nps was determined by magnetic susceptibility measurements which indicated them to be a room temperature ferromagnet. This was only possible if Co is in metallic form; $Co(OH)_2$ is not a room temperature ferromagnet. To provide an indirect evidence, the Co@COF pyrolyzed under N_2 at 800C was analyzed using PXRD. Peaks for Co metals appeared in the data, no peaks corresponding to Co_3O_4, CoO or $Co(OH)_2$ were found. This confirmed that the composite had Co metal nanoparticles with a mere hydroxylated surface. Exploiting the composites high aqueous stability, hydrogen generation from aqueous/methanolic $NaBH_4$ was studied employing it as the catalyst. The evolved hydrogen was measured with a gas displacement cell and the catalyst showed a better rate and lower activation energy for the H_2 generation (48 kJ/mol) compared to other reported catalysts.[211] Importantly, in a tandem reaction, the evolved

hydrogen was utilized for the reduction of nitro and nitrile compounds in one-pot. The high catalytic conversion was quantified by the yield of aromatic (>95%) and aliphatic amines (>80%) with selectivity towards primary amines. The turnover frequency for the nitrile reduction is 25 to 30 h^{-1} which was quite significant for non-noble metal-based catalysts (Figure 1.22). The mechanism of the reduction involves a redox cycle which was further corroborated by the cyclic voltammetry analysis of the Co@COF composite (Co^{2+}/Co^{3+} redox activity is observed).[212]

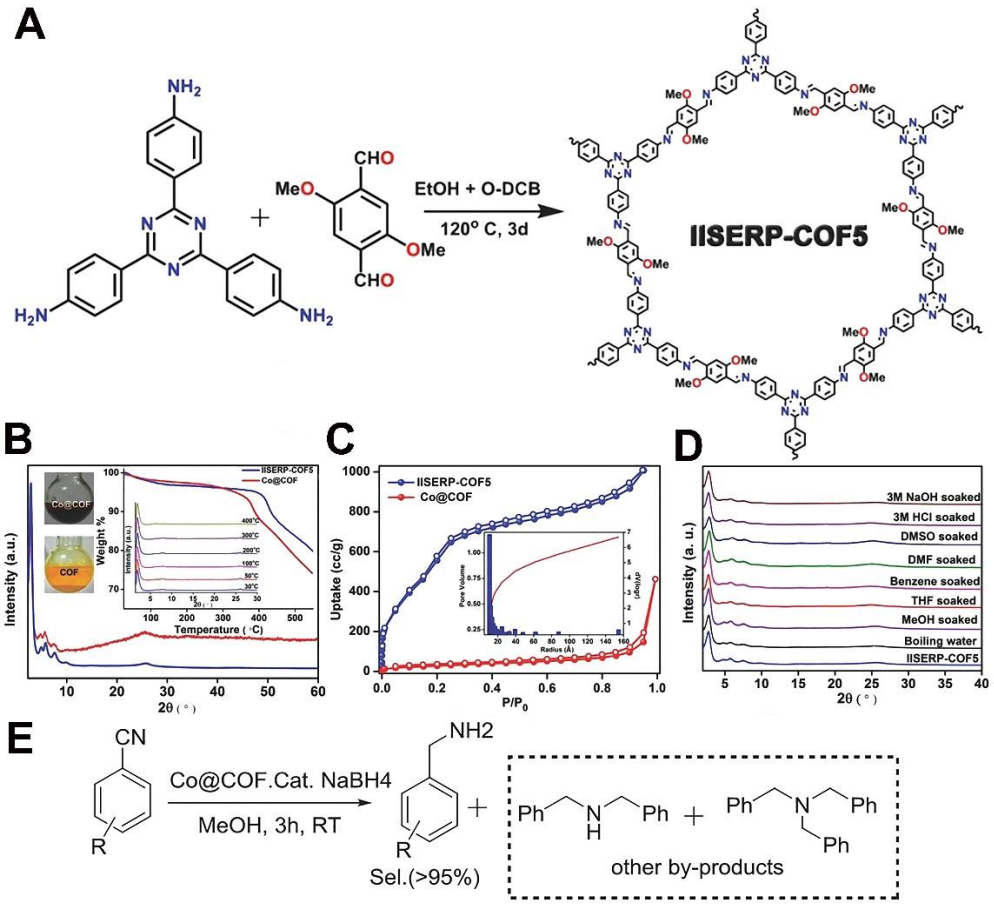

Figure 1.22. (A) Schematic representation of IISERP-COF5 preparation. (B) PXRD of the pristine COF and Co@COF. Inset shows the thermal stability of the COF from TGA and variable temperature PXRD. (C) N_2 isotherms at 77K for both the COF and composite. (D) PXRDs depicting chemical stability of the COF when exposed to different harsh chemicals. (E) Schematic of nitrile reduction by Co@COF. *(Adopted from ref. 212 from the Wiley Online Library with permission).*

These selected examples, presented above, strongly convey the potential of COF to act as porous support in the generation of a heterogeneous catalyst. This opens up an avenue for developing a superior heterogeneous catalyst for a variety of challenging organic transformations carried out in harsh chemical conditions.

1.6. References:

1. S. Das, P. Heasman, T. Ben, S. Qiu, *Chem. Rev.* **2016**, *117*, 1515-1563.
2. R. G. Taylor, C. G. Bezzu, M. Carta, K. J. Msayib, J. Walker, R. Short, B. M. Kariuki, N. B. McKeown, *Chem. Eur. J.* **2016**, *22*, 2466-2472.
3. Y. Jiao, F. H. Stillinger, S. Torquato, *Phys. Rev. let.* **2008**, *100*, 245504.
4. S. Krause, V.r Bon, I. Senkovska, D. M. Toebbens, D. Wallacher, R. S. Pillai, G. Maurin, S, Kaskel, *Nat. Commun*. **2018**, *9*, 1573.
5. Z. Li, X. Feng, Y. Zou, Y. Zhang, H. Xia, X. Liu, Y. Mu, *Chem. Commun.* **2014**, *50*, 13825-13828.
6. Z. Li, Y. Zhi, X. Feng, X. Ding, Y. Zou, X. Liu, Y. Mu, *Chem. Eur. J.* **2015**, *21*, 12079-12084.
7. L. Stegbauer, M. W. Hahn, A. Jentys, G. k. Savasci, C. Ochsenfeld, J. A. Lercher, B. V. Lotsch, *Chem. Mater.* **2015**, *27*, 7874-7881.
8. M. Dogru, T. Bein, *Chem. Commun*. **2014**, *50*, 5531– 5546.
9. K. Yuan, C. Liu, J. Han, G. Yu, J. Wang, H. Duan, Z. Wang, X. Jian, *RSC Adv.* **2016**, *6*, 12009-12020.
10. K. Wang, H. Huang, D. Liu, C. Wang, J. Li, C. Zhong, *Environ. Sci. Technol.* **2016**, *50*, 4869-4876.
11. T. Ben, C. Pei, D. Zhang, J. Xu, F. Deng, X. Jing, S. Qiu, *Energy Environ. Sci.* **2011**, *4*, 3991-3999.
12. S. S. Dhankhar, N. Sharma, S. Kumar, T. J. D. Kumar, C. M. Nagaraja, *Chem. Eur. J.* **2017**, *23*, 16204–16212.
13. B. Li, Y. Zhang, R. Krishna, K. Yao, Y. Han, Z. Wu, D. Ma, Z. Shi, T. Pham, B. Space, *J. Am. Chem. Soc.* **2014**, *136*, 8654-8660.
14. T. Hasell, M. Miklitz, A. Stephenson, M. A. Little, S. Y. Chong, R. Clowes, L. Chen, D. Holden, G. A. Tribello, K. E. Jelfs, *J. Am. Chem. Soc.* **2016**, *138*, 1653-1659.
15. S. S. Dhankharand, C. M. Nagaraja, *New J. Chem.* **2019**, *43*, 2163-2170.
16. M. Gupta, N. Chatterjee, D. De, R. Saha, P. K. Chattaraj, C. L. Oliver, P. K. Bharadwaj, *Inorg. Chem.* **2020**, *59*, 1810-1822.
17. Z.-A. Qiao, S.-H. Chai, K. Nelson, Z. Bi, J. Chen, S. M. Mahurin, X. Zhu, S. Dai, *Nat. commun.* **2014**, *5*, 3705.
18. Q. Song, S. Jiang, T. Hasell, M. Liu, S. Sun, A. K. Cheetham, E. Sivaniah, A. I. Cooper, *Adv. Mater.* **2016**, *28*, 2629-2637.
19. Q. Fang, S. Gu, J. Zheng, Z. Zhuang, S. Qiu, Y. Yan, *Angew. Chem. Int. Ed.* **2014**, *53*, 2878-2882.
20. H. Xu, J. Gao, D. Jiang, *Nat. chem.* **2015**, *7*, 905.
21. M´. Gimenez-Marques, A. Santiago-Portillo, S. Navalon, M.´Alvaro, V. Briois, F. Nouar, H. Garcia, C. Serre, *J. Mater. Chem. A* **2019**, *7*, 20285–20292.
22. K. Iwase, T. Yoshioka, S. Nakanishi, K. Hashimoto, K. Kamiya, *Angew. Chem. Int. Ed.* **2015**, *54*, 11068-11072.
23. P. Thomas, C. Pei, B. Roy, S. Ghosh, S. Das, A. Banerjee, T. Ben, S. Qiu, S. Roy, *J. Mater. Chem. A* **2015**, *3*, 1431-1441.
24. Q. Wang, K. Domen, *Chem. Rev*. **2020**, *120*, 919-985.
25. H. Furukawa, O. M. Yaghi, *J. Am. Chem. Soc.* **2009**, *131*, 8875–8883.
26. Y. Zhi, Z. Yao, W. Jiang, H. Xia, Z. Shi, Y. Mu, X. Liu, *ACS Appl. Mater. Interfaces* **2019**, *11*, 37578-37585.
27. Z. Xie, C. Wang, K. E. deKrafft, W. Lin, *J. Am. Chem. Soc.* **2011**, *133*, 2056-2059.
28. J.-X. Jiang, Y. Li, X. Wu, J. Xiao, D. J. Adams, A. I. Cooper, *Macromolecules* **2013**, *46*, 8779-8783.
29. L. Pan, M.-Y. Xu, L.-J. Feng, Q. Chen, Y.-J. He, B.-H. Han, *Polym. Chem.* **2016**, *7*, 2299-2307.
30. L. Chen, Y. Honsho, S. Seki, D. Jiang, *J. Am. Chem. Soc.* **2010**, *132*, 6742-6748.
31. K. V. Rao, R. Haldar, T. K. Maji, S. J. George, *Phys. Chem. Chem. Phys.* **2016**, *18*, 156-163.
32. S. Dalapati, E. Jin, M. Addicoat, T. Heine, D. Jiang, *J. Am. Chem. Soc.* **2016**, *138*, 5797-5800.

33. Y. Hong, J. W. Lam, B. Z. Tang, *Chem. Commun.* **2009**, 4332-4353.
34. V. S. Vyas, R. Rathore, *Chem. Commun.* **2010**, *46*, 1065-1067.
35. X. Liu, Y. Xu, D. Jiang, *J. Am. Chem. Soc.* **2012**, *134*, 8738-8741.
36. S. Dalapati, S. Jin, J. Gao, Y. Xu, A. Nagai, D. Jiang, *J. Am. Chem. Soc.* **2013**, *135*, 17310-17313.
37. Z. Xiang, D. Cao, *Macromol. rapid commun.* **2012**, *33*, 1184-1190.
38. F. Xu, X. Chen, Z. Tang, D. Wu, R. Fu, D. Jiang, *Chem. Commun.* **2014**, *50*, 4788-4790.
39. Y. Kou, Y. Xu, Z. Guo, D. Jiang, *Angew. Chem. Int. Ed.* **2011**, *50*, 8753-8757.
40. J.-S. M. Lee, T.-H. Wu, B. M. Alston, M. E. Briggs, T. Hasell, C.-C. Hu, A. I. Cooper, *J. Mater. Chem. A* **2016**, *4*, 7665-7673.
41. F. Xu, H. Xu, X. Chen, D. Wu, Y. Wu, H. Liu, C. Gu, R. Fu, D. Jiang, *Angew. Chem. Int. Ed.* **2015**, *54*, 6814-6818.
42. C. R. DeBlase, K. E. Silberstein, T.-T. Truong, H. D. Abruña, W. R. Dichtel, *J. Am. Chem. Soc.* **2013**, *135*, 16821-16824.
43. C. R. Mulzer, L. Shen, R. P. Bisbey, J. R. McKone, N. Zhang, H. c. D. Abruña, W. R. Dichtel, *ACS cent. Sci.* **2016**, *2*, 667-673.
44. S. Khatua, A. K. Bar, J. A. Sheikh, A. Clearfield, S. Konar *Chem. Eur. J.* **2018**, *24*, 872-880.
45. B. Guo, T. Ben, Z. Bi, G. M. Veith, X.-G. Sun, S. Qiu, S. Dai, *Chem. Commun.* **2013**, *49*, 4905-4907.
46. Y. Li, S. Roy, T. Ben, S. Xu, S. Qiu, *Phys. Chem. Chem. Phys.* **2014**, *16*, 12909-12917.
47. H. Xu, S. Tao, D. Jiang, *Nat. mater.* **2016**, *15*, 722.
48. H. Ma, B. Liu, B. Li, L. Zhang, Y.-G. Li, H.-Q. Tan, H.-Y. Zang, G. Zhu, *J. Am. Chem. Soc.* **2016**, *138*, 5897-5903.
49. Q. Fang, J. Wang, S. Gu, R. B. Kaspar, Z. Zhuang, J. Zheng, H. Guo, S. Qiu, Y. Yan, *J. Am. Chem. Soc.* **2015**, *137*, 8352-8355.
50. E. Derouane, J. C. Vedrine, R. R. Pinto, P. Borges, L. Costa, M. Lemos, F. Lemos, F. R. Ribeiro, *Catal. Rev.* **2013**, *55*, 454-515.
51. L.-E. Sandoval-Díaz, J.-A. González-Amaya, C.-A. Trujillo, *Microporous and Mesoporous Mater.* **2015**, *215*, 229-243.
52. A. Tuel, S. Moussa-Khouzami, Y. B. Taarit, C. Naccache, *J. mol. catal.* **1991**, *68*, 45-52.
53. G. Wu, Y. Wang, L. Wang, W. Feng, H. Shi, Y. Lin, T. Zhang, X. Jin, S. Wang, X. Wu, *Chem. Eng. J.* **2013**, *215*, 306-314.
54. H. Y. Luo, J. D. Lewis, Y. Román-Leshkov, *Annu. Rev. Chem. Biomol. Eng.* **2016**, *7*, 663-692.
55. R. Bai, Q. Sun, N. Wang, Y. Zou, G. Guo, S. Iborra, A. Corma, J. Yu, *Chem. Mater.* **2016**, *28*, 6455-6458.
56. H. Guo, G. Zhu, I. J. Hewitt, S. L. Qiu, *J. Am. Chem. Soc*. **2009**, *131*, 1646.
57. S. Lv, K. Zhang, L. Zhu, D. Tang, R. N., D. Knopp, *Anal. Chem*. **2019**, *91*, 12055-12062.
58. A. Nuhnen, M. Klopotowski, H. B. T. Jeazet, S. Sorribas, B. Zornoza, C. Téllez, J. Coronas C. Janiak, *Dalton Trans.* **2020**, DOI: 10.1039/C9DT03222C.
59. S. Nandi, S. Collins, D. Chakraborty, D. Banerjee, P. K. Thallapally, T. K. Woo, R. Vaidhyanathan, *J. Am. Chem. Soc.* **2017**, *139*, 1734-1737.
60. A. Samanta, A. Zhao, G. K. H. Shimizu, P. Sarkar, R. Gupta *Ind. Eng. Chem. Res*. **2012**, *51*, 1438−1463.
61. S. Nandi, R. Maity, D. Chakraborty, H. Ballav, R. Vaidhyanathan, *Inorg. Chem*. **2018**, *57*, 5267−5272.
62. J.-R. Li, R. J. Kuppler, H.-C. Zhou, *Chem. Soc. Rev*. **2009**, *38*, 1477-1504.
63. S. Mollick, S. Mukherjee, D. Kim, Z. Qiao, A. V. Desai, R. Saha, Y. D. More, J. Jiang, M. S. Lah, S. K. Ghosh, *Angew. Chem. Int. Ed.* **2019**, *58*, 1041-1045.
64. S. Nandi, D. Chakraborty, R. Vaidhyanathan, *Chem. Commun*. **2016**, *52*, 7249-7252.
65. A. Karmakar, R. Illathvalappil, B. Anothumakkool, A. Sen, P. Samanta, A. V. Desai, S. Kurungot, S. K. Ghosh, *Angew. Chem. Int. Ed.* **2016**, *55*, 10667-10671.

66. R.-B. Lin, Y. He, P. Li, H. Wang, W. Zhou, B. Chen, *Chem. Soc. Rev.* **2019**, *48*, 1362-1389.
67. S. Amirjalayer, R. Q. Snurr, R. Schmid, *J. Phys. Chem. C* **2012**, *116*, 4921-4929.
68. S. S. Han, H. Furukawa, O. M. Yaghi, W. A. Goddard Iii, *J. Am. Chem. Soc.* **2008**, *130*, 11580-11581.
69. C. J. Doonan, D. J. Tranchemontagne, T. G. Glover, J. R. Hunt, O. M. Yaghi, *Nat. chem.* **2010**, *2*, 235.
70. A. Nagai, Z. Guo, X. Feng, S. Jin, X. Chen, X. Ding, D. Jiang, *Nat. commun.* **2011**, *2*, 536.
71. Z. Chang, D.-S. Zhang, Q. Chen, X.-H. Bu, *Phys. Chem. Chem. Phys.* **2013**, *15*, 5430-5442.
72. W. Wang, M. Zhou, D. Yuan, *J. Mater. Chem. A* **2017**, *5*, 1334-1347.
73. Q. Xu, K. C. Kharas, B. J. Croley, A. K. Datye, *ChemCatChem* **2011**, *3*, 1004-1014.
74. X. Wang, S.-m. Lu, J. Li, Y. Liu, C. Li, *Catal. Sci. Technol.* **2015**, *5*, 2585-2589.
75. J.-L. Wang, C. Wang, K. E. deKrafft, W. Lin, *ACS Catal.* **2012**, *2*, 417-424.
76. Q. Sun, Z. Lv, Y. Du, Q. Wu, L. Wang, L. Zhu, X. Meng, W. Chen, F. S. Xiao, *Chem. Asian J.* **2013**, *8*, 2822-2827.
77. W.-J. Yoo, S. Kobayashi, *Green Chem.* **2014**, *16*, 2438-2442.
78. M. Jiang, L. Yan, Y. Ding, Q. Sun, J. Liu, H. Zhu, R. Lin, F. Xiao, Z. Jiang, J. Liu, *J. Mol.r Catal. A: Chem.* **2015**, *404*, 211-217.
79. T. Iwai, T. Harada, H. Shimada, K. Asano, M. Sawamura, *ACS Catal.* **2017**, *7*, 1681-1692.
80. L. Tan, B. Tan, *Chem. Soc. Rev.* **2017**, *46*, 3322-3356.
81. S. Kramer, N. R. Bennedsen, S. Kegnæs, *ACS Catal.* **2018**, *8*, 6961-6982.
82. Q. Zhao, A. Whittaker, X. Zhao, *Materials* **2018**, *11*, 2567.
83. L. Bai, Q. Gao, Y. Zhao, *J. Mater. Chem. A* **2016**, *4*, 14106-14110.
84. S. Haldar, K. Roy, S. Nandi, D. Chakraborty, D. Puthusseri, Y. Gawli, S. Ogale, R. Vaidhyanathan, *Adv. Energy Mater.* **2018**, *8*, 1702170.
85. S. Haldar, R. Kushwaha, R. Maity, R. Vaidhyanathan, *ACS Materials Lett.* **2019**, *1*, 490-497.
86. P. Bhanja, S. K. Das, K. Bhunia, D. Pradhan, T. Hayashi, Y. Hijikata, S. Irle, A. Bhaumik, *ACS Sustainable Chem. Eng.* **2017**, *6*, 202-209.
87. S. Dutta, A. Bhaumik, K. C.-W. Wu, *Energy Environ.l Sci.* **2014**, *7*, 3574-3592.
88. Y. Zhi, K. Li, H. Xia, M. Xue, Y. Mu, X. Liu, *J. Mater. Chem. A* **2017**, *5*, 8697-8704.
89. R. S. Sprick, J.-X. Jiang, B. Bonillo, S. Ren, T. Ratvijitvech, P. Guiglion, M. A. Zwijnenburg, D. J. Adams, A. I. Cooper, *J. Am. Chem. Soc.* **2015**, *137*, 3265-3270.
90. N. Kang, J. H. Park, K. C. Ko, J. Chun, E. Kim, H. W. Shin, S. M. Lee, H. J. Kim, T. K. Ahn, J. Y. Lee, *Angew. Chem. Int. Ed.* **2013**, *52*, 6228-6232.
91. V. S. Vyas, F. Haase, L. Stegbauer, G. Savasci, F. Podjaski, C. Ochsenfeld, B. V. Lotsch, *Nat. commun.* **2015**, *6*, 8508.
92. M. Liras, M. Iglesias, F. l. Sánchez, *Macromolecules* **2016**, *49*, 1666-1673.
93. X. Ding, B. H. Han, *Angew. Chem. Int. Ed.* **2015**, *54*, 6536-6539.
94. X. Chen, M. Addicoat, E. Jin, L. Zhai, H. Xu, N. Huang, Z. Guo, L. Liu, S. Irle, D. Jiang, *J. Am. Chem. Soc.* **2015**, *137*, 3241-3247.
95. W. Huang, B. C. Ma, D. Wang, Z. J. Wang, R. Li, L. Wang, K. Landfester, K. A. Zhang, *J. Mater. Chem. A* **2017**, *5*, 3792-3797.
96. C. Wu, Y. Liu, H. Liu, C. Duan, Q. Pan, J. Zhu, F. Hu, X. Ma, T. Jiu, Z. Li *J. Am. Chem. Soc.* **2018**, *140*, 10016-10024.
97. S. T. Meek, J. A. Greathouse, M. D. Allendorf, *Adv. Mater.* **2011**, *23*, 249-267.
98. S. R. Batten, N. R. Champness, X.-M. Chen, J. Garcia-Martinez, S. Kitagawa, L. Öhrström, M. O'Keeffe, M. P. Suh, J. Reedijk, *CrystEngComm* **2012**, *14*, 3001-3004.
99. D. Tanaka, S. Kitagawa, *Chem. Mater.* **2007**, *20*, 922-931.
100. H. Li, M. Eddaoudi, M. O'Keeffe, O. M. Yaghi, *Nature* **1999**, *402*, 276.

101. M. P. Suh, H. J. Park, T. K. Prasad, D.-W. Lim, *Chem. Rev*. **2012**, *112*, 782-835.
102. A. R. Millward, O. M. Yaghi, *J. Am. Chem. Soc.* **2005**, *127*, 17998-17999.
103. J.-R. Li, J. Sculley, H.-C. Zhou, *Chem. Rev*. **2012**, *112*, 869-932.
104. Y. He, W. Zhou, G. Qian, B. Chen, *Chem. Soc. Rev.* **2014**, *43*, 5657-5678.
105. M. M. Sena, C. P. Morrow, R. J. J. Kirkpatrick, M. Krishnan, *Chem. Mater*. **2015**, *27*, 6946-6959.
106. S. Roy, A. Chakraborty, T. K. Maji, *Coord. Chem. Rev.* **2014**, *273*, 139-164.
107. R. Haldar, K. Prasad, P. K. Samanta, S. Pati, T. K. Maji, *Cryst. Growth Des.* **2015**, *16*, 82-91.
108. B. Li, M. Chrzanowski, Y. Zhang, S. Ma, *Coord. Chem. Rev.* **2016**, *307*, 106-129.
109. A. Pal, S. Chand, D. Madden, D. Franz, L. Ritter, A. Johnson, B. Space, T. Curtin, M. C. Das, *Inorg. Chem*. **2019**, *58*, 11553-11560.
110. A. Dey, S. K. Mandal, K. Biradha, *CrystEngComm* **2013**, *15*, 9769-9778.
111. J. Liu, P. K. Thallapally, B. P. McGrail, D. R. Brown, J. Liu, *Chem. Soc. Rev.* **2012**, *41*, 2308-2322.
112. Z. R. Herm, B. M. Wiers, J. A. Mason, J. M. van Baten, M. R. Hudson, P. Zajdel, C. M. Brown, N. Masciocchi, R. Krishna, J. R. Long, *Science* **2013**, *340*, 960-964.
113. B. P. Biswal, A. Bhaskar, R. Banerjee, U. K. Kharul, *Nanoscale* **2015**, *7*, 7291-7298.
114. P. K. Thallapally, J. Tian, M. Radha Kishan, C. A. Fernandez, S. J. Dalgarno, P. B. McGrail, J. E. Warren, J. L. Atwood, *J. Am. Chem. Soc.* **2008**, *130*, 16842-16843.
115. M. Jiang, B. Li, X. Cui, Q. Yang, Z. Bao, Y. Yang, H. Wu, W. Zhou, B. Chen, H. Xing, *ACS Appl. Mater. Interfaces* **2018**, *10*, 16628-16635.
116. J. Liu, L. Chen, H. Cui, J. Zhang, L. Zhang, C.-Y. Su, *Chem. Soc. Rev.* **2014**, *43*, 6011-6061.
117. A. Corma, H. García, F. Llabrés i Xamena, *Chem. Rev.* **2010**, *110*, 4606-4655.
118. M. Yoon, R. Srirambalaji, K. Kim, *Chem. Rev.* **2011**, *112*, 1196-1231.
119. U. Mueller, M. Schubert, F. Teich, H. Puetter, K. Schierle-Arndt, J. Pastre, *J. Mater. Chem.* **2006**, *16*, 626-636.
120. P. Asha, D. Kuznetsov, S. Mandal, *Inorg. Chem*. **2019**, *58*, 1377-1381.
121. Y. Cui, Y. Yue, G. Qian, B. Chen, *Chem. Rev.* **2011**, *112*, 1126-1162.
122. T. Kundu, S. Mitra, D. Díaz Díaz, R. Banerjee, *ChemPlusChem* **2016**, *81*, 728-732.
123. K. Banerjee, K. Biradha, *New J. Chem.* **2016**, *40*, 1997-2006.
124. S. S. Nagarkar, B. Joarder, A. K. Chaudhari, S. Mukherjee, S. K. Ghosh, *Angew. Chem. Int. Ed.* **2013**, *52*, 2881-2885B.
125. Chen, L. Wang, Y. Xiao, F. R. Fronczek, M. Xue, Y. Cui, G. Qian, *Angew. Chem. Int. Ed.* **2009**, *48*, 500-503.
126. S. S. Nagarkar, S. M. Unni, A. Sharma, S. Kurungot, S. K. Ghosh, *Angew. Chem. Int. Ed.* **2014**, *53*, 2638-2642.
127. S. Saha, E. M. Schön, C. Cativiela, D. Diaz Diaz, R. Banerjee, *Chem. Eur. J.* **2013**, *19*, 9562-9568.
128. N. Sikdar, D. Dutta, R. Haldar, T. Ray, A. Hazra, A. J. Bhattacharyya, T. K. Maji, *J. Phys. Chem. C* **2016**, *120*, 13622-13629.
129. R. K. Tripathy, A. K. Samantara, J. N Behera, *Dalton Trans*. **2019**, *48*, 10557.
130. M. Shao, Q. Chang, J.-P. Dodelet, R. Chenitz, *Chem. Rev.* **2016**, *116*, 3594-3657.
131. A. Mahmood, W. Guo, H. Tabassum, R. Zou, *Adv. Energy Mater*. **2016**, *6*, 1600423.
132. K. Huang, J.-Y. Zhang, F. Liu, S. Dai, *ACS Catal*. **2018**, *8*, 9079−9102.
133. S. Xu, Y. Luo, B. Tan, *Macromol. rapid commun.***2013**, *34*, 471-484.
134. T. A. Makal, J.-R. Li, W. Lu, H.-C. Zhou, *Chem. Soc. Rev*. **2012**, *41*, 7761-7779.
135. J. Germain, J. M. Fréchet, F. Svec, *J. Mater. Chem.* **2007**, *17*, 4989-4997.
136. S. Kandambeth, K. Dey, R. Banerjee, *J. Am. Chem. Soc*. **2018**, *141*, 1807-1822.
137. K. Konavarapu, K. Biradha, *Cryst. Growth Des.* **2018**, *19*, 362-368.
138. S.-Y. Ding, W. Wang, *Chem. Soc. Rev.* **2013**, *42*, 548-568.

139. D. Mullangi, S. Nandi, S. Shalini, S. Sreedhala, C. P. Vinod, R. Vaidhyanathan, *Sci. rep.* **2015**, *5*, 10876.
140. D. Mullangi, V. Dhavale, S. Shalini, S. Nandi, S. Collins, T. Woo, S. Kurungot, R. Vaidhyanathan, *Adv. Energy Mater.* **2016**, *6*, 1600110.
141. S. Haldar, D. Chakraborty, B. Roy, G. Banappanavar, K. Rinku, D. Mullangi, P. Hazra, D. Kabra, R. Vaidhyanathan, *J. Am. Chem. Soc.* **2018**, *140*, 13367-13374.
142. K. C. Ranjeesh, R. Illathvalappil, S. D. Veer, J. Peter, V. C. Wakchaure, Goudappagouda, K. V. Raj, S. Kurungot, S. S. Babu, *J. Am. Chem. Soc.* **2019**, *141*, 14950-14954.
143. S. Yao, X. Yang, M. Yu, Y. Zhang, J.-X. Jiang, *J. Mater. Chem. A* **2014**, *2*, 8054-8059.
144. S. Mane, Z.-Y. Gao, Y.-X. Li, D.-M. Xue, X.-Q. Liu, L.-B. Sun, *J. Mater. Chem. A* **2017**, *5*, 23310-23318.
145. S. K. Kundu, A. Bhaumik, *ACS Sustainable Chem. Eng.* **2016**, *4*, 3697-3703.
146. J. Sun, T. Jarvi, L. Conopask, S. Satyapal, M. J. Rood, M. Rostam-Abadi, *Energy Fuels* **2001**, *15*, 1241-1246.
147. C. D. Wood, B. Tan, A. Trewin, F. Su, M. J. Rosseinsky, D. Bradshaw, Y. Sun, L. Zhou, A. I. Cooper, *Adv. Mater.* **2008**, *20*, 1916-1921.
148. A. Zecchina, S. Bordiga, J. G. Vitillo, G. Ricchiardi, C. Lamberti, G. Spoto, M. Bjørgen, K. P. Lillerud, *J. Am. Chem. Soc.* **2005**, *127*, 6361-6366.
149. B. Panella, M. Hirscher, S. Roth, *Carbon* **2005**, *43*, 2209-2214.
150. N. L. Rosi, J. Eckert, M. Eddaoudi, D. T. Vodak, J. Kim, M. O'Keeffe, O. M. Yaghi, *Science* **2003**, *300*, 1127-1129.
151. J. L. Rowsell, O. M. Yaghi, *Angew. Chem. Int. Ed.* **2005**, *44*, 4670-4679.
152. X. Zhao, B. Xiao, A. J. Fletcher, K. M. Thomas, D. Bradshaw, M. J. Rosseinsky, *Science* **2004**, *306*, 1012-1015.
153. M. Nijkamp, J. Raaymakers, A. Van Dillen, K. De Jong, *Appl. Phys. A* **2001**, *72*, 619-623.
154. J. L. Rowsell, O. M. Yaghi, *J. Am. Chem. Soc.* **2006**, *128*, 1304-1315.
155. J.-Y. Lee, C. D. Wood, D. Bradshaw, M. J. Rosseinsky, A. I. Cooper, *Chem. Commun.* **2006**, 2670-2672.
156. Z. Ying, Y. Dong, J. Wang, Y. Yu, Y. Zhou, Y. Sun, C. Zhang, H. Cheng, F. Zhao, *Green Chem.* **2016**, *18*, 2528-2533.
157. V. K. Das, R. R. Devi, P. K. Raul, A. J. Thakur, *Green Chem.* **2012**, *14*, 847-854.
158. G. Pettit, M. Kalnins, T. Liu, E. Thomas, K. Parent, *J. Org. Chem.* **1961**, *26*, 2563-2566.
159. R. A. Molla, P. Bhanja, K. Ghosh, S. S. Islam, A. Bhaumik, S. M. Islam, *ChemCatChem* **2017**, *9*, 1939-1946.
160. R. Banerjee, A. Phan, B. Wang, C. Knobler, H. Furukawa, M. O'Keeffe, O. M. Yaghi, *Science* **2008**, *319*, 939-943.
161. Y. S. Li, F. Y. Liang, H. Bux, A. Feldhoff, W. S. Yang, J. Caro, *Angew. Chem. Int. Ed.* **2010**, *49*, 548-551.
162. H. Bux, F. Liang, Y. Li, J. Cravillon, M. Wiebcke, J. r. Caro, *J. Am. Chem. Soc.* **2009**, *131*, 16000-16001.
163. Y. Pan, Z. Lai, *Chem. Commun.* **2011**, *47*, 10275-10277.
164. T. H. Bae, J. S. Lee, W. Qiu, W. J. Koros, C. W. Jones, S. Nair, *Angew. Chem. Int. Ed.* **2010**, *49*, 9863-9866.
165. C. Zhang, Y. Dai, J. R. Johnson, O. Karvan, W. J. Koros, *J. Membr. Sci.* **2012**, *389*, 34-42.
166. K. Zhang, R. P. Lively, M. E. Dose, A. J. Brown, C. Zhang, J. Chung, S. Nair, W. J. Koros, R. R. Chance, *Chem. Commun.* **2013**, *49*, 3245-3247.
167. U. P. Tran, K. K. Le, N. T. Phan, *ACS Catal.* **2011**, *1*, 120-127.
168. L. T. Nguyen, K. K. Le, H. X. Truong, N. T. Phan, *Catal. Sci. Technol.* **2012**, *2*, 521-528.
169. C. Chizallet, S. Lazare, D. Bazer-Bachi, F. Bonnier, V. Lecocq, E. Soyer, A.-A. Quoineaud, N. Bats, *J. Am. Chem. Soc.* **2010**, *132*, 12365-12377.

170. G. Lu, S. Li, Z. Guo, O. K. Farha, B. G. Hauser, X. Qi, Y. Wang, X. Wang, S. Han, X. Liu, *Nat. Chem.* **2012**, *4*, 310.
171. T. T. Isimjan, H. Kazemian, S. Rohani, A. K. Ray, *J. Mater. Chem.* **2010**, *20*, 10241-10245.
172. G. Lu, J. T. Hupp, *J. Am. Chem. Soc.* **2010**, *132*, 7832-7833.
173. X. Lin, G. Gao, L. Zheng, Y. Chi, G. Chen, *Anal. Chem.* **2013**, *86*, 1223-1228.
174. S. Eslava, L. Zhang, S. Esconjauregui, J. Yang, K. Vanstreels, M. R. Baklanov, E. Saiz, *Chem. Mater.* **2012**, *25*, 27-33.
175. C.-Y. Sun, C. Qin, X.-L. Wang, G.-S. Yang, K.-Z. Shao, Y.-Q. Lan, Z.-M. Su, P. Huang, C.-G. Wang, E.-B. Wang, *Dalton Trans.* **2012**, *41*, 6906-6909.
176. R. Vaidhyanathan, S. S. Iremonger, G. K. Shimizu, P. G. Boyd, S. Alavi, T. K. Woo, *Science* **2010**, *330*, 650-653.
177. P. Nugent, Y. Belmabkhout, S. D. Burd, A. J. Cairns, R. Luebke, K. Forrest, T. Pham, S. Ma, B. Space, L. Wojtas, *Nature* **2013**, *495*, 80.
178. S. Xiang, Y. He, Z. Zhang, H. Wu, W. Zhou, R. Krishna, B. Chen, *Nat. commun.* **2012**, *3*, 954.
179. P. M. Bhatt, Y. Belmabkhout, A. Cadiau, K. Adil, O. Shekhah, A. Shkurenko, L. J. Barbour, M. Eddaoudi, *J. Am. Chem. Soc.* **2016**, *138*, 9301-9307.
180. J. M. Taylor, R. Vaidhyanathan, S. S. Iremonger andG. K. H. Shimizu, *J. Am. Chem. Soc*. **2012**, *134*, 14338.
181. S. Nandi, U. Werner-Zwanzigerband, R. Vaidhyanathan, *J. Mater. Chem. A* **2015**, *3*, 21116–21122.
182. S. Nandi, J. Rother, D. Chakraborty, R. Maity, U. Werner-Zwanzigerdand, R. Vaidhyanathan, *J. Mater. Chem. A* **2017**, *5*, 8431–8439.
183. M. I. Hoffert, K. Caldeira, G. Benford, D. R. Criswell, C. Green, H. Herzog, A. K. Jain, H. S. Kheshgi, K. S. Lackner, J. S. Lewis, *science* **2002**, *298*, 981-987.
184. D. Banerjee, A. J. Cairns, J. Liu, R. K. Motkuri, S. K. Nune, C. A. Fernandez, R. Krishna, D. M. Strachan, P. K. Thallapally, *Acc. Chem. Res.* **2014**, *48*, 211-219.
185. D. Banerjee, C. M. Simon, A. M. Plonka, R. K. Motkuri, J. Liu, X. Chen, B. Smit, J. B. Parise, M. Haranczyk, P. K. Thallapally, *Nat. communications* **2016**, *7*, ncomms11831.
186. K. V. Lawler, Z. Hulvey, P. M. Forster, *Chem. Commun.* **2013**, *49*, 10959-10961.
187. H. Wang, K. Yao, Z. Zhang, J. Jagiello, Q. Gong, Y. Han, J. Li, *Chem. Sci.* **2014**, *5*, 620-624.
188. Z. Hulvey, K. V. Lawler, Z. Qiao, J. Zhou, D. Fairen-Jimenez, R. Q. Snurr, S. V. Ushakov, A. Navrotsky, C. M. Brown, P. M. Forster, *J. Phys. Chem. C* **2013**, *117*, 20116-20126.
189. X. Chen, A. M. Plonka, D. Banerjee, R. Krishna, H. T. Schaef, S. Ghose, P. K. Thallapally, J. B. Parise, *J. Am. Chem. Soc.* **2015**, *137*, 7007-7010.
190. P. K. Thallapally, J. W. Grate, R. K. Motkuri, *Chem. Commun.* **2012**, *48*, 347-349.
191. L. Chen, P. S. Reiss, S. Y. Chong, D. Holden, K. E. Jelfs, T. Hasell, M. A. Little, A. Kewley, M. E. Briggs, A. Stephenson, *Nat. mater.* **2014**, *13*, 954.
192. A. P. Cote, A. I. Benin, N. W. Ockwig, M. O'Keeffe, A. J. Matzger, O. M. Yaghi, *Science* **2005**, *310*, 1166-1170.
193. H. M. El-Kaderi, J. R. Hunt, J. L. Mendoza-Cortés, A. P. Côté, R. E. Taylor, M. O'Keeffe, O. M. Yaghi, *Science* **2007**, *316*, 268-272.
194. X. Feng, X. Ding, D. Jiang, *Chem. Soc. Rev.* **2012**, *41*, 6010-6022.
195. S. Kandambeth, A. Mallick, B. Lukose, M. V. Mane, T. Heine, R. Banerjee, *J. Am. Chem. Soc.* **2012**, *134*, 19524-19527.
196. B. P. Biswal, S. Chandra, S. Kandambeth, B. Lukose, T. Heine, R. Banerjee, *J. Am. Chem. Soc.* **2013**, *135*, 5328-5331.
197. H. Wei, S. Chai, N. Hu, Z. Yang, L. Wei, L. Wang, *Chem. Commun.* **2015**, *51*, 12178-12181.
198. C. F. Martín, E. Stöckel, R. Clowes, D. J. Adams, A. I. Cooper, J. J. Pis, F. Rubiera, C. Pevida, *J. Mater. Chem.* **2011**, *21*, 5475-5483.
199. D. Yuan, W. Lu, D. Zhao, H. C. Zhou, *Adv. Mater.* **2011**, *23*, 3723-3725.

200. M. G. Rabbani, A. K. Sekizkardes, Z. Kahveci, T. E. Reich, R. Ding, H. M. El-Kaderi, *Chem. Eur. J.* **2013**, *19*, 3324-3328.
201. A. F. El-Mahdy, C.-H. Kuo, A. Alshehri, C. Young, Y. Yamauchi, J. Kim, S.-W. Kuo, *J. Mater. Chem. A* **2018**, *6*, 19532-19541.
202. S. Haldar, K. Roy, R. Kushwaha, S. Ogale, R. Vaidhyanathan, *Adv. Energy Mater.* **2019**, *9*, 1902428.
203. N. Huang, X. Chen, R. Krishna, D. Jiang, *Angew. Chem. Int. Ed.* **2015**, *54*, 2986-2990.
204. N. Huang, R. Krishna, D. Jiang, *J. Am. Chem. Soc.* **2015**, *137*, 7079-7082.
205. Q. Gao, X. Li, G.-H. Ning, H.-S. Xu, C. Liu, B. Tian, W. Tang, K. P. Loh, *Chem. Mater.* **2018**, *30*, 1762-1768.
206. P. Das, S. K. Mandal, *Chem. Mater.* **2019**, *31*, 1584-1596.
207. S.-Y. Ding, J. Gao, Q. Wang, Y. Zhang, W.-G. Song, C.-Y. Su, W. Wang, *J. Am. Chem. Soc.* **2011**, *133*, 19816-19822.
208. D. Kaleeswaran, R. Antony, A. Sharma, A. Malani, R. Murugavel, *ChemPlusChem* **2017**, *82*, 1253-1265.
209. S. Lu, Y. Hu, S. Wan, R. McCaffrey, Y. Jin, H. Gu, W. Zhang, *J. Am. Chem. Soc.* **2017**, *139*, 17082-17088.
210. X. Shi, Y. Yao, Y. Xu, K. Liu, G. Zhu, L. Chi, G. Lu, *ACS appl. Mater. Interfaces* **2017**, *9*, 7481-7488.
211. H. Zhang, T. Ling, X.-W. Du, *Chem. Mater.* **2015**, *27*, 352.
212. D. Mullangi, D. Chakraborty, A. Pradeep, V. Koshti, C. P. Vinod, S. Panja, S. Nair, R. Vaidhyanathan, *Small* **2018**, *14*, 1801233.

Part 1: Xe/Kr separation using Porous Frameworks.

Chapter 2

Hyper-Crosslinked Porous Organic Frameworks with Ultra-micropores for Selective Xenon Capture

2.1. Introduction:

Emerging energy demand in the developing world is resulting in the depletion of conventional fuel sources mainly fossil fuel. An alternate clean energy source is now becoming mandatory for economic development and national security. However, many radioactive wastes primarily (Xe, Kr) are being released from the power plant during the associated nuclear fission process.[1] Of this, the nonradioactive isotope of Xe is of value in various applications in the optical lighting, medical sector, space technology etc.[2-4] Therefore, selective capture of Xe from its analogous noble gas Kr and other gases found in the nuclear off-gas stream (1300 ppm Xe, 130 ppm Kr, 78% N_2, 21% O_2, 0.9% Ar, 0.03% CO_2) is imperative.[2,5]

Currently, cryogenic separation is the industrially opted process for separating Xe/Kr from Used Nuclear Fuel (UNF) which utilizes the difference in their boiling points (Xe = -108.1°C and Kr = -153.2°C). But this process is energy demanding and associated with explosion hazards. Alternatively, the off-gas stream could become a potential source of Xe. Adsorptive separation by porous solids brings additional advantages to the energy associated with the selective Xe capture. The efficiency (capacity + selectivity) of the solid sorbent could be a directing factor to the energy and economy of the adsorptive separations.[2] Solid sorbents like porous carbon,[5] zeolites,[6] metal-organic frameworks,[2] porous membranes (particularly zeolite, MOF and aluminophosphate based membranes),[6-10] and organic cages[11] are being extensively investigated for selective Xe capture. But the number of investigations on Xe separation is limited compared to other gas separations (CO_2/N_2, CO_2/CH_4, CO_2/H_2, etc.). The off-gas stream contains other harsh chemicals and humidity along with the mixture of Xe/Kr at an elevated temperature. This is an important criterion for the solid sorbents to possess high thermal and chemical stability to be able to function as a potential candidate for noble gas capture. Porous organic polymers[12,13] are one of the most important classes of materials made of covalent bonds which have been studied for different applications such as gas separation, storage.[14-18] During the last decade, diverse chemical reactions are employed to develop porous polymers such as Schiff chemistry,[19] azo-bond formation,[20,21] Bakelite chemistry,[16,17] Friedel-Crafts reactions,[22-25] click chemistry[26] and been investigated for several gas separation applications. However, to the best of our knowledge, a report on Xe/Kr separation using organic polymers is absent. If such porous polymers can be built using non-hydrolyzable covalent bonds, it is of immense value. Here, we have investigated the selective

Xe capture possibilities of C-C bonded porous polymers made using simple Friedel-Crafts reaction catalyzed by $AlCl_3$. The formation of C-C bonds in the polymers bring additional advantages of stability, durability, and reproducibility due to soft synthetic protocols.

2.2. Materials and methods:

1,3,5-tris(bromomethyl)-2,4,6-trimethyl benzene was synthesized according to previously reported procedure with slight modification.[27]

Synthesis of the IISERP-POF6:

The polymers were synthesized via Fridel-Crafts alkylation reaction. 0.75 mmol (96 mg) naphthalene and 0.5 mmol (200 mg) tribromide compound were dissolved in 40 ml of dry dichloromethane (DCM). Then 3.75 mmol $AlCl_3$ (500 mg) was added slowly. The mixture was gently heated at 40°C for 24 hours under an N_2 atmosphere. After that, the mixture was taken out, filtered, washed with DCM and then suspended in 20 ml 3M HCl to remove unreacted $AlCl_3$. The final product was purified by Soxhlet extraction using Dimethylformamide (DMF) and Tetrahydrofuran (THF) mixture to eliminate oligomeric impurities yielding a yellow-colored polymer (Yield ~80%). Observed elemental analysis; C: 82.65%, H: 13.82%.

Synthesis of the IISERP-POF7:

0.75 mmol (152 mg) pyrene and 0.5 mmol (200 mg) tribromide compound were dissolved in 40 ml of dry dichloromethane (DCM). Then 3.75 mmol $AlCl_3$ (500 mg) was added slowly. The mixture was gently heated at 40°C for 24 hours under a N_2 atmosphere. After that, the mixture was taken out, filtered, washed with DCM and then suspended in 20 ml 3M HCl to eliminate unreacted $AlCl_3$. The final product was purified by Soxhlet extraction using DMF and THF mixture to eliminate oligomeric impurities yielding a brown colored polymer (Yield ~80%). Observed elemental analysis; C: 81.34%, H: 15.75%.

Synthesis of the IISERP-POF8:

0.75 mmol (183 mg) pyrene and 0.5 mmol (200 mg) tribromide compound were dissolved in 40 ml of dry dichloromethane (DCM). Then 3.75 mmol $AlCl_3$ (500 mg) was added slowly. The mixture was gently heated at 40°C for 24 hours under an N_2 atmosphere. After that, the mixture was taken out, filtered, washed with DCM and then suspended in 20 ml 3M HCl to dissolve unreacted $AlCl_3$. The final product was purified by Soxhlet extraction using DMF

and THF mixture to eliminate impurities yielding a brown colored polymer (Yield ~80%). Observed elemental analysis; C: 86.52%, H: 12.21%.

Gram scale synthesis of IISERP-POF6:

As a representative, IISERP-POF6 had been synthesized in gram scale to demonstrate the ability to be used on an industrial scale. In a typical synthesis, 7.5 mmol (1.83 g) naphthalene and 5 mmol (2 g) tribromide compound were dissolved in 300 ml of dry dichloromethane (DCM). Then 37.5 mmol $AlCl_3$ (5 g) was added slowly. The mixture was gently heated at 40°C for 36 hours under N_2 atmosphere. After that, the mixture was taken out, filtered, washed with DCM and then suspended in 200 ml 3M HCl to dissolve unreacted $AlCl_3$. The final product was soxhletted using DMF and THF mixture to eliminate oligomeric impurities yielding a yellow-colored polymer (Yield ~75%). Observed elemental analysis; C: 79.54%, H: 16.88%.

Stability studies in harsh conditions:

To check the stability of the polymers, they were dispersed in 9M HCl, 9M NaOH, boiling water and the stability were confirmed by N_2 adsorption at 77 K and IR spectra.

2.3. Analytical characterizations:

Powder X-ray diffraction:

Powder X-Ray Diffraction data were recorded out Rigaku Miniflex-600 instrument and processed using PDXL software.

Thermo gravimetric Analysis:

Thermal analysis (thermo-gravimetric) of the polymers was carried out using NETSZCH TGA-DSC system. TGAs were performed under 20 ml/min N_2 gas flow (purge + protective) and the heating rate was maintained 5 K/min from 25°C to 550°C.

IR spectroscopy:

IR spectra were recorded using a Nicolet ID5 attenuated total reflectance IR spectrometer which operates at ambient temperature. Anhydrous KBr pellets were used to record the data.

Field Emission Scanning Electron Microscopy:

FE-SEM images were collected using Ultra Plus Field Emission Scanning Electron Microscope with integral charge compensator and embedded EsB and AsB detectors. Oxford X-max instruments 80 mm^2. (Carl Zeiss NTS, Gmbh), Imaging conditions: 2 kV, WD=2 mm, 200 kX, Inlens detector. For preparing the polymers for imaging, the samples were ground thoroughly, dispersed in methanol and were sonicated for 5 min. After that, the well-dispersed polymers in methanol were drop casted on the silicon wafer and dried in vacuum for 12 hours.

HR-Transmission Electron Microscopy (HRTEM):

Jeol JEM220FS high-resolution transmission electron microscope (HR-TEM) equipped with a field emission source operating at 200 KeV was used for collecting the TEM images. The well-dispersed sample was drop casted on a Cu grid.

2.4. Adsorption studies:

All the adsorptions were carried out using a 3-FLEX pore and surface area analyzer, Micromeritics and few cases 'Autosorb IQ', Quantachrome.

Langmuir fits:

In most cases, the isotherms were fit to the Single-Site Langmuir (SSL) equation. The isotherms were fit by solving the Langmuir equation using the solver function in Microsoft Excel following a similar protocol.[28] Utilizing this routine circumvents some of the problems associated with favoring either high- or low-pressure regions when linearizing the Langmuir equation and offers a balanced approach.

Single-Site Langmuir (SSL)

$$q_i = q_m \frac{k_i}{1 + k_i P} P$$

Dual-Site Langmuir (DSL)

$$q_i = q_{m,1} \frac{K_1}{1 + K_1 P} P + q_{m,2} \frac{K_2}{1 + K_2 P} P$$

Virial analysis:

The Xe & Kr adsorption data for the polymers were measured from 0- 1bar at 278, 288 and 298 K and were fitted by the following virial equation.

ln(P) = ln(Va)+(A0+A1*Va +A2*Va^2 …+ A6*Va^6)/T+(B0+B1*Va)

Where P is pressure, Va is amount adsorbed, T is temperature, and A0, A1, A2 …, A4 and B0, B1 are temperature independent empirical parameters.

Ideal Adsorption Solution Theory (IAST):

IAST calculations were employed as described by Prausnitz et al.[29] The equation that is involved in selectivity calculations has been given below.

$$S_{1,2} = \frac{q_1/q_2}{p_1/p_2}$$

Breakthrough studies:

For the breakthrough measurements, ~0.250 g of pre-activated (160°C under vacuum) sample of the POF was packed in a 6.35 cm long and 0.5-cm diameter column. This was further activated at 50°C under flowing helium overnight. Pressurization of the 0.25" (6.35 mm) diameter column packed with POF was accomplished with a syringe pump (Teledyne ISCO) directly connected to the system through a series of 0.07 mm (ID) segments of tubing (PEEK) and valves. System pressure was maintained by coordinated adjustments to the syringe pump flow rate and the needle metering valve (Tescom). An inline pressure transducer was used to verify column pressure. The column was cooled to room temperature and a premixed mixture of Xe and Kr was introduced with a flow rate of 20 ml/min at a total pressure of 15 psi (1.02 atm). Effluent gas chemistry was tracked with a Stanford Research residual gas analyzer (RGA). Masses (a.m.u.) corresponding to Xe (131), Kr (84) and He (4) were monitored throughout the experiments. The flow rate (20 ml/min) through the needle metering valve created a sampling pressure of 5 $\times 10^{-5}$ torr to 3.0 $\times 10^{-4}$ Torr in the RGA and was maintained throughout the experiments. Indications of Xe and Kr breaking through the column were indicated by an increase in the pressure for masses 131 and 84 respectively.

2.5. Results and discussions:

Synthesis and characterization of the polymers:

Polymers are isolated as brown powders and purified by Soxhlet extraction using different organic solvents like Methanol, THF, DMF, etc (Figure 2.1A). Rigorous EDAX analysis was performed to ensure the absence of any unreacted brominated sites in the oligomeric compounds (see appendix). Amorphous nature was established from the PXRD pattern

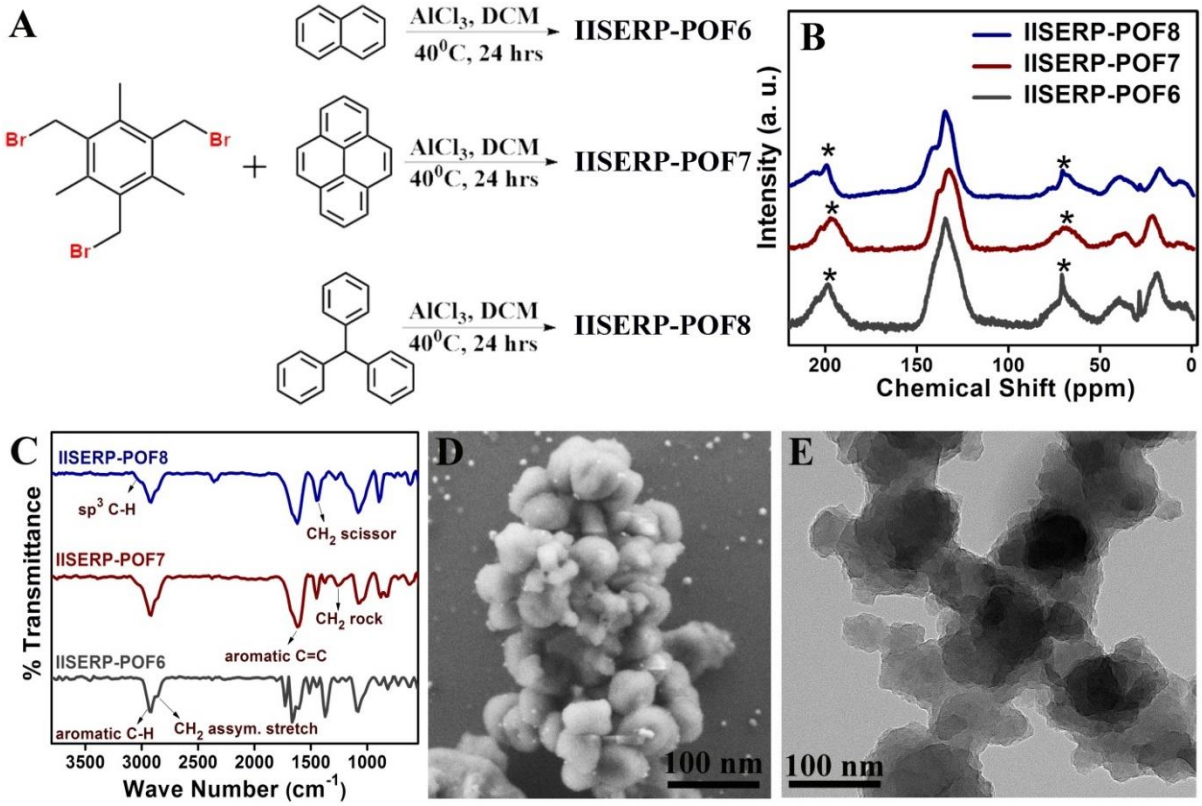

Figure 2.1. (A) Schematic of polymer synthesis. (B) Solid-state ^{13}C MASNMR spectra displaying the characteristics of chemical shifts. The * marked peaks correspond to the spinning side-bands. (C) IR spectra of the polymers featuring the bond environment. (D) FESEM images of IISERP-POF6 showing spherical morphology, with the spheres ranging from ~8 nm to a micron in diameter. (E) HRTEM image of IISERP-POF6

(Figure A.2.1A). Exceptional thermal (Figure A.2.1B), as well as chemical stability, make these polymers potential candidates for any industrial applications. Moreover, they are synthesizable in gram scales with absolute retention of the inherent properties. The cross condensation has been established by solid-state ^{13}C Magic Angle Spinning Nuclear Magnetic Resonance (MASNMR) spectroscopy (Figure 2.1B) and Infra-Red (IR) spectra (Figure 2.1C). The peak at around δ=130–135 ppm in the solid-state NMR is assigned to the aromatic carbons of the polymers. Meanwhile, the co-condensation of the building blocks has been validated by the appearance of two broad peaks at around δ=40 and δ=20 ppm which correspond to the methylene and methyl carbons. The mere shifts in the δ value of the NMR spectra of the respective three polymers appear due to the variance of aromatic rig current of the three different aromatic units (naphthalene, pyrene, and triphenylmethane). IR spectra of the respective polymers corroborate to the SSNMR showing the characteristics vibrations present in the polymeric network. The peaks at 2920 cm^{-1}, 2850 cm^{-1} signify aromatic C-H

and asymmetric CH_2 stretching vibrations. The peaks correspond to ~1440 cm^{-1}, 12050 cm^{-1} and 1620 cm^{-1} narrates the CH_2 scissoring, CH_2 rocking, and aromatic C=C bond stretching. IISERP-POF8 possesses its unique sp^3 C-H vibration at 3040 cm^{-1} (Figures 2.1C, A.2.2). The morphology of all the polymers was envisioned from the Field Emission Scanning Electron Microscopy (FESEM) (Figures 2.1D, A.2.3-A.2.6, tables A.2.1-A.2.3). A spherical morphology is observed. which is prominent in Bakelite based and phenol-formaldehyde based polymers due to their hydrophobic nature.[16,17,30] This is further supported by the High-Resolution Transmission Electron Microscopic (HRTEM) images which appear stacked spheres of polymers with a dimension of 80 to 120 nm (Figure 2.1E, A.2.7).

N_2 adsorption isotherms and stability studies:

The porosity of the polymers is investigated by N_2 adsorption at 77K where the polymers display a combination of type-I and type-IV isotherms with a prominent hysteresis (Figure 2.2A).[31] The hysteresis arises from the fact that the polymers are devoid of ordered porous architecture. Being amorphous and crosslinked, the polymers possess hierarchical pores which are responsible for the observed mesoporosity and hysteresis (Figure 2.2B). Brunauer-Emmett-Teller (BET) surface areas were estimated to be 890, 630 and 813 m^2/g for IISERP-POF6, IISERP-POF7 and IISERP-POF8 respectively (Figure A.2.8). A Non-local Density Functional Theory (NLDFT) was fitted to the N_2 adsorption isotherms at 77K and these reveal the presence of hierarchical pores with the major pore dimension of 6 Å (Figure 2.2B). Pore size distribution obtained from CO_2 273K is comparable to that from N_2 77K data (Figure A.2.9). The polymers possess a significant degree of ultra-micropores which is a potential character to render selectivity during gas capture. However, the absence of heteroatoms in the pore results in moderate CO_2 capacity and selectivity for the polymers. The exceptional chemical stability of these polymers towards acid and base was established from BET surface area analysis recorded after treating samples with 9N HCl and 9N NaOH, which showed retention of surface area or isotherm type. The polymers are obtained at a large gram scale to demonstrate the applicability to the industrial scales with absolute retention of the surface area and pore volume. We have synthesized multiple batches of the polymers in gram scale (~5 g) using the same condition (40°C for 36 hrs) and measured the porosities. The N_2 uptake of these samples at 77K matched well with the uptakes found for the samples from mg scale synthesis (Figures 2.2C, 2.2D, and A.2.10-A.2.12).

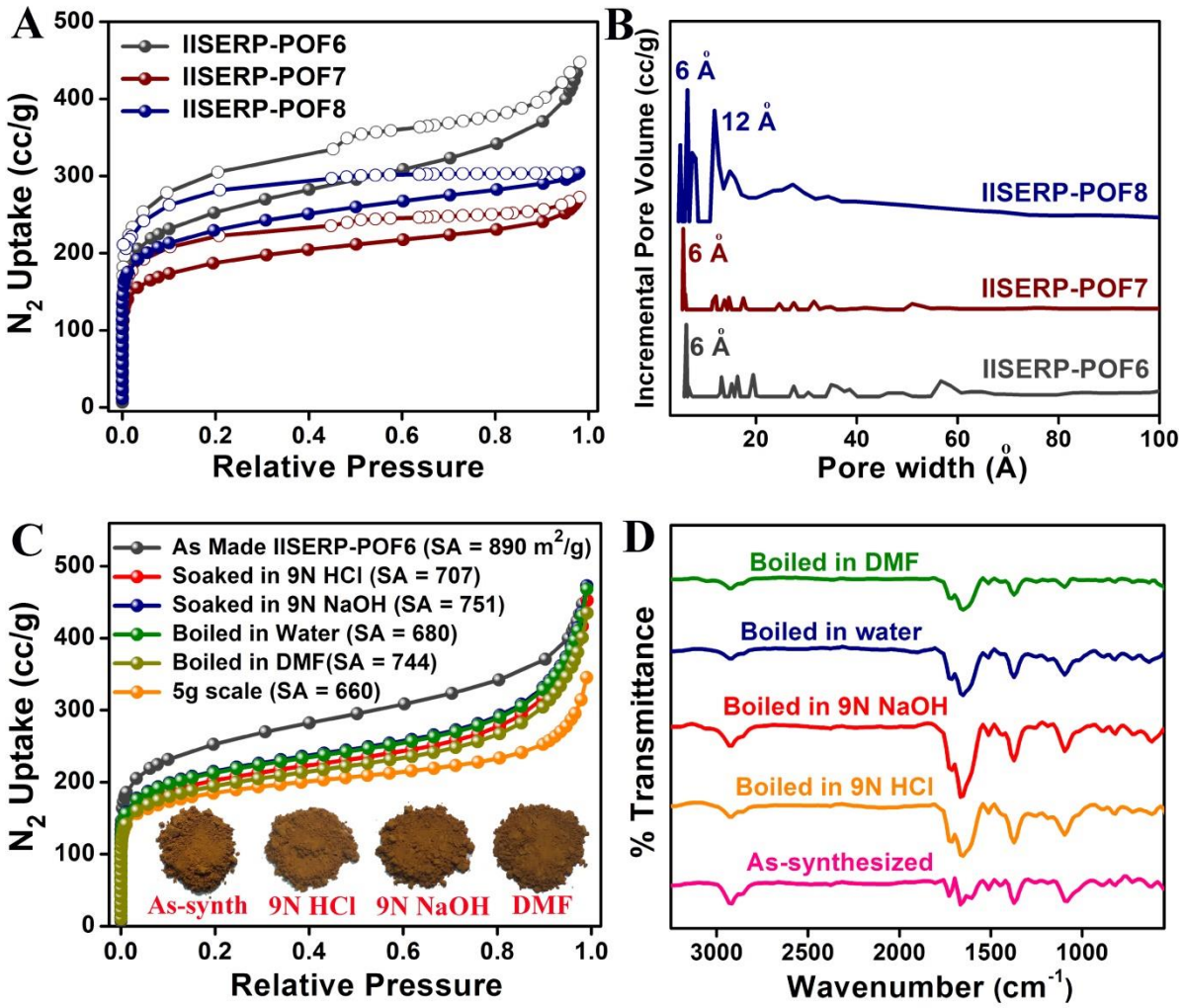

Figure 2.2. (A) N_2 adsorption isotherms for the polymers at 77K. (B) Pore size distribution obtained from NLDFT fitting. The stability of IISERP-POF6 evaluated from (C) 77K N_2 isotherms and (D) IR spectra.

Xe/Kr adsorption studies:

The Xe/Kr isotherms were collected at three different temperatures (278K, 288K, and 298K) up to 1 bar pressure. All of these polymers show selective uptake of Xe over Kr at these temperatures, but the isotherms don't saturate at 1 bar. The Xe uptakes are 37.7, 34.6 and 38.5 cc/g (P/P_0 = 1) for IISERP-POF6, IISERP-POF7 and IISERP-POF8, respectively (Figures 2.3). These uptakes are comparable with some of the well-known Xe adsorbing porous materials like IRMOF_1 (44.3 cc/g),[32] Noria (34.7),[33] SBMOF1 (31 cc/g),[34] CROFOUR_1_Ni and CROFOUR_2_Ni (40.3 cc/g and 36 cc/g) (P/P_0 = 1).[35] Although, there are MOFs, organic cages are known to have very high Xe capacity at 1 bar, 298K (Ag @ Ni_MOF74, 108 cc/g; Activated carbon, 94.1 cc/g; MOF-Cu-H , 71.5 cc/g; SBMOF2, 63.4 cc/g; CC3, 53.8 cc/g) (P/P_0 = 1)[5,11,36-38] (Table 2.1), the C-C bonded polymers bring

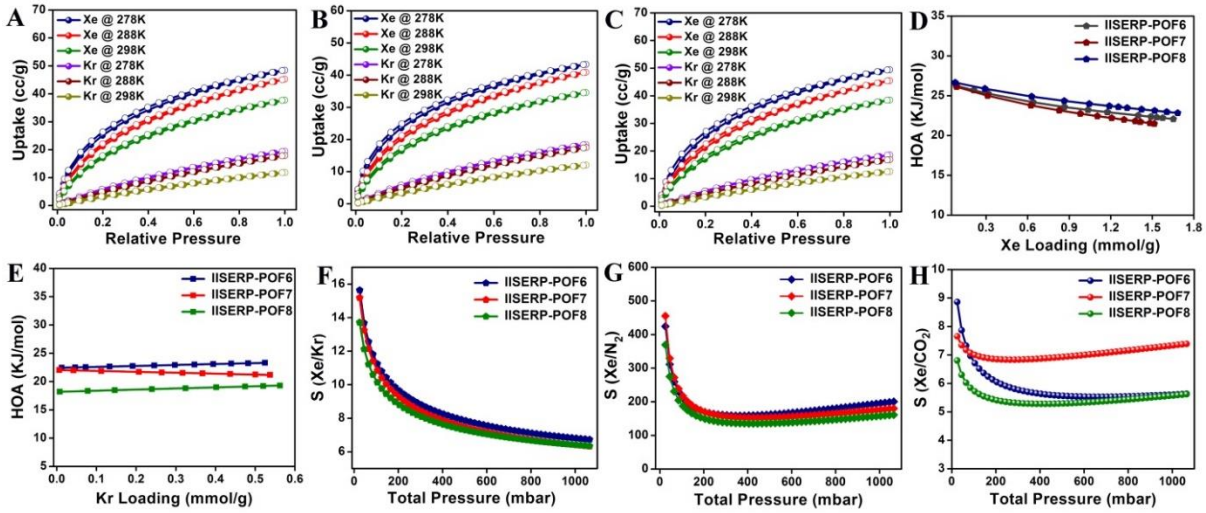

Figure 2.3. (A, B, C) Xe and Kr adsorption isotherms for IISERP-POF6, IISERP-POF7, and IISERP-POF8 at different temperatures. (D) The heat of Adsorption for Xe calculated from the Virial method. (E) The heat of Adsorption for Kr calculated from the Virial model. (F) Xe/Kr selectivity at 298 K calculated from IAST model employing a nominal composition of 20Xe:80Kr. (G) Xe/N_2 selectivity at 298 K calculated using IAST method with a nominal composition of 1Xe:99N_2. (H) Xe/CO_2 selectivity at 298 K calculated from IAST model using a nominal composition of 1Xe:99CO_2.

exceptional stability and durability when employed to work under harsh conditions as well as desired as membranes. Virial method was employed to calculate the Heat of Adsorption (HOA) of Xe and Kr isotherms collected at 278, 288 and 298 K. The zero loading HOA value for Xe was found to be 26 kJ/mol (Figure 2.3D and Figures A.3.13-A.2.15), which is slightly higher than that for Kr (~22 kJ/mol) (Figure 2.3E and A.2.16, tables A.2.4 and A.2.5). This suggests that Xe has a stronger interaction with the polymeric frameworks than Kr. This observation agrees with the Xe/Kr selectivity. Ideal Adsorption Solution Theory (IAST) was adopted to determine the Xe/Kr selectivity with a composition of 20/80 (Xe/Kr). The Xe/Kr selectivity values were 6.7, 6.3 and 6.3 for IISERP-POF6, IISERP-POF7, and IISERP-POF8, respectively at 1 bar and 298K (Figure 2.3F and A.2.17, tables A.2.6-A.2.8). These Xe/Kr selectivities are lower than only a few of the top-performing MOFs and cages[11,31-33] and is higher than the selectivities shown by Zeolites (s(Xe/Kr) = 4-6),[6] Porous Carbon (~3)[5] and is comparable to some of the well-known MOFs (Ni-MOF-74: 5-6; IRMOF-1: 3; UTSA-49: 9.2; Ag@NiMOF-74: 6.8), organic cages (12.5) (Table 2.1).[5,11,32,36,39] Importantly, it is quite substantial for a first-time report using a porous polymer, and we believe that there is significant room for improvement.

Xenon recovery from nuclear off-gas stream involves their separation from a mixture of other gases which balances the stream. Also, Xe is present at an exceptionally low concentration in

the off-gas stream compared to N_2 and CO_2 Surprisingly, these polymers display significantly high Xe selectivity over nitrogen (IAST selectivity: s(Xe/N_2): 200, 180, 160 for IISERP-POF6, 7 and 8 at 298 K, 1 bar, employing a nominal composition of 1Xe:99N_2 (Figures 2.3G and A.2.18). These values are much higher than those reported with other porous materials (Carbon-ZX: 120; Carbon-Z: 80; HKUST: 80; PCN-14: 26; ZIF-8: 18.3; IRMOF-1: 5.2)[40,41] (Tables A.2.9-A.2.11). Also, these polymers express promising Xe/CO_2 separation ability. The Xe/CO_2 selectivities obtained from IAST were found to be 5.6, 7.4 and 5.6 for IISERP-POF6, 7 and 8, respectively, for a composition of 1Xe:99CO_2 at 298K and 1 bar (Figure 2.3H). These selectivities are higher than ZIF-8 and porous carbon.[40] Notably, the energy input (based on the synthesis temperature and pressure) in the synthesis of these polymers is substantially smaller compared to benchmark porous materials like MOF and porous carbons. Xe has a higher dipole moment compared to the Kr, N_2, CO_2 which contributes to the preferential adsorption of Xe. This would promote a stronger interaction of Xe with the aromatic groups of the porous polymers, and therefore to higher Xe uptakes.

Dynamic mixed-gas separation:

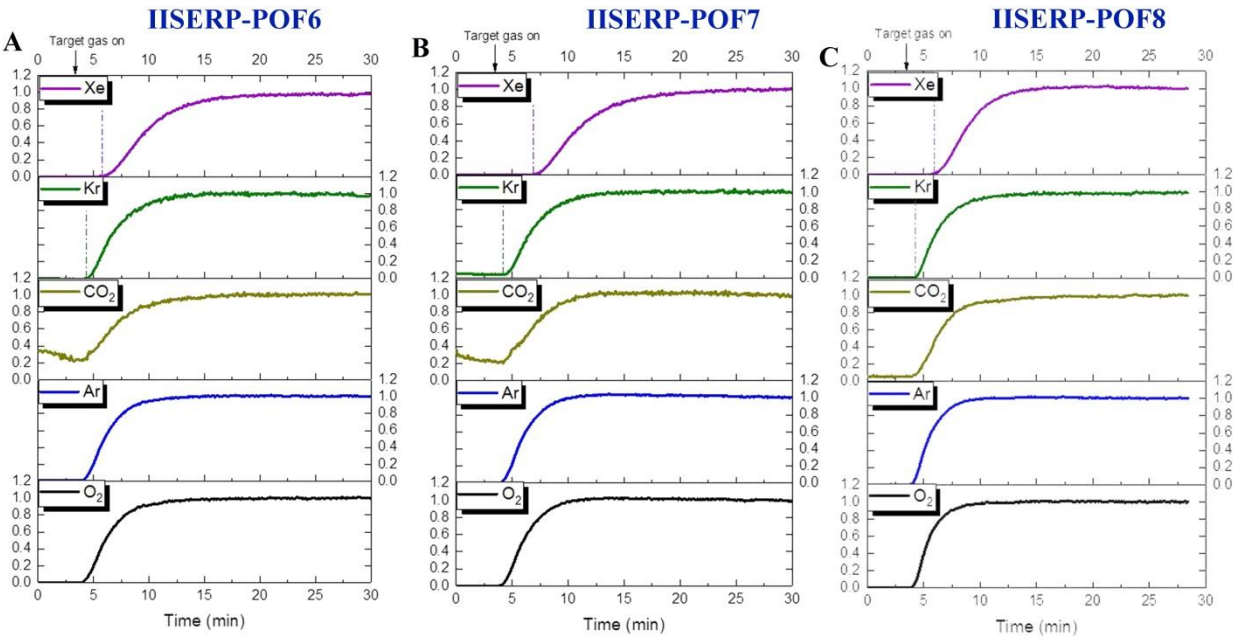

Figure 2.4. Breakthrough curves for different polymers. The polymers illustrate the dynamic separation of Xe under nuclear processing conditions.

It is important to demonstrate the ability of the polymers to perform the separation under a more realistic condition. To do so, we performed breakthrough separation for each of the polymers where a mixture of Xe/Kr (1300 ppm Xe/ 130 ppm Kr, UNF) was passed through a

column packed with the polymers (~200-300 mg) which was pre-activated. The retention time of a particular gas was monitored and it is found that Xe showed noticeably better retention compared to the other gases (Kr, CO_2, O_2, and Ar) for all the three polymers. Among all, IISERP-POF7 has the highest retention time for Xe (8.5 min) compared Kr (3.8 min) which is also reflected in the selectivity value (2.3) obtained in dynamic condition (Figure 2.4). Similar results were obtained for IISERP-POF6 and IISERP-POF8 which also exhibit selective retention of Xe with selectivities of 1.7 and 1.5 (Table 2.2). This illustrates the Xe/Kr separation performance of the polymers under the dynamic condition with significant Xe/Kr selectivities.

Table 2.1. Comparison of the Xe/Kr selectivities of the polymers with some of the high-performing porous materials.

S.No.	Material	Xe Uptake (cc/g) at 1bar and 298K (P/P_0 =1)	S(Xe/Kr) at 1 bar, 298K for (20Xe:80Kr)
1	CROFOUR-1-Ni	40.3	22[a]
2	MOF-Cu-H	71.5	16.7[a], 15.8[b]
3	SBMOF-1	31	16[b]
4	CROFOUR-2-Ni	36	15.5[a]
5	CC3	53.7	12.5[a]
6	Ag@MOF-74Ni	103	11.5[a]
7	$Co_3(HCOO)_6$	44.8	11[a]
8	SBMOF-2	63.4	10[a]
9	HKUST-1	~120	6.90[b]
10	**IISERP_POF6**	**37.7**	**6.7[a]**
11	**IISERP_POF7**	**34.6**	**6.3[a]**
12	**IISERP_POF8**	**38.5**	**6.3[a]**
13	PCN-14	~160	6.5[c]
14	NOTT series	~100-150	5.5-7[c]
15	MOF-74-Mg	125.4	6[c]
16	MOF-74-Ni	94.1	4[c]
17	IRMOF-series	-	2.8-4.2[b]
18	Activated Carbon	94	3[c]

[a]Selectivity calculated using *IAST* modeling. [b]Selectivity calculated from Henry's constant. [c]Selectivity calculated from breakthrough experiment.

Table 2.2. Summarized parameters of the Xe/Kr breakthrough experiments performed using POFs at room temperature.

Adsorbent	Gas	Time (min)	Conc. (ppm)	Xe/Kr selectivity
IISERP-POF6	Xe	7.5133	1282	1.7
IISERP-POF6	Kr	4.3083	132	
IISERP-POF7	Xe	8.5678	1282	2.3
IISERP-POF7	Kr	3.803	132	
IISERP-POF8	Xe	5.8587	1282	1.5
IISERP-POF8	Kr	3.8361	132	

2.6. Conclusion:

In summary, three new exceptionally stable C-C bonded hyper-crosslinked porous organic polymers have been developed using very mild synthesis methods. The ultra-microporous character enables good Xe/Kr, Xe/N_2 and Xe/CO_2 separation. These advantages combine with their easy scalability make them potential candidates for large-scale separation of Used Nuclear Fuel (UNF) off-gas stream; however, further work needs to be done to improve their capacity and Xe/Kr selectivity.

2.7. References:

1. B. W. Brook, A. Alonso, D. A. Meneley, J. Misak, T. Blees, J. B. van Erp, *Sustainable Mater. Technol.* **2014**, *1*, 8-16.
2. D. Banerjee, A. J. Cairns, J. Liu, R. K. Motkuri, S. K. Nune, C. A. Fernandez, R. Krishna, D. M. Strachan, P. K. Thallapally, *Acc. Chem. Res.* **2014**, *48*, 211-219.
3. T. Wu, J. Lucero, M. A. Sinnwell, P. K. Thallapally, M. A. Carreon, *Chem. Commun.* **2018**, *54*, 8976-8979.
4. S. K. Elsaidi, D. Ongari, W. Xu, M. H. Mohamed, M. Haranczyk, P. K. Thallapally, *Chem. Eur. J.* **2017**, *23*, 10758-10762.
5. J. Liu, P. K. Thallapally, D. Strachan, *Langmuir* **2012**, *28*, 11584-11589.
6. X. Feng, Z. Zong, S. K. Elsaidi, J. B. Jasinski, R. Krishna, P. K. Thallapally, M. A. Carreon, *J. Am. Chem. Soc.* **2016**, *138*, 9791-9794.
7. T. Wu, J. Lucero, M. A. Sinnwell, P. K. Thallapally, M. A. Carreon, *Chem. Commun.* **2018**, *54*, 8976-8979.
8. T. Wu, J. Lucero, J. M. Crawford, M. A. Sinnwell, P. K. Thallapally, M. A. Carreon, *J. Membr. Sci.* **2019**, *573*, 288-292.
9. T. Wu, X. Feng, S. K. Elsaidi, P. K. Thallapally, M. A. Carreon, *Ind. Eng. Chem. Res.* **2017**, *56*, 1682-1686.
10. T. Wu, J. Lucero, Z. Zong, S. K. Elsaidi, P. K. Thallapally, M. A. Carreon, *ACS Appl. Nano Mater.* **2017**, *1*, 463-470.
11. L. Chen, P. S. Reiss, S. Y. Chong, D. Holden, K. E. Jelfs, T. Hasell, M. A. Little, A. Kewley, M. E. Briggs, A. Stephenson, *Nat. Mater.* **2014**, *13*, 954.
12. L. Tan, B. Tan, *Chemical Society Reviews* **2017**, *46*, 3322-3356.
13. D. Wu, F. Xu, B. Sun, R. Fu, H. He, K. Matyjaszewski, *Chem. Rev.* **2012**, *112*, 3959-4015.
14. M. J. Bojdys, J. Jeromenok, A. Thomas, M. Antonietti, *Adv. Mater.* **2010**, *22*, 2202-2205.
15. W. Lu, D. Yuan, D. Zhao, C. I. Schilling, O. Plietzsch, T. Muller, S. Bräse, J. Guenther, J. Blümel, R. Krishna, *Chem. Mater.* **2010**, *22*, 5964-5972.
16. S. Nandi, U. Werner-Zwanziger, R. Vaidhyanathan, *J. Mater. Chem. A* **2015**, *3*, 21116-21122.
17. S. Nandi, J. Rother, D. Chakraborty, R. Maity, U. Werner-Zwanziger, R. Vaidhyanathan, *J. Mater. Chem. A* **2017**, *5*, 8431-8439.
18. K. T. Jackson, M. G. Rabbani, T. E. Reich, H. M. El-Kaderi, *Polym. Chem.* **2011**, *2*, 2775-2777.
19. Y. Jin, Y. Zhu, W. Zhang, *CrystEngComm* **2013**, *15*, 1484-1499.

20. H. A. Patel, S. H. Je, J. Park, D. P. Chen, Y. Jung, C. T. Yavuz, A. Coskun, *Nat. commun.* **2013**, *4*, 1357.
21. S. K. Gupta, D. Kaleeswaran, S. Nandi, R. Vaidhyanathan, R. Murugavel, *ACS Omega* **2017**, *2*, 3572-3582.
22. P. Puthiaraj, W.-S. Ahn, *Industrial & Engineering Chemistry Research* **2015**, *55*, 7917-7923.
23. S. Wang, C. Zhang, Y. Shu, S. Jiang, Q. Xia, L. Chen, S. Jin, I. Hussain, A. I. Cooper, B. Tan, *Sci. adv.* **2017**, *3*, e1602610.
24. A. Modak, J. Mondal, A. Bhaumik, *ChemCatChem* **2013**, *5*, 1749-1753.
25. S. K. Kundu, A. Bhaumik, *ACS Sustainable Chem. Eng.* **2015**, *3*, 1715-1723.
26. M. Albuszis, P. J. Roth, W. Pauer, H.-U. Moritz, *Polym. Chem.* **2014**, *5*, 5689-5699.
27. S. B. Maity, P. K. Bharadwaj, *Inorg. Chem.* **2013**, *52*, 1161-1163.
28. M. Saleh, H. M. Lee, K. C. Kemp, K. S. Kim, *ACS Appl. Mater. Interfaces* **2014**, *6*, 7325-7333.
29. A. L. Myers, J. M. Prausnitz, *AIChE Journal* **1965**, *11*, 121-127.
30. Y. Wang, Y. Xie, Y. Zhang, S. Tang, C. Guo, J. Wu, R. Lau, *Chemical Engineering Research and Design* **2016**, *114*, 258-267.
31. M. Thommes, K. Kaneko, A. V. Neimark, J. P. Olivier, F. Rodriguez-Reinoso, J. Rouquerol, K. S. Sing, *Pure Appl. Chem.* **2015**, *87*, 1051-1069.
32. S. T. Meek, S. L. Teich-McGoldrick, J. J. Perry, J. A. Greathouse, M. D. Allendorf, *J. Phys. Chem. C* **2012**, *116*, 19765-19772.
33. R. S. Patil, D. Banerjee, C. M. Simon, J. L. Atwood, P. K. Thallapally, *Chem. Eur. J.* **2016**, *22*, 12618-12623.
34. D. Banerjee, C. M. Simon, A. M. Plonka, R. K. Motkuri, J. Liu, X. Chen, B. Smit, J. B. Parise, M. Haranczyk, P. K. Thallapally, *Nat. commun.* **2016**, *7*, ncomms11831.
35. M. H. Mohamed, S. K. Elsaidi, T. Pham, K. A. Forrest, H. T. Schaef, A. Hogan, L. Wojtas, W. Xu, B. Space, M. J. Zaworotko, *Angew. Chem. Int. Ed.* **2016**, *55*, 8285-8289.
36. J. Liu, D. M. Strachan, P. K. Thallapally, *Chemical Communications* **2014**, *50*, 466-468.
37. S. Xiong, Y. Gong, S. Hu, X. Wu, W. Li, Y. He, B. Chen, X. Wang, *J. Mater. Chem. A* **2018**, *6*, 4752-4758.
38. X. Chen, A. M. Plonka, D. Banerjee, R. Krishna, H. T. Schaef, S. Ghose, P. K. Thallapally, J. B. Parise, *J. Am. Chem. Soc.* **2015**, *137*, 7007-7010.
39. S. Xiong, Q. Liu, Q. Wang, W. Li, Y. Tang, X. Wang, S. Hu, B. Chen, *J. Mater. Chem. A* **2015**, *3*, 10747-10752.
40. S. Zhong, Q. Wang, D. Cao, *Sci. Rep.* **2016**, *6*, 21295.
41. J. J. Perry IV, S. L. Teich-McGoldrick, S. T. Meek, J. A. Greathouse, M. Haranczyk, M. D. Allendorf, *J. Phys. Chem. C* **2014**, *118*, 11685-11698.

Chapter 2 has been adopted form the reference "Chakraborty *et al*. *ACS Appl. Mater. Interfaces* **2019**, *11*, 13279-13284." With permission from the American Chemical Society.

2.8. Appendix of Chapter 2:

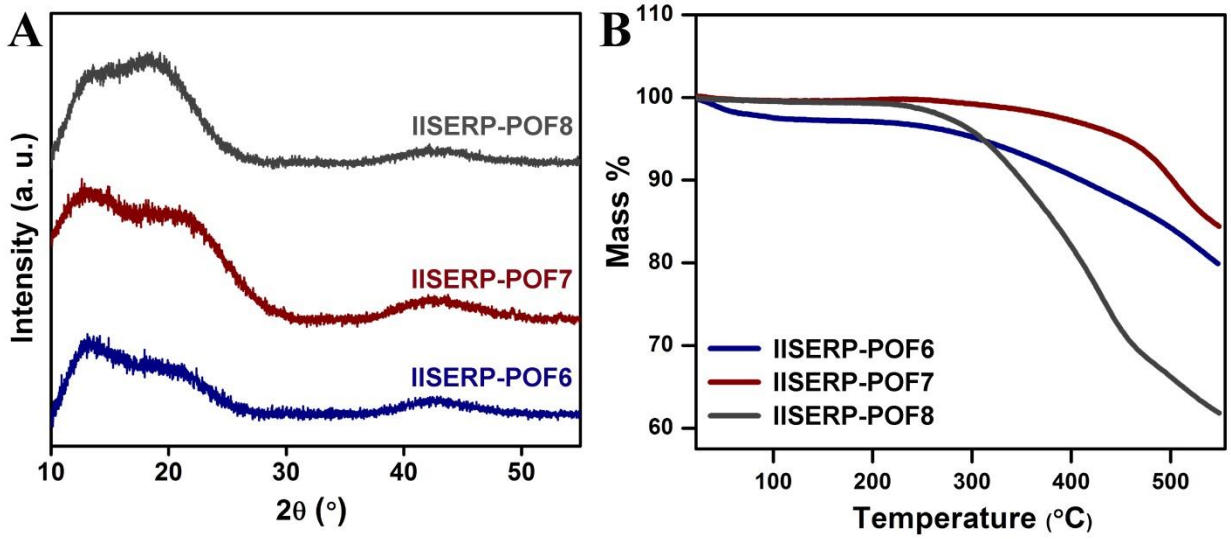

Figure A.2.1. (A) Powder X-Ray Diffraction pattern of the polymers showing amorphous nature (B) Thermo Gravimetric Analysis (TGA) curves for the corresponding polymers showing the polymers are thermally stable up to ~200°C.

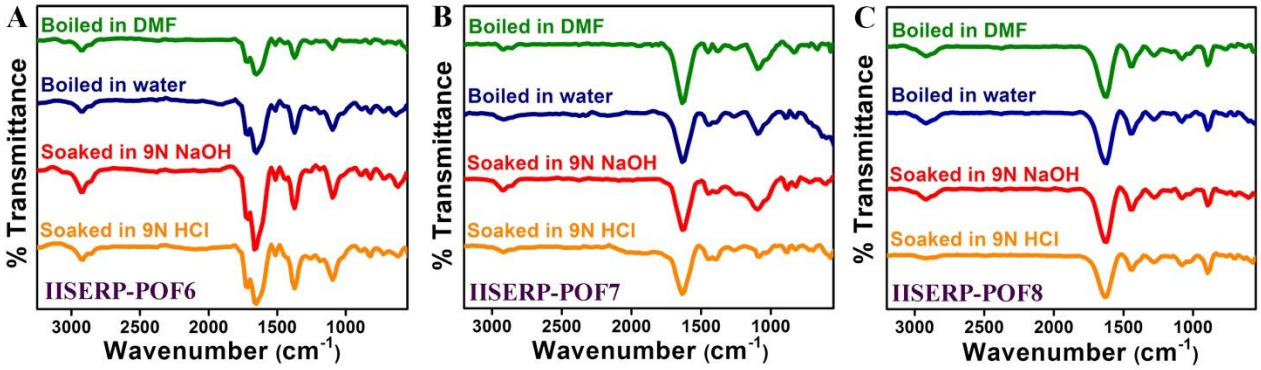

Figure A.2.2. Infra-Red (IR) spectra of **POFs** subjected to different chemical treatments. These spectra exemplify the stability of the polymer in different chemical environments. (*Source: Infrared and Raman Spectra of Inorganic and Coordination Compounds, Part B, Applications in Coordination, Organometallic, and Bioinorganic Chemistry, 6th Edition, Kazuo Nakamoto*).

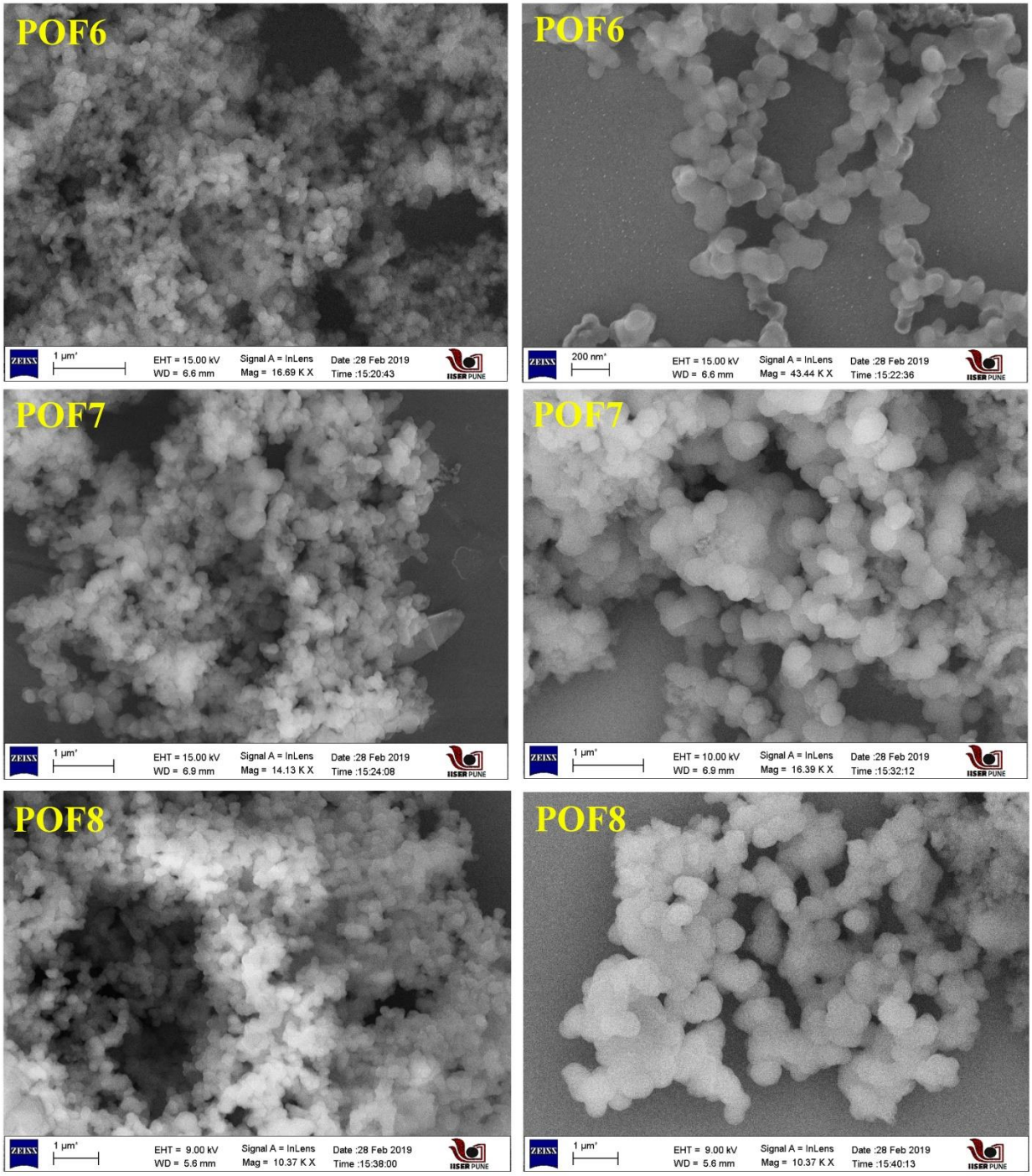

Figure A.2.3. Field Emission Scanning Electron Microscopic (FESEM) images of the polymers. The polymers exhibit a spherical morphology.

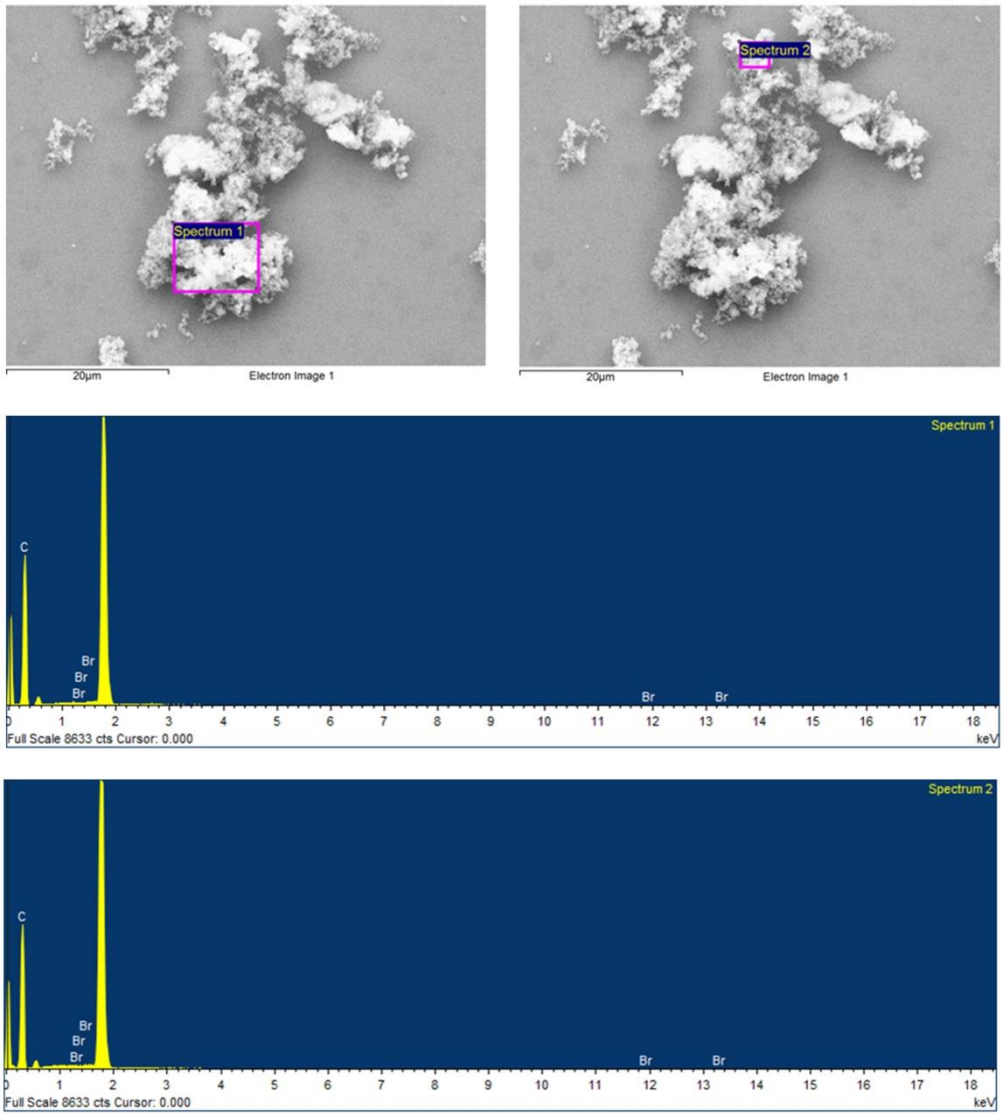

Figure A.2.4. Energy Dispersive X-ray (EDX) images of **IISERP-POF6** showing the respective elements present in the polymer.

Table A.2.1: Atomic and elemental composition obtained from EDX analysis of **IISERP-POF6**.

	Spectrum 1		**Spectrum 2**	
Element	**Weight %**	**Atomic %**	**Weight %**	**Atomic %**
C K	98.08	99.71	99.17	99.56
Br L	1.92	0.29	2.83	0.44

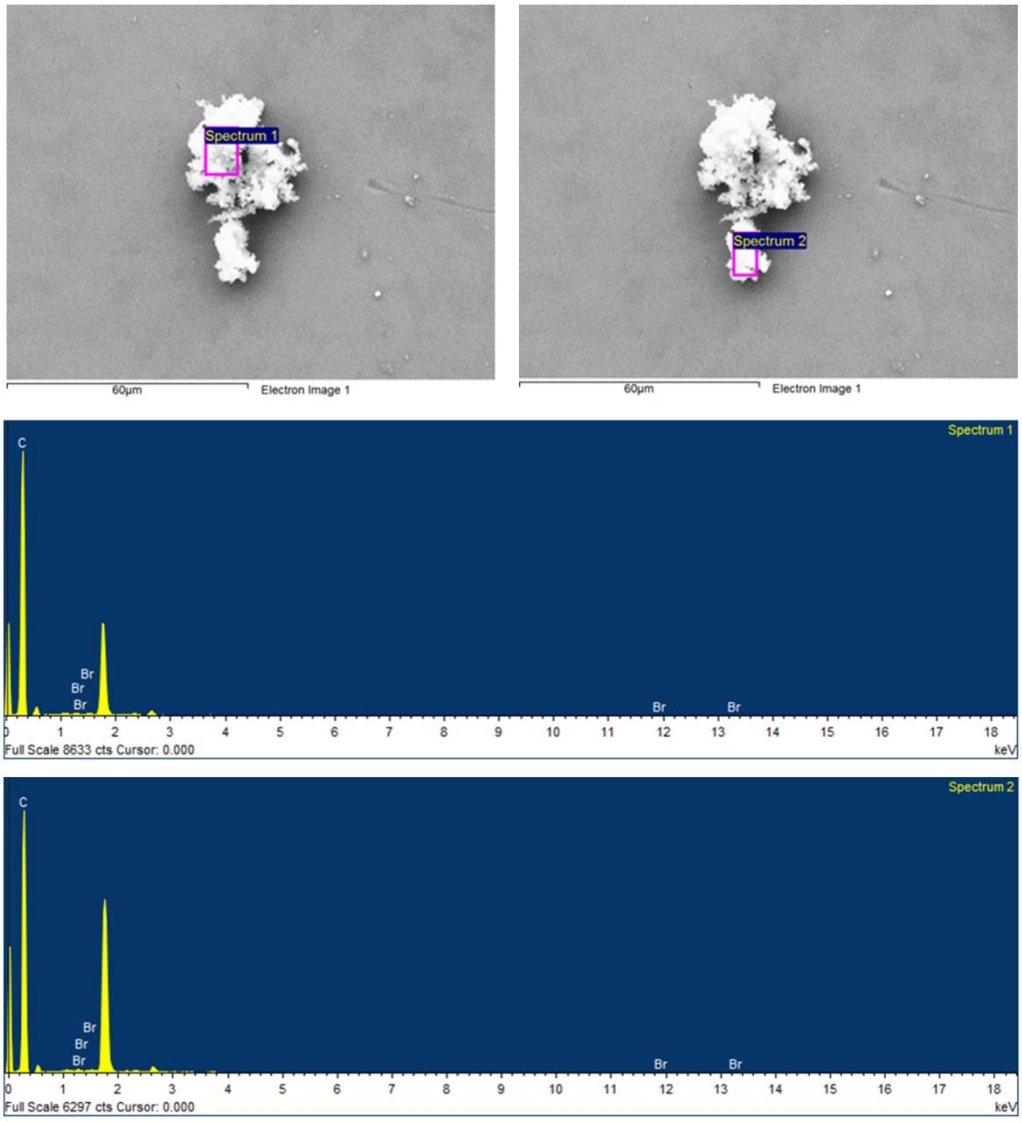

Figure A.2.5. Energy Dispersive X-ray (EDX) images of **IISERP-POF7** showing the respective elements present in the polymer.

Table A.2.2. Atomic and elemental composition obtained from EDX analysis of **IISERP-POF7**.

	Spectrum 1		**Spectrum 2**	
Element	**Weight %**	**Atomic %**	**Weight %**	**Atomic %**
C K	98.96	99.84	98.93	99.84
Br L	1.04	0.16	1.07	0.16

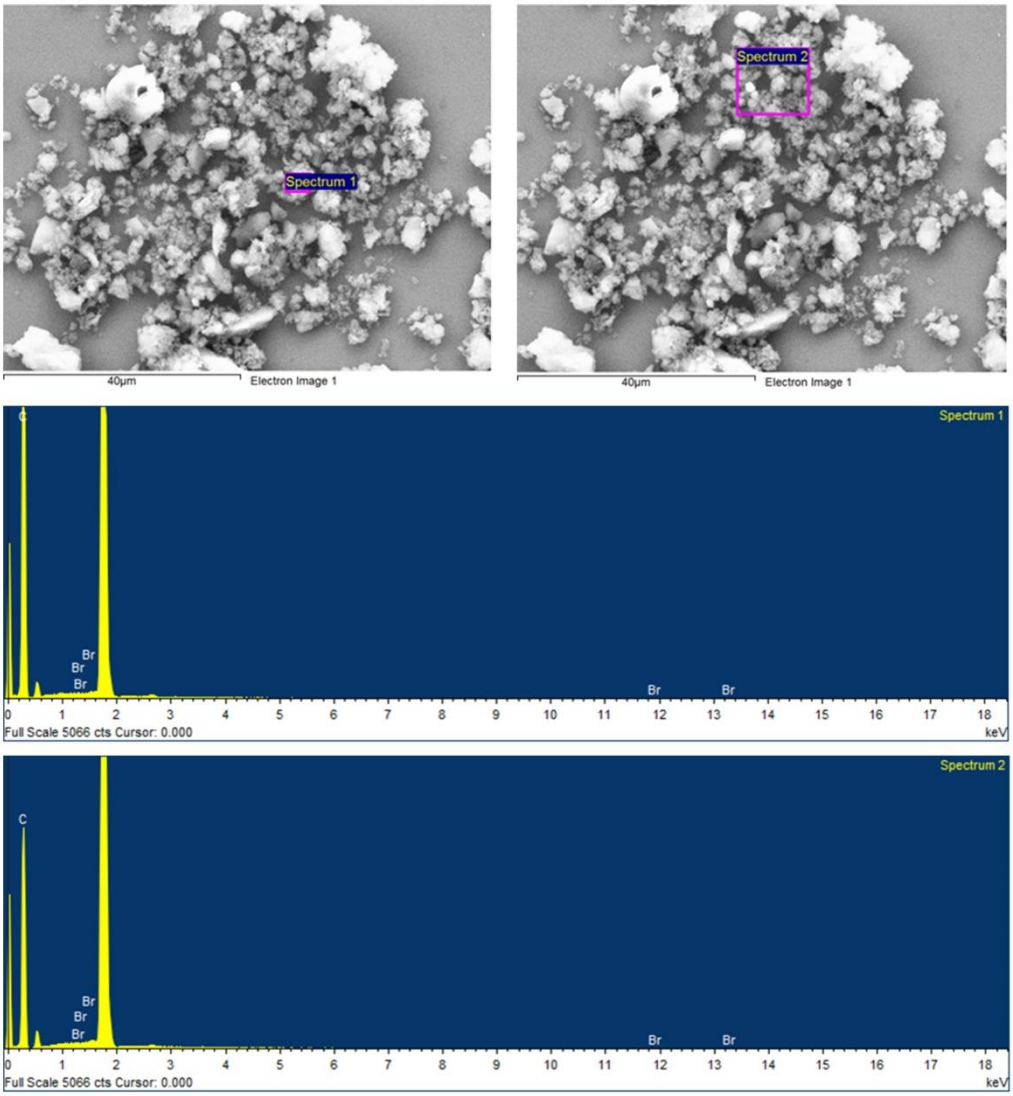

Figure A.2.6. Energy Dispersive X-ray (EDX) images of **IISERP-POF8** showing the respective elements present in the polymer.

Table A.2.3. Atomic and elemental composition obtained from EDX analysis of **IISERP-POF8**.

	Spectrum 1		**Spectrum 2**	
Element	**Weight %**	**Atomic %**	**Weight %**	**Atomic %**
C K	98.22	99.73	98.70	99.49
Br L	1.78	0.27	1.30	0.51

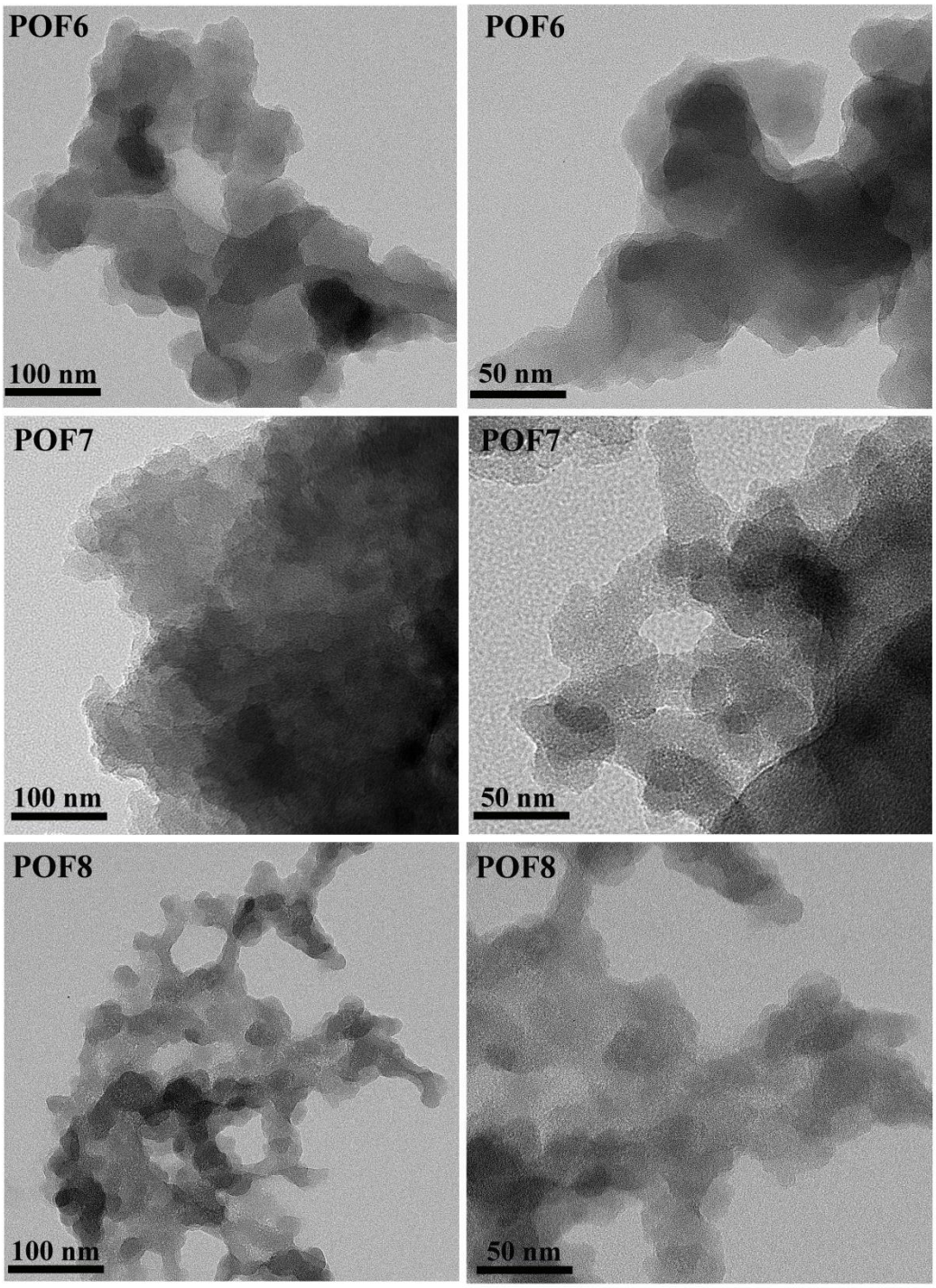

Figure A.2.7. High-Resolution Transmission Electron Microscopic (HRTEM) images of the three polymers.

Table A.2.4: Fitted Virial parameters for Xe.

Parameters	IISERP-POF6	IISERP-POF7	IISERP-POF8
A0	-3208.061845	-3200.490362	-3243.346928
A1	619.2541303	718.1017016	501.8488689
A2	-270.7945347	-328.0339082	-198.7313009
A3	59.84408912	81.72084534	45.48335781

A4	0	-0.459100703	0
B0	15.22197341	15.12487157	15.5214489
B1	0	-0.038330415	0

Table A.2.5. Fitted Virial parameters for Kr.

Parameters	IISERP-POF6	IISERP-POF7	IISERP-POF8
A0	-2697.304481	-2651.063435	-2187.629647
A1	-204.0152665	192.5161732	-237.3467145
B0	16.29700252	16.0864836	14.48544663
B1	1.280113504	0	1.442828328

Table A.2.6. Fitted IAST parameters for Xe/Kr (20Xe:80Kr composition) selectivity at 298 K and 288 K for IISERP-POF6.

Constants	Gas A		Gas B	
	288 K	298 K	288 K	298 K
qA1	3.849746839	3.082682691	2.536684261	2.324022715
qA2	0	0	0	0
kA1	0.008437009	0.006507509	0.000457617	0.000416795
kA1	0	0	0	0
nA1	0.678442665	0.731527453	0.992821604	0.954831647
nA1	0	0	0	0
HA1	0.032480347	0.020060586	0.001160829	0.000968641
HA1	0	0	0	0

Table A.2.7. Fitted IAST parameters for Xe/Kr (20Xe:80Kr composition) selectivity at 298 K and 288 K for IISERP-POF7.

Constants	Gas A		Gas B	
	288 K	298 K	288 K	298 K
qA1	3.849746839	3.082682691	2.536684261	2.324022715
qA2	0	0	0	0
kA1	0.008437009	0.006507509	0.000457617	0.000416795
kA1	0	0	0	0
nA1	0.678442665	0.731527453	0.992821604	0.954831647
nA1	0	0	0	0
HA1	0.032480347	0.020060586	0.001160829	0.000968641
HA1	0	0	0	0

Table A.2.8. Fitted IAST parameters for Xe/Kr (20Xe:80Kr composition) selectivity at 298 K and 288 K for IISERP-POF8.

Constants	Gas A		Gas B	
	288 K	298 K	288 K	298 K
qA1	4.048261507	3.49427188	2.539073057	2.32658096
qA2	0	0	0	0
kA1	0.005828481	0.004462894	0.000397678	0.000356362
kA1	0	0	0	0

nA1	0.748253836	0.780912786	1.00583943	0.984825712
nA1	0	0	0	0
HA1	0.023595216	0.015594564	0.001009733	0.000829105
HA1	0	0	0	0

Table A.2.9. Fitted IAST parameters for Xe/N_2 ($1Xe:99N_2$ composition) selectivity at 298 K for all the polymers.

Constants	Gas A			Gas B		
	POF6	POF7	POF8	POF6	POF7	POF8
qA1	3.584327049	3.083585995	3.454944772	0.067818734	0.081464087	0.083108822
qA2	0	0	0	0	0	0
kA1	0.005114634	0.006541535	0.004416721	0.000332957	0.000284879	0.000244613
kA1	0	0	0	0	0	0
nA1	0.748628779	0.730605945	0.785567598	1.317373312	1.318282045	1.318445365
nA1	0	0	0	0	0	0
HA1	0.018332521	0.020171385	0.015259528	2.25807E-05	2.32074E-05	2.03295E-05
HA1	0	0	0	0	0	0

Table A.2.10. Fitted IAST parameters for Xe/CO_2 ($1Xe:99CO_2$ composition) selectivity at 298 K for all the polymers.

Constants	Gas A			Gas B		
	POF6	POF7	POF8	POF6	POF7	POF8
qA1	3.584327049	3.08117948	3.454944772	5.502305792	4.950602554	5.058374449
qA2	0	0	0	0	0	0
kA1	0.005114634	0.006461629	0.004416721	0.000599257	0.001373547	0.00075008
kA1	0	0	0	0	0	0
nA1	0.748628779	0.732785981	0.785567598	0.966857085	0.821108768	0.932937072
nA1	0	0	0	0	0	0
HA1	0.018332521	0.019909438	0.015259528	0.003297297	0.006799885	0.003794186
HA1	0	0	0	0	0	0

Table A.2.11. Comparison of the Xe/N_2 selectivities of the polymers with some benchmark porous materials.

Serial no.	Material	Xe/N_2 selectivity at 298K, 1bar ($1Xe:99N_2$)	Ref.
1	IISERP-POF6	200[a]	This Work
2	IISERP-POF7	180[a]	This Work
3	IISERP-POF8	160[a]	This Work
4	Carbon-ZX	120[a]	*Sci. Rep.* **2016**, *6*, 21295.
5	ZIF8	~40[a]	*Sci. Rep.* **2016**, *6*, 21295.
6	PCN-14	24.7[b]	*J. Phys. Chem. C* **2014**, *118*, 11685.
7	NOTT series	18.1-21[b]	*J. Phys. Chem. C* **2014**, *118*,

			11685.
8	HKUST-1	20.7[b]	*J. Phys. Chem. C* **2014**, *118*, 11685.
9	IRMOF series	8.6-10.7[b]	*J. Phys. Chem. C* **2012**, *116*, 19765.
10	MOF-74 series	5.3-18.2[b]	*J. Phys. Chem. C* **2012**, *116*, 19765.

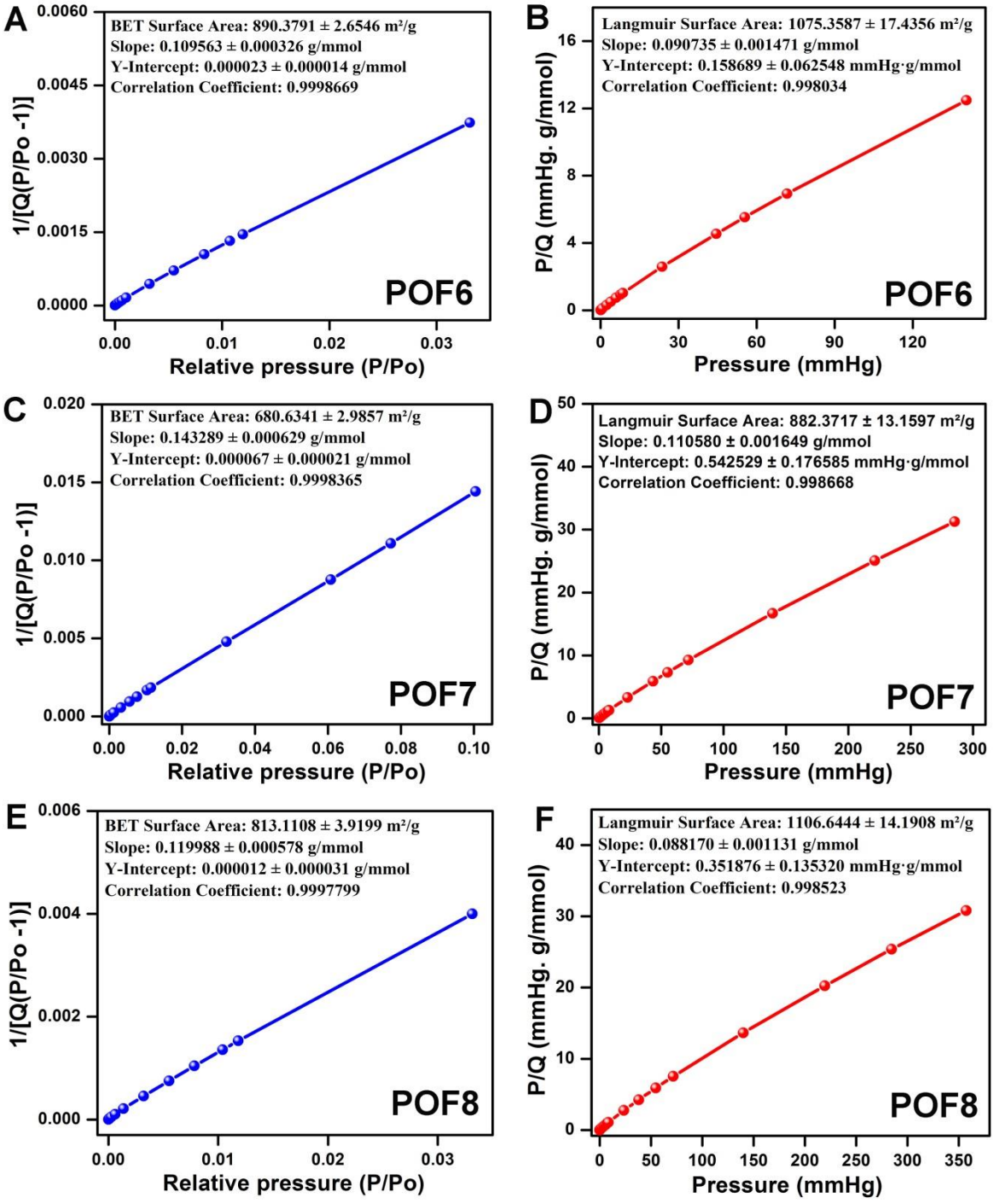

Figure A.2.8. BET, Langmuir fits and surface area reports obtained from N_2 77 K adsorption isotherms for the polymers.

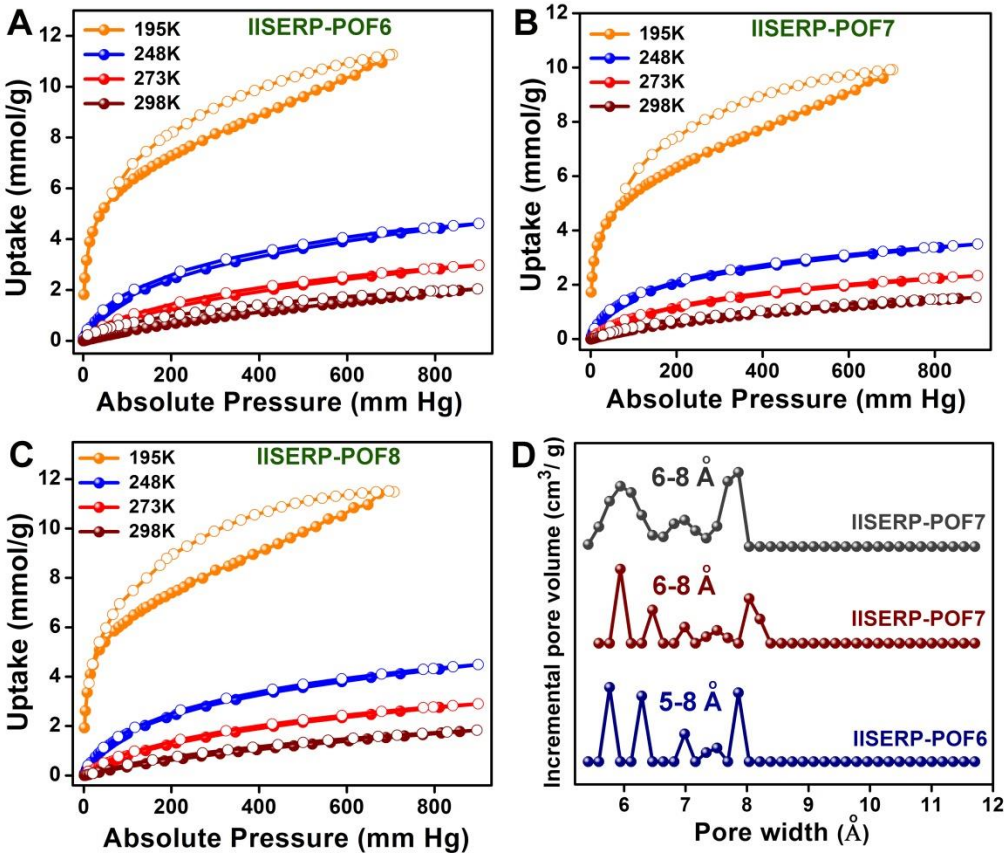

Figure A.2.9. (A, B, C) CO_2 isotherms of the respective polymers at different temperatures. (D) Pore size distribution obtained from NLDFT fit using CO_2 isotherm at 273K.

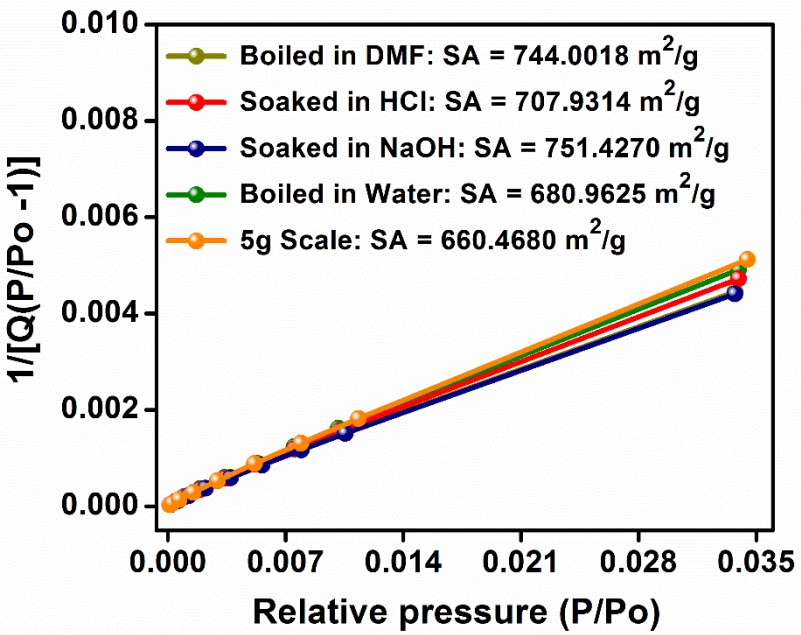

Figure A.2.10. BET transform plots for **IISERP-POF6** treated with different chemicals to demonstrate stability.

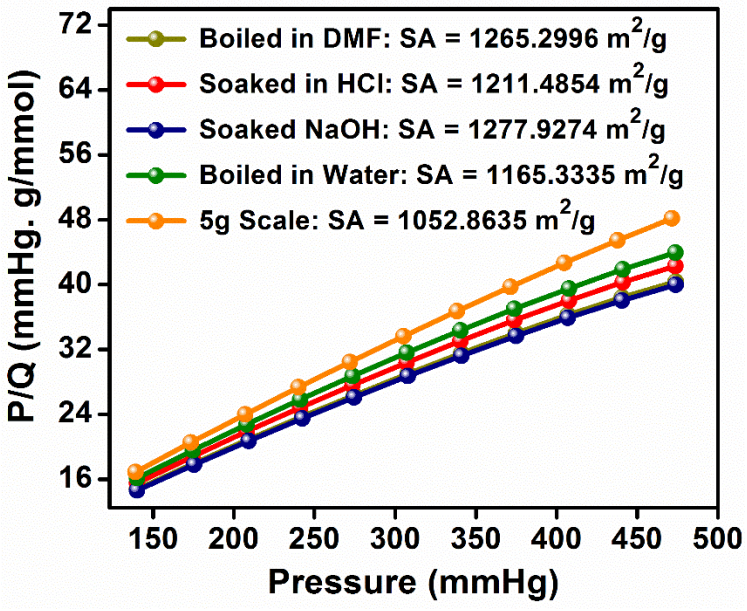

Figure A.2.11. Langmuir transform plots for **IISERP-POF6** treated with different chemicals to demonstrate stability.

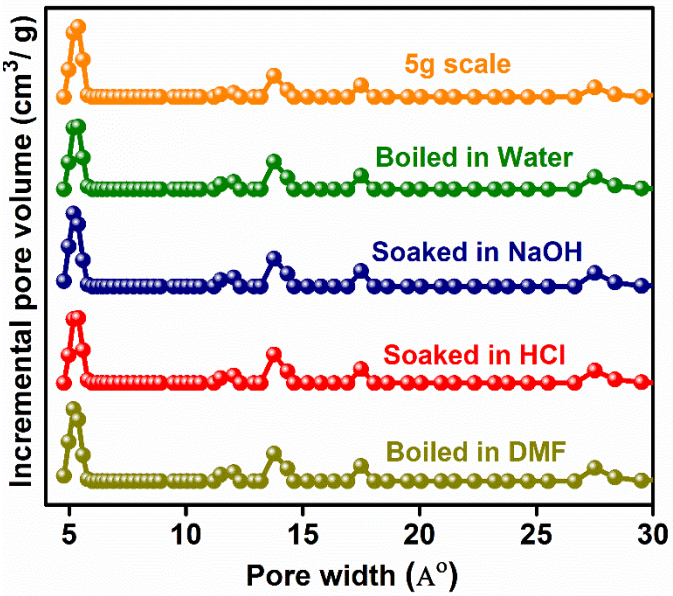

Figure A.2.12. NLDFT pore size distribution plots for **IISERP-POF6** treated with different chemicals to demonstrate stability.

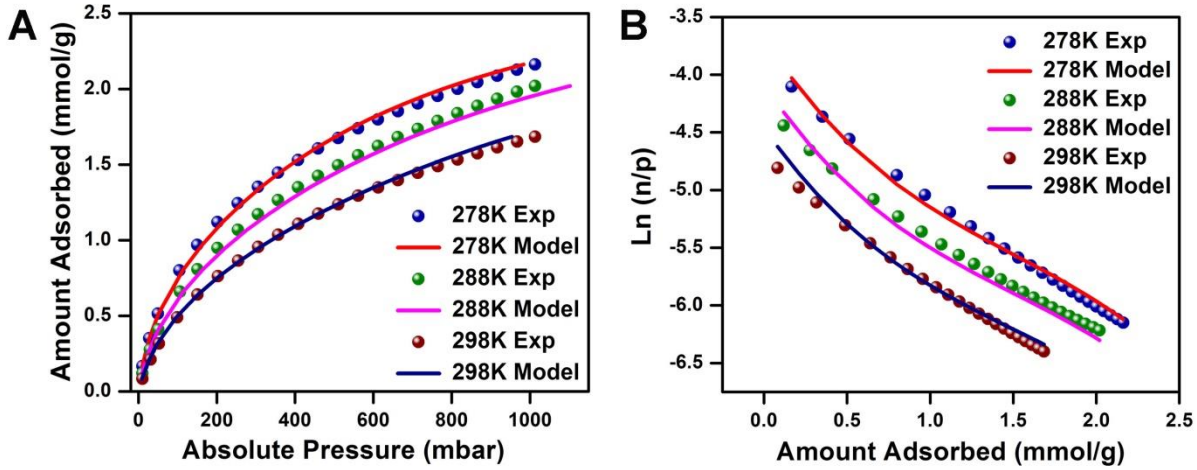

Figure A.2.13. (A) Comparison of experimental Xe isotherms with the isotherms calculated from virial model for **IISERP-POF6** at three different temperatures, 278 K, 288 K, and 298 K. (B) Virial plots for Xe adsorption at three different temperatures, 278 K, 288 K, and 298 K.

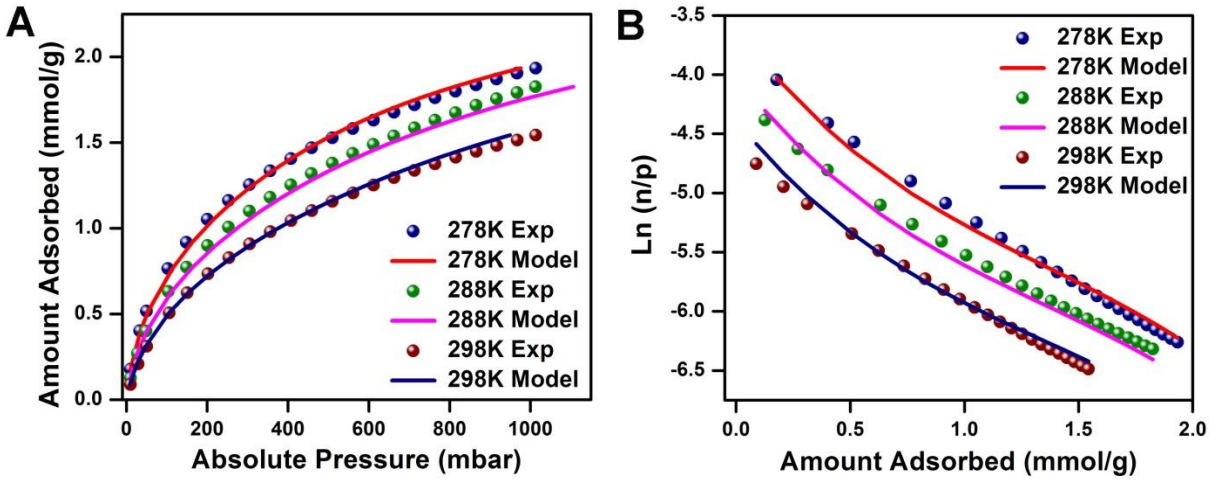

Figure A.2.14. (A) Comparison of experimental Xe isotherms with the isotherms calculated from virial model for **IISERP-POF7** at three different temperatures, 278 K, 288 K, and 298 K. (B) Virial plots for Xe adsorption at three different temperatures, 278 K, 288 K, and 298 K.

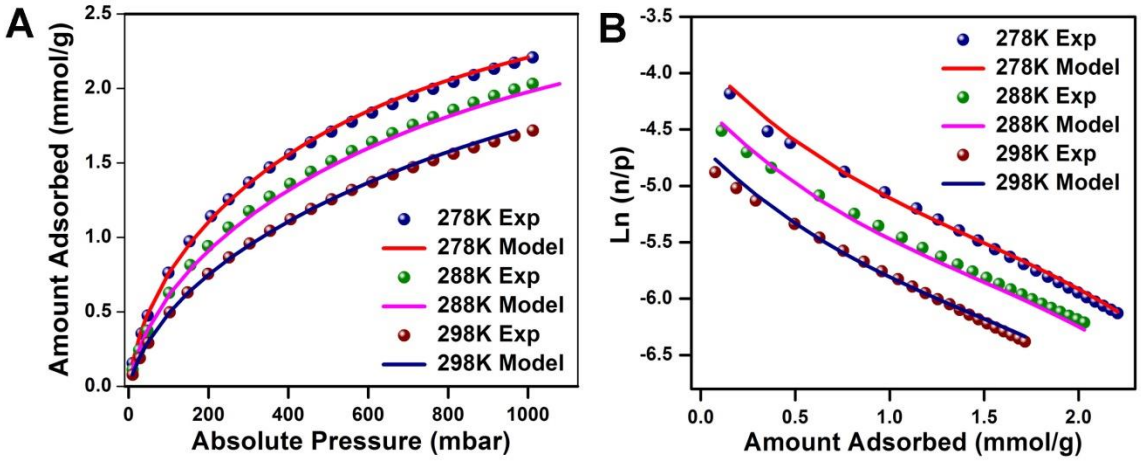

Figure A.2.15. (A) Comparison of experimental Xe isotherms with the isotherms calculated from virial model for **IISERP-POF8** at three different temperatures, 278 K, 288 K, and 298 K. (B) Virial plots for Xe adsorption at three different temperatures, 278 K, 288 K, and 298 K.

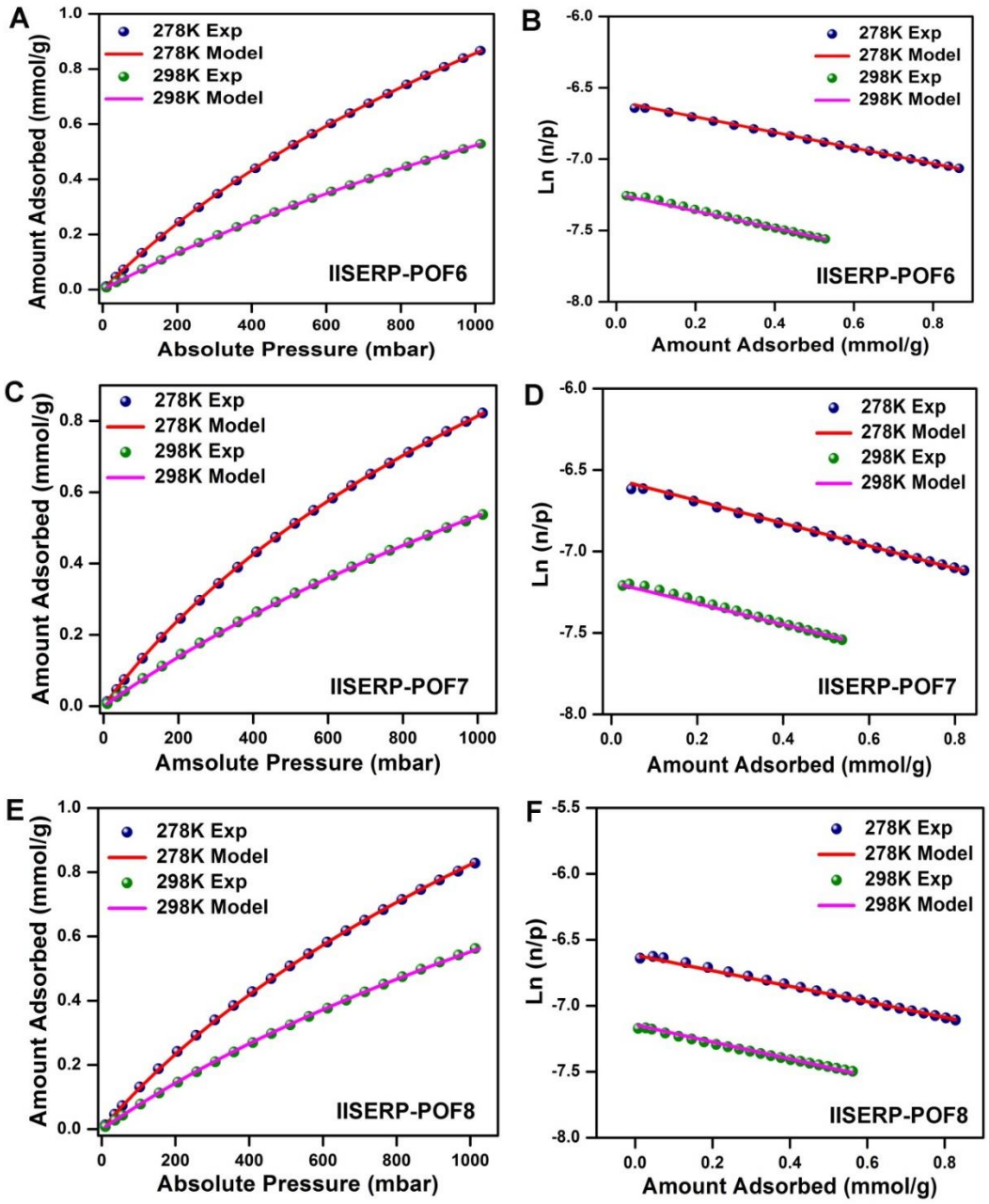

Figure A.2.16. Virial model fitting using Kr adsorption isotherms at two different temperatures, 278 K and 298 K.

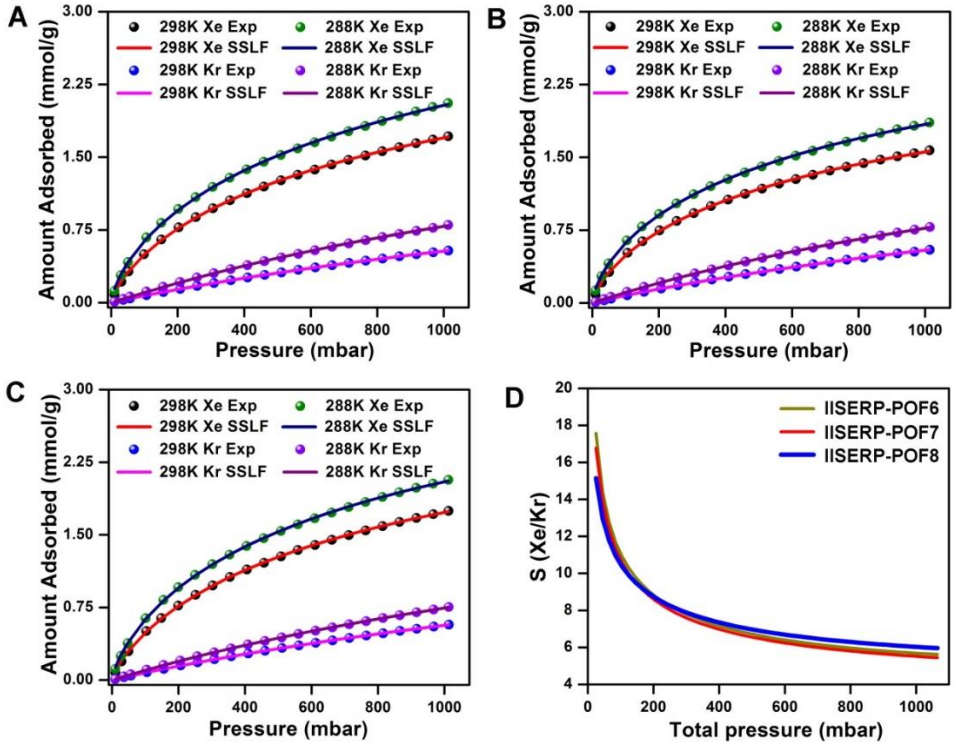

Figure A.2.17. (A, B, C) IAST fitting curves for Xe and Kr at different temperatures, 288 K and 298 K. **(A: IISERP-POF6; B: IISERP-POF7; IISERP-POF8)** (D) Xe/Kr selectivity at 288 K.

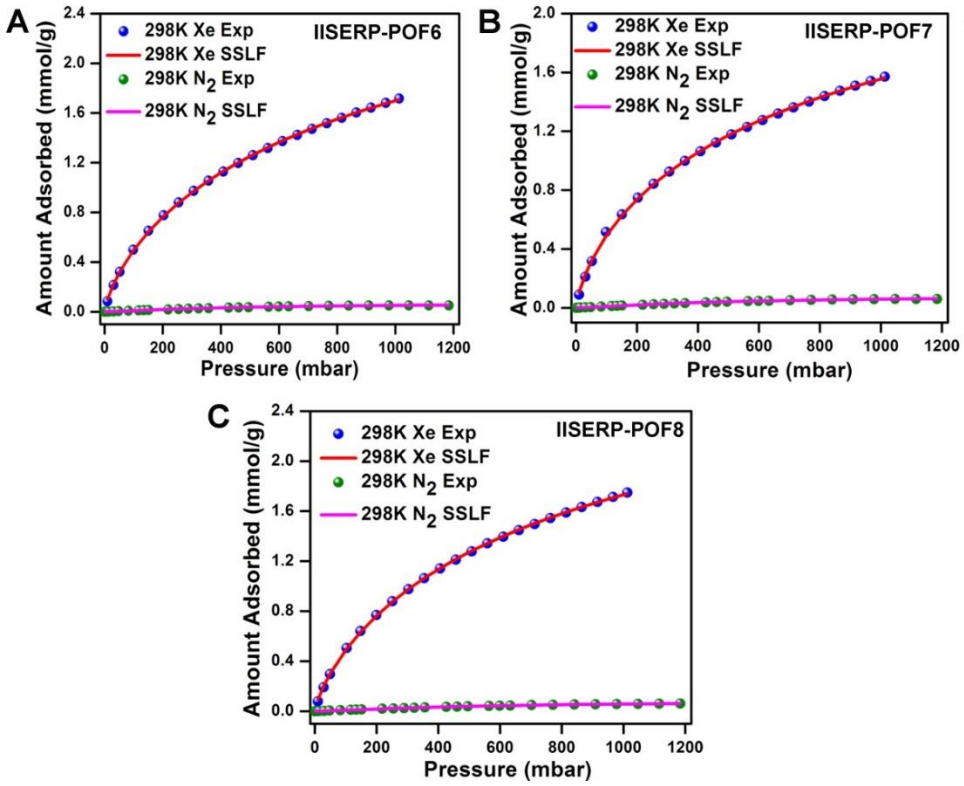

Figure A.2.18. IAST fitting curves for Xe and N_2 at 298 K.

Chapter 3

An Ultra-microporous Metal-Organic Framework with Exceptional Xe Capacity

Chapter 3

3.1. Introduction:

Molecular confinement is known to impose profound effects on the chemistry of encapsulated gas molecules.[1] For example, biological systems such as proteins exhibit unparalleled efficiency and selectivity in molecular binding and transport through confinement and cooperative effects.[1] In this regard, biological systems such as proteins offer the ultimate example of unique chemistry under confinement. Structural investigation of Xe adsorption in various proteins and biomolecules suggest the most prominent binding site is within the small hydrophobic pockets with pore size (4 – 5 Å) where Xe interacts weakly via van der Waals forces.[2] Similar observations on the importance of hydrophobic pockets were made in other classes of protein structures including myoglobin, haemoglobin and adenylate kinase.[3] Traditional porous materials such as activated carbon and aluminosilicate zeolites have been tested for Xe adsorption, but the role of confinement and pore size have not always been investigated. In this regard, nanoporous materials, MOFs have shown to be ideal candidate materials to probe the mechanism of weakly interacting noble gases because MOFs are atomically precise materials with tunable pore sizes. Further, the ability to carry out detailed computational analysis from determined structures.[2,3-14] MOFs offer several advantages over traditional porous sorbents including high internal surface area and functionalized pore surface.[15,16] MOFs and related porous organic cages, in particular, NiMOF-74, cobalt formate, CC3 (porous imine cage) and SBMOF-1 (Calcium 4,4 -sulfonyldibenzoate) have shown promising Xe adsorption and selectivity over other competing gases such as Kr under conditions pertinent to nuclear reprocessing.[2,7,17-19] In particular, SBMOF-1 that was selected as part of a computationally inspired materials discovery strategy exhibit the highest Xe uptake under the nuclear reprocessing condition.[7,20]

Experimental and computational studies have previously indicated that an optimal Xe selective material should have a similar pore size as the kinetic diameter of Xe (4.1 Å).[20-22] In this direction, SBMOF-1 with its optimally sized unidimensional channels showed a Xe capacity (13.2 mmol/kg) with high selectivity. However, considering that their low surface area yields only a moderate uptake at low pressures (145 m^2/g, ~1.4 mmol/g of Xe at 1bar and 298K), there is definite room for enhancing the capture capacities. Further, in our continued search for Xe selective materials, we looked for primarily two characteristics: (a) MOFs with effective pore size close to 4.0 Å, but with a higher surface than SBMOF-1 and (b) absence of open metal sites for high selectivity towards Xe over other gases including CO_2. MOFs with open

metal sites tend to be selective towards CO_2 because of its large quadrupole moment which leads to the issue of co-adsorption of CO_2 along with Xe, making the overall adsorption (recovery) process more complicated.[23] In this communication, we report an ultra-microporous nickel isonicotinate MOF, IISERP-MOF2,[1,24] that shows excellent Xe adsorption capacity compared to benchmark Xe selective material such as SBMOF-1.[7]

3.2. Materials and methods:

Synthesis of the IISERP-MOF2:

IISERP-MOF2 was synthesized according to the reported literature. The bulk phase purity of the sample was determined by Powder X-Ray Diffraction.

3.3. Analytical characterization:

Powder X-ray diffraction:

Powder X-Ray Diffraction data were recorded out Rigaku Miniflex-600 instrument and processed using PDXL software.

3.4. Adsorption studies:

All the adsorptions were carried out using a 3-FLEX pore and surface area analyzer, Micromeritics and few cases 'Autosorb IQ', Quantachrome.

Langmuir fits:

In most cases, the isotherms were fit to the Single-Site Langmuir (SSL) equation. The isotherms were fit by solving the Langmuir equation using the solver function in Microsoft Excel following a similar protocol previously reported.[24] Utilizing this routine circumvents some of the problems associated with favoring either high- or low-pressure regions when linearizing the Langmuir equation and offers a balanced approach.

Single-Site Langmuir (SSL)

$$q_i = q_m \frac{k_i}{1 + k_i P} P$$

Dual-Site Langmuir (DSL)

$$q_i = q_{m,1} \frac{K_1}{1 + K_1 P} P + q_{m,2} \frac{K_2}{1 + K_2 P} P$$

Virial analysis:

The Xe & Kr adsorption data for the polymers were measured from 0- 1bar at 278, 288 and 298 K and were fitted by the following virial equation.

ln(P) = ln(Va)+(A0+A1*Va +A2*Va^2 …+ A6*Va^6)/T+(B0+B1*Va)

Where P is pressure, Va is amount adsorbed, T is temperature, and A0, A1, A2 …, A4 and B0, B1 are temperature independent empirical parameters.

Ideal Adsorption Solution Theory (IAST):

IAST calculations were employed as described by Prausnitz et al.[25] The equation that is involved in selectivity calculations has been given below.

$$S_{1,2} = \frac{q_1/q_2}{p_1/p_2}$$

3.5. Results and discussions:

Xe and other gas adsorption studies:

The 1's framework structure is made up of isolated nickel octahedra connected by 4-pyridine dicarboxylate to form a two-fold interpenetrated diamondoid framework with one-dimensional ultra-microporous channels of approximate diameter 4.7 Å (Figures 3.1A, A.3.1-A.3.3, Table A.3.1). The high thermal stability, absence of open metal sites and moderate surface area (470 m^2/g) makes 1 an attractive candidate to study for noble gas adsorption studies.[24] Further, the PYC linker can be replaced with other functionalized PYC linkers or extended PYC linkers to understand the role of functional groups and confinement effects. We, therefore, synthesized 1, characterized and then measured pure-component adsorption isotherm for Xe along with CO_2, N_2, and O_2 as a function of temperature (278K, 288K, 298K) up to 1 bar pressure (Figures 3.1B, 3.1C, and A.3.4).

The Xe adsorption isotherm in 1 saturates at low pressure (~P/P_0 = 0.2) even at room temperature, indicating a high affinity towards Xe compared to other gases including Kr (Figure 3.1B). The Xe sorption capacity 1 bar and 298K was found to be ~3.2 mmol/g, significantly higher (~2X) than SBMOF-1 (1.4 mmol/g) and 1.5X than CC3 (2.4 mmol/g) under similar experimental conditions (Figure 3.1C).[7,17,19] Interestingly, at lower partial pressures (P/P_0 = 0.1), the difference is more pronounced with 1, which exhibits an unprecedented uptake capacity of 1.33 mmol/g, which is way higher than the benchmark

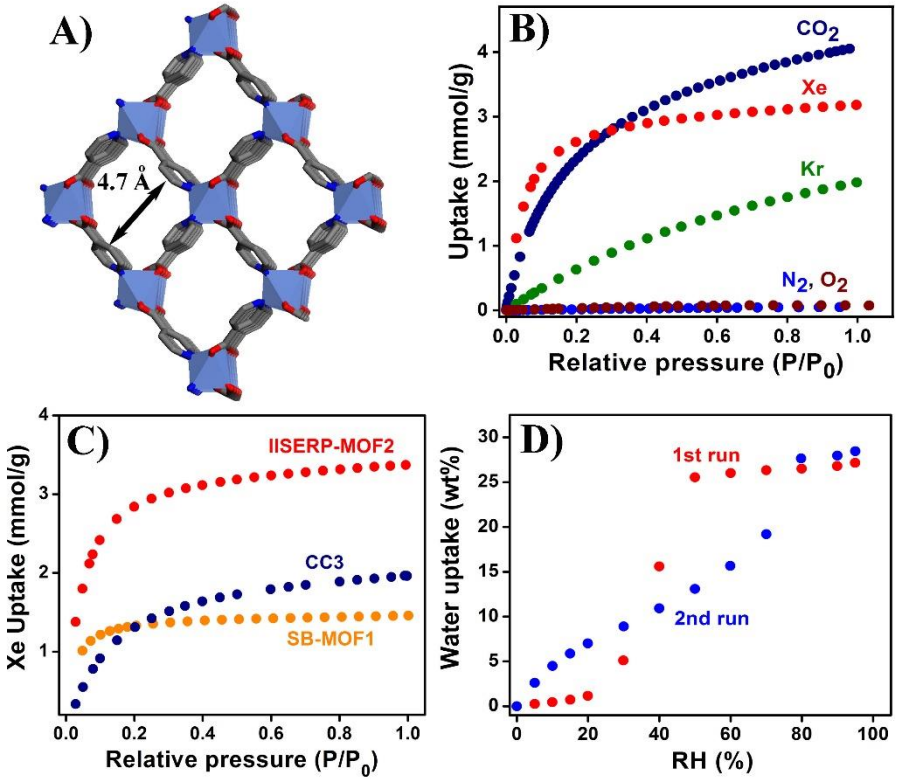

Figure 3.1. (A) Chemical structure, Pore-size, PXRD and the 3-D framework of IISERP-MOF2 showing 1-D channels 3-D framework (B) Adsorption isotherms for different gases done using IISERP-MOF2 at 298K. (C) Comparative Xe adsorption isotherms for different high-performance MOF materials. (D). The heat of Adsorption of Xe and Kr obtained from the Virial method.

Xe selective materials such as SBMOF-1 (0.75 mmol/g), CC3 (0.44 mmol/g) and NiMOF-74 (0.35 mmol/g) respectively (Figure 3.1C). The exceptionally high Xe sorption capacities of 1, is attributed to the higher surface area (470 m^2/g vs. 145 m^2/g in comparison to SBMOF-1)[7,24] and similar pore size. On the contrary, the Kr adsorption isotherm exhibits a smaller slope and does not saturate at 1 bar, at all three collection temperatures, indicating a much weaker affinity towards Kr (Figure 3.1B). The total Kr uptake capacity of 1 at room temperature was found to be 1.97 mmol/g, significantly lower than that of Xe (Figure 3.1B). Further, the Xe heats of adsorption (Q_{st}), a measure of adsorbate-adsorbent interaction was calculated based on the Virial equation by fitting the adsorption data at three different temperatures of 278K, 288K, and 298K (Figures 3.1D, and A.3.5). The value was found to be 32 kJ mol^{-1}, which is comparable to benchmark materials, SBMOF-1 (37 kJ mol^{-1}) and CROFOUR-1 (36 kJ mol^{-1}) and considerably higher than HKUST-1 (27 kJ mol^{-1}), NiMOF-74 (22 kJ mol^{-1}), MOF-5 (15 kJ mol^{-1}) and cobalt for-mate (28 kJ mol^{-1}) respectively.[7,9,12,13]

The difference in Xe vs. Kr affinity is also apparent in the Kr Q_{st}, which is calculated to be 20 kJ mol^{-1} (Figures 3.1D and A.3.6). We further collected the adsorption isotherm for other

gaseous components of air such as N_2, O_2, and CO_2. As expected, 1 has almost no affinity for any gas except CO_2, which is evident from their low uptake capacity (Figure 3.1B). For CO_2, 1 exhibits a type –I isotherm with a total uptake of 4.015 mmol/g at 1 bar and 298K, slightly higher than its total Xe uptake. However, based on the single-component isotherms, 1 has a stronger affinity towards Xe over CO_2 as evident from the steep Xe uptake at lower pressure (< 100 mbar) region and early saturation. This particular observation can be attributed to the lack of open metal site and close size match between adsorbed Xe and pore width.

Selectivity studies:

Ideal adsorbed solution theory (IAST),[25] capable of predicting gas selectivities, including Xe/Kr,[7,18] in MOF, is employed to estimate the Xe/Kr and Xe/CO_2 selectivity at various conditions including very low concentrations of Xe such as (1300 ppm Xe, 130 ppm Kr, 300 ppm CO_2, 0.9% Ar, 20.1% O_2, 78.9% N_2) and under condition pertinent to Xe recycling in the medical industry (65% Xe, 27% O_2, 5% CO_2 and 3.3% N_2). The predicted Xe/Kr and Xe/CO_2 selectivities at different pressures and mixture compositions are shown in table 3.1. At 1300 ppm Xe and 130 ppm Kr, the selectivity was calculated to be 18.51 (Figures A.3.7 and A.3.8). These values are comparable to benchmark MOFs such as SBMOF-1, CROFOUR-1, and CC3 under similar conditions.

Theoretical insights:

In order to further testify the exceptional Xe-selectivity of 1, computational simulations were performed to identify adsorption sites that are selective towards Xe. Purification of Xe from the Xe/Kr mixture that is left behind after the cryogenic distillation of O_2 from the air has a typical composition of 20%Xe:80%Kr @ 298K, 1bar. The current record holder for this Xe/Kr separation process is SBMOF-1, with a selectivity of 70.6 (source: The CoRE database), determined using Grand Canonical Monte Carlo (GCMC). SBMOF-1 has an experimentally determined Henry's selectivity of 16. Here, we verified the selectivity reported by Banerjee for SBMOF-1, HKUST-1, and IRMOF-1 using our simulation protocols. For comparison, we calculated the selectivities using Henry's method, a competitive model, IAST, and GCMC. For Henry's, competitive, and IAST models, experimental data were fit to Sips isotherms. For GCMC calculations, we used Lennard-Jones (LJ) parameters, while the frameworks used DREDING LJ parameters and if none were available UFF. These values were also calculated for 1 in the same way. For the competitive, IAST, and GCMC calculations they were calculated at 0.2 bar Xe and 0.8 bar Kr. As shown in Table 3.1, Henry's selectivity is different from those

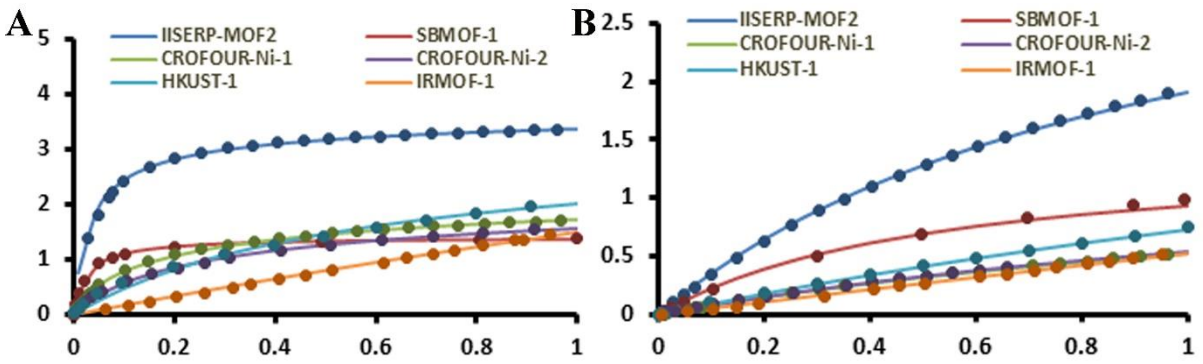

Figure 3.2. Comparison of the experimental and simulated Top: Xe and Bottom: Kr adsorption data for IISERP-MOF2 and other relevant MOFs at 298 K.

found in the literature as they have been calculated using different methods. Here we have calculated Henry's selectivity from an automated protocol that first fits the data to the Sips isotherm model. The slope was then calculated using the low-pressure data from the fitted model. This modus operandi was consistently applied to all the MOFs. The other important factor to note here that the competitive selectivity for SBMOF-1 seems to be overly high compared to the other methods, (22 vs. 16). This is mainly because, for SBMOF-1, the Kr uptake does not saturate even at 1bar, this makes the saturation capacity to be overestimated causing the Langmuir constant to be underestimated. This causes the competitive model to overestimate as it is heavily dependent on the Langmuir constants.

Figure 3.2 shows the experimental and simulated adsorption data for Xe and Kr on both 1 and SBMOF-1. The first thing to note is that 1's overall adsorption capacity for Xe is much greater than SBMOF-1 (3.37 mmol/g vs. 1.38 mmol/g). To the best of our knowledge, this is the first time UFF LJ parameters have been used for the simulation of Xe/Kr adsorption; and we achieve good agreement with experimental results (Figures A.3.9 and A.3.10). Also, the data obtained helps validate the GCMC results. With these results and caveats considered, it is reasonable to say that 1 has a better Xe/Kr selectivity than SBMOF-1, with a value of 19 compared to 16.

To further find the superior Xe sorption capacity, we performed ABSL on both MOFs at 0.2 bar Xe and 0.8 Kr at 298 K. Figures 3.3 and A.3.11 show the binding sites of both Xe and Kr in 1 and SBMOF-1, respectively. From the figures, it is seen that Xe in 1 lay slightly closer to the framework atoms than the Krypton counterpart. In SBMOF-1 however, Kr and Xe occupy nearly the same space, so much so that when using the CPK filling model, the Xe location in the MOF. From ABSL it was found that the Xe and Kr are closer to the framework atoms in SBMOF-1 than in 1. From the ABSL calculations, we discern that SBMOF-1 completely

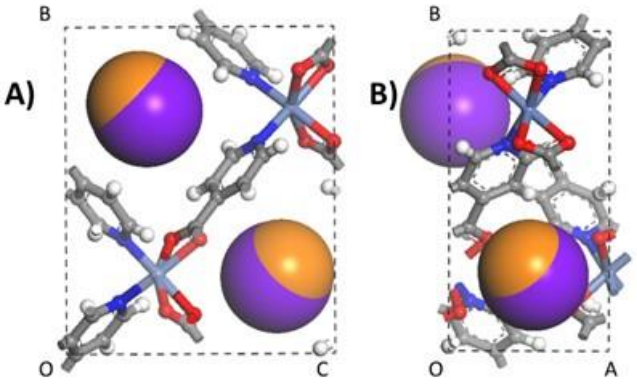

Figure 3.3. Binding site locations of Xenon and Krypton in IISERP-MOF-2 (1), Xenon is colored purple, and Krypton in orange.

envelopes contained more close atoms to Xe (20 atoms within 120% of the combined VdW radii of the framework atom and guest) compared to 1 (5 atoms within 120%) at a closer distance (3.37 Å minimum distance for SBMOF-1 compared to 3.84 Å for 1). This shows both Xe and Kr share a relatively similar binding. Along with the binding site locations, the energetics of the adsorption of the Xe and Kr in each MOF were investigated. Table 3.2 lists the binding energies found for the guest molecules; all binding sites have a notable difference in their binding energies. It was found that the heats of adsorption/binding energies were higher in SBMOF-1 for both Xe and Kr.

The better Xe/Kr selectivity of IISERP-MOF-2 (1) can be explained by comparing its binding energies with other competing materials. The relative binding energy difference between Xe and Kr for both the SBMOF-1 and IISERP-MOF2 it is 9.1 kJ/mol, which is significantly smaller than what is observed, for example, CO_2 and N_2 in Mg-MOF74 (20.1 kJ/mol), and the Xe/Kr selectivity in IISERP-MOF2 is 18.51.[26] In stark contrast, the Mg-MOF74 with CO_2 and N_2 binding energy difference of 20.1 kJ/mol yields a selectivity of only 31.[27] This could mean a much smaller difference in binding energies between Xe and Kr could have a substantial impact on the selectivities.

^{129}Xe NMR study:

To further understand the Xe adsorption in 1, high pressure ^{129}Xe NMR experiments were conducted at different temperatures. As shown in Figure 3.4, the peak appeared at ~0 ppm attributes to gaseous Xe molecule and the broad peak with an isotropic chemical shift of 127.7 ppm is due to the Xe gas adsorbed within the confined space.[28] The increased chemical shift of adsorbed Xe in comparison with gas phase in 1 is explained by the interaction of gaseous

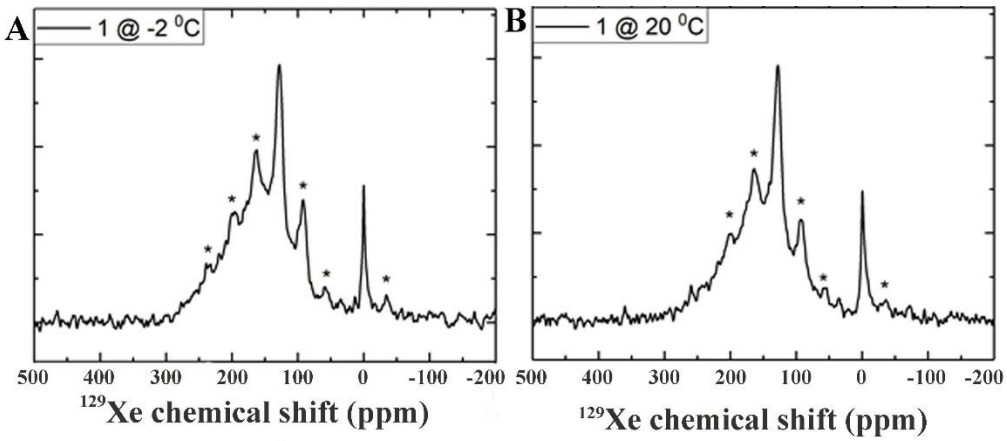

Figure 3.4. ^{129}Xe NMR spectra for 1 obtained at temperature -2 and 20 °C with a spinning rate of 3 kHz. The asterisks denote spinning side-bands.

Xe with MOF particles. Further, it was documented in the literature there is a clear correlation between the pore size and chemical shift of the adsorbed Xe in porous materials. For example, using ^{129}Xe NMR chemical shift, pore sizes of various unknown pore structure of silica-based materials were predicted.[29] The chemical shift of 127.7 ppm in 1 suggests the pore size of ~5 Å which is in line with our pore size calculations using the single-crystal X-ray structure.

Table 3.1. Selectivities of SBMOF-1, IRMOF-1, HKUST-1, and IISERP-MOF-2 (1) calculated using different methods.

	Literature	Henry's	Competitive	IAST	GCMC
SBMOF-1	16.21	15.63	22.25	16.47	16.23
IRMOF-1	3.28	3.18	2.96	2.97	2.72
HKUST-1	8.46	10.41	6.11	8.23	6.35
IISERP-MOF2	-	19.16	19.23	18.51	18.59

Table 3.2. Comparison of the binding energies for Xe and Kr in IISERP-MOF-2 vs. SBMOF-1.

	SBMOF-1	IISERP-MOF-2
Xe Heat of Adsorbtion (kJ/mol)	34.2	32.2
Xe Binding Energy (kJ/mol)	34.6	30.2
Kr Heat of Adsorption (kJ/mol)	25.4	22.8
Kr Binding Energy (kJ/mol)	25.5	21.1

3.6. Conclusion:

In conclusion, we report an ultra-microporous MOF with outstanding Xe selectivity high sorption capacity at low pressures. The Xe adsorption and selectivity were found to be dependent on the optimal pore size of the material and is commensurate with the surface area with respect to the current benchmark material, SBMOF-1. Our results indicate that the selectivity and sorption capacities towards Xe will continue to improve in the near and long-term with the advent of new materials with improved functionalities.

3.7. References:

1. A. S. Tanwar, V. D. Goyal, D. Choudhary, S. Panjikar, R. Anand, *PLOS ONE* **2013**, *8*, e77781.
2. (a) D. Banerjee, A. J. Cairns, J. Liu, R. K. Motkuri, S. K. Nune, C. A. Fernandez, R. Krishna, D. M. Strachan, P. K. Thallapally, *Acc. Chem. Res*. **2014**, *48*, 211-219; (c) D. Chakraborty, S. Nandi, M. A. Sinnwell, J. Liu, R. Kushwaha, P. K. Thallapally, R. Vaidhyanathan, *ACS Appl. Mater. Interfaces* **2019**, *11*, 13279−13284. (d) U. Muller, M. Schubert, F. Teich, H. Puetter, K. Schierle-arndt, J. Pastre, J. Mat. Chem. 2006, 16, 626.
3. T. Prange, M. Schiltz, L. Pernot, N. Colloc'h, S. Longhi, W. Bourguet, R. Fourme, *Proteins* **1998**, *30*, 61-73.
4. R. D. Sanders, D. Q. Ma, M. Maze, *Brit Med Bull* **2004**, *71*, 115-135.
5. D. Banerjee, C. M. Simon, S. K. Elsaidi, M. Haranczyk, P. K. Thallapally, *Chem* **2018**, *4*, 466-494.
6. [a] D. Banerjee, C. M. Simon, A. M. Plonka, R. K. Motkuri, J. Liu, X. Y. Chen, B. Smit, J. B. Parise, M. Haranczyk, P. K. Thallapally, J. Am. Chem. Soc., 2015, 137, 7007. [b] S. K. Ghose, Y. Li, A. Yakovenko, E. Dooryhee, L. Ehm, L. E. Ecker, A. C. Dippel, G. J. Halder, D. M. Strachan, P. K. Thallapally, J. Phy Chem. Lett, 2015, 6, 1790 [c] J. J. Perry, S. L. Teich -McGoldrick, S. T. Meek, J. A. Greathouse, M. Haranczyk, M. D. Allendorf, J. Phys. Chem, C., 2014, 118, 11685. [d] Y. S. Bae, B. G. Hauser, Y. J. Colon, J. T. Hupp, O. K. Farha, R. Q. Snurr, *Micropor Mesopor Mat*, 2013, 169, 176
7. D. Banerjee, C. M. Simon, A. M. Plonka, R. K. Motkuri, J. Liu, X. Y. Chen, B. Smit, J. B. Parise, M. Haranczyk, P. K. Thallapally, *Nat. Commun*. **2016**, *7*, 11831.
8. P. Bergonzo, U. Kogelschatz, I. W. Boyd, *Appl Surf Sci* **1993**, *69*, 393-397.
9. A. S. Dorcheh, D. Denysenko, D. Volkmer, W. Donner, M. Hirscher, *Micro. Meso. Mater*. **2012**, *162*, 64-68.
10. H. Wang, K. X. Yao, Z. J. Zhang, J. Jagiello, Q. H. Gong, Y. Han, J. Li, *Chem. Sci*. **2014**, *5*, 620-624.
11. S. K. Elsaidi, M. H. Mohamed, C. M. Simon, E. Braun, T. Pham, K. A. Forrest, W. Xu, D. Banerjee, B. Space, M. J. Zaworotko, P. K. Thallapally, *Chem. Sci*. **2017**, *8*, 2373–2380.
12. M. H. Mohamed, S. K. Elsaidi, T. Pham, K. A. Forrest, H. T. Schaef, A. Hogan, L. Wojtas, W. Xu, B. Space, M. J. Zaworotko, P. K. Thallapally, *Angew. Chem. Int. Ed*. **2016**, *55*, 8285-8289.
13. P. K. Thallapally, J. W. Grate, R. K. Motkuri, *Chem. Commun*. **2012**, *48*, 347-349.
14. Z. Hulvey, K. V. Lawler, Z. Qiao, J. Zhou, D. Fairen-Jimenez, R. Q. Snurr, S. V. Ushakov, A. Navrotsky, C. M. Brown, P. M. Forster, *J. Phys. Chem. C* **2013**, *117*, 20116-20126.
15. H. C. Zhou, J. R. Long, O. M. Yaghi, *Chem. Rev*. **2012**, *112*, 673-674.
16. O. M. Yaghi, M. O'Keeffe, N. W. Ockwig, H. K. Chae, M. Eddaoudi, J. Kim, *Nature* **2003**, *423*, 705-714.

17. J. Liu, P. K. Thallapally, D. Strachan, *Langmuir* **2012**, *28*, 11584-11589.
18. J. Liu, D. M. Strachan, P. K Thallapally, *Chem. Commun*. **2014**, *50*, 466−468.
19. (a) L. Chen, P. S. Reiss, S. Y. Chong, D. Holden, K. E.Jelfs, T. Hasell, M. A. Little, A. Kewley, M. E. Briggs, A. Stephenson, K. M. Thomas, J. A. Armstrong, J. Bell, J. Busto, R. Noel, J. Liu, D. M. Strachan, P. K. Thallapally, A. I. Cooper, *Nat. Mater*. **2014**, *13*, 954−960; (b) L. Li, L. Guo, Z. Zhang, Q. Yang, Y. Yang, Z. Bao, Q. Ren, J. Li, *J. Am. Chem. Soc*. **2019**, *141*, 9358−9364; (c) L. Yu, S. Xiong, Y. Lin, L. Li, J. Peng, W. Liu, X. Huang, H. Wang, J. Li, *Inorg. Chem*. **2019**, doi.org/10.1021/acs.inorgchem.9b02449.
20. (a) C. M. Simon, R. Mercado, S. K. Schnell, B. Smit, M. Haranczyk, M. *Chem. Mater*. **2015**, *27*, 4459-4475. (b) D. Kakan, J. A. Greathouse, C. L. Staiger, J. P. Perry, M. D. Allendorf, D. S. Sholl, J. Mat. Chem., A. 2015, 3, 23539. (c) S. Panter, P. Zarabadi -poor, *ACS Omega* **2018**, *3*, 18535 (e) T. Vazhappilly, T. K. Ghanty, B. N. Jagatap, *J. Phys. Chem. C* **2016**, *120*, 10968.
21. B. J. Sikora, C. E. Wilmer, M. L. Greenfield, R. Q. Snurr, *Chem. Sci*. **2012**, *3*, 2217-2223.
22. C. E. Wilmer, M. Leaf, C. Y. Lee, O. K. Farha, B. G. Hauser, J. T. Hupp, R. Q. Snurr, *Nat. Chem*. **2012**, *4*, 83-89.
23. J. Liu, P. K. Thallapally, B. P. McGrail, D. R. Brown, J. Liu, *Chem. Soc. Rev*. **2012**, *41*, 2308-2322.
24. S. Nandi, S. Collins, D. Chakraborty, D. Banerjee, P. K. Thallapally, T. K. Woo, R. Vaidhyanathan, *J. Am. Chem. Soc*. **2017**, *139*, 1734-1737.
25. A. L. Myers, J. M. Prausnitz, *AICHE J*. **1965**, *11*, 121.
26. L. Valenzano, B. Civalleri, S. Chavan, G. T. Palomino, C. O. Areán, S. Bordiga, *J. Phys. Chem. C* **2010**, *114*, 11185.
27. A. N. Dickey, A. O. Yazaydın, R. R. Willis, R. Q. Snurr, *THE CANADIAN JOURNAL OF CHEMICAL ENGINEERING* **2012**, *90*, 825.
28. H. C. Hoffmann, B. Assfour, F. Epperlein, N. Klein, S. Paasch, I. Senkovska, S. Kaskel, G. Seifert, E. Brunner, J. Am. Chem. Soc., 2011, 133, 8681 [b] M. Oschatz, H. C. Hoffman, J. Pallmann, J. Schaber, L. Borchardt, WE. Nickel, I. Senkovska, S. Rico -Frances, J. Silvestrto-albero, S. Kaskel, E. Brunner, *Chem. Mater*. **2014**, *26*, 3280.
29. V. V. Terskikh, I. L. Moudrakovski, S. R. Breeze, S. Lang, C. I. Ratcliffe, J. A. Ripmeester, A. Sayari, *Langmuir* **2002**, *18*, 5653.

3.8. Appendix of Chapter 3:

Table A.3.1. Crystallographic parameters.

Crystal Structure Information	
Chemical formula	$Ni(4PyC)_2.DMF$
Formula weight	374.98
Crystal system	Monoclinic
Space group	*Pn*
Crystal color	Colorless prismatic crystal
Unit-cell parameter	a(Å) =6.2528(4) , b(Å) = b=12.5234(8), c(Å) =10.2768(6) , α = 90°, β = 91.269(2)°, γ = 90°, V(Å) = 804.54(9) $Å^3$
Temperature	150(2)
No. of formula units in unit cell (Z)	2
Density (g cm^{-1})	1.552
F(000)	388
Reflection Data	
No. of reflections meas.	2950
No. of obs. reflections	2938
λ (Å)	1.54178
R_{merge}	0.0334
θ_{max}	68.5
θ_{min}	3.53
R_{all}	0.0380
R_{obs}	0.0379
$wR_{2(all)}$	0.1033
Goodness-of-fit (GOOF)	1.055

Table A.3.2. Fitted Virial parameters for Xe and Kr.

Parameters	Xe	Kr
A0	-4133.994786	-2571.62304
A1	159.6838126	21.25775491
A2	-66.89678436	27.95379623
A3	116.8056215	0
A4	-38.8282651	0
A5	16.59836383	0
A6	-2.552968493	0
B0	17.11003072	14.33444069
B1	0.470784794	0
B2	-1.077293476	0

B3	0.200762598	0
B4	-0.025472412	0
B5	-1.3112E-06	0

Table A.3.3. Fitted IAST parameters for Xe/Kr (20Xe:80Kr composition) selectivity at 298 K **IISERP-MOF2**.

Constants	Xe	Kr
qA1	3.372732202	3.988676493
qA2	0	0
kA1	0.019815984	0.000794322
kA1	0	0
nA1	0.987558857	1.033957098
nA1	0	0
HA1	0.066834006	0.003168292
HA1	0	0

Table A.3.4. Fitted IAST parameters for Xe/CO_2 (1Xe:99CO_2 composition) selectivity at 298 K **IISERP-MOF2**.

Constants	Xe	CO_2
qA1	3.372732202	5.396488104
qA2	0	0
kA1	0.019815984	0.00761617
kA1	0	0
nA1	0.987558857	0.87323473
nA1	0	0
HA1	0.066834006	0.041100571
HA1	0	0

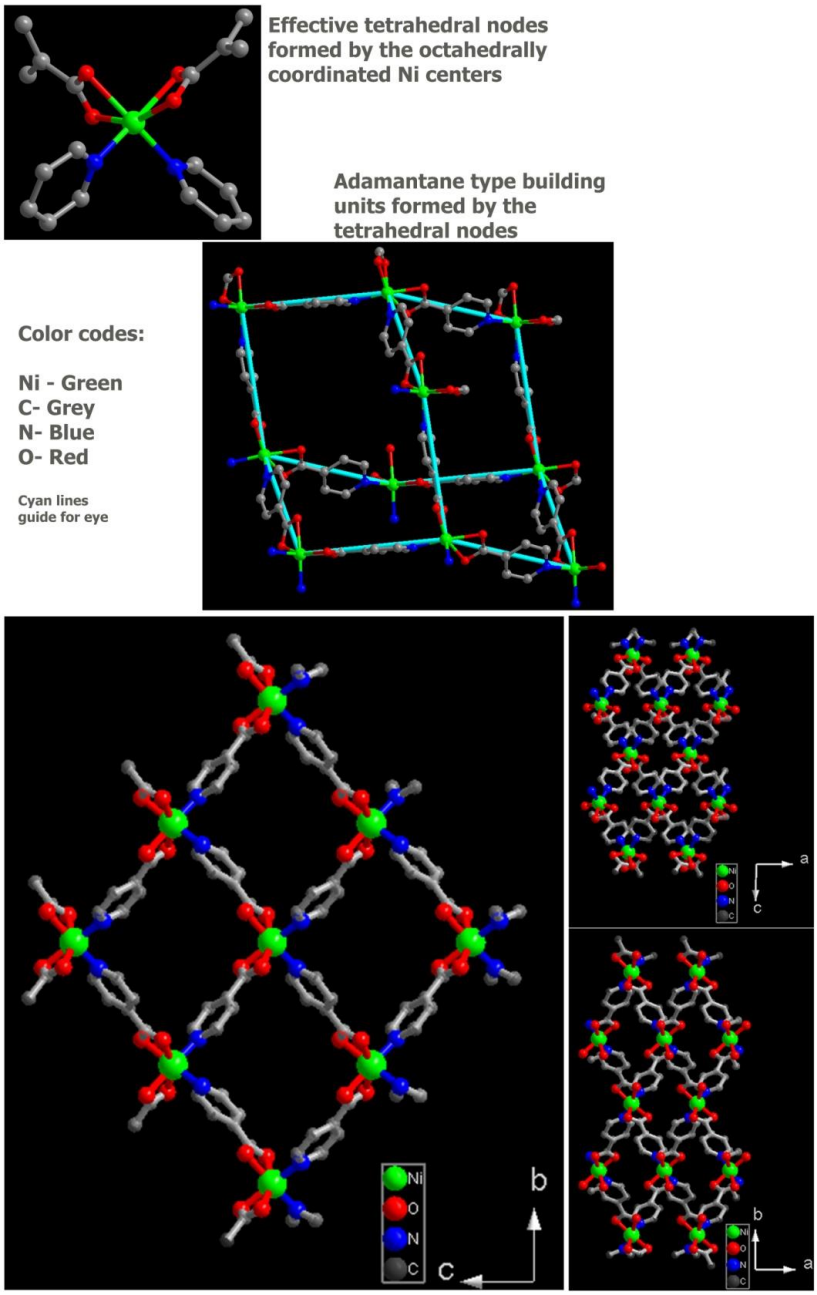

Figure A.3.1. The diamondoid framework construction of 1, showing the structure along different directions. There are uniform 1D channels along the a-axis.

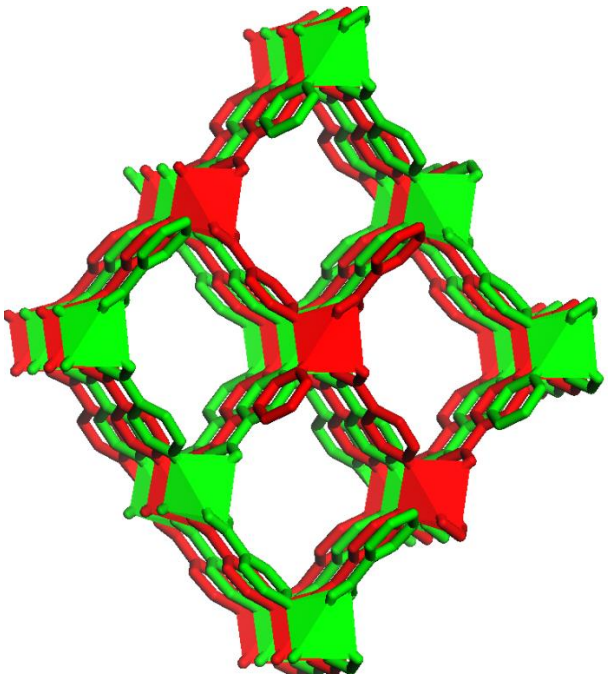

Figure A.3.2. A 2-fold interpenetrated diamondoid framework of 1, showing the uniform 1D channel along a-axis.

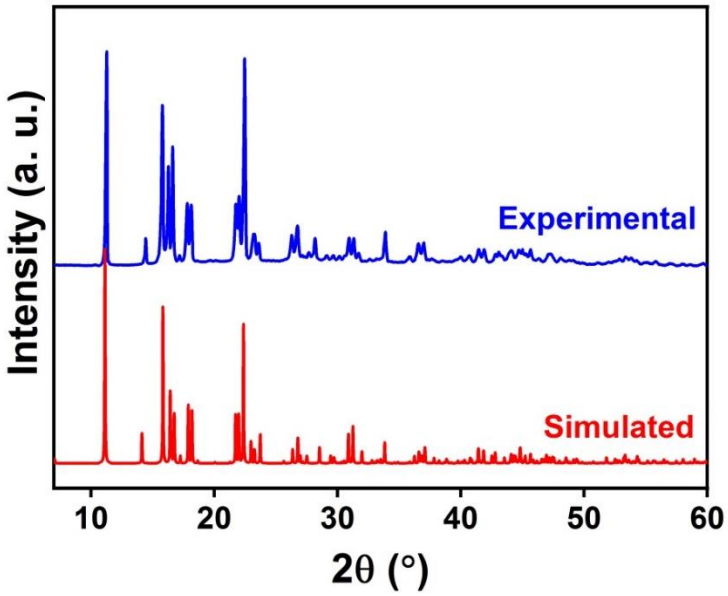

Figure A.3.3. Powder X-Ray Diffraction data of IISERP-MOF2 showing bulk phase purity of the MOF.

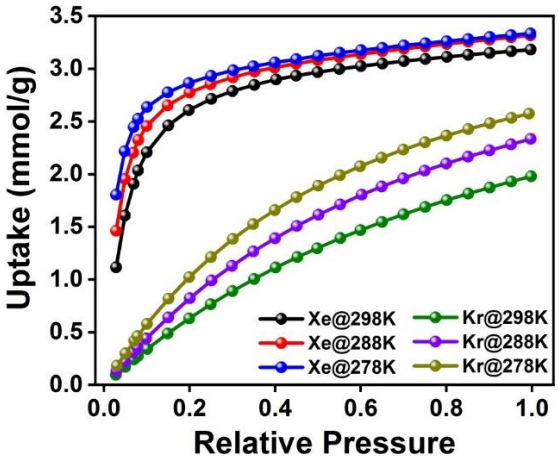

Figure A.3.4. Xe and Kr isotherms of IISERP-MOF2 at different temperatures.

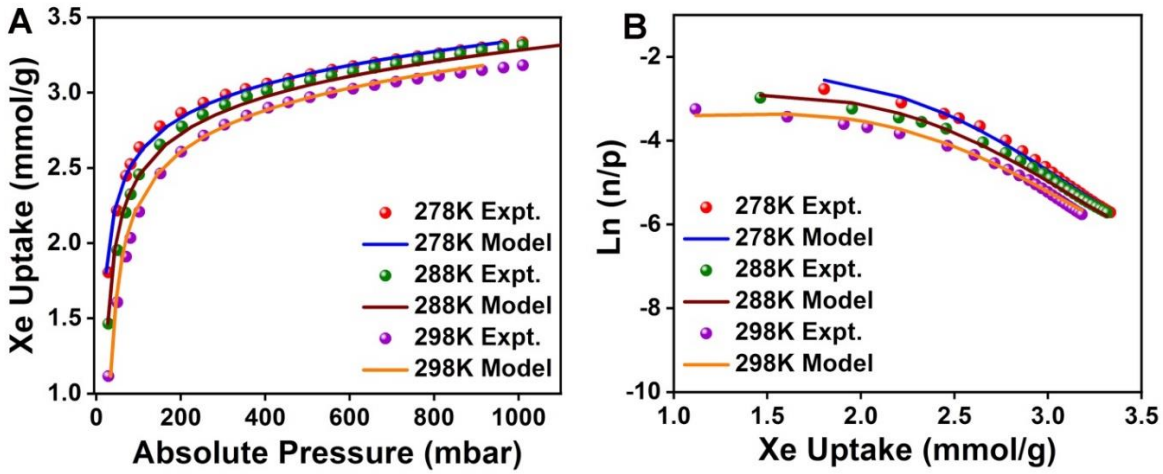

Figure A.3.5. (A) Comparison of experimental Xe isotherms with the isotherms calculated from virial model for **IISERP-MOF2** at three different temperatures, 278 K, 288 K, and 298 K. (B) Virial plots for Xe adsorption at three different temperatures, 278 K, 288 K, and 298 K.

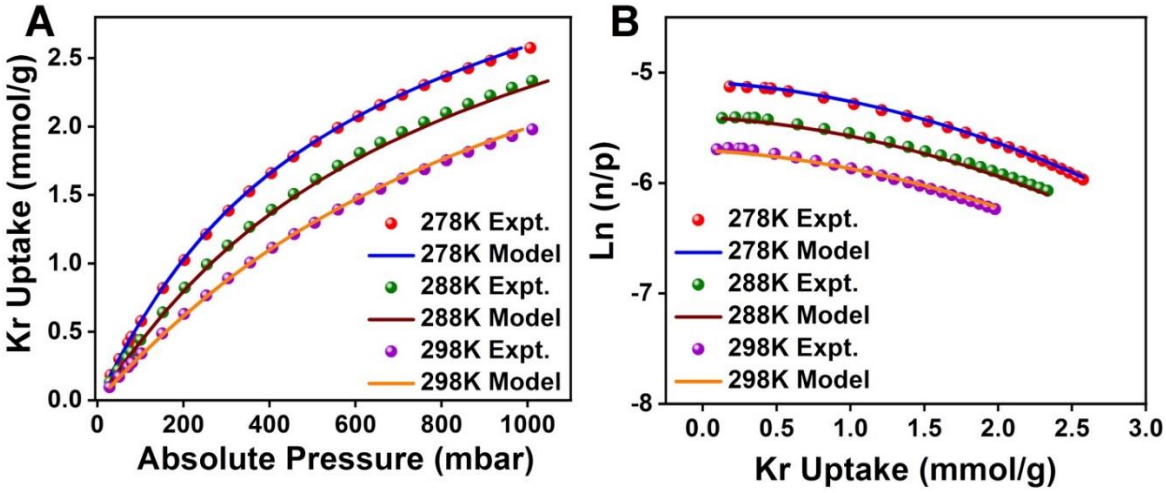

Figure A.3.6. (A) Comparison of experimental Kr isotherms with the isotherms calculated from virial model for **IISERP-MOF2** at three different temperatures, 278 K, 288 K, and 298 K. (B) Virial plots for Kr adsorption at three different temperatures, 278 K, 288 K, and 298 K.

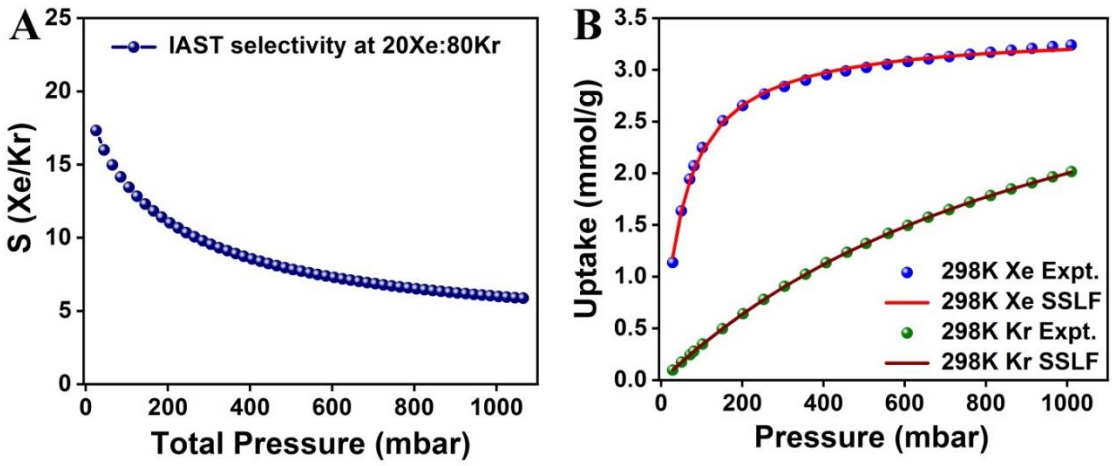

Figure A.3.7. (A) IAST selectivity of 20Xe:80Kr at 298K. (B) IAST fittings of Xe and Kr at 298K.

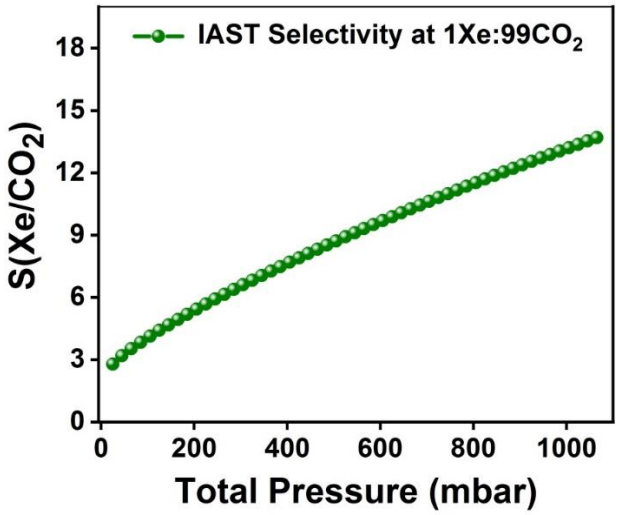

Figure A.3.8. IAST selectivity of 1Xe:99CO_2 at 298K.

Computational Details:

Notes on Xe/Kr separation using different MOF materials.

We have studied IISERP-MOF-2 (also known as Ni-4PyC-2) for its ability to separate Xe and Kr, particularly for use in nuclear fuel reprocessing. The idea behind the noble gas separation from nuclear fuel reprocessing is that radioactive ^{85}Kr has a long half-life, and should, therefore, be removed to not contaminate the atmosphere. In contrast, radioactive ^{127}Xe would decay by the time fuel is reprocessed and is less of a concern. A high purity Xe could then be repurposed for uses such as lighting, propulsion, imaging, anesthesia, and insulation. In this way, it would be beneficial to have a facile Xe/Kr separation process, as current technologies rely on cryogenic separations which are costly.

Using nanoporous materials, such as MOFs, is not a new concept, as the researchers have already performed experimental and computational studies for this very process. In 2016, Banerjee and co-workers performed high throughput simulations of Xe/Kr separations on over 125,000 hypothetical and experimental MOFs. From this analysis, they determined that a MOF, known as SBMOF-1, to be one of the best materials available for the separation with an estimated selectivity of ~70 Xe/Kr. In their work, they went on to synthesize the material and run experimental single component isotherms for both Xe and Kr to determine an experimental selectivity. When they used the data from their experimental work, they found the selectivity dropped to 16.21 Xe/Kr. This value was still the best-reported value even after their literature review, with the next closest 12.8 Xe/Kr. It should also be noted that in their work, they found that SBMOF-1 seemed to be saturated at 1 bar of Xe, with a saturation limit of ~1.4 mmol/g.

Spurred on by this work the selectivity and adsorptions of Xe and Kr were studied for IISERP-MOF-2. What was first noted was that IISERP-MOF-2 had a higher adsorption capacity for Xe, saturating at 3.53 mmol/g, compared to SBMOF-1, which saturated at ~1.4 mmol/g. It is difficult to tell the saturation capacities of Kr for each as they did not reach it for either material, however at 298 K and 1 bar, IISERP-MOF-2 had adsorption of Kr of 1.9 mmol/g compared to SBMOF-1 which had adsorption of ~1 mmol/g. The IISERP-MOF-2 adsorption isotherms for Xe and Kr are shown in Figure A.3.4. The adsorption isotherms were fitted to a Sips isotherm, as well the materials were computationally evaluated for the noble gas adsorptions. Both of these are discussed in detail later on.

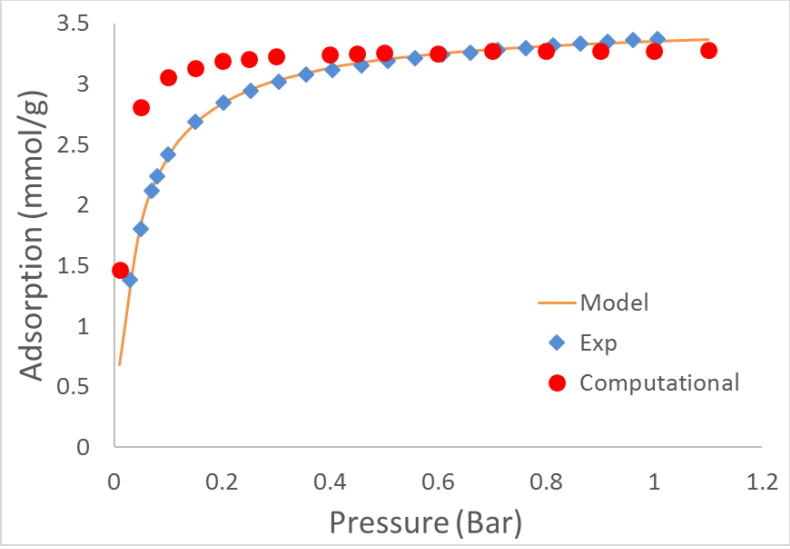

Figure A.3.9. Adsorption isotherms of Xe on IISERP-MOF-2 showing the experimentally determined values, a fitted model, and computationally determined values.

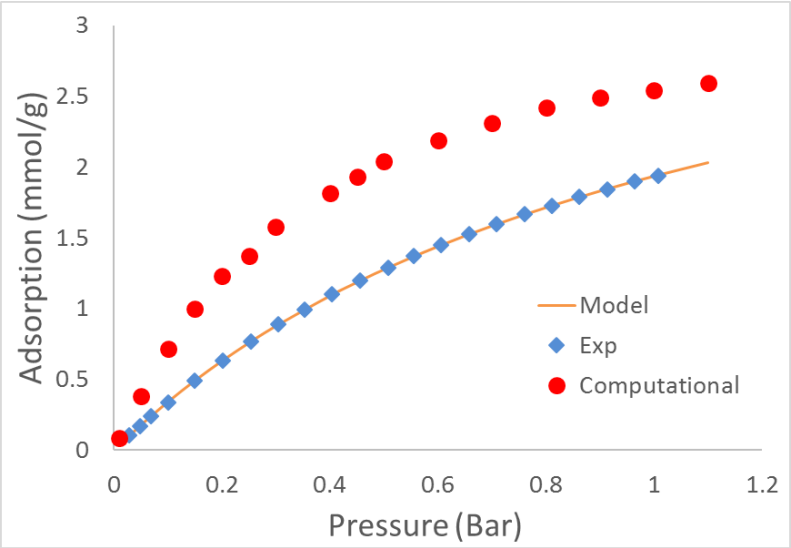

Figure A.3.10. Adsorption isotherms of Kr on IISERP-MOF-2 showing the experimentally determined values, a fitted model, and computationally determined values.

The selectivity is a bit more difficult to definitively determine the values as there are multiple ways to calculate the value. Experimentally, Banerjee and co-workers used the Henry's coefficients for the gases to calculate the selectivity. These values were calculated by looking at the low-pressure uptake for each gas (< 0.01 bar for Xe and 0.05 for Kr) and determine the straight line for adsorption as a function of pressure. SBMOF-1 has a Henry's coefficient of 38.42 mmol/(g-bar) for Xe and 2.37 mmol/(g-bar) for Kr. This gave the selectivity of SBMOF-1 of Xe/Kr of 16.21. As there was not adsorption data that low experimentally, I first fitted the data to the Sips isotherm model, shown in Eq 1. The Sips model fits the saturation capacity, adsorption constant, and degree of heterogeneity; q_s, k, and n respectively to calculate the amount adsorbed, q, at a given pressure, p. Both the Xe and Kr are shown to be well fitted by the model, as shown in Figures A.3.9 and A.3.10, as well as the low RMSE values of 0.014 and 0.0027 respectively. Using the models, and consider the adsorption up to 0.01 bar for Xe and 0.05 bar for Kr, the Henry coefficients were 67.8 mmol/(g-bar) and 3.54 mmol/(g-bar) respectively. Using these values gives a selectivity of 19.1 Xe/Kr, outperforming SBMOF-1's value of 16.2. For scale, the next best material was known as CC3 and had a selectivity of 12.8.

Eq. 1 $$q(p) = \frac{q_s(k*p)^n}{(1+(k*p)^n)}$$

Although these values showed a better selectivity than what was found for SBMOF-1, I used other selectivity determination methods to verify the results. One such method is known as a competitive model, which takes into account on a numerical basis, the competitive nature of guest molecules. To perform this model, the fitted Sips isotherms were once again used, with the difference being that in the calculation of the adsorption of guest *i*, a term is added into the denominator to show the competitive nature of guest *j*, as shown in Eq. 2. Using these equations for both the Xe and Kr and the parameters

from the fitted Sips. When using these values, and relevant pressures of 0.2 bars of Xe and 0.8 bars of Kr, gives a selectivity of 19.2 Xe/Kr. The same fitted parameters could also be used in IAST and give a selectivity of 18.5.

Eq. 2 $$q_i(p_i, p_j) = \frac{q_{s,i}(k_i * p_i)^{n_i}}{\left(1+(k_i * p_i)^{n_i}+(k_j * p_j)^{n_j}\right)}$$

The final work we did was to look at the computational results, which are shown in Figures A.3.9 and A.3.10 for Xe and Kr respectively. As this was the first-time testing Xe and Kr adsorption computationally, first the simulation parameters were validated. This was done by modifying both the CIF and the forcefields. To determine the ideal CIFs and forcefields, 2 CIFs (VASP optimized and not), 2 framework forcefields (DREIDING and UFF), and two force fields for each guest. This meant that there was a total of 8 simulations for each guest atom. Each combination had the RMSE calculated between the simulation results and the results from the fitted Sips models. For both Xe and Kr the best CIF was found to be the VASP optimized structure, while the DREIDING forcefield gave the lowest RMSE. Using those parameters, a binary GCMC simulation was performed. The selectivity from the GCMC calculation was found to be 28.6 Xe/Kr.

In summary, SBMOF-1 was stated to be the best MOF for Xe/Kr separation with a Xe saturation capacity of ~1.4 mmol/g and a selectivity of 16.2 Xe//Kr. IISERP-MOF-2, however, has a saturation capacity of Xe of 3.5 mmol/g with selectivities calculated by Henry's coefficient of 19.1, Sips competitive model of 19.2, IAST of 18.5 and a GCMC value of 28.6.

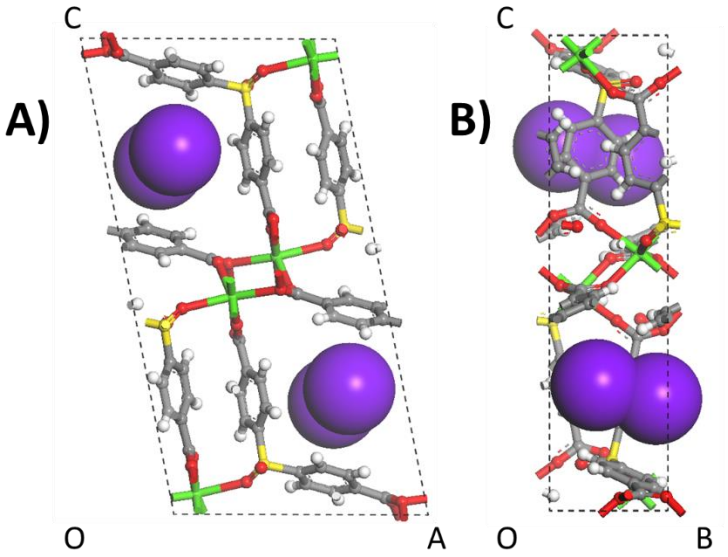

Figure A.3.11. Binding site locations of Xenon and Krypton in SBMOF-1, Xenon is coloured purple, and Krypton in orange. Krypton cannot be seen as it's binding locations are in the center of the Xenon locations.

Part 2: Organo-catalysis using Porous Framework Supported Nanoclusters.

Chapter 4

Ag Nanoparticles Supported on a Resorcinol-phenylenediamine Based COF for Chemical Fixation of CO_2

Chapter 4

4.1. Introduction:

Rising atmospheric CO_2 concentration due to the heightened use of fossil fuels has serious implications on global warming triggered climate change. So, it is highly desirable not only to develop stable materials to capture CO_2 but also to convert it into value-added products.[1-3] CO_2 is a source of small C1 building block for the synthesis of a variety of organic molecules,[4] including heterocyclic molecules.[5] Although CO_2 is abundant in the atmosphere, it possesses reluctance to react with other compounds due to its inherent stability and inertness.[4,6] Hence, it is beneficial to develop new catalysts to capture and fix CO_2 in an energy-efficient process. There are seminal examples where CO_2 has been fixed as a part of an organic backbone. For example, CO_2 forms cyclic carbonates with epoxides,[7,8] can carboxylate terminal alkynes, alkenes, amines, propargyl alcohols, propargyl amines.[9-13] In this regard, a promising example is the propargyl alcohols which react with CO_2 to yield α-alkylidene cyclic carbonates, biologically important core.[14] Organometallic compounds are the well-investigated catalysts for this reaction, but they face serious problems such as synthesis, storage, and their utilizations are laborious and, in some cases, challenging.[15,16] Metal-free and metal-based catalysts bring about CO_2 fixation. However, such reactions require high pressure of CO_2 and preeminent temperatures.[17-26] The main challenge lies in performing the reaction under ambient conditions without compromising the selectivity and yield of the products. Developing recyclable heterogeneous catalyst bring added advantages. Recently, few supported metal catalysts have been tried e.g. Ag NPs/SMR,[27] AgX@carbon,[28] ionic liquid supported AgI/OAc-.[29] Nevertheless, the matrix only supports the growth of nanoparticles serving as passive support. To a large extent, this is due to the limitations in the characterization techniques available for these types of composites. Using crystalline porous materials such as covalent organic frameworks (COFs) as supports could provide meaningful insights in decoding the activity of these heterogeneous catalysts.

COFs are fascinating synthetic porous materials due to their modular structural and functional character and high surface area.[30,31] The dimensionality (2D and 3D) and the degree of crystallinity solely depend on the judicious choice of the building blocks.[32,33] Most importantly, heteroatom decorated pore walls are the active sites for anchoring/growing catalytically active nps.[34] COFs find application in diverse fields of research such as gas separation and storage,[35] heterogeneous catalysis,[36a,36-38] energy storage, and conversion,[39] biological application[40,] and optics.[41] Earlier, in our group, we have developed efficient heterogeneous COF-np composite

catalysts for organic transformations (Heck coupling, nitro and nitrile compound reduction using $NaBH_4$) and electrocatalytic oxygen evolution reaction.[34a,42-43] Several experimental and theoretical inputs prove the active nature of the COF. COF not only supports the growth of small-sized nPs but also renders a synergistic structural and electronic influence on the catalytic process.[37a] Here, we report a microporous resorcinol-phenylenediamine COF which has exceptional stability and possesses significant CO_2 capacity and selectivity. Further, Silver nanoparticles are grown and the composite is used for the chemical fixation of CO_2 with propargyl alcohols to synthesize α-alkylidene cyclic carbonates. The activity of the COF is verified. There are very few reports on CO_2 conversion using COF where epoxides and propargyl amines are being used to prepare cyclic carbonates.[8d, 13c] But, to the best of our knowledge, this is the first report of COF based heterogeneous catalysts to convert CO_2 into α-alkylidene cyclic carbonates using propargyl alcohols with high selectivity and yields.

4.2. Materials and methods:

All the chemicals have been purchased from Sigma Aldrich and used without further purification. 2,4-dihydroxybenzene-1,3,5-tricarbaldehyde (Triformyl resorcinol) has been prepared using previously reported procedure.[44]

Synthesis of IISERP-COF15:

0.2 mmol triformyl resorcinol and 0.2 mmol phenylene diamine were dissolved in a solvent combination of 4 mL dioxane and 4 mL mesitylene. The mixture was stirred for 1 hour and then 0.5 ml of 6N acetic acid was added to it. The final reaction mixture was transferred in a pyrex tube and heated at 120°C for 3 days. The dark brown precipitate was obtained which was filtered and finally washed through soxhlet extraction using DMF, THF mixture. Yield (82%), Formula for COF $C_{36}N_6O_4H_{24}$, M. Wt. 604.623 g/mol, CHN Observed is C = 85.29; H = 3.81; N = 10.85. Calc. C = 79.97; H = 4.48; N = 15.55.

Stability studies of IISERP-COF15:

To study the stability of IISERP-COF15, it was soaked in 6N HCl, 6N H_2SO_4, 6N NaOH and even boiled in water. Samples were characterized by Powder X-Ray Diffraction (PXRD), Infra-Red spectroscopy (IR) and porosity measurements.

Synthesis of Ag@COF:

Silver nPs have been encapsulated into the COF by simply heating the mixture of COF and

$AgNO_3$ in dimethyl sulfoxide (DMSO).[10] In a typical synthesis, 100 mg of COF was dispersed in 20 ml of Ethanol. A 5ml solution (DMSO) containing 15 mg of $AgNO_3$ was added to it followed by sonication. The mixture was heated at 80°C for 24 hours. After that, the mixture was cooled, filtered and washed with dimethylformamide (DMF) and ethanol. The solid product was dried under vacuum. 6.3% Ag content was quantified by Inductively Coupled Plasma (ICP) analysis. CHN: C = 83.51; H = 4.75; N = 11.68.

General procedure of catalytic reaction:

10 mol% Ag@COF was dispersed in 3 mL of DMF and 1 mmol propargyl alcohol, 0.1 mmol 1,8-Diazabicyclo[5.4.0]undec-7-ene (DBU) were added to it. The reaction was performed at room temperature under CO_2 atmosphere (CO_2 balloon). The reaction was completed within 4 hours. The crude mixture was centrifuged to get the solid catalyst back and the product mixture was extracted with dichloromethane and washed with a saturated NaCl solution to get rid of DMF. Finally, the product mixture was purified using column chromatography on silica gel with 10% ethyl acetate and hexane mixture as eluent. The products were characterized by ^1H, ^{13}C Nuclear Magnetic Resonance spectroscopy (NMR), High Resolution Mass Spectroscopy (HRMS).

4.3. Analytical characterizations:

Powder X-ray diffraction:

All the Powder X-Ray diffractions have been carried out using a Bruker instrument with a Cu Kα (λ = 1.541 Å) source and processed using PDXL software. Variable temperature PXRD (VTPXRD) was recorded on a Pt plate sample holder and under a vacuum of 10^{-3} bar.

Thermo gravimetric Analysis:

NETSZCH TGA-DSC instrument has been used for TGA analysis. The sample was heated under N_2 flow of 20 ml/min (purge + protective) from 25°C to 600°C with a heating rate of 10 K/min.

IR spectroscopy:

IR spectra were obtained using a Nicolet ID5 attenuated total reflectance IR spectrometer in a range of 4000-600 cm^{-1}. Pellets are made using KBr to carry out the experiments.

Nuclear Magnetic Resonance spectroscopy (NMR):

NMR spectra for the catalytic products were recorded on a 400 MHz Jeol ECS-400, Bruker 400 MHz and solid-state magic angle spinning NMR spectra for COF was obtained in Bruker 500 MHz.

Field Emission-SEM:

SEM images and EDX analyses were carried out using an Ultra Plus Field Emission Scanning Electron Microscope with an integral charge compensator and embedded EsB and AsB detectors. The solid samples were dispersed in THF and sonicated for 10 mins. The dispersed samples were drop casted on silicon wafer and dried in a vacuum oven for overnight.

HR-Transmission electron microscopy (HRTEM):

TEM images were recorded using Jeol JEM220FS high-resolution transmission electron microscope (HR-TEM) equipped with a field emission source operating at 200 KeV. Solid sample was dispersed in THF and was drop casted on a Cu grid.

Adsorption studies:

All the adsorptions were performed using a 3-FLEX pore and surface area analyzer and few cases using Micromeritics ASAP. Before adsorption, the samples were soaked in Methanol for solvent exchange and evacuation.

Cyclic Voltammetry (CV):

Cyclic Voltammetry studies were performed using CH-instruments. A typical three-electrode assembly is used where saturated calomel electrode (SCE) and Pt wire were used as reference and counter electrodes respectively. The solid material was coated on the glassy carbon surface and was used as the working electrode. The electrolyte was 1M $tBuNH_4PF_6$ in Acetonitrile.

X-ray photoelectron spectroscopy (XPS):

XPS measurements were carried out using Thermo Kalpha+ spectrometer using micro-focused and monochromated AlKα radiation with energy 1486.6 eV. The base pressure of the spectrometer was better than 10^{-8} mbar during spectral acquisition. The pass energy for the spectral acquisition was kept at 50 eV for individual core-levels. The electron flood gun was utilized for providing charge compensation during data acquisition. The samples for XPS analysis were prepared inside the glove box and transferred to a vacuum transfer module which

was subsequently evacuated in the anti-chamber of the glove box. The samples were loaded onto the spectrometer using this vacuum transfer module and subsequently pumped down by turbomolecular pumps connected to the load lock chamber. This allowed us to efficiently transferring the samples without being exposed to the atmosphere. The peak fitting of the individual core-levels was done using XPS peak software with a Shirley type background.

Synthesis of starting materials:

Anhydrous acetone/butanone (2 mmol), aryl acetylene (2 mmol), and potassium t-butoxide (2 mmol) were mixed using a mortar and pestle, the mixture was kept at room temperature for 20 min. The product was extracted with 10% aqueous sodium chloride, filtered, washed with water, and dried to give as colorless crystal/brown oil.[45]

4.4. Structure solution:

The different modules employed in the Materials Studio V6 were used to perform all the calculations. The structure solution was carried out by employing a protocol that involves indexing the experimental PXRD using XCELL program. The Reflex module of the Materials Studio V6.0 (MS) was used to determine the space group which suggested that P6 is the highest possible choice of symmetry with a normalized FOM > 50. Hence the cell was constructed with the indexed unit cell in this space group. Atomic manipulations were carried out using the Materials Studio to build an initial model satisfying the connectivity requirements. On introducing the heteroatoms into the structure, the space group P6 reduced to P1. This model was then geometry optimized using a period tight-binding DFT routine (DFTB) embedded within the Material Studio. The final structure adopts a P2/m space group with a unit cell with following parameters: a = 22.1232; b = 22.1232; c = 3.5166; β = 120°. A comparison of the simulated powder XRD (PXRD) pattern of the eclipsed/staggered form vs. the experimental one is being presented here (Figure A.4.1). The unit cell and the atomic coordinates of the refined structure are presented in Table A.4.1. For the geometry optimizations of the periodic COF structures, dispersion corrected tight-binding Density Functional Theory (DFTB) was employed. The Smart algorithm was used with the force fields chosen from the Slater-Koster library. The Divide and Conquer Eigen solver implemented and the self-consistent charges with a SCC tolerance of $1x\ 10^{-8}$ were used. UFF-based Lennard-Jones dispersion corrections were included in Energy, Force and Displacement calculations and the cell were optimized. Thermal smearing with a smearing parameter of 0.005 Ha was applied. In all cases, brilliant convergence was accomplished in less than 500 SCC cycles.

4.5. Adsorption studies:

All the adsorptions were carried out using a 3-FLEX pore and surface area analyzer, Micromeritics and few cases 'Autosorb IQ', Quantachrome.

Langmuir fits:

In most cases, the isotherms were fit to the Single-Site Langmuir (SSL) equation. The Langmuir equation was solved using the solver function in Microsoft Excel following a similar protocol to Keller et al.[46] Utilizing this routine circumvents some of the problems associated with favoring either high- or low-pressure regions when linearizing the Langmuir equation and offers a balanced approach.

Single-Site Langmuir (SSL)

$$q_i = q_m \frac{k_i}{1 + k_i P} P$$

Dual-Site Langmuir (DSL)

$$q_i = q_{m,1} \frac{K_1}{1 + K_1 P} P + q_{m,2} \frac{K_2}{1 + K_2 P} P$$

Virial analysis:

The CO_2 adsorption data for the COF were measured from 0- 1bar at 248, 273 and 298 K and were fitted by the following virial equation.

ln(P) = ln(Va)+(A0+A1*Va +A2*Va^2 …+ A6*Va^6)/T+(B0+B1*Va)

Where P is pressure, Va is amount adsorbed, T is temperature, and A0, A1, A2 …, A4 and B0, B1 are temperature independent empirical parameters.

Ideal Adsorption Solution Theory (IAST):

IAST calculations were employed as described by Prausnitz et al.[47] The equation that is involved in selectivity calculations has been given below.

$$S_{1,2} = \frac{q_1/q_2}{p_1/p_2}$$

Breakthrough studies:

Breakthrough measurements are performed using Rubotherm Breakthrough analyzer. About ~250 mg of sample was pre-heated at 160°C externally. A column (3 cm long and having an internal diameter of 0.7 cm) is packed with the sample and again activated at 50°C for 12 hours under vacuum using PFEIFFER vacuum plus system. All the measurements were done at 298K and 1.5 bar. The total gas flow for CO_2/N_2 and CO_2/CH_4 is maintained at 20 ml/min and 10 ml/min respectively. The relative concentration of the gases is monitored via Cirrus 2 mass spectrometer which is equipped with a capillary heater. The internal pressure of the capillary is maintained at 10^{-6} torr. Masses corresponding to N_2 (14), CH_4 (16) and CO_2 (44) are monitored.

4.6. Results and discussions:

Synthesis and structural modeling of IISERP-COF15:

IISERP-COF15 was synthesized via a conventional Schiff base condensation reaction between triformyl-resorcinol and phenylenediamine under solvothermal conditions. The aldehyde and amine were dissolved in a mixture of dioxane and mesitylene (1:1 v/v) and 0.5 mL 6N acetic acid were added as a catalyst. The mixture was flash frozen and heated in a pyrex tube at 120°C for three days (Scheme A.2.1). The resulting solid product was purified by soxhlet extraction using dimethylformamide (DMF) and tetrahydrofuran (THF). The presence of high intensity low angle peak and several high angle peaks in the PXRD confirm the crystalline nature of the COF.

A two-dimensional (2D) COF structure was modeled in agreement with the experimental powder X-Ray diffraction, using the Material Studio Programme. The structure is formed by π-stacking of layers having hexagonal windows well agreement with the pore dimension obtained experimentally (Figure 4.1). For the structure solution, we followed a similar routine as reported in our earlier works.[34a, 37a,42,43] To determine the best possible space group, we have indexed the powder X-ray pattern in the XCELL program which yielded P6 (FOM: > 50) space group as the best-fitted highest symmetry. Atomic manipulations are adopted to construct an initial hexagonal cell. Still, the presence of the asymmetrically positioned atom lowers the symmetry to monoclinic. This structure was further geometry-optimized using a tight-binding density functional theory algorithm embedded in the Materials Studio. The lowest energy structure adopts a P2/m space group (a = 22.12; b = 22.12; c = 3.52; β = 120°, table A.4.1).

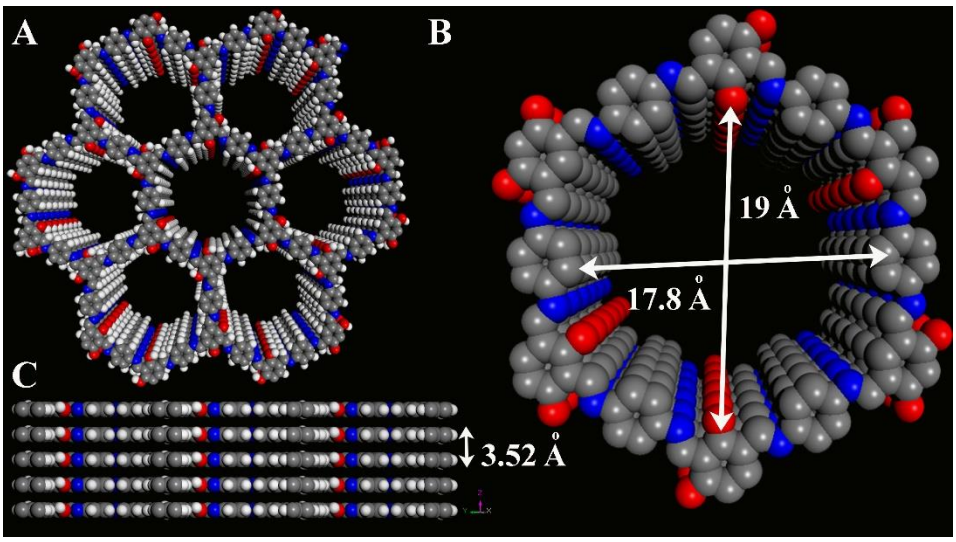

Figure 4.l. (A) Three-dimensional structure of the COF viewed along the c-axis showing the hexagonal pores. (B) Single-channel view of the COF illustrating the heteroatoms lining its pore-wall. (C) View of π-stacked layers with an AAA…. arrangement. Color codes; Gray: Carbon; Blue: Nitrogen; Red: Oxygen; White: Hydrogen.

The diffraction pattern of this model was refined against the experimental PXRD using the Pawley routine; it yielded an excellent fit (Figure 2A, refined cell: a = 22.04; b = 21.50; c = 3.52; α = 89.75°, γ = 89.85°, β = 119.91°; Rp = 4.5 and wRp = 6.56). The experimental PXRD has been compared with the eclipsed and staggered forms (Figure A.4.1). The COF crystalizes in eclipsed with a uniform one-dimensional (1D) pores of size ~14 Å (factoring the van der Waal radii of the atoms), which agrees well with the experimentally determined pore size from N_2 isotherm (Figures 4.1 and 4.2A).

Characterization of IISER-COF15:

The solid-state magic-angle spinning NMR (SS-MAS NMR) spectrum confirms the COF formation. Peaks in the range of δ= 110 to 120 ppm have been assigned to the aromatic carbons. Notably, the peak at δ= 182 ppm suggests that the -OH groups are tautomerized to keto form through intralayer hydrogen transfer (Figure A.4.2).[34a, 41a] Further, the peak at δ= 148 ppm is seen due to the imine bond (-C=N) formation in the COF. While the characteristic chemical shift due to C=C-N is observed at δ= 134 ppm suggesting the existence of the COF in the keto form under the ambient conditions. The Infra-Red (IR) stretching band at 1607 cm^{-1} is ascribed to the carbonyl vibration. Peaks at 1513 and 1457 cm^{-1} are observed due to the stretching of C=N and C=C-N bonds, respectively (Figure A.4.3).[34a] Thermal stability has been established from thermo gravimetric analysis (TGA) (Figure A.4.4). An initial mass loss (29%) is observed due to the loss of occluded solvent molecules trapped within the COF pores. The variable

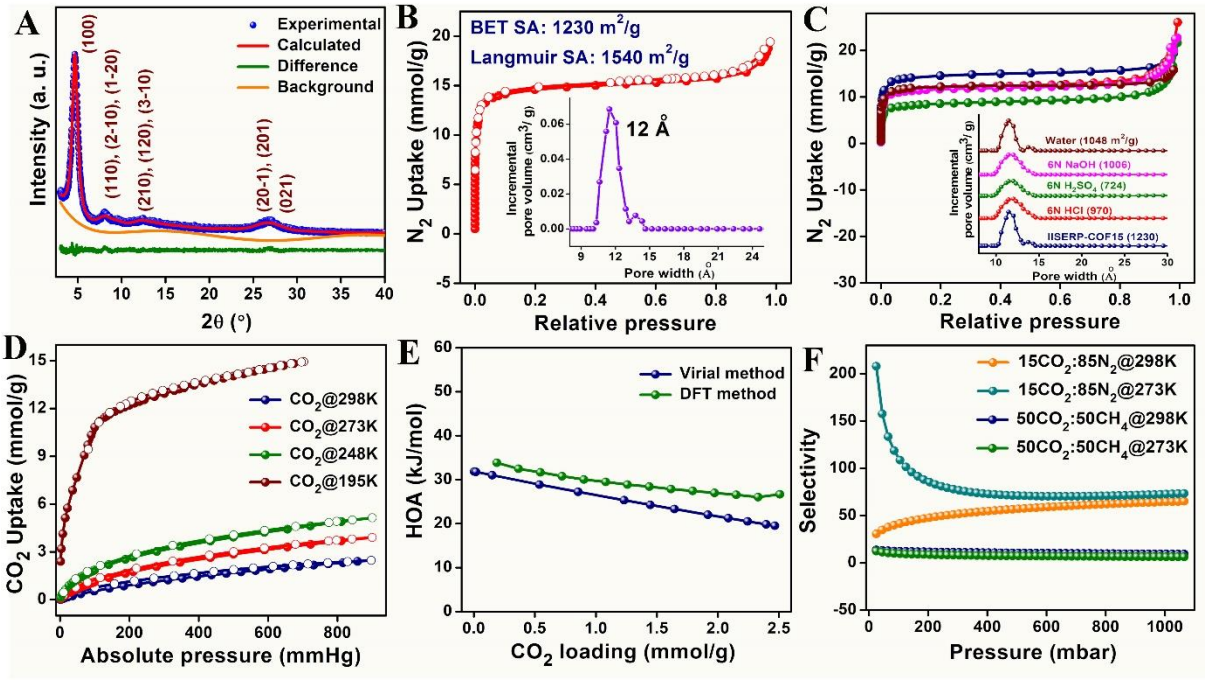

Figure 4.2. (A) Pawley fitting of the powder XRD of the COF. (B) N_2 adsorption isotherm collected at 77K; the surface areas are presented. Inset shows the pore size distribution of the COF obtained using the NLDFT model. (C) The stability of the COF to different chemical treatment is demonstrated by the N_2 adsorption isotherms and the associated pore-size distribution (inset) carried out using the treated samples. (D) CO_2 adsorption isotherms at different temperatures. (E) The heat of adsorption (HOA) for the CO_2. (F) Selectivity plots demonstrating selective CO_2 capture by the COF.

temperature PXRD (VTPXRD) shows that the COF retains its crystallinity even after heating at 250°C (Figure A.4.5).

N_2 adsorption isotherms and stability studies:

The permanent porosity of the COF was established from N_2 adsorption at 77K. The COF has a type-I adsorption isotherm with a saturation N_2 uptake of 15 mmol/g. The COF possesses significantly high Brunauer−Emmet−Teller (BET) and Langmuir surface areas 1230 and 1540 m^2/g respectively, calculated from the N_2 at 77K isotherm (Figures 4.2B and A.4.6). The non-local density functional theory (NLDFT) yields a pore-size of 12 Å and a pore volume of 0.6332 cm^3/g at P/P_0 0.96 (inset of figure 4.2B) (spherical pore model of carbon standard). The stability of IISERP-COF15 has been confirmed under various harsh chemical conditions such as 6N HCl, 6N H_2SO_4, 6N NaOH and even in boiling water for 24 hours (Figure 4.2C). Further, 77K N_2 adsorptions carried out on the post-chemically-treated samples and the extracted pore size distributions; approve the structural stability which validates well with the retention of crystallinity observed from the PXRD (inset of figure 4.2C). The exceptional stability arises due to the microporous network, keto-enol tautomerism and interlayer hydrogen bonding.

Thus, IISERP-COF15 could be a potential candidate for gas separation application particularly when the harsh environment is involved.

CO_2 adsorption studies:

The abundant heteroatom decorated sites within the micropores of the COF could provide facile interaction sites for CO_2. In order to verify this, CO_2 adsorptions were measured at four different temperatures. The COF shows moderate CO_2 uptake at room temperature (2.5 mmol/g, 1 bar). It exhibits a saturation CO_2 uptake of 15 mmol/g at 195K (Figure 2D). The zero-loading heat of adsorption (HOA) values were 32 kJ/mol and 33 kJ/mol as estimated from virial and DFT calculations, respectively (Figure 4.2E). This optimal HOA value supports a well-adjusted reversible physisorption-desorption cycle of CO_2. Further, the ideal adsorption solution theory (IAST) was adopted to calculate the selectivity of CO_2 over other gases (Figure 4.2F). The CO_2/N_2 selectivity is obtained employing a typical composition of $15CO_2$:$85N_2$ (relevant to post-combustion CO_2 capture) and it is observed that the COF has substantially high CO_2 selectivity at two different temperatures (65 at 298K and 73 at 273K, @ 1 bar). The selectivity values are comparable to the recently reported COFs.[35] The CO_2/CH_4 selectivity has also been calculated using a typical composition of $50CO_2$:$50CH_4$ (related to syngas capture) and the COF reveals selective capture of CO_2 over methane at 1 bar (selectivity: 9.3 at 298K and 6.4 at 273K) (Figures A.4.7-A.4.10, tables A.4.2-A.4.4). Thus, the porous network provides favorable sites for dipole-quadrupolar interaction of CO_2 with the framework. The spherical morphology of the COF has been evidenced by scanning electron microscopic images. The energy dispersive X-Ray analysis and the mapping show homogeneous distribution of elements in the COF (Figures A.4.11-A.4.13).

Dynamic mixed-gas separation studies:

Breakthrough studies are performed to demonstrate the dynamic separation of CO_2/N_2 and CO_2/CH_4 by IISERP-COF15. CO_2/N_2 separation is performed in a 20% CO_2 and 80% N_2 mixture at 1.5 bar pressure (total flow 20 ml/min). A retention time of 11.7 min/g is obtained for CO_2 which means one gram of material is able to generate a pure stream of N_2 from the mixture for 11 mins. CH_4/CO_2 separation is performed at a 50-50% composition (total flow 10 ml/min) and a retention time of 16 min/g is obtained. Breakthrough cycling shows absolute retention of activity in the subsequent cycle (Figure 4.3). Thus, IISERP-COF15 is able to show selective CO_2 adsorption in equilibrium as well as dynamic conditions.

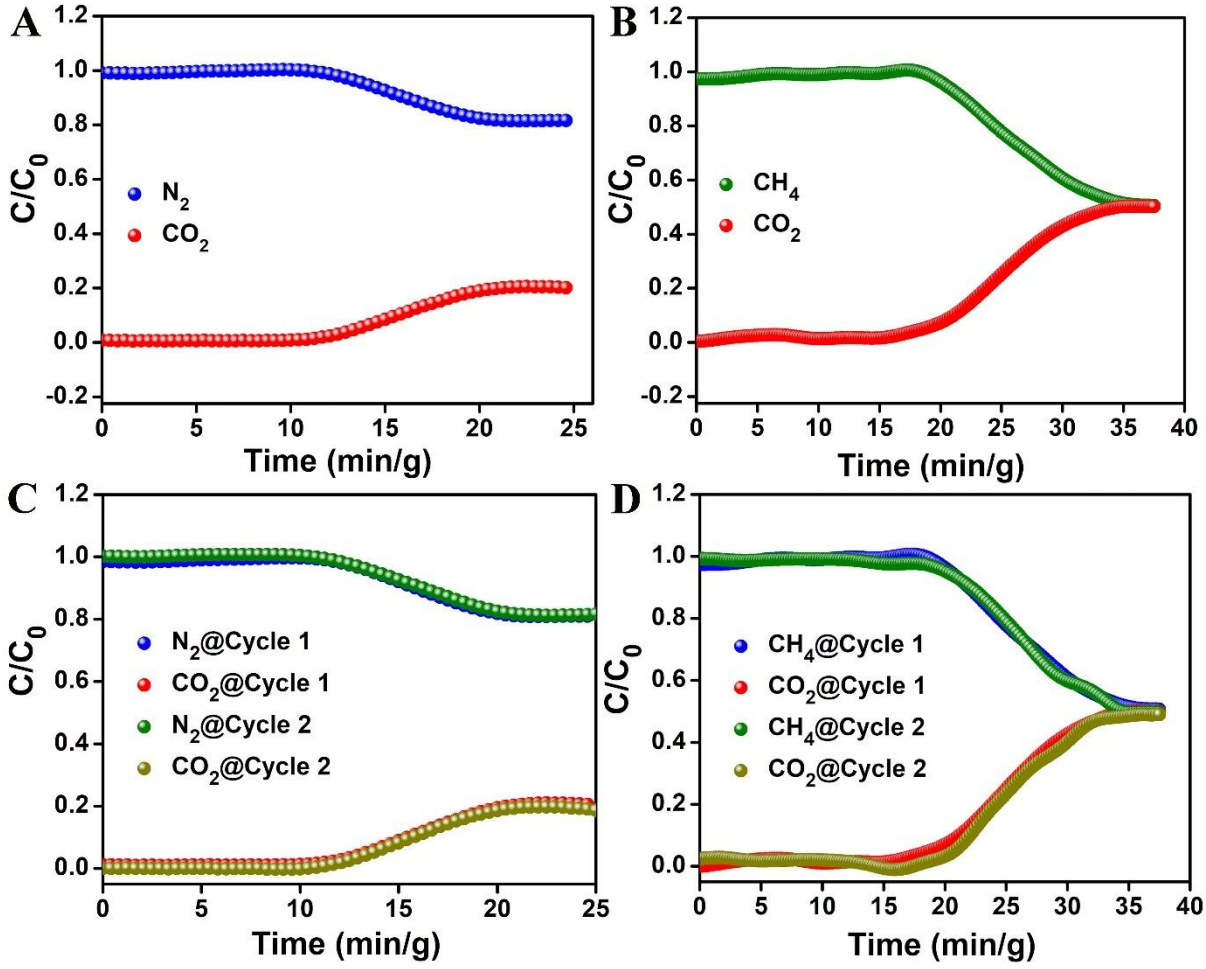

Figure 4.3. (A, B) Breakthrough studies for CO_2/N_2 and CO_2/CH_4. (C, D) Breakthrough cycling studies showing absolute retention of the separation performance of IISERP-COF15.

Synthesis and characterization of Ag@COF:

It has been observed that the silver metal/salts are active catalysts for chemical fixation of CO_2 with propargyl alcohols.[10] Our COF is having a substantial amount of selective CO2 capacity and the pore is highly functionalized. Realizing these facts, we choose to grow that Ag np that can be an active metal for CO_2 conversion,[10] we have utilized the micropores of the COF to grow small-sized uncapped silver nPs. The heteroatoms in the structure have an interaction with the metal nPs which holds the nPs firmly, preventing the leaching from the support. To load the nPs, the COF is suspended in dimethylsulphoxide (DMSO) along with $AgNO_3$ and the was heated at 80°C for 24 hours under an N_2 atmosphere to prevent any areal oxidation. This deliberate treatment generates small-sized Ag nPs on the COF. The PXRD of the composite has the characteristics low angle peaks of the COF and the peaks due to Ag nPs at higher 2θ values: 38.1° (hkl: 111), 44.1° (200), 64.1° (220) and 77.1° (311) (JCPDS file no: 89-3722) (Figure 4.4A).[48] Interestingly the Ag@COF composite did not exhibit any appreciable N_2

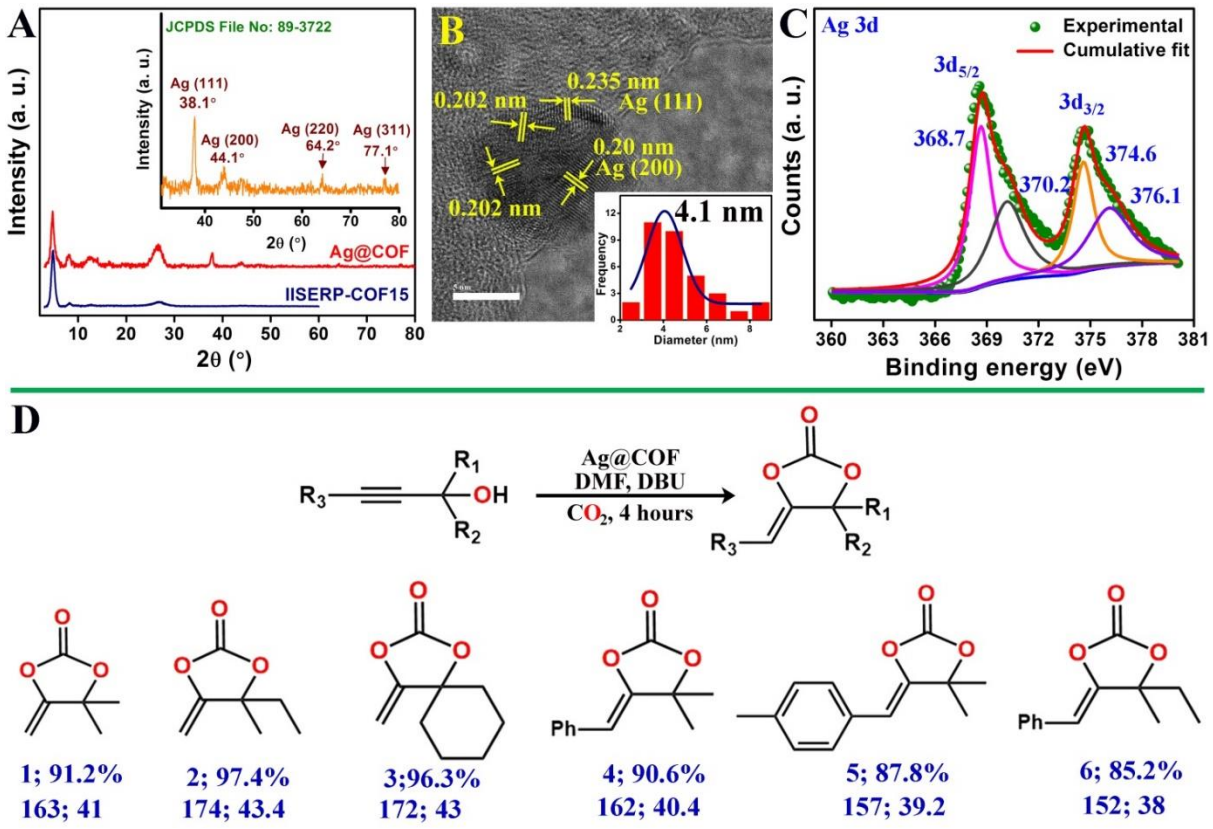

Figure 4.4. (A) PXRD of the Ag@COF. Inset is showing the indexed peaks of the Ag nanoparticles (B) High resolution TEM image of the Ag@COF. The lattice fringes of the planes of Ag nPs are indexed accordingly. (C) XPS spectrum of the Ag nP showing the splitting of 3d orbital. (D) Details of CO_2 fixation reaction with yields, TONs, and TOFs.

uptake even at 77K, however, it shows a substantial amount of CO_2 capacity (1.3 mmol/g) at 298K and 1 bar (Figures A.4.9 and A.4.10). This is important to note that upon loading Ag, the interaction sites for CO_2 are reduced, still, a significant degree of heteroatoms is free to interact with CO_2. Thus, the COF is not only serving as the support for small-sized Ag nps, but also provides a synergistic role through selective CO_2 adsorption.

The composite retains spherical morphology comparable to the parent COF (Figure A.4.11). The EDX analysis reveals that the composite has ~5% Ag loading, which is further supported by inductively coupled plasma (ICP) analysis (6.3% Ag loading). Elemental mapping verifies the homogeneous distribution of Ag on the COF (Figures A.4.11, A.4.14-A.4.18). The phase of the silver was established by high-resolution transmission electron microscopic (HRTEM) studies. Lattice fringes with d-spacing of 0.235 and 0.20 nm appear due to the exposure of Ag (111) and Ag (200) planes, respectively (Figure 4.4B). A statistical estimate of the TEM images shows the average size of the Ag nPs to be 3-5 nm (Figures A.4.19, A.4.20, A.4.21). The heteroatoms in the COF's pore provide active centers to the growth of such small-sized nPs.

Further, X-ray photoelectron spectroscopy prominently classifies the Ag(0) nPs. Two spin-orbit doublets are obtained at 368.7 ($3d_{5/2}$) and 374.6 eV ($3d_{3/2}$) with 6eV spacing corresponding to the Ag(0) (Figure 4.4C). No peaks corresponding to the oxidized form of Ag were observed.[49] Notably, The Ag $3d_{5/2}$ appears at a slightly higher value, 368.7 (instead of 368.2 eV) due to the interaction of Ag with C=N (Ag $0^{\delta+}$).[49] The peak at 399.7 eV for N1s spectrum corresponds to the Ag-N interaction, which corroborates the slight positive shift of the Ag $3d_{5/2}$ peak. The satellites of Ag peaks arise due to the asymmetric line-shapes.[49] Ag-O interaction is also confirmed from the O1s spectrum (530.8 eV for Ag-O) (Figure A.4.22).[50] All these observations admit that the COF can be compatible support to grow small-sized active Ag nPs.

Chemical fixation of CO_2 using Ag@COF as the catalyst:

Dispersion of active Ag metal nPs on the CO_2 selective COF synergistically funds to the facile conversion of CO_2 to cyclic carbonates. Importantly, the catalysis is performed at ambient conditions under a CO_2 balloon. It is noteworthy to mention that this reaction is usually performed under high pressure of CO_2. 1 mmol of propargyl alcohol and 0.1 mmol of 1,8-Diazabicyclo[5.4.0]undec-7-ene (DBU) were dissolved in 3 mL of DMF and the mixture was charged with a CO_2 balloon (table A.4.5). The optimized reaction required 10 mol% of the catalyst. It takes four hours to achieve complete conversion of the propargyl alcohol to α-alkylidene cyclic carbonates. Substrate scope has been studied and in all the cases ~90% yield is obtained (see appendix). The turnover numbers (TON) are greater than 150 and turn over frequencies (TOF) are around 40 h^{-1}, which indicates the superior performance of this relatively cheaper noble metal catalyst (Figure 4.4D). However, the TON is not remarkably high because only certain facets of the Ag nPs are exposed to the surface for catalytic activity, other atoms are buried in the COF pore. Also, the atoms in the core of the cluster are not accessible to the CO_2 and reactants.[34a,36b]

For a heterogeneous catalyst, recyclability is a critical aspect. For this Ag@COF catalyst, we registered complete retention of activity over five cycles of the reaction (Figure 4.5A). The post catalysis samples were characterized via PXRD, IR, SEM, TEM and XPS (Figures 4.5B and 4.5C). The PXRD shows that the peaks for the COF and the Ag are retained. However, after five reaction cycles, the intensities of the Ag peaks increase slightly, while the FWHM drops. This is due to the agglomeration of the nPs during the reaction. But, still, the PXRD is indexed to the Ag in zero oxidation state. We performed EDX (Figures A.4.16 and A.4.17) and

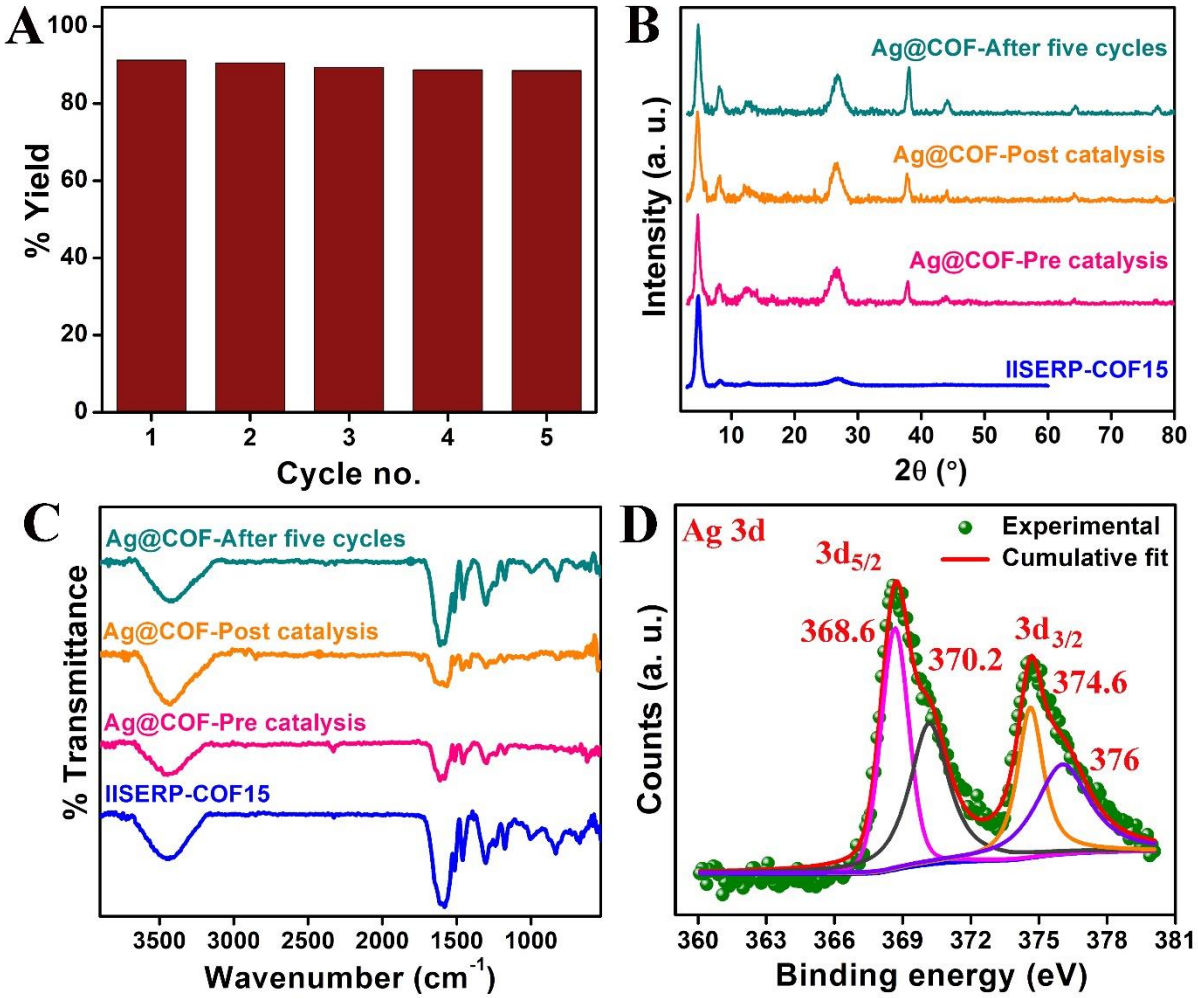

Figure 4.5. (A) A histogram plot showing the recyclability of the Ag@COF catalyst via the retention of activity over five consecutive cycles. (B) Comparison of the PXRD patterns and (C) IR spectra of the different Ag@COF samples. (D) Ag 3d XPS spectra of the spent-catalyst.

ICP analysis of the supernatant solution yielded no trace of silver representing the integrity of the Ag with the framework. Lattice fringes from the TEM of the spent catalyst were indexed to the Ag (111) and Ag (200) planes confirming the existence of Ag(0) in the composite (Figure A.4.21). The XPS spectra corroborate the observations. The Ag $3d_{5/2}$ and Ag $3d_{3/2}$ peaks are obtained at 368.6 and 374.6 eV along with two satellites at 370.2 and 376 eV, respectively (Figure 4.5D). All these studies indicate that Ag@COF is an effective heterogeneous catalyst for the chemical fixation of CO_2.

We did not perform any experiment or theoretical investigation for the mechanism of the reaction as it is well established in the literature.[27,28,29] In a typical reaction, the alkyne bond is activated by the co-ordination of the Ag nanoparticles. Base, here DBU deprotonates the alcoholic –OH group which does a nucleophilic attack on CO_2 This results in the formation of cyclic carbonates after an intramolecular ring closure reaction. Finally, the Ag@COF goes back

to its original form for the subsequent cycles. To support the claim, we have performed cyclic voltammetry (CV) of the neat COF and Ag@COF. In CV, the irreversible oxidation peak at 0.12 V vs. NHE corresponding to the Ag/Ag^+, indicates that the composite is redox-active (Figure A.4.23). This activity is an important indication of the redox process during the CO_2 fixation which is well documented in the literature.[51] Here, COF has an active role by providing support for the growth of Ag nPs, also the selective CO_2 adsorption promotes the reaction. COF provides an ideal nano-reactor where the Ag nps and CO_2 reside in close proximity in the nano-confinement.

4.7. Conclusion:

Chemical fixation is a significant route to develop a cleaner and greener approach for CO_2 mitigation. Heterogeneous catalysts are the most capable participants along this line. Here, we have demonstrated a stable COF-based catalyst that effectively fixes CO_2 with propargyl alcohols to yield α-alkylidene cyclic carbonates. Microporous architecture, high surface area and the presence of heteroatoms enable selective CO_2 capture at different temperatures. The heat of adsorption value suggests the facile regeneration of CO_2 during adsorption-desorption cycles. The COF hosts small-sized active Ag nPs which effectively converts the CO_2 to cyclic carbonates. The composite has remarkable cyclability with retention of the catalytic sites over five cycles. The COF is active support which not only grows active nps, but also provides perfect nanoconfinement for CO_2 and the reactants leading to complete fixation of CO_2. Our findings highlight the COF's role in heterogeneous catalysis and inspire the development of a recyclable heterogeneous catalyst for different CO_2 assisted organic transformations.

4.8. References:

1. H. Zhong, Y. Su, X. Chen, X. Li, R. Wang, *ChemSusChem* **2017**, *10*, 4855-4863.
2. S. Wang, K. Song, C. Zhang, Y. Shu, T. Li, B. Tan, *J. Mater. Chem. A* **2017**, *5*, 1509-1515.
3. S. Nandi, S. Collins, D. Chakraborty, D. Banerjee, P. K. Thallapally, T. K. Woo, R. Vaidhyanathan, *J. Am. Chem. Soc.* **2017**, *139*, 1734-1737.
4. M. Cokoja, C. Bruckmeier, B. Rieger, W. A. Herrmann, F. E. Kühn, *Angew. Chem., Int. Ed.* **2011**, *50*, 8510-8537.
5. L. J. Murphy, K. N. Robertson, R. A. Kemp, H. M. Tuononen, J. A. C. Clyburne, *Chem. Commun.* **2015**, *51*, 3942-3956; b) P. Bhanja, A. Modak, A. Bhaumik, *ChemCatChem* **2019**, *11*, 244-257; c) W.-F. Zheng, W. Zhang, J. Huang, Y. Yu, H. Qian, S. Ma, *Org. Chem. Front.* **2018**, *5*, 1900–1904.
6. T. Sakakura, J.-C. Choi, H. Yasuda, *Chem. Rev.* **2007**, *107*, 2365-2387.
7. a) A. Decortes, A. M. Castilla, A. W. Kleij, *Angew. Chem., Int. Ed.* **2010**, *49*, 9822-9837; b) J. Lyu, X. Zhang, P. Li, X. Wang, C. T. Buru, P. Bai, X. Guo, O. K. Farha, *Chem. Mater.* **2019**, *31*, 4166−4172; c) M. H. Beyzavi, R. C. Klet, S. Tussupbayev, J. Borycz, N. A. Vermeulen, C. J. Cramer, J. F. Stoddart, J. T. Hupp, O. K. Farha, *J. Am. Chem. Soc.* **2014**, *136*, 15861−15864;

d) A. Chakraborty, A. Achari, M. Eswaramoorthy, T. K. Maji, *Chem. Commun*. **2016**, *52*, 11378-11381.
8. a) G. Dutta, A. K. Jana, S. Natarajan, *Chem. Asian J*. **2018**, *13*, 66-72; b) V. Sharma, D. De, R. Saha, R. Das, P. K. Chattaraj, P. K. Bharadwaj, *Chem. Commun*. **2017**, *53*, 13371—13374; c) W.-Y. Gao, Y. Chen, Y. Niu, K. Williams, L. Cash, P. J. Perez, L. Wojtas, J. Cai, Y.-S. Chen, S. Ma, *Angew. Chem. Int. Ed*. **2014**, *53*, 2615 –2619; d) Y. Zhi, P. Shao, X. Feng, H. Xia, Y. Zhang, Z. Shi, Y. Mua, X. Liu, *J. Mater. Chem. A* **2018**, *6*, 374–382.
9. a) S. Li, J. Sun, Z. Zhang, R. Xie, X. Fang, M. Zhou, *Dalton Trans.* **2016**, *45*, 10577-10584; b) B. Yu, J.-N. Xie, C.-L. Zhong, W. Li, L.-N. He, *ACS Catal*. **2015**, *5*, 3940−3944; c) Y. Yuan, C. Chen, C. Zeng, B. Mousavi, S. Chaemchuen, F. Verpoort, *ChemCatChem* **2017**, *9*, 882-887; d) X.-H. Liu, J.-G. Ma, Z. Niu, G.-M. Yang, P. Cheng, *Angew. Chem. Int. Ed*. **2015**, *54*, 988 – 991; e) M. Arndt, E. Risto, T. Krause, L. J. Gooßen, *ChemCatChem* **2012**, *4*, 484–487.
10. Q.-Q. Dang, C.-Y. Liu, X.-M. Wang, X.-M. Zhang, *ACS Appl. Mater. Interfaces* **2018**, *10*, 27972-27978.
11. C. M. Williams, J. B. Johnson, T. Rovis, *J. Am. Chem. Soc.* **2008**, *130*, 14936-14937.
12. J. Hu, J. Ma, Q. Zhu, Z. Zhang, C. Wu, B. Han, *Angew. Chem., Int. Ed.* **2015**, *54*, 5399-5403.
13. a) K. Sekine, T. Yamada, *Chem. Soc. Rev.* **2016**, *45*, 4524-4532; b) Y.-G. Chen, B. Shuai, C. Ma, X.-J. Zhang, P. Fang, T.-S. Mei, *Org. Lett*. **2017**, *19*, 2969−2972; c) S. Ghosh, R. A. Molla, U. Kayal, A. Bhaumik, S. M. Islam, *Dalton Trans*. **2019**, *48*, 4657–4666.
14. H. Zhang, H.-B. Liu, J.-M. Yue, *Chem. Rev.* **2014**, *114*, 883-898.
15. Y. Kayaki, M. Yamamoto, T. Ikariya, *J. Org. Chem.* **2007**, *72*, 647-649.
16. Y. Kayaki, M. Yamamoto, T. Ikariya, *Angew. Chem., Int. Ed.* **2009**, *48*, 4194-4197.
17. Y.-B. Wang, Y.-M. Wang, W.-Z. Zhang, X.-B. Lu, *J. Am. Chem. Soc*. **2013**, *135*, 11996-12003.
18. Y.-B. Wang, D.-S. Sun, H. Zhou, W.-Z. Zhang, X.-B. Lu, *Green Chem.* **2014**, *16*, 2266-2272.
19. S. Kikuchi, S. Yoshida, Y. Sugawara, W. Yamada, H.-M. Cheng, K. Fukui, K. Sekine, I. Iwakura, T. Ikeno, T. Yamada, *Bull. Chem. Soc. Jpn*. **2011**, *84*, 698-717.
20. S. Yoshida, K. Fukui, S. Kikuchi, T. Yamada, *J. Am. Chem. Soc.* **2010**, *132*, 4072-4073.
21. Z.-Z. Yang, Y. Zhao, H. Zhang, B. Yu, Z. Ma, G. Ji, Z. Liu, *Chem, Comm.* **2014**, *50*, 13910-13913.
22. Z. Yang, B. Yu, H. Zhang, Y. Zhao, Y. Chen, Z. Ma, G. Ji, X. Gao, B. Han, Z. Liu, *ACS Catal.* **2016**, *6*, 1268-1273.
23. Y. Inoue, J. Ishikawa, M. Taniguchi, H. Hashimoto, *Bull. Chem. Soc. Jpn.* **1987**, *60*, 1204-1206.
24. W. Yamada, Y. Sugawara, H. M. Cheng, T. Ikeno, T. Yamada, *Eur. J. Org. Chem*. **2007**, 2604–2607.
25. Y. Gu, F. Shi, Y. Deng, *J. Org. Chem.* **2004**, *69*, 391-394.
26. J. Hu, J. Ma, Q. Zhu, Q. Qian, H. Han, Q. Mei, B. Han, *Green Chem.* **2016**, *18*, 382-385.
27. M. Cui, Q. Qian, Z. He, J. Ma, X. Kang, J. Hu, Z. Liu, B. Han, *Chem. Eur. J.* **2015**, *21*, 15924-15928.
28. J. Qiu, Y. Zhao, H. Wang, G. Cui, J. Wang, *RSC Adv*. **2016**, *6*, 54020-54026.
29. Y. Yuan, Y. Xie, C. Zeng, D. Song, S. Chaemchuen, C. Chen, F. Verpoort, *Green Chem.* **2017**, *19*, 2936-2940.
30. a) M. S. Lohse, T. Bein, *Adv. Funct. Mater.* **2018**, *28*, 1705553-1705624; b) S. Kandambeth, K. Dey, R. Banerjee, *J. Am. Chem. Soc.* **2019**, *141*, 1807−1822; c) L. Ascherl, E. W. Evans, M. Hennemann, D. D. Nuzzo, A. G. Hufnagel, M. Beetz, R. H. Friend, T. Clark, T. Bein, F. Auras, Nat. Commun. **2018**, *9*, No. 3802; d) X. Zhao, P. Pachfule, S. Li, T. Langenhahn, M. Ye, C. Schlesiger, S. Praetz, J. Schmidt, A. Thomas, *J. Am. Chem. Soc*. **2019**, *141*, 6623−6630; e) S. Kandambeth, A. Mallick, B. Lukose, M. V. Mane, T. Heine, R. Banerjee, *J. Am. Chem. Soc*. **2012**, *134*, 19524−19527.
31. a) N. Huang, P. Wang, D. Jiang, *Nat. Rev. Mat.* **2016**, *1*, 16068-16087; b) X. Feng, X. Dinga, D. Jiang, *Chem. Soc. Rev*. **2012**, *41*, 6010–6022; c) T. Banerjee, F. Haase, G. K. Savasci, K. Gottschling,C. Ochsenfeld, B. V. Lotsch, *J. Am. Chem. Soc*. **2017**, *139*, 16228−16234; d) S. K. Konavarapu, K. Biradha, Cryst. Growth Des. **2019**, *19*, 362−368; e) P. Das, S. K. Mandal,

Chem. Mater. **2019**, *31*, 1584−1596 f) Q. Sun, B. Aguila, L. D. Earl, C. W. Abney, L. Wojtas, P. K. Thallapally, S. Ma, *Adv. Mater*. **2018**, No. 1705479.
32. C. S. Diercks, O. M. Yaghi, *Science* **2017**, *355*, 1585-1593.
33. a) A. M. Evans, L. R. Parent, N. C. Flanders, R. P. Bisbey, E. Vitaku, M. S. Kirschner, R. D. Schaller, L. X. Chen, N. C. Gianneschi, W. R. Dichtel, *Science* **2018**, *361*, 52-57; b) D. R.-S.-Miguel, F. Zamora, *Chem. Soc. Rev*. **2019**, *48*, 4375-4386.
34. a) D. Chakraborty, S. Nandi, D. Mullangi, S. Haldar, C. P. Vinod, R. Vaidhyanathan, *ACS Appl. Mater. Interfaces* **2019**, *11*, 15670-15679; b) S. M. J. Rogge, A. Bavykina, J. Hajek, H. Garcia, A. I. Olivos-Suarez, A. Sepu´lveda-Escribano, A. Vimont, G. Clet, P. Bazin, F. Kapteijn, M. Daturi, E. V. Ramos-Fernandez, F. X. Llabre´s i Xamena, V. Van Speybroeck, J. Gascon, *Chem. Soc. Rev*. **2017**, *46*, 3134—3184.
35. a) Y. Zeng, R. Zou, Y. Zhao, *Adv. Mater.* **2016**, *28*, 2855-2873; b) N. Huang, R. Krishna, D. Jiang, *J. Am. Chem. Soc*. **2015**, *137*, 7079−7082; c) H. Wei, S. Chai, N. Hu, Z. Yang, L. Wei, L. Wang, *Chem. Commun*. **2015**, *51*, 12178—12181; d) Y. Ge, H. Zhou, Y. Ji, L. Ding, Y. Cheng, R. Wang, S. Yang, Y. Liu, X. Wu, Y. Li, J. *Phys. Chem. C* **2018**, *122*, 27495−27506; e) A. Modak, S. Jana, *Microporous and Mesoporous Materials* **2019**, *276*, 107-132.
36. a) D. Mullangi, S. Nandi, S. Shalini, S. Sreedhala, C. P. Vinod, R. Vaidhyanathan, *Sci. rep.* **2015**, *5*, 10876; b) D. Mullangi, D. Chakraborty, A. Pradeep, V. Koshti, C. P. Vinod, S. Panja, S.l Nair, R. Vaidhyanathan, *Small* **2018**, *14*, 1801233; c) D. Kaleeswaran, R. Antony, A. Sharma, A. Malani, R. Murugavel, *ChemPlusChem* **2017**, *82*, 1253−1265.
37. a) S. Nandi, S. K. Singh, D. Mullangi, R. Illathvalappil, L. George, C. P. Vinod, S. Kurungot, R. Vaidhyanathan, *Adv. Energy Mater.* **2016**, *6*, 1601189-1601200; b) S.-Y Ding, J. Gao, Q. Wang, Y. Zhang, W.-G. Song, C.-Y Su, W. Wang, *J. Am. Chem. Soc*. **2011**, *133*, 19816−19822; c) Q. Fang, J. Wang, S. Gu, R. B. Kaspar, Z. Zhuang, J. Zheng, H. Guo, S. Qiu, Yushan Yan, *J. Am. Chem. Soc*. **2015**, *137*, 8352-8355; d) S. Lu, Y. Hu, S. Wan, R. McCaffrey, Y. Jin, H.i Gu, W. Zhang, *J. Am. Chem. Soc*. **2017**, *139*, 17082−17088.
38. a) Y. Zhang, Y. Hu, J. Zhao, E. Park, Y. Jin, Q. Liu, W. Zhang, *J. Mater. Chem. A* **2019**, *7*, 16364-16371; b) Y. Han, M. Zhang, Y.-Q. Zhang, Z.-H. Zhang, *Green Chem*. **2018**, *20*, 4891-4900.
39. a) S. Haldar, K. Roy, S. Nandi, D. Chakraborty, D. Puthusseri, Y. Gawli, S. Ogale, R. Vaidhyanathan, *Adv. Energy Mater.* **2018**, *8*, 1702170-1702181; b) A. Halder, M. Ghosh, A. Khayum M, S. Bera, M. Addicoat, H. S. Sasmal, S. Karak, S. Kurungot, R. Banerjee, *J. Am. Chem. Soc*. **2018**, *140*, 10941−10945; c) T. Banerjee, K. Gottschling,G.kcen Savasci, C. Ochsenfeld, B. V. Lotsch, *ACS Energy Lett*. **2018**, *3*, 400−409; d) P. Bhanja, K. Bhunia, Sa.j K. Das, D. Pradhan, R. Kimura, Y. Hijikata, S. Irle, A. Bhaumik, *ChemSusChem* **2017**, *10*, 921 – 929.
40. S. Mitra, H. S. Sasmal, T. Kundu, S. Kandambeth, K. Illath, D. Díaz Díaz, R. Banerjee, *J. Am. Chem. Soc.* **2017**, *139*, 4513-4520.
41. a) S. Haldar, D. Chakraborty, B. Roy, G. Banappanavar, K. Rinku, D. Mullangi, P. Hazra, D. Kabra, R. Vaidhyanathan, *J. Am. Chem. Soc*. **2018**, *140*, 13367-13374; b) C. Krishnaraj, A. M. Kaczmarek, H. S. Jena, K. Leus, N. Chaoui, J. Schmidt, R. V. Deun, P. V. D.Voort, *ACS Appl. Mater. Interfaces* **2019**, *11*, 27343−27352.
42. D. Mullangi, V. Dhavale, S. Shalini, S. Nandi, S. Collins, T. Woo, S. Kurungot, R. Vaidhyanathan, *Adv. Energy Mater.* **2016**, *6*, 1600110.
43. D. Chakraborty, S. Nandi, R. Illathvalappil, D. Mullangi, R. Maity, S. K. Singh, S. Haldar, C. P. Vinod, S. Kurungot, R. Vaidhyanathan, *ACS Omega* **2019**, 10.1021/acsomega.9b01777.
44. S. Haldar, D. Chakraborty, B. Roy, G. Banappanavar, K. Rinku, D. Mullangi, P. Hazra, D. Kabra, R. Vaidhyanathan, *J. Am. Chem. Soc.* **2018**, *140*, 13367−13374.
45. H. Miyamoto, S. Yasaka, K. Tanaka, *Bull. Chem. Soc. Jpn*. **2001**, *74*, 185-186.
46. M. Saleh, H. Lee, K. C. Kemp, K. S. Kim, *ACS Appl. Mater. Interfaces* **2014**, *6*, 7325.
47. A. L. Myers, J. M. Prausnitz, *AIChE J*. **1965**, *11*, 121.
48. K. Anandalakshmi, J. Venugobal, V. Ramasamy, *Appl. Nanosci*. **2016**, *6*, 399-408.
49. A. Dolatkhah, P. Jani, L. D. Wilson, *Langmuir* **2018**, *34*, 10560−10568.

50. N. Wei, H. Cui, Q. Song, L. Zhang, X. Song, K. Wang, Y. Zhang, J.Li, J. Wen, J. Tian, *Applied Catalysis B: Environmental* **2016**, doi:10.1016/j.apcatb.2016.05.040.
51. M. Giovanni, M. Pumera, *Electroanalysis* **2012**, *24*, 615 – 617.

Chapter 4 has been adopted form the reference "Chakraborty *et al*. *Chem. Asian J.* **2019,** *14,* 4767-4773." With permission from the Wiley Online Library.

Appendix of Chapter 4:

Table A.4.1. Atomic coordinates of the IISERP-COF15.

Space group: P2/m; Crystal system: Monoclinic.

Unit cell parameters: a = 22.1232; b = 22.1232; c = 3.5166; β = 120°.

Atom	x	y	z
C1	0.52308	0.57097	0.50046
C2	0.56885	0.54575	0.50003
C3	0.54617	0.47478	0.49957
N4	0.40567	0.5494	0.50029
C5	0.42222	0.6142	0.49988
C6	0.37218	0.63841	0.49971
C7	0.30234	0.59384	0.49998
C8	0.43023	0.95917	0.50022
C9	0.45912	0.03107	0.49982
C10	0.52879	0.07226	0.49969
N11	0.44344	0.85439	0.49997
C12	0.3795	0.81238	0.50012
C13	0.35281	0.73728	0.49971
C14	0.39646	0.70944	0.49944
C15	0.04452	0.47322	0.49995
C16	0.97555	0.42882	0.50028
C17	0.93059	0.4551	0.50011
N18	0.13984	0.59196	0.49991
C19	0.18499	0.57215	0.4998
C20	0.25766	0.62105	0.49995
C21	0.28332	0.69327	0.49998
O22	0.27739	0.52378	0.49983
O23	0.24098	0.72119	0.50014

Table A.4.2. Parameters for virial equation fitting:

Parameters	IISERP-COF15
A0	-2951.162772
A1	-110.0743939
A2	117.6941644
A3	0
B0	15.10078922
B1	1.059887854
B2	-0.508260504
B3	0

Table A.4.3. Parameters for the IAST fitting for CO_2/N_2 ($15CO_2$:$85N_2$ composition) at 273K and 298K.

Constants	Gas A		Gas B	
	273 K	298 K	273 K	298 K
qA1	11.78884011	6.160535346	0.15964648	1.281039191
qA2	0	0	0	0
kA1	0.003095883	0.000797777	0.000401595	0.00026649
kA1	0	0	0	0
nA1	0.718040532	0.939845588	1.210235768	0.725721546
nA1	0	0	0	0
HA1	0.03649687	0.004914735	6.41133E-05	0.000341384
HA1	0	0	0	0

Table A.4.4. Parameters for the IAST fitting for CO_2/CH_4 ($50CO_2$:$50CH_4$ composition) at 273K and 298K.

Constants	Gas A		Gas B	
	273 K	298 K	273 K	298 K
qA1	11.56957807	6.709843892	2.483991464	2.325340081
qA2	0	0	0	0
kA1	0.003106718	0.000857601	0.00076661	0.00015621
kA1	0	0	0	0
nA1	0.721399821	0.914556743	0.882725927	0.972028992
nA1	0	0	0	0
HA1	0.035943412	0.00575437	0.001904252	0.00036324
HA1	0	0	0	0

Table A.4.5. Comparative table of the catalytic performances of different catalysts used for CO_2 fixation into propargyl alcohols.

Sr. No.	Catalyst	Reaction condition	%Yields of the cyclic carbonates	References
1	$P(n\text{-}C_4H_9)_3$	Supercritical CO_2 at 10 MPa; 100°C, 15 hours.	>90	*J. Org. Chem.* **2007**, *72*, 647-649.
2	N-Heterocyclic Olefin (NHO)	2 MPa CO_2; 60°C, 12 hours	>80	*J. Am. Chem. Soc.* **2013**, *135*, 11996−12003.
3	N-Heterocyclic carbenes	4.5 MPa CO_2; 60°C, 12 hours	>95	*Angew. Chem. Int. Ed.* **2009**, *48*, 4194 –4197.
4	Alkoxide-functionalized imidazolium betaines	2 MPa CO_2; 60°C, 5 hours	>95	*Green Chem.* **2014**, *16*, 2266–2272.
5	AgOAc	1 MPa CO_2; RT, 5 hours	80-90	*Bull. Chem. Soc. Jpn.* **2011**, *84*, 698-717.
6	AgOAc and optically active ligands	1 MPa CO_2; 0°C, 48 hours	98	*J. Am. Chem. Soc.* **2010**, *132*, 4072–4073.
7	F-MOP-3-Ag	1 MPa CO_2; 25°C, 10 hours	>99	*Chem. Commun.* **2014**, *50*, 13910-13913.

8	poly(PPh_3)-azo-Ag	1 MPa CO_2; 25°C, 18 hours	>90	*ACS Catal.* **2016**, *6*, 1268−1273.
9	[BMIm][$PhSO_3$]/CuCl	0.5-1 MPa CO_2; 90-120°C, 8 hours	>90	*J. Org. Chem.* **2004**, *69*, 391-394.
10	ZnI_2/NEt_3	1 MPa CO_2; 30°C, 10 hours	99	*Green Chem.* **2016**, *18*, 382-385.
11	AgNPs/SMR	1 MPa CO_2; 25°C, 10 hours	>90	*Chem. Eur. J.* **2015**, *21*, 15924-15928.
12	AgX@carbon	0.1 MPa CO_2; RT, 4 hours	>90	*RSC Adv.* **2016**, *6*, 54020-54026.
13	AgI/OAc^- (AgI/IL)	0.1 MPa CO_2; 45°C, 2.5 hours	>90	*Green Chem.* **2017**, *19*, 2936-2940.
14	**Ag@COF**	**0.1 MPa CO_2; 25°C, 4 hours**	**>90**	**This Work**

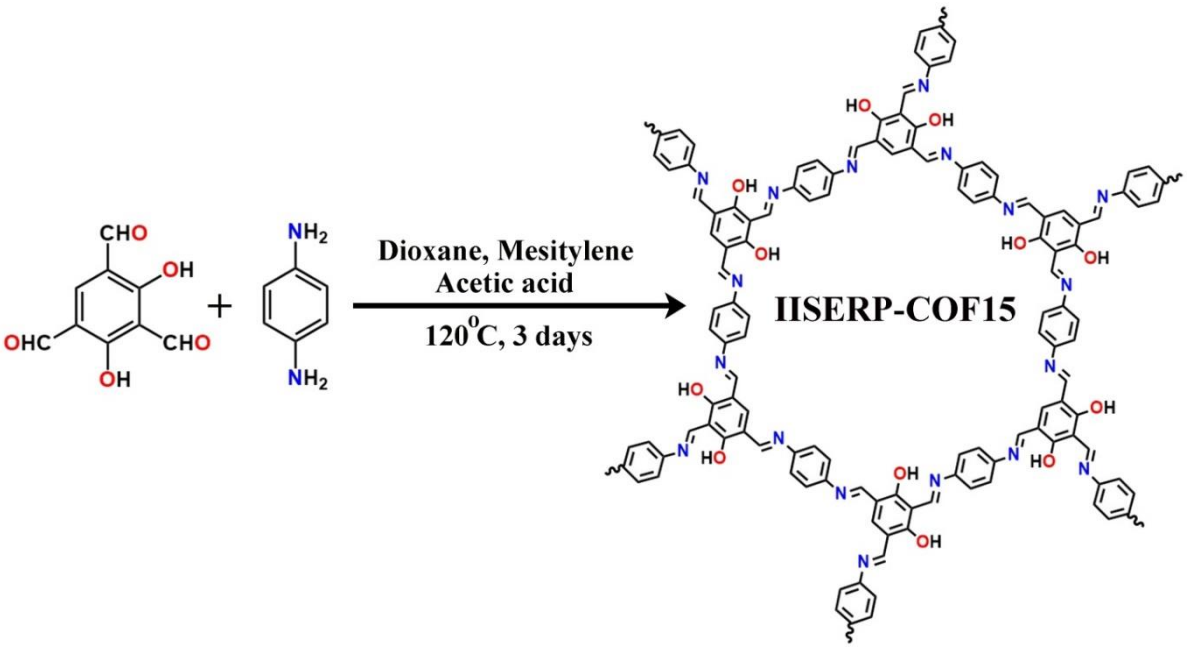

Scheme A.4.1. Schematic representation of the synthesis procedure of IISERP-COF15.

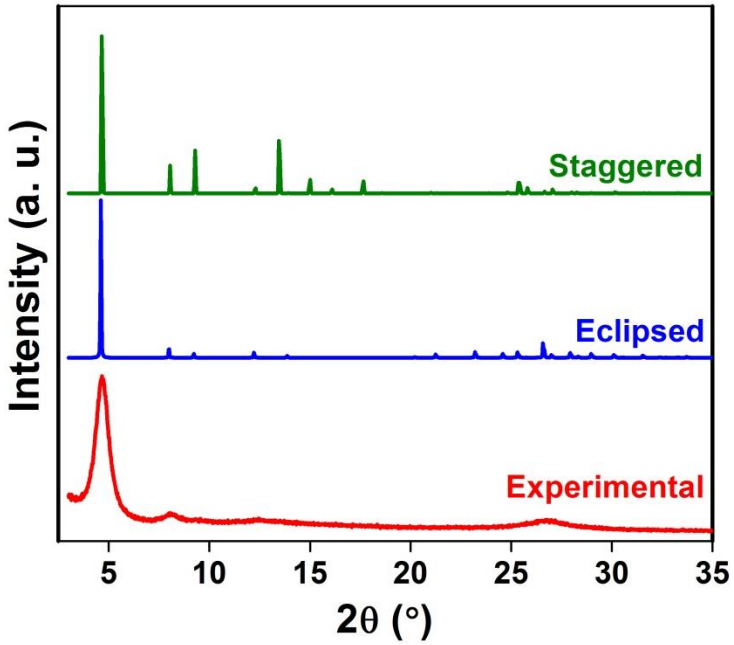

Figure A.4.1. Comparison of the experimental and the simulated PXRDs of IISERP-COF15.

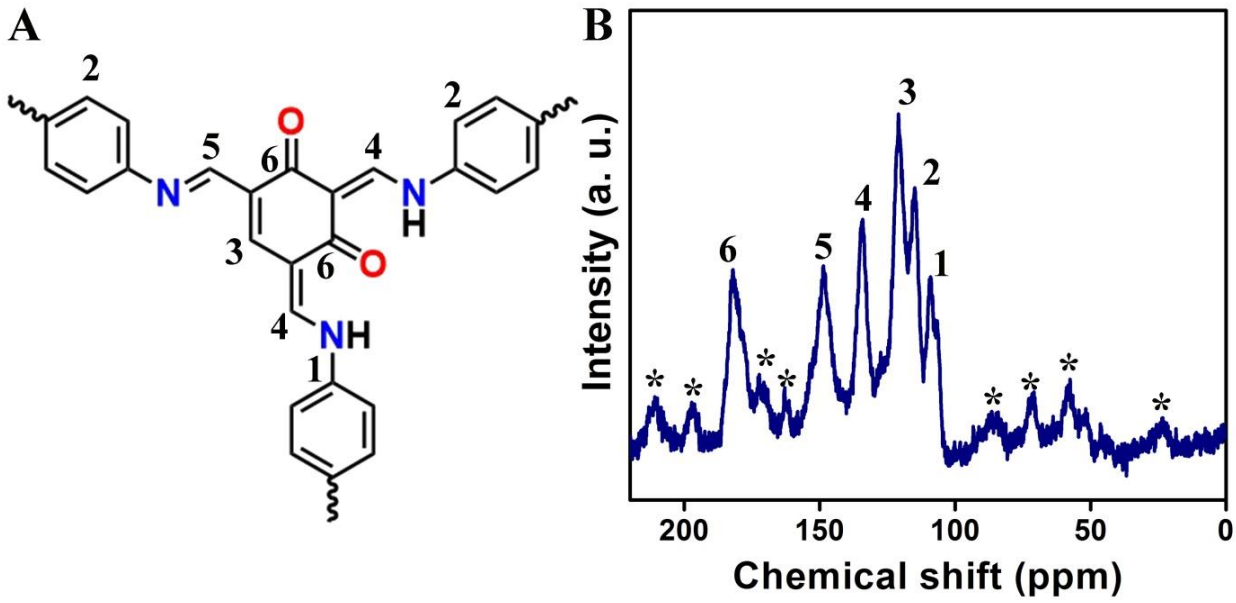

Figure A.4.2. Solid-state ^{13}C Magic Angle Spinning NMR spectrum of IISERP-COF15 showing the characteristics peaks. '*' marked peaks are the spinning sidebands.

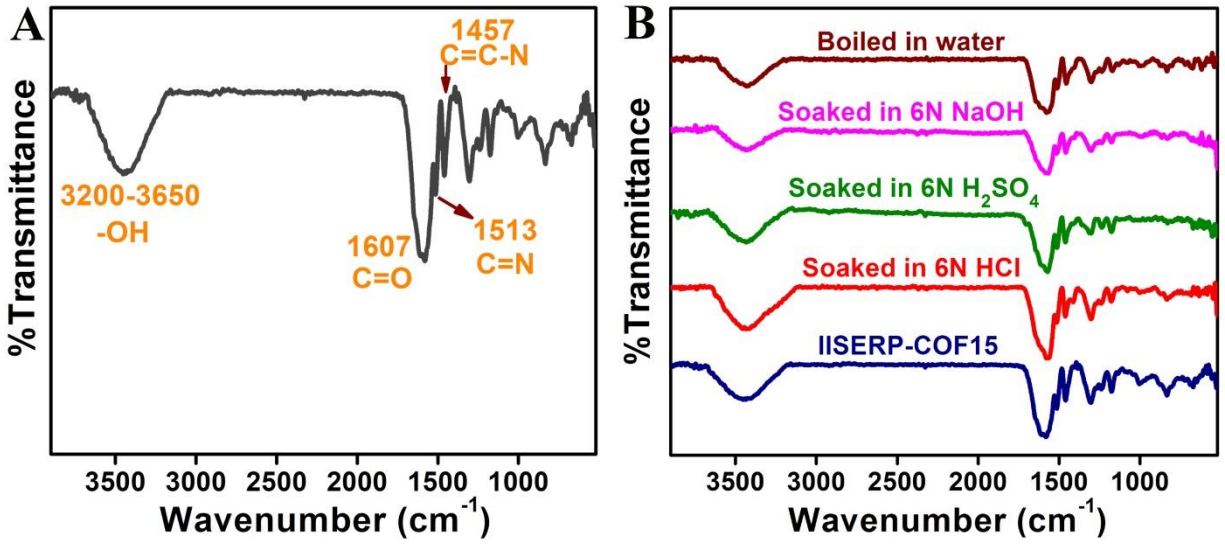

Figure A.4.3. (A) Infra-Red (IR) spectra of IISERP-COF15 showing the characteristics of stretching frequencies. (B) IR spectra showing the stability of IISERP-COF15 towards different chemical treatments e.g. acids, bases and even to boiling in water for 24 hours.

Discussion: IISERP-COF15 exists predominantly in the keto form under ambient conditions. C=O stretching frequency is observed at 1607 cm^{-1}. Moreover, the 1457 cm^{-1} peak corresponding to –C=C-N supports the existence of COF in the keto form in the solid-state. Imine bond vibrates at 1513 cm^{-1} and the –OH vibration is observed at ~3400 cm^{-1}. (*Source: Infrared and Raman Spectra of Inorganic and Coordination Compounds, Part B, Applications in Coordination, Organometallic, and Bioinorganic Chemistry, 6th Edition, Kazuo Nakamoto*).

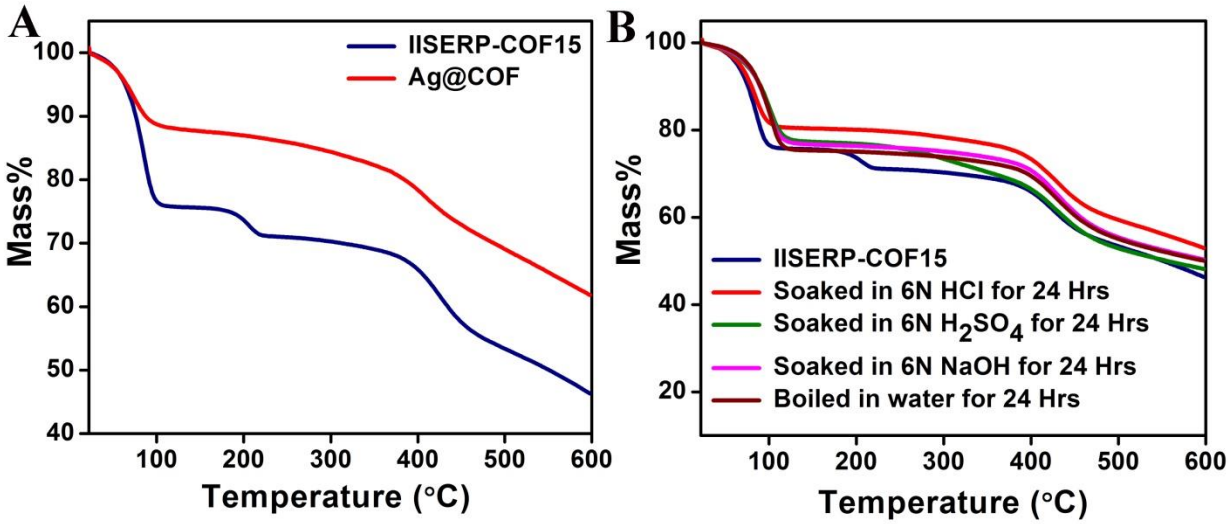

Figure A.4.4. (A) TGA plots of IISERP-COF15 and Ag@COF showing that the materials are stable up to 300°C. (B) TGA of the COF treated with different chemicals depicting the thermal stabilities.

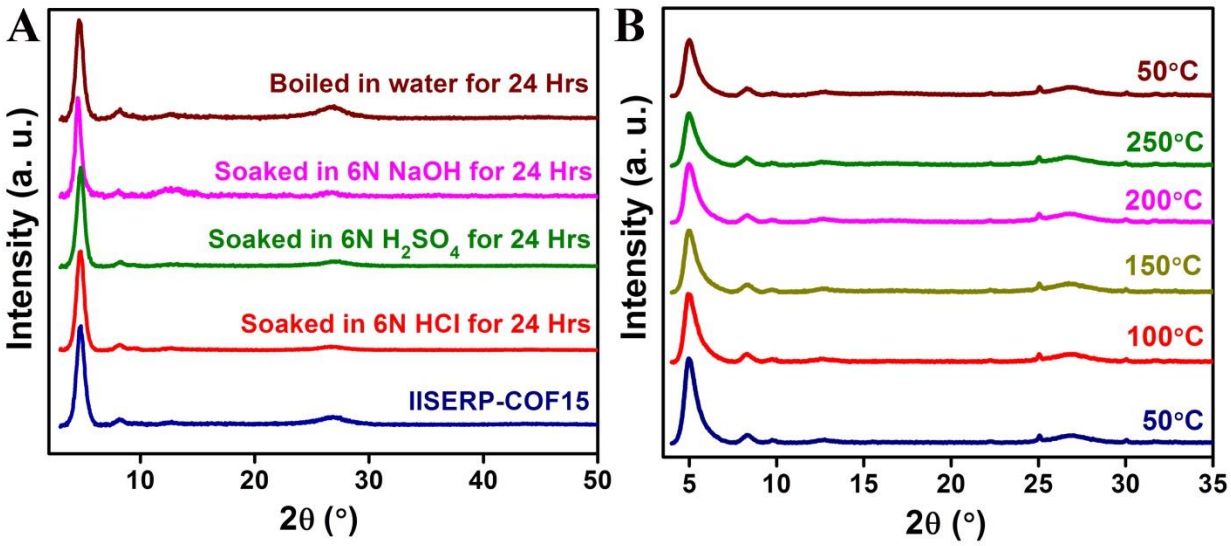

Figure A.4.5. (A) Powder X-Ray Diffraction (PXRD) patterns depicting the stability of the COF towards different chemical treatments. (B) Variable temperature PXRD of the COF showing the retention of crystallinity upon heating. Note: small peaks at 2θ ~25° and ~30° is observed due to the presence of an impurity in the Pt sample holder (These could not be cleaned satisfactorily. Also, the empty holder was checked and these peaks remain).

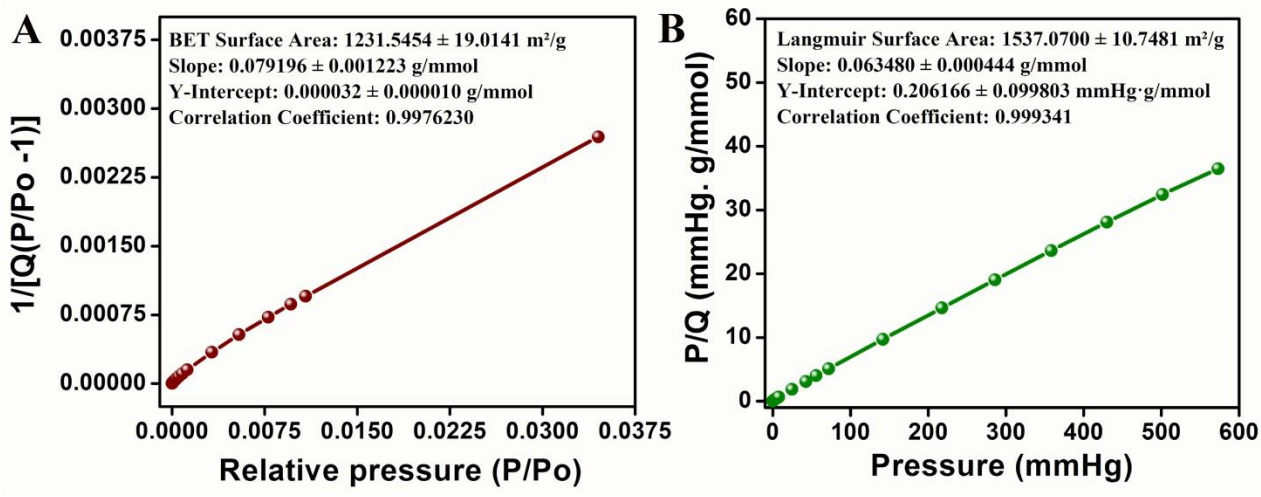

Figure A.4.6. BET (A) and Langmuir (B) surface area plots for the COF.

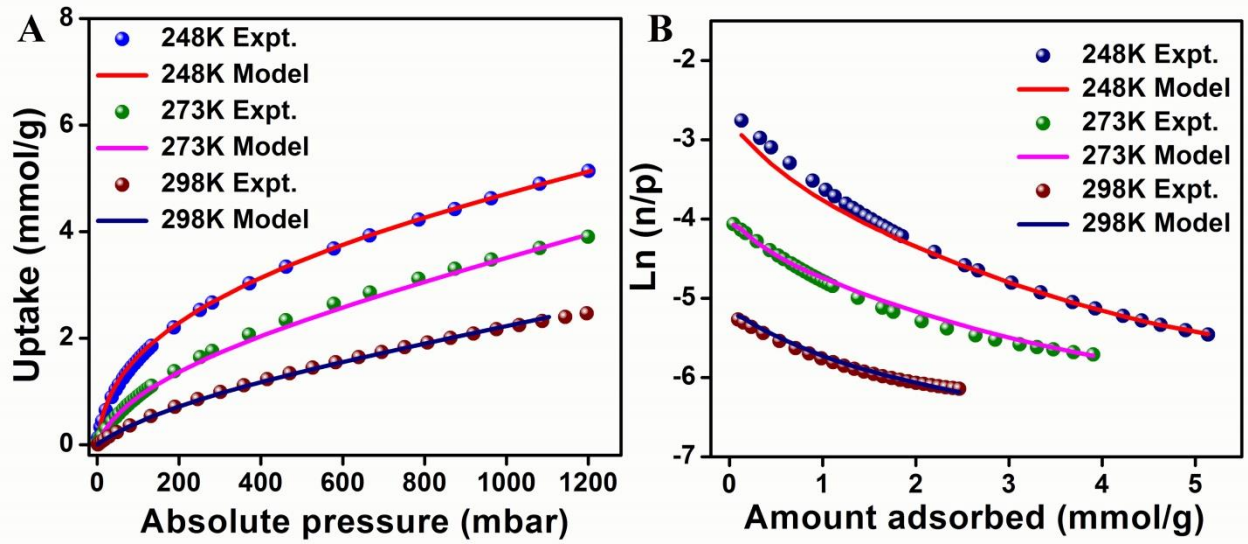

Figure A.4.7. (A) Comparison of the experimental CO_2 isotherms with the isotherms calculated from virial model for the COF at 248 K, 273 K, and 298 K. (B) Virial plots for the CO_2 adsorption at three different temperatures, 278 K, 288 K, and 298 K.

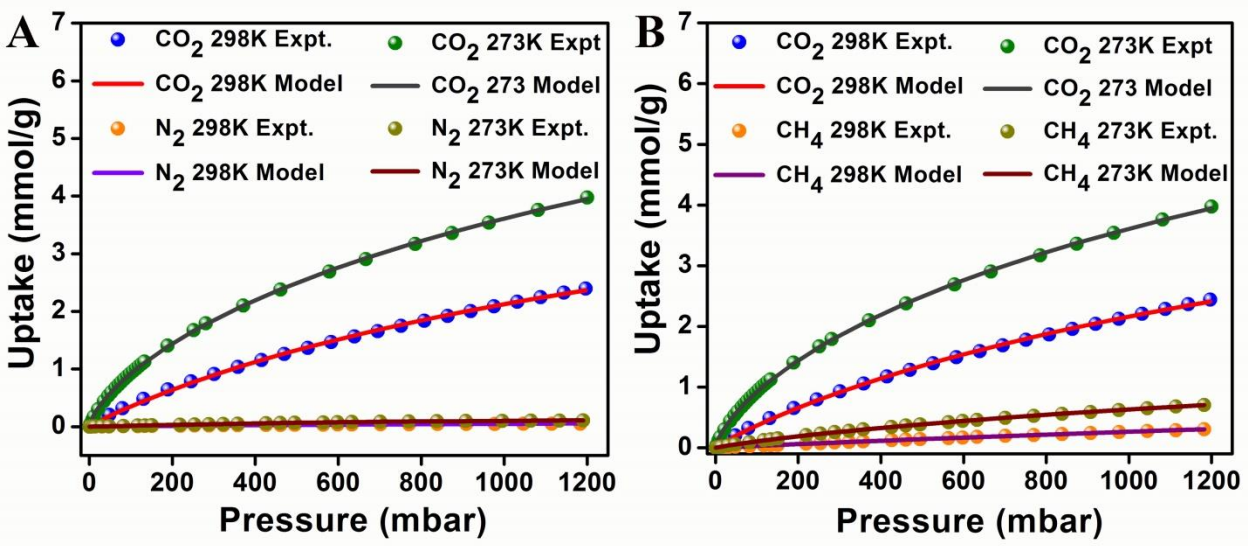

Figure A.4.8. IAST selectivity, fitting curves for the gas mixture of CO_2/N_2 (A) and CO_2/CH_4 (B) at two different temperatures, 298K and 273K.

Note: Depending on the different uptake of CO_2 and N_2/CH_4 at different partial pressure one will obtain the selectivity values as a function of the total pressure of the gas mixture. Based on the gas composition the partial pressure will be different. Hence you will get different selectivity for a different composition.

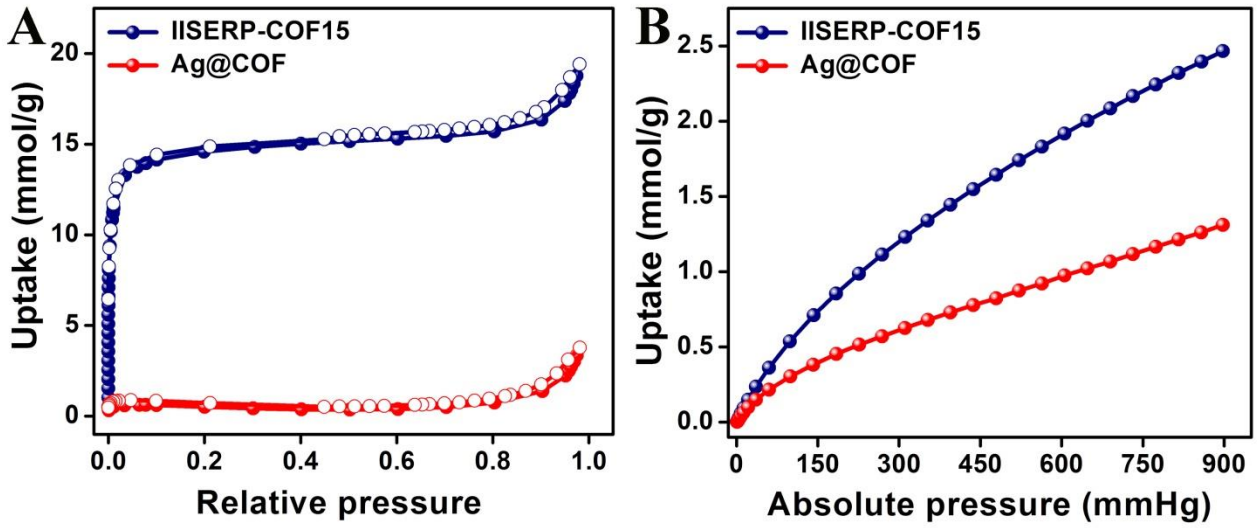

Figure A.4.9. N_2@77K (A) and CO_2@298K (B) isotherms for IISERP-COF15 and Ag@COF.

Note: Probably the nanoparticles don't fill the entire pore rather just plug the entry of the pore. Certain facets are exposed to catalytic activity. Rests of the atoms are inside the pore and are inactive. That's why the composite becomes almost nonporous. Another important aspect is that N_2 and CO_2 have different binding sites in the framework and fortunately, nitrogen sites are specifically blocked. As a result, we are able to get a reasonable amount of CO_2 uptake, but no nitrogen upon Ag loading.

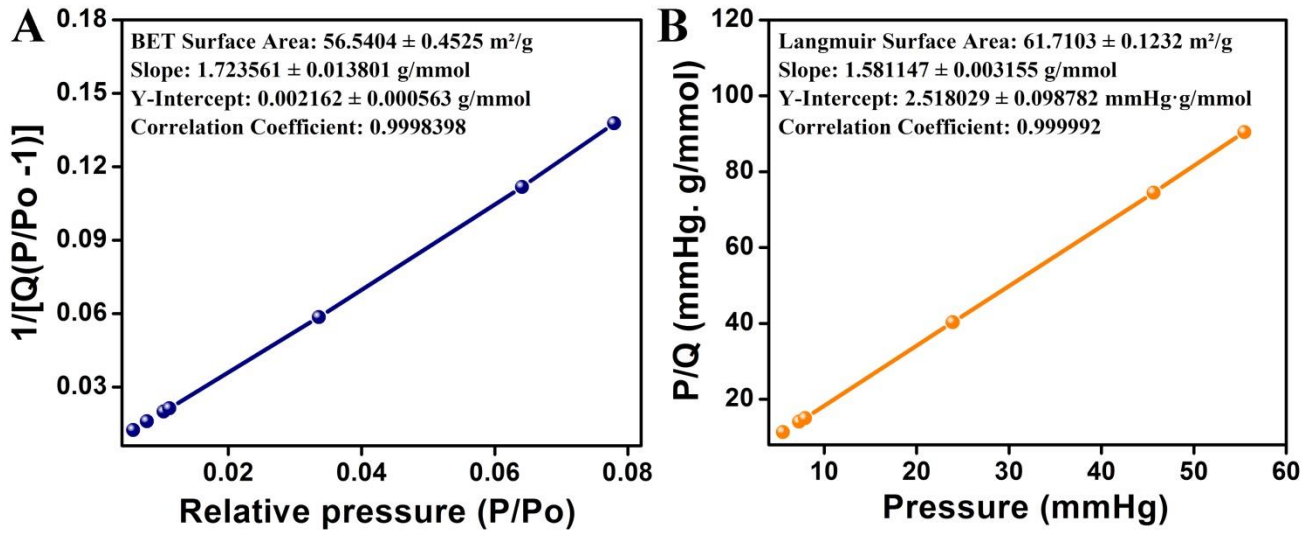

Figure A.4.10. BET (A) and Langmuir (B) surface area plots for the Ag@COF.

Microscopy studies:

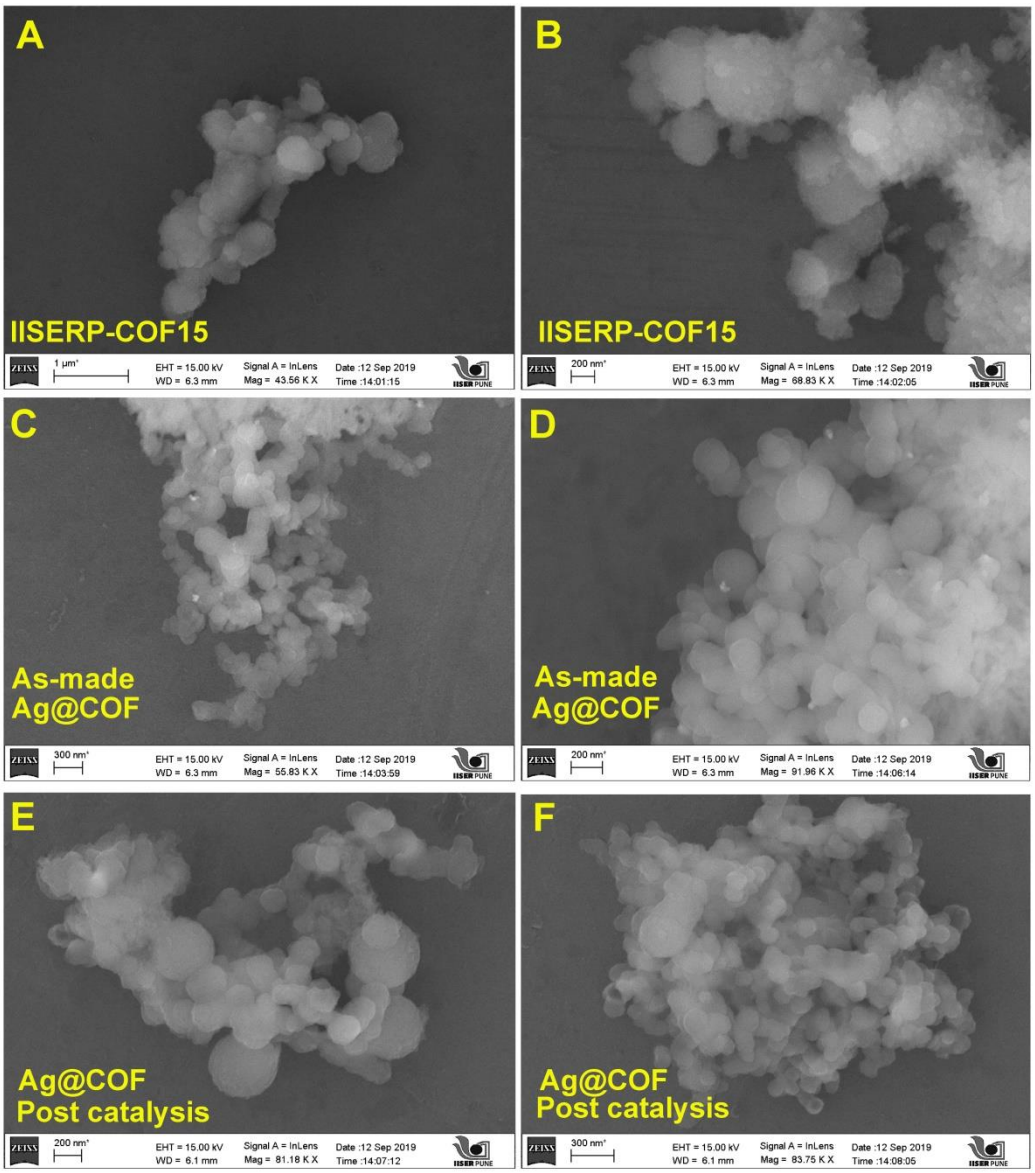

Figure A.4.11. (A), (B) SEM images of IISERP-COF15 showing the spherical morphology. SEM images of the catalyst before (C) and after (D) catalysis. Note that the spherical shape is retained.

Element	Weight%	Atomic%
C K	54.54	60.25
N K	17.39	16.48
O K	28.06	23.27
Totals	100.00	

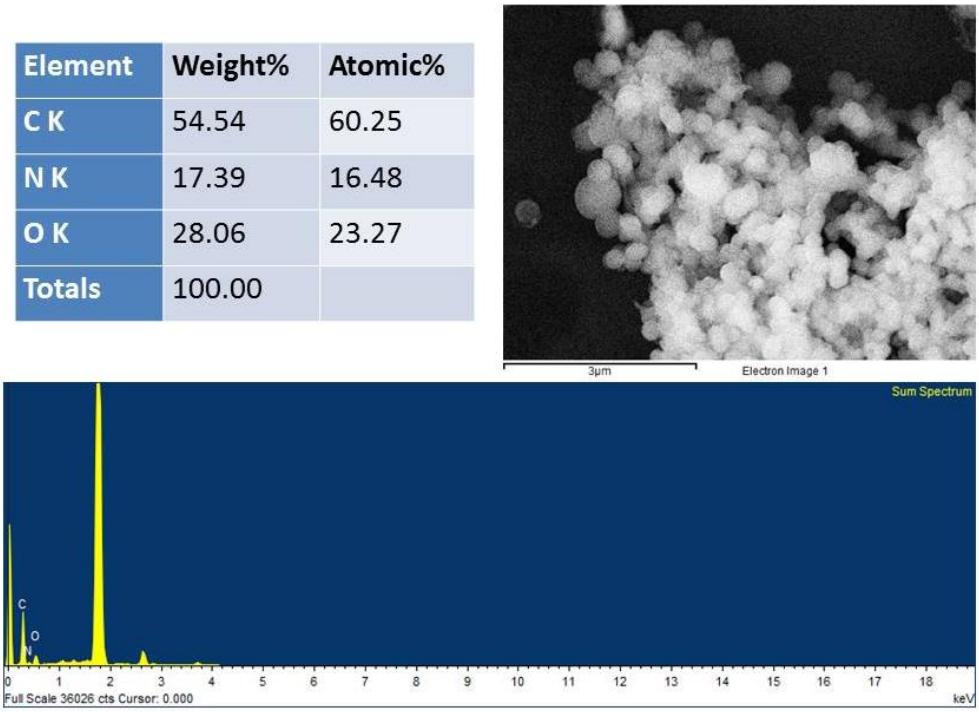

Figure A.4.12. Energy dispersive X-Ray spectrum of IISERP-COF15.

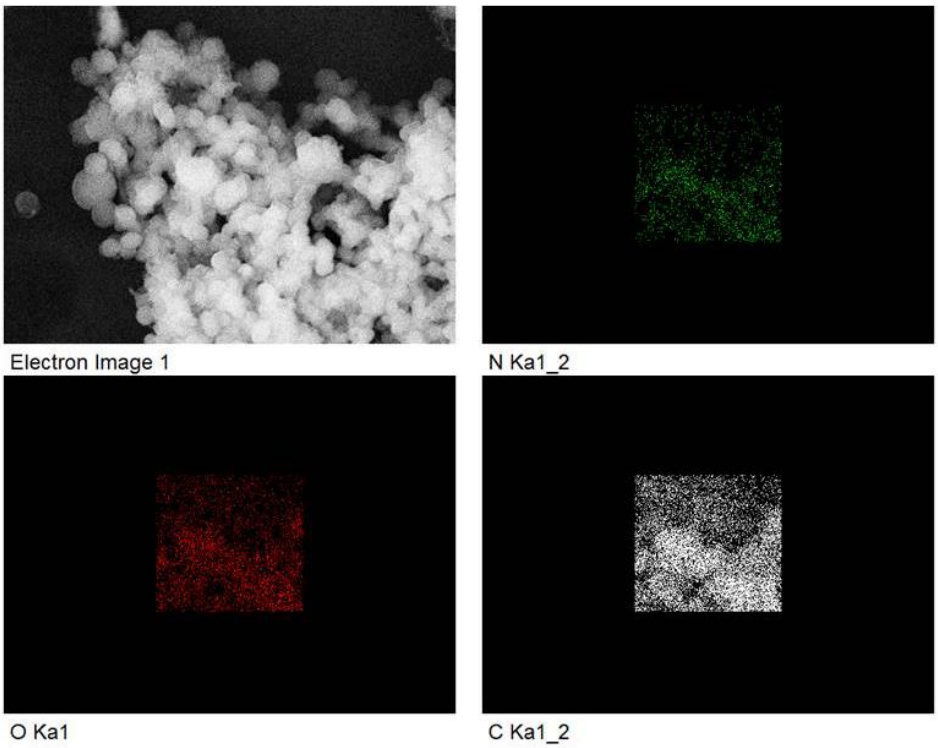

Figure A.4.13. Elemental mapping for the IISERP-COF15 showing the homogeneous distribution of the elements in the COF.

Element	Weight%	Atomic%
C K	53.35	61.33
N K	22.48	22.16
O K	18.25	15.75
Ag L	5.92	0.76
Totals	100.00	

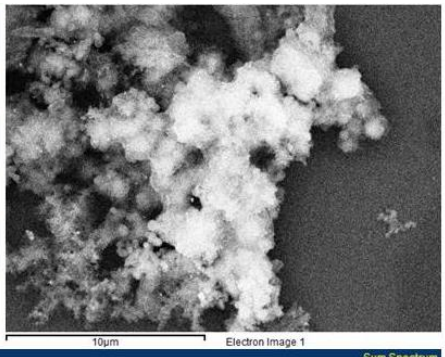

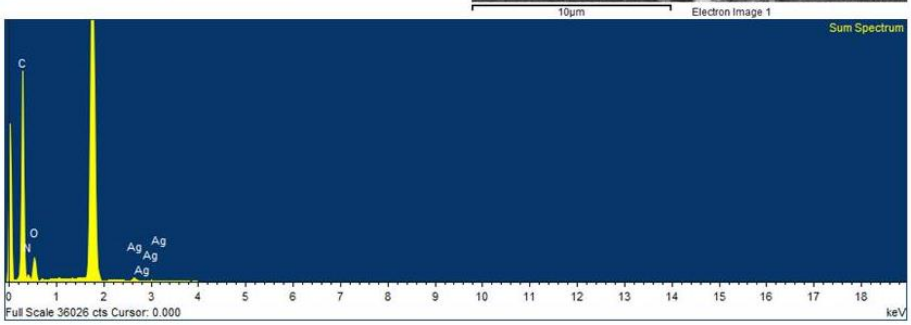

Figure A.4.14. Energy dispersive X-Ray spectrum of Ag@COF before catalysis.

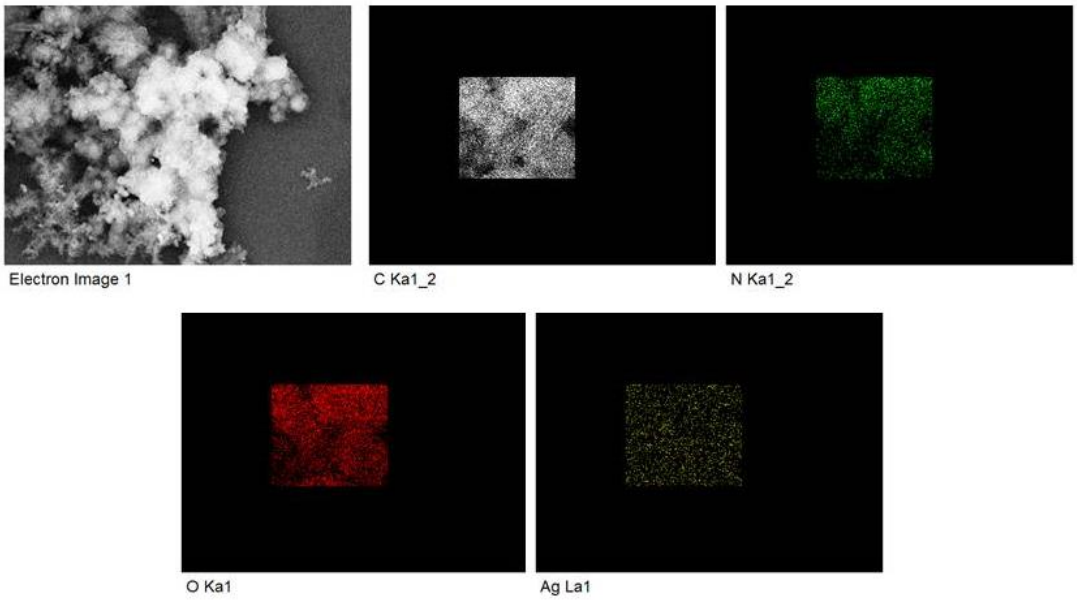

Figure A.4.15. Elemental mapping for the Ag@COF before catalysis showing the homogeneous distribution of the elements in the COF.

Element	Weight%	Atomic%
C K	56.85	64.48
N K	20.44	19.37
O K	16.92	15.48
Ag L	5.80	0.70
Totals	100.00	

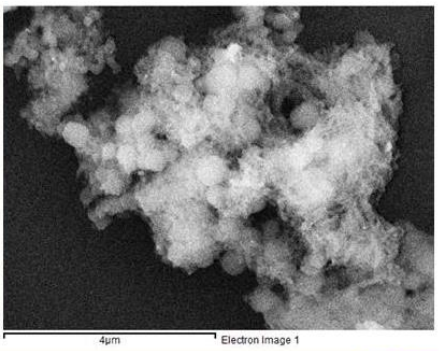

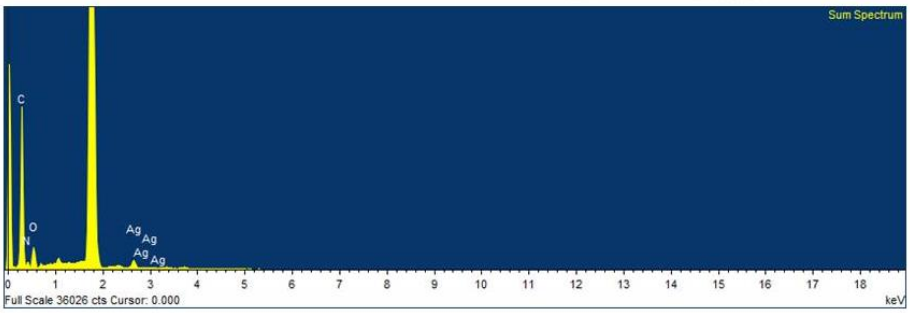

Figure A.4.16. Energy dispersive X-Ray spectrum of Ag@COF after catalysis.

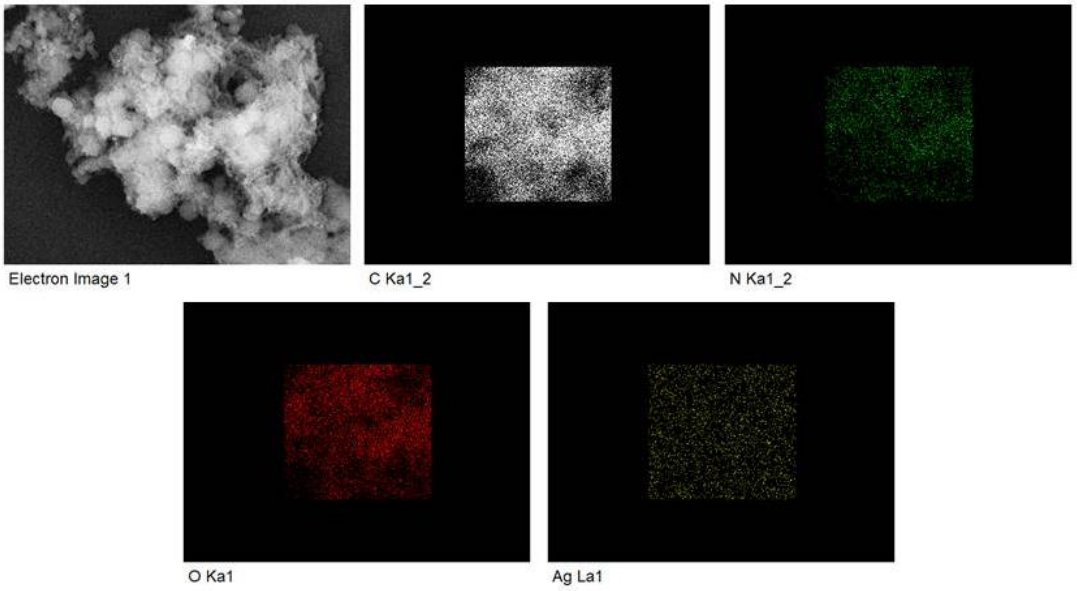

Figure A.4.17. Elemental mapping for the Ag@COF after catalysis showing the homogeneous distribution of the elements in the COF.

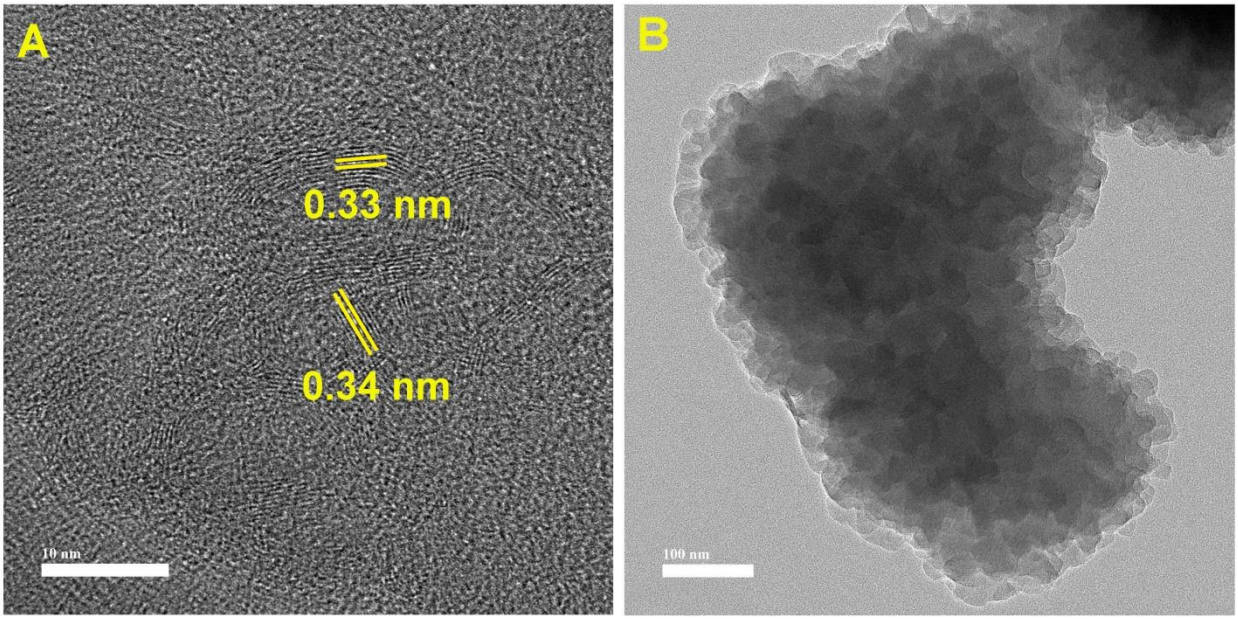

Figure A.4.18. TEM images of IISERP-COF15 at two different magnifications. Lattice fringes (d = 0.33 nm) are observed which depicts the highly crystalline nature of the COF.

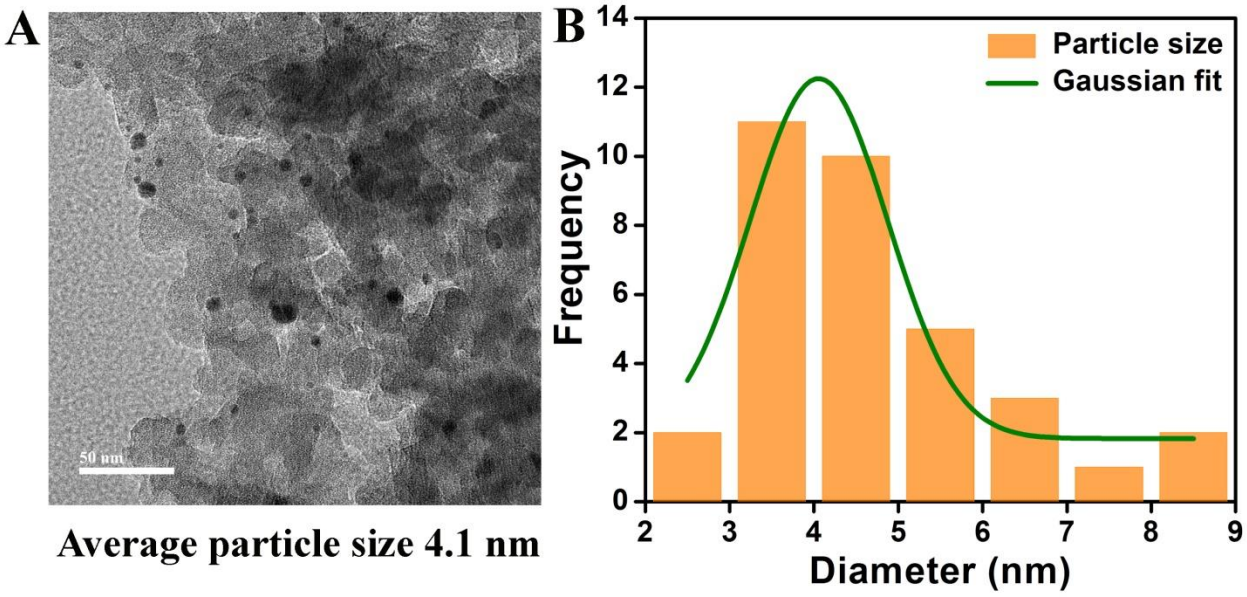

Figure A.4.19. (A) and (B), the particle size distribution of as-made Ag@COF that was used for the catalysis. The composite has an average particle size of 4.1 nm.

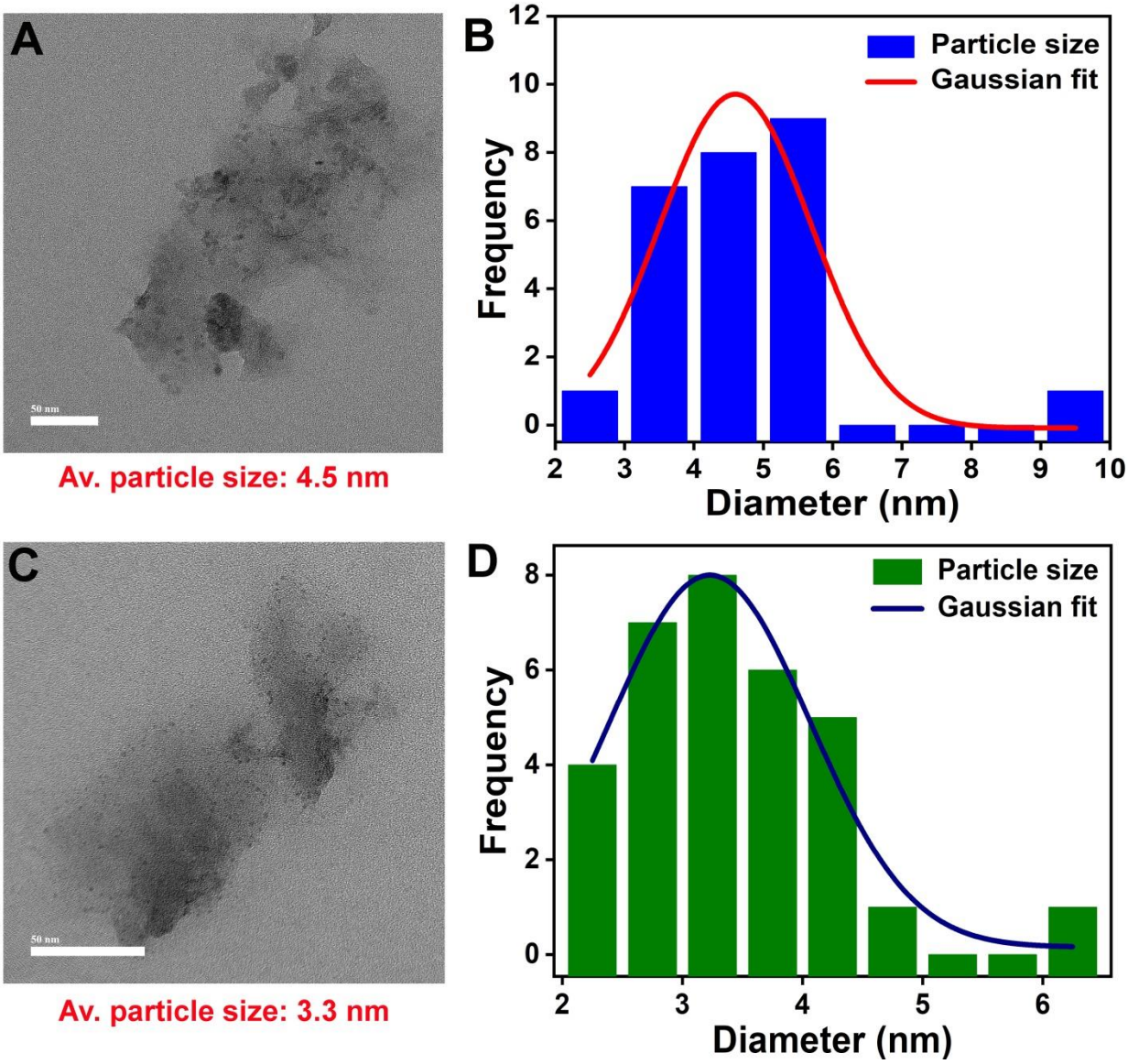

Figure A.4.20. Particle size distributions of Ag nanoparticle on COF in different regions. It has been observed that the average particle size ranges from 3-5 nm. This confirms that the Ag particles are homogeneously distributed on the COF with uniform size.

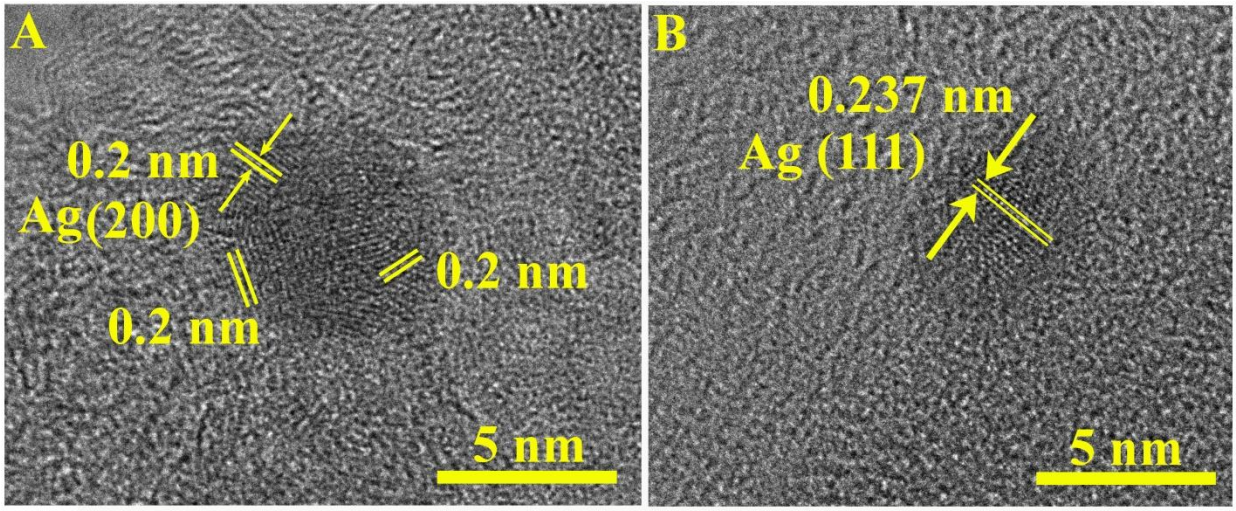

Figure A.4.21. Lattice fringes from the spent-catalyst that was recovered after the reaction (5 cycles) which have been indexed to the Ag(*111*) and Ag(*200*) planes.

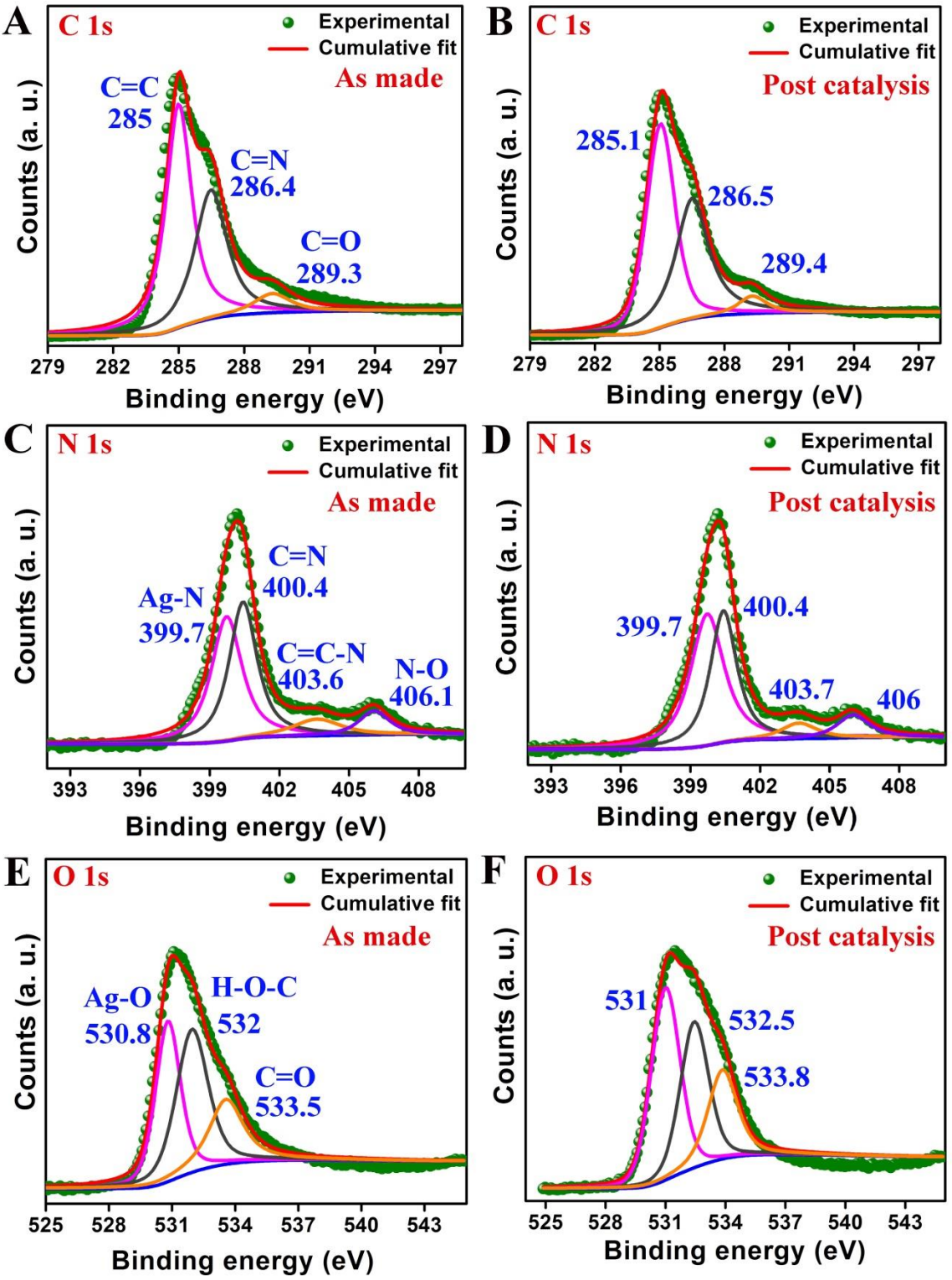

Figure A.4.22. Detailed XPS spectra of C1s, N1s, and O1s for the Ag@COF before and after catalysis.

Nuclear Magnetic Resonance spectroscopic data for the organic compounds:

2-methyl-4-phenylbut-3-yn-2-ol (S1)

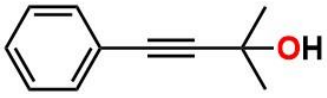

^{1}H NMR (400 MHz, $CDCl_3$): δ = 7.45 – 7.43 (m, 2H), 7.35 – 7.30 (m, 3H), 1.64 (s, 6H).
^{13}C NMR (101 MHz, $CDCl_3$): δ = 131.6, 128.2, 122.7, 93.8, 82.1, 65.6, 31.50.
HRMS: calcd. for $C_{11}H_{13}O$ $[M+H]^+$ 161.1033, found 161.1045.

2-methyl-4-(p-tolyl)but-3-yn-2-ol (S2)

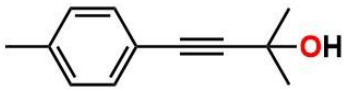

^{1}H NMR (400 MHz, $CDCl_3$): δ = 7.31 (d, J = 8 Hz, 2H), 7.12 (d, J = 8 Hz, 2H), 2.36 (s, 3H), 1.64 (s, 6H).
^{13}C NMR (101 MHz, $CDCl_3$): δ = 138.3, 131.5, 129.0, 119.6, 93.1, 82.2, 65.6, 31.5, 21.4.
HRMS: calcd. for $C_{12}H_{15}O$ $[M+H]^+$ 175.1123, found 175.1128.

3-methyl-1-phenylpent-1-yn-3-ol (S3)

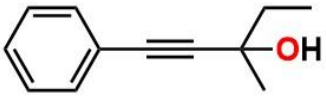

^{1}H NMR (400 MHz, $CDCl_3$): δ = 7.49 – 7.41 (m, 2H), 7.34 – 7.28 (m, 3H), 1.92 – 1.73 (m, 2H), 1.60 (s, 3H), 1.13 (t, J = 6 Hz, 3H).
^{13}C NMR (101 MHz, $CDCl_3$): δ = 138.3, 131.5, 129.0, 119.6, 93.1, 82.2, 65.6, 31.5, 21.4.
HRMS: calcd. for $C_{12}H_{15}O$ $[M+H]^+$ 175.1123, found 175.1130.

4,4-dimethyl-5-methylene-1,3-dioxolan-2-one (1)

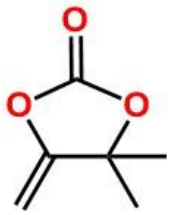

^{1}H NMR (400 MHz, $CDCl_3$): δ = 4.74 (d, J = 4.0 Hz, 1H), 4.29 (d, J = 4.0 Hz, 1H), 1.59 (s, 6H).
^{13}C NMR (101 MHz, $CDCl_3$): δ = 158.8, 151.4, 85.4, 84.7, 27.7.
HRMS: calcd. for $C_6H_9O_3$ $[M+H]^+$ 129.0552, found 129.0566.

4-ethyl-4-methyl-5-methylene-1,3-dioxolan-2-one (2)

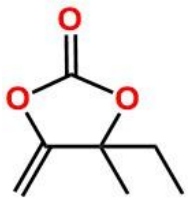

^{1}H NMR (400 MHz, $CDCl_3$): δ = 4.76 (d, J = 4.0 Hz, 1H), 4.26 (d, J = 4.0 Hz, 1H), 1.97 – 1.69 (m, 2H), 1.55 (s, 3H), 0.94 (t, J = 8.0 Hz, 3H).
^{13}C NMR (101 MHz, $CDCl_3$): δ = 157.3, 151.5, 87.6, 85.6, 33.3, 25.9, 7.2.
HRMS: calcd. for $C_7H_{11}O_3$ $[M+H]^+$ 143.0708, found 143.0716.

4-methylene-1,3-dioxaspiro[4.5]decan-2-one (3)

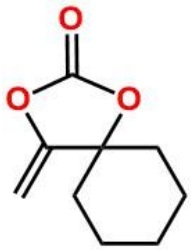

^{1}H NMR (400 MHz, $CDCl_3$): δ = 4.67 (d, J = 4.0 Hz, 1H), 4.24 (d, J = 4.0 Hz, 1H), 1.93 – 1.91 (M, 2H), 1.77 – 1.48 (m, 7H).
^{13}C NMR (101 MHz, $CDCl_3$): δ = 158.7, 151.5, 86.5, 85.6, 36.5, 24.3, 21.6.
HRMS: calcd. for $C_9H_{13}O_3$ $[M+H]^+$ 169.0865, found 169.0874.

5-benzylidene-4,4-dimethyl-1,3-dioxolan-2-one (4)

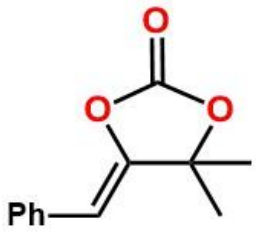

^{1}H NMR (400 MHz, $CDCl_3$): δ = 7.58 – 7.56 (m, 2H), 7.40 – 7.36 (m, 2H), 7.31 – 7.26 (m, 1H), 5.54 (s, 1H), 1.72 (s, 6H).
^{13}C NMR (101 MHz, $CDCl_3$): δ = 151.3, 150.7, 132.4, 128.6, 128.5, 127.6, 101.6, 85.6, 27.7.
HRMS: calcd. for $C_{12}H_{13}O_3$ $[M+H]^+$ 205.0865, found 205.0922.

4,4-dimethyl-5-(4-methylbenzylidene)-1,3-dioxolan-2-one (5)

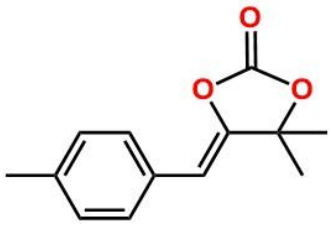

^{1}H NMR (400 MHz, $CDCl_3$): δ = 7.48 – 7.45 (m, 2H), 7.20 – 7.18 (m, 2H), 5.51 (s, 1H), 2.38 (s, 3H), 1.71 (s, 6H).
^{13}C NMR (101 MHz, $CDCl_3$): δ = 151.5, 150.0, 137.5, 129.6, 129.4, 128.4, 101.5, 85.5, 27.7, 21.3.
HRMS: calcd. for $C_{13}H_{15}O_3$ $[M+H]^+$ 219.1021, found 219.1038.

5-benzylidene-4-ethyl-4-methyl-1,3-dioxolan-2-one (6)

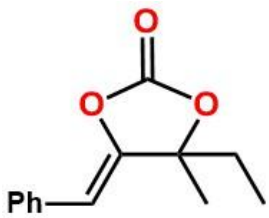

^{1}H NMR (400 MHz, $CDCl_3$): δ = δ 7.46 – 7.43 (m, 2H), 7.25 – 7.19 (m, 2H), 7.15 – 7.10 (m, 1H), 5.37 (s, 1H), 1.93 – 1.65 (m, 2H), 1.53 (s, 3H), 0.89 (t, J = 8 Hz, 3H).
^{13}C NMR (101 MHz, $CDCl_3$): δ = 151.6, 149.6, 132.6, 128.7, 128.4, 127.6, 102.0, 88.6, 33.7, 26.1, 7.5.
HRMS: calcd. for $C_{13}H_{15}O_3$ $[M+H]^+$ 219.1021, found 219.1029.

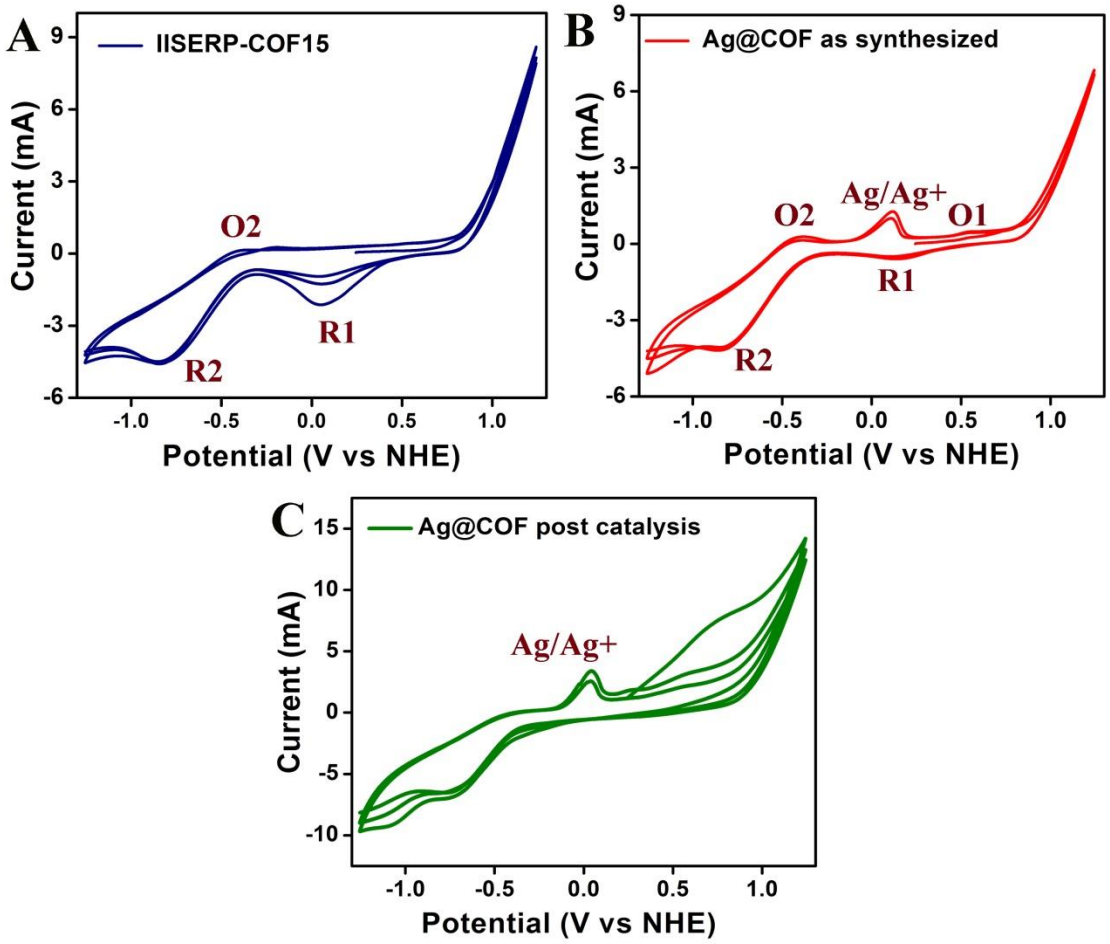

Figure A.4.23. (A) Cyclic voltammetry of IISERP-COF15 showing the redox-active peaks, R1: -0.4 V vs NHE is due to the imine bond reduction, R2: -0.8 V *vs*. NHE is for the keto group reduction. O2 is the oxidation peak for the keto group. (B) CV of Ag@COF. The oxidation peak of Ag is obtained at 0.12 V vs NHE. O1: 0.52 vs NHE is due to oxidation of the imine bond. (C) The CV of recovered Ag@COF sample after catalysis.

Chapter 5

Cu/Cu_2O Nanoparticles Supported by a Phenol-Pyridyl COF as Heterogeneous Catalyst for the Synthesis of Unsymmetrical Diynes via Glaser-Hay Coupling

Chapter 5

5.1. Introduction:

Covalent Organic Frameworks (COF) are metal-free porous crystalline polymers. In recent years, they have gained immense attention.[1-8] Owing to their chemically tuneable modular structure and pore architecture, COFs have been applied to the several fields of material sciences starting from gas storage and separation,[9-11] sensing,[12-14] energy storage and conversion,[15-28] pro-ton conduction[29-31], optics[32-36] and catalysis.[37-49] Inclusion of inorganic cluster in the network has been an effective strategy to introduce novel functions.[37-39] Depending upon the dimension of the pore, the size of the nanoparticle can be controlled enhancing the performance of the particle. Moreover, heteroatoms in the COF help to grow active nanoparticles in the pore. Such COF-nP composites serve as heterogeneous catalysts and carry a number of advantages like recyclability, easy handling, scalability. Importantly, the activity is modulated through "by-design" strategy of the composite.[16,18,37-49] The lability of the groups presents in the catalysts plays an important role in the final outcome. Effect of the matrix on such groups are also a very important point to be addressed (e.g., a self-standing pyridyl vs. the one embedded on a graphene framework).[50-52] Similarly, heteroatoms in the COF pore can stabilize the intermediate of the reaction leading to a particular product.

Unsymmetrical 1,3-diynes are an important core in organic and biologically active molecules and key motifs in many natural products and functional materials.[53-56] This provides a room to unlock diverse chemistry by partial reduction of the triple bond and metal coordination.[57-59] Thus, developing procedures synthesize diynes, in particular, unsymmetrical diynes is worthwhile. Though homogeneous catalysts[60-68] have been systematically developed for the synthesis of homocoupled 1,3-diynes through the Glaser-Hay coupling, attempts to make unsymmetrical 1,3-diynes by coupling two different aryl or alkyl substrates have been marred by poor selectivity.[69-83] Very few heterogeneous Cu-based catalysts are reported, but they give predominantly homocoupling products.[84-91] Recently, Yin and co-workers reported a Cu-based homogeneous catalyst, an active species is generated with N1,N1,N2,N2-tetramethylethylenediamine (TMEDA) in chloroform and catalyzes the heterocoupling of alkynes quite effectively.[92]

An important feature of the catalysis is that there is a complex formation with chloride ion generated from chloroform and the species is counterbalanced by the protonated amine moiety. But the drawback is the consumption of Cu powder and the homogeneous nature restricts recyclability of the catalyst. Inspired by the chemistry involved in the reaction, here we report

a COF which can support highly active Cu nanoparticles. This Cu@COF is used as a heterogeneous catalyst for Gaser-Hay heterocoupling. A thorough analytical characterizations prove the integrity and recyclability of the catalyst which are absent in case of the homogeneous catalyst. The mechanism has been studied by different experimental tools and theoretical inputs. It has been found from the DFT optimization that the co-existing hetero-coupled configuration possesses the lowest relative energy compared to the homo-coupled ones. The effect of COF also has been established from a series of control reactions.

The high chemical stability of the COF and its strong interactions with the Cu centers renders the catalyst to be highly recyclable which can be made in grams. To the best of our knowledge, this is the first report of a Cu@COF-based heterogeneous catalyst for selective Gaser-Hay heterocoupling.

5.2. Materials and methods:

Synthesis of 2,4,6-tris(4-nitrophenyl)pyridine::

The amine building block was synthesized by following the reported procedure in two steps.[93] In the first step, 10 mmol of 4-Nitrobezaldehyde and 20 mmol of 4-Nitroacetophenone were dissolved in 25 ml of acetic acid. Then 10 g of ammonium acetate was added to this mixture and refluxed at 110°C for 3 hours. The deep orange precipitate was obtained which was filtered and washed with acetic acid and cold Ethanol. The crude product was used to the next step without any further purification.

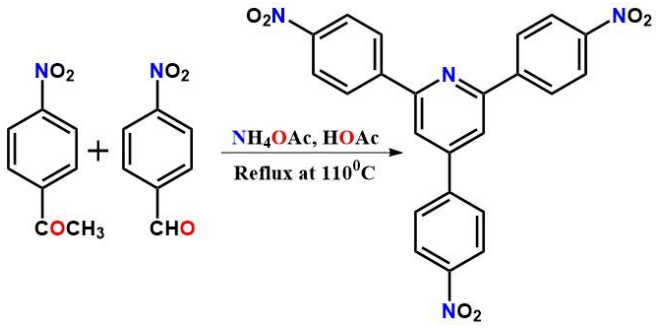

Synthesis of 4,4',4''-(pyridine-2,4,6-triyl)trianiline:

1.5 g of 2,4,6-tris(4-nitrophenyl)pyridine was dissolved in 20 ml EtOH. About 60 mg of $FeCl_3$ and 200 mg of activated carbon were added to this solution and heated under reflux conditions for 30 mins. To this, 4 ml of hydrazine hydrate in 4 ml EtOH was added and the mixture was refluxed for 12 hours. The mixture was filtered as hot and the filtrate was poured in distilled

water. A yellow precipitate appeared, which was filtered, washed with water and dried at 60°C overnight.

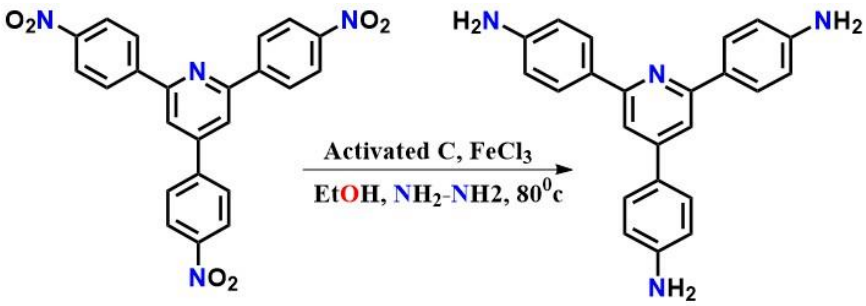

Synthesis of 2-hydroxybenzene-1,3,5-tricarbaldehyde:

The trifornyl phenol was prepared following the reported procedure.[94] A 250 ml RB was equipped with 4.7 g (50 mmol) phenol, 50 ml TFA, 15.4 g (110 mmol) hexamine and the mixture was heated at 120°C for 20 hours. The temperature was maintained at 150°C for another 3 hours before lowering to 120°C again. The mixture was then brought down to 100°C and was treated with 100 ml 3N HCl solution. Contents were maintained at 100°C for another 3 hours. Finally, the mixture was cooled to room temperature overnight. The resulting brown precipitate was filtered, washed with water and was recrystallized from DMF.

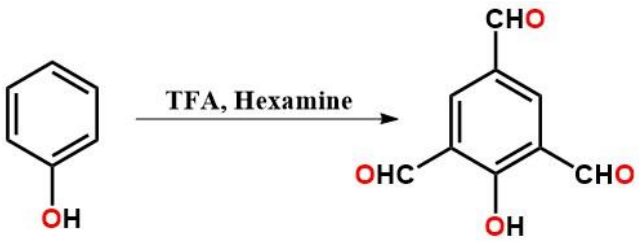

Synthesis of IISERP-COF9:

4,4',4"-(pyridine-2,4,6-triyl)trianiline (71.4 mg, 0.2 mmol) and 2-hydroxybenzene-1,3,5-tricarbaldehyde (36 mg, 0.2 mmol) were added in a pyrex tube and dissolved in 8 ml o-Dichlorobenzene and 2 ml Butanol mixture. 1 ml Acetic acid was added to this mixture and was stirred well. The pyrex tube was then flash-frozen using liquid nitrogen and sealed. The contents in the sealed tube were heated at 120°C for 3 days. After cooling to room temperature, the deep brown precipitate was filtered and washed with DMF, THF, MeOH. The powder was dried at 80°C, overnight. The final product was cleaned through soxhlet extraction. Yield (82%), Formula for COF $C_{32}N_4OH_{20}$, M. Wt. 476.536 g/mol, CHN Observed is C = 84.77; H = 5.527; N = 8.79. Calc. C = 80.65; H = 4.23; N = 11.76.

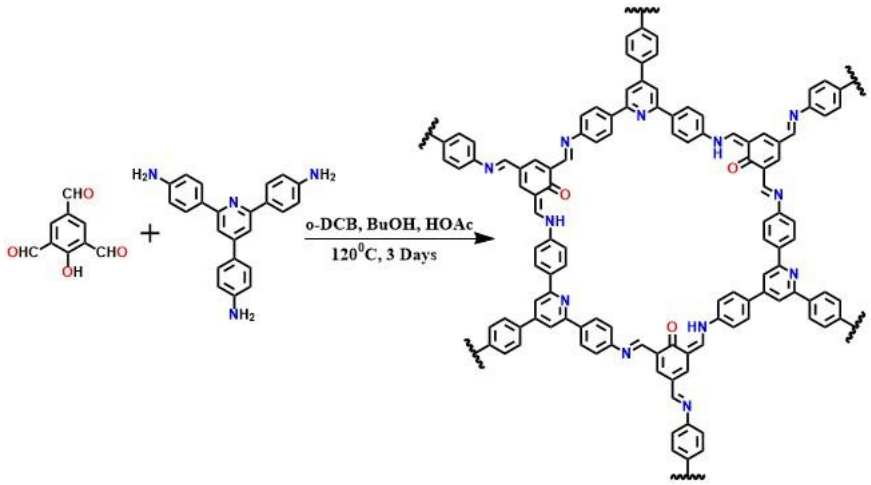

Scheme 5.1. Schematic representation of COF synthesis.

Synthesis of Cu@IISERP-COF9:

100 mg COF was dispersed in 15 ml THF and sonicated for 30 mins in a 100 ml RB. To this suspension, 60 mg $CuCl_2$ in 2 ml H_2O was added. Contents were stirred at RT for 12 hrs and then the solid was extracted by filtration. The solid was washed with water and methanol. Then it was dried at 120°C under vacuum. This solid was then resuspended in a 3:1 water + methanol mixture and the mixture was heated at 80°C. At 80°C, the reduction of Cu^{2+} was carried out by the addition of 5 ml 1M ascorbic acid in water. Contents were allowed to stir for 20 hrs. Finally, the precipitate was filtered and washed with copious amounts of H_2O, MeOH, THF and dried under vacuum. CHN observed: C = 50.70; H = 5.243; N = 7.81. Remark: We could not track the loading of Cu^{2+} or the Cu^0 as a function of color change due to the deep red color of the parent COF. Note: When ascorbic acid is not used, the Cu^{2+} reduced only by the COF yields predominantly Cu(I) and not Cu(0).

Gram scale synthesis of IISERP-COF9:

4,4',4"-(pyridine-2,4,6-triyl)trianiline (3.57 g) and 2-hydroxybenzene-1,3,5-tricarbaldehyde (1.8 g) were added in an autoclave and dissolved in 80 ml o-Dichlorobenzene and 20 ml Butanol. 10 ml Acetic acid was added to this mixture and it was stirred well. The Teflon liner was then flash-frozen by liquid nitrogen and sealed. Finally, it was heated at 120°C for 3 days. After cooling to room temperature, the deep brown precipitate was filtered and washed with DMF, THF, MeOH. The powder was dried at 80°C, overnight. The final product was cleaned through soxhlet extraction.

Stability studies of IISERP-COF9:

To study the stability IISERP-COF9, the COF was soaked in 6N HCl, 6N H_2SO_4, 6N NaOH and boiled in water. Then the samples were characterized by Powder X-Ray Diffraction (PXRD), Infra-Red spectroscopy (IR) and porosity measurements.

5.3. Analytical characterizations:

Powder X-ray diffraction:

Powder X-Ray has been carried out using a Bruker instrument with a Cu Kα (λ = 1.541 Å) source and processed using PDXL software.

Thermo gravimetric Analysis:

NETSZCH TGA-DSC instrument has been used for TGA analysis. The sample was heated under N_2 flow of 20 ml/min (purge + protective) from 25°C to 600°C with a heating rate of 5 K/min.

IR spectroscopy:

IR spectra were obtained using a Nicolet ID5 attenuated total reflectance IR spectrometer in a range of 4000-600 cm^{-1}. KBr pellets were made with the sample to record IR.

Nuclear Magnetic Resonance spectroscopy (NMR):

NMR spectra for the catalytic products were recorded on a 400 MHz Jeol ECS-400, Bruker 400 MHz and solid-state magic angle spinning NMR spectra for COF was obtained in Bruker 500 MHz.

Field Emission-SEM:

Ultra Plus Field Emission Scanning Electron Microscope with integral charge compensator and embedded EsB and AsB detectors was used for recording the SEM images and EDX analysis. During sample preparation, the solid samples were dispersed in THF and sonicated for 10 mins. The dispersed samples were drop casted on silicon wafer and dried in a vacuum oven for overnight.

HR-Transmission electron microscopy (HRTEM):

FEI (Jeol FEG 2100F is the model) high-resolution transmission electron microscope (HR-

TEM) equipped with a field emission source operating at 300 KeV was used for collecting the TEM images. The well-dispersed sample was drop casted on a Cu grid.

Adsorption studies:

All the adsorptions were performed using a 3-FLEX pore and surface area analyzer and few cases using Micromeritics ASAP.

Cyclic Voltammetry (CV):

Cyclic Voltammetry studies are performed using an AMETEK instrument and the data was analyzed with Versa Studio software. A three-electrode assembly is used where Ag/AgCl and Pt wire are used as reference and counter electrodes. Traditional materials with low electrical conductivity are either mixed with conductive additives (e. g. conducting carbon, CNT, etc.) or coated on a current collector electrode like glassy carbon or Tory carbon paper. As the COF/Cu@COF has low electrical conductivity, they are coated on a conducting Toray paper and this is used as a working electrode. Toray paper is being served as the current collector. The material is not being coated on a glassy carbon electrode as the accessible area (0.07065 cm^2) is smaller compared to a Toray paper. This has helped to access the Cu particles buried inside the COF matrix. The electrolyte was prepared by preparing 1M $tBuNH_4PF_6$ in Acetonitrile.

Gas chromatography (GC):

GC was performed on AOC-20i Auto Sampler GC system using RTX5 (30 m* 0.32 mm * 0.25 µm) columns, Split ratio 5:1, FID temperature 250 °C. Dodecane was used as an internal standard.

X-Ray photoelectron spectroscopy (XPS):

XPS measurements were carried out using Thermo Kalpha+ spectrometer using micro focussed and monochromated AlKα radiation with energy 1486.6 eV. The base pressure of the spectrometer was better than 10^{-8} mbar during spectral acquisition. The pass energy for the spectral acquisition was kept at 50 eV for individual core-levels. The electron flood gun was utilized for providing charge compensation during data acquisition. The samples for XPS analysis were prepared inside the glove box and transferred to a vacuum transfer module which was subsequently evacuated in the anti-chamber of the glove box. The samples were loaded onto the spectrometer using this vacuum transfer module and subsequently pumped down by

turbomolecular pumps connected to the load lock chamber. This allowed to efficiently transferring the samples without being exposed to the atmosphere. The peak fitting of the individual core-levels was done using XPSpeak software with a Shirley type background.

General procedure for the catalytic reaction:

In general, the catalytic reactions were done in an open atmosphere. Firstly, 0.0992 mol% Cu @ IISERP-COF9 was dispersed in 0.3 ml $CHCl_3$ and 0.1 ml dioxane mixture solvent. To this 0.1 mmol Tetramethylethylenediamine (TMEDA) was added followed by the addition of 0.5 mmol of aromatic alkyne and 0.42 mmol aliphatic alkyne. The mixture was heated at 80°C. The progress of the reaction was monitored by Thin Layer Chromatography. The reaction was found to be completed within 4 hours. The crude mixture was centrifuged to get the solid catalyst back and the product mixture was extracted with dichloromethane and washed with a saturated NH_4Cl solution to get rid of TMEDA. Finally, the product mixture was purified using column chromatography on silica gel with 10% ethyl acetate and hexane mixture as eluent. The products were characterized by ^{1}H, ^{13}C Nuclear Magnetic Resonance spectroscopy (NMR), High Resolution Mass Spectroscopy (HRMS) and Gas Chromatography (GC) using dodecane as an internal standard.

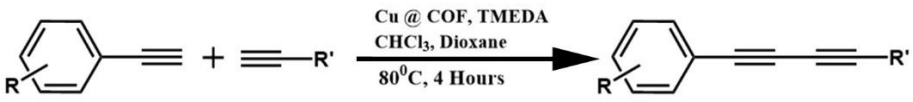

5.4. Results and discussions:

Synthesis and structural modeling of IISERP-COF9:

IISERP-COF9 has been prepared via the Schiff base condensation reaction of Triformyl phenol and 4,4',4''-(pyridine-2,4,6-triyl)trianiline in solvothermal condition (dichlorobenzene-butanol solvent mixture at 120°C for 3 days) (Scheme 5.1). The isolated solid was Soxhletted to purify in dimethyl formamide (DMF) and tetrahydro furan (THF) under reflux conditions. The crystalline nature of the COF has been established from Powder X-Ray Diffraction (PXRD) (Figure A.5.1).

A 2D structure made up of hexagonal layers consistent with the experimentally observed powder X-ray pattern was modeled using the Material Studio program (Figure 5.1). For the structure solution, a similar routine has been adopted as in our earlier work.[16-18] In brief, the XCELL program was used to index the powder X-ray diffraction (PXRD) pattern and the best

possible space group as being P6 (FOM: >20) has been identified. Following this, a model structure was constructed in a hexagonal cell. However, the presence of asymmetrically positioned pyridyl and hydroxyl groups lower the symmetry to triclinic.

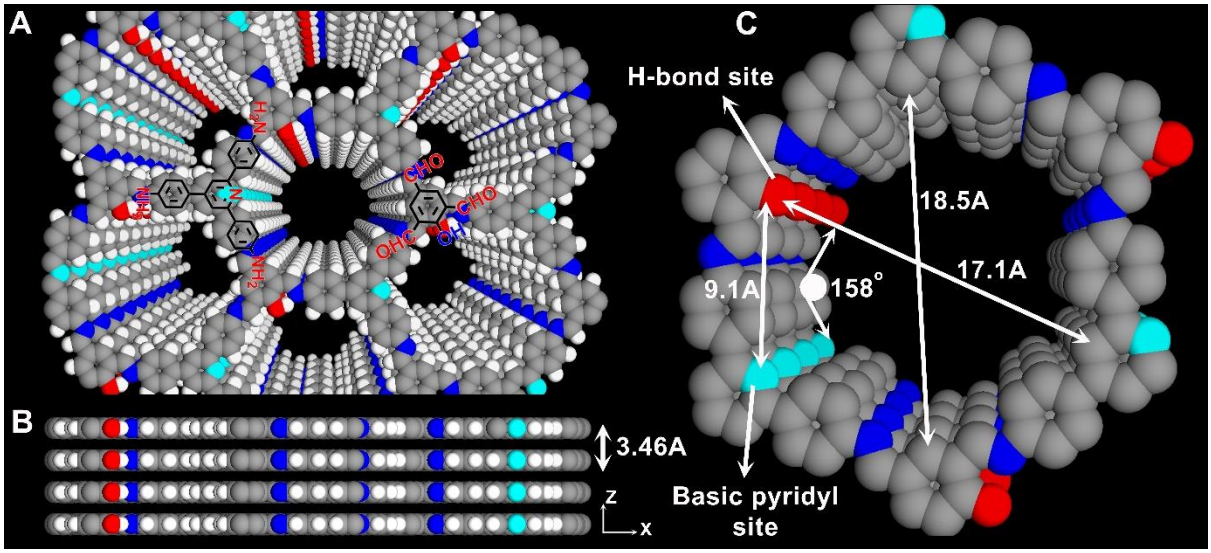

Figure 5.1. (A) The three-dimensional structure of IISERP-COF9 showing uniform 1-D channels along the y-axis. (B) *AAAA*... packing of the π-stacked eclipsed layers. (C) View of a single channel showing the periodic lining of the channels by the hydrogen bonding hydroxyl and basic pyridyl sites (shown in cyan color), and the channel dimensions.

This triclinic structure was geometry optimized using a tight-binding density functional theory (DFTB) algorithm embedded in the Materials Studio. Finally, in the optimized geometry the structure attains a Pm space group (Initial cell in Pm: a = 18.66; b = 18.66; c = 3.51; β= 120.0°, Table A.5.1). The experimental PXRD pattern was refined against this model using a Pawley refinement which yielded an excellent fit (Figure 5.2A, Refined cell: a = 18.23; b = 17.93; c = 3.51; β= 117.74°; Rp = 2.44 and wRp = 3.15). The relative intensities of the high angle peaks suggested the presence of eclipsed form in the structure (Figure A.5.1). The eclipsed configuration has uniform 1-D pores of ~13.5Å (factoring the van der Waal radii of the atoms), which matches well with the experimentally determined pore size from N_2 isotherm at 77K. The optimal geometry of the Schiff bonded monomers allow the active sites, hydroxyl (h-bond site) and the pyridyl (basic site) to be positioned proximally at angles that favor synergistic interactions with the metal atoms individually or conjointly (Figure 5.1B).

Characterizations of IISERP-COF9:

The thermal stability of the COF has been established from Thermo Gravimetric Analysis (TGA) (Figure A.5.2) and Variable Temperature PXRD (VTPXRD) (Figure A.5.3). Solid-state

^{13}C magic-angle spinning NMR spectra disclose the characteristics peaks of the COF (Figure A.5.4). The broad peaks in the range of δ = 114 ppm to 124 ppm correspond to the aromatic carbons. The peak from the imine bonds (-C=N) of the Schiff linkages appears at δ = 156 ppm. The –OH groups in the triformyl phenol undergo reversible proton transfer and keto-enol tautomerism as established by Ning *et al.*[94] We observe that the dried solid exists predominantly in keto-form, while in protic solvents they adopt the enolic conformation. The peak at δ = 197 ppm designates to the -C=O i.e. the keto form at ambient temperature. The observation corroborates well with the Infra-Red (IR) spectra of the COF (keto: 1614 cm^{-1} aromatic –C-H: ~2900 cm^{-1}; -C=C-N: 1435 cm^{-1}, C=N: 1510 cm^{-1}) (Figure A.5.5). Importantly, from the IR spectra of the evacuated sample (exists in keto form), the presence of both C=N and C-N are detected which is due to the stabilization of the Schiff bonds by the tautomerization of the hydroxyl positioned beta to it. If there had been a phloroglucinol core,[17,95] one would observe only the C-N band for the keto form. The COF has a permanent porous network observed by the N_2 isotherm at 77 K. It displays a type-I adsorption isotherm with a rapid nitrogen uptake at low partial pressure region (Figure 5.2B). The COF possesses very high Brunauer–Emmet–Teller (BET) and Langmuir surface area, 1172 m^2/g and 1503 m^2/g, respectively (Figure A.5.6). A Non-Local Density Functional Theory (NLDFT) fit generated a pore size of 13 Å, which agrees well with the eclipsed model of the COF. The COF is remarkably stable in harsh acidic and basic conditions, even in boiling water due to the keto-enol tautomerism and microporous network (Figure 5.2C and D, A.5.7). The COF loses some of its crystallinity when treated with 6N NaOH. Surprisingly, the presence of only one hydroxyl unit compared to the phloroglucinol analog,[17,95] renders the keto-enol tautomerized stabilization to the Schiff bonds in the COF (Figure A.5.8). Field Emission Scanning Electron Microscopy (FESEM) images of the COF discloses its spherical morphology. (Figures A.5.9-A.5.11) The AFM image of a sample prepared by sonicating for 30mins in methanol also showed the presence of isolated spherical particles (Figure A.5.12). Nevertheless, it can be seen from the Field Emission Transmission Electron Microscopy (FETEM) that these spheres are made up of aggregated COF flakes (Figure A.5.13).

Cu@COF characterizations:

The richness of the heteroatoms (pyridyl and hydroxyl groups) in the COF pores inspires us to grow *"capping agent-free"* Cu nanoparticles. At first, the Cu^{2+} ions are adsorbed into the THF suspension of the COF. These pore-confined Cu^{2+} species are then reduced with ascorbic acid

at 80°C.[96] But the reduction of Cu (II) can result in Cu(0) and/or Cu(I) species. Also, prolonged exposure of the composite to air may partially oxidize Cu(0) to Cu(I). The PXRD pattern of the Cu@IISERP-COF9 (Cu@COF) showed only the peaks corresponding to COF (Figure A.5.14). No reflections for Cu were detected suggesting the Cu species to be extremely small-sized nanoparticles or amorphous in nature.

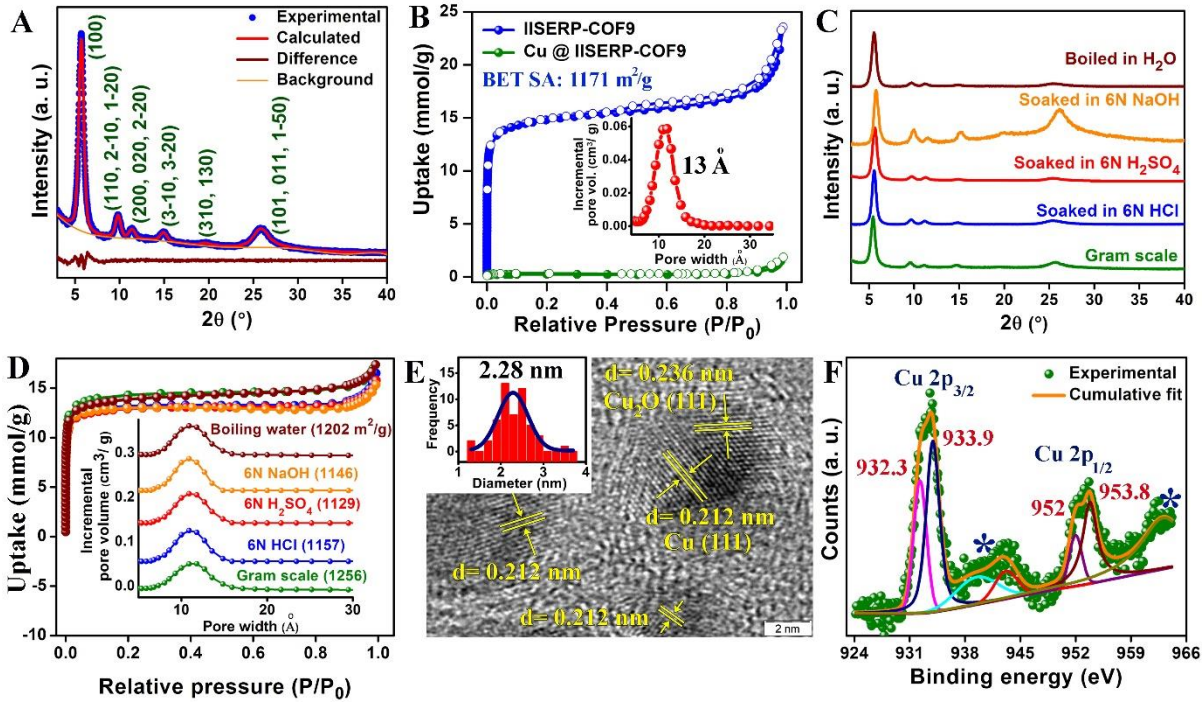

Figure 5.2: (A) Fitting obtained from the Pawley refinement using the COF's PXRD. (B) Comparison of the 77K N_2 adsorption isotherms of IISERP-COF9 and Cu@COF. The BET surface area and the pore size obtained from NLDFT (inset) for the neat COF are given. (C &D) Chemical stability of the IISERP-COF9 from PXRD and 77K N_2 adsorption studies. (E) HRTEM image of the Cu@COF showing the lattice fringes appeared due to Cu and Cu_2O exposed facets. The inset shows the particle size distribution obtained from HRTEM. (F) The XPS spectrum of the Cu@COF showing the peaks corresponding to Cu(0) and Cu(I) and the '*' indicates the satellite peaks which appear due to the higher oxidation state of Cu.

The N_2 isotherm of the Cu@COF measured at 77K shows negligible nitrogen uptake suggesting that the nanoparticles are dispersed in the COF (Figure 5.2B). The spherical morphology is retained for the Cu@COF similar to the neat COF as observed from the FESEM and FETEM images (Figures A.5.15-A.5.16). The Energy Dispersive X-ray (EDX) analysis indicated the homogeneous distribution of Cu and the loading to be at 6.3 weight percent, which agrees well with the 7 wt% determined from the Inductively Coupled Plasma (ICP) analysis (Figure A.5.17). While the elemental mapping revealed the regular dispersion of Cu into the COF and also displays that they remain as isolated clusters (Figure A.5.18-A.5.19). To identify the phase of the Cu species embedded in the COF, high-resolution TEM (HRTEM) images of

the Cu@COF were recorded. The observed lattice fringes indexed to metallic Cu and Cu(I) oxide. The d-spacing of 0.212 nm is assigned to the (111) plane of the cubic Cu nP (ICSD-4349326) and the d-spacing of 0.236 nm is occurring from the (111) plane of the Cu_2O nanoparticle (ICSD 063281). These indicate that the Cu nPs were not amorphous. A statistical estimate of the particle size distribution from HRTEM images collected at two different magnifications exhibits that the Cu nPs have an average size range of 2 to 3nm (Figure 5.2E, A.5.20). The richness of heteroatoms, metal-binding units play a key role to stabilize such small nps which is difficult to achieve from the conventional route.[97] Further, the prominent characterization of the nanoparticles has been done by X-Ray Photo Electron Spectroscopy (XPS). The Cu 2p XPS spectra exhibit peaks at 932.3, 933.9, 952 and 953.8 eV, which are assigned to the Cu $2p_{3/2}$ and Cu $2p_{½}$ levels of the metallic Cu and Cu(I) from Cu_2O (Figure 5.2F).[98-102] Additionally, two shake-up peaks appear at 944 eV and 964 eV. The shake-up peaks or satellite peaks signify the higher oxidation states of Cu.[98-102] The N 1s spectra show two peaks at 398.5 and 400.3 eV 398.5 eV ascribed to the weak Cu-N interaction between Schiff nitrogen and Cu, while the peak at 400.3 is allocated for C=N bonds in the COF (Figure A.5.21).[103,104] The freshly prepared Cu@COF was burnt under dry Ar atmosphere at 600°C to identify the actual phase of nps in the composite. After pyrolysis, this carbon coated np composite was quickly transferred to an air-sensitive PXRD holder equipped with a Kapton window and evacuated before performing X-ray diffraction. The PXRD of this pyrolyzed product displayed characteristic peaks for the Cu (ICSD-4349326) and Cu_2O nanoparticles (ICSD 063281, Figure A.5.22).

Glaser-Hay catalysis:

The Cu@COF can be considered as a copper powder dispersed in an insoluble COF matrix. This makes the catalyst the solid Cu powder which is known to be an excellent catalyst for Glaser-hay coupling in the presence of a suitable amine.[92] However, the activity towards the selectivity of hetero coupling is been evading the other heterogeneous Cu catalysts.[84-91] The catalytic reaction was carried out in the $CHCl_3$-dioxane solvent system with an optimal catalyst loading of 0.0992 mol%. The reaction was carried out in the open air and it finished within four hours. The catalyst was removed by centrifugation from the reaction mixture and ready for further use. The product mixture has been extracted with an organic solvent and conventional column chromatography is employed to purify the product. The average percent yield of the hetero coupled products is around 70% which is quite remarkable (Figure 5.3).

Turn Over Number (TON) for the products is greater than 150 and Turn Over Frequency (TOF) has been obtained for each of the product and this lies around 45 h^{-1} which are quite reasonable for a non-noble metal-based catalyst. The cause of not being able to achieve exceptionally high

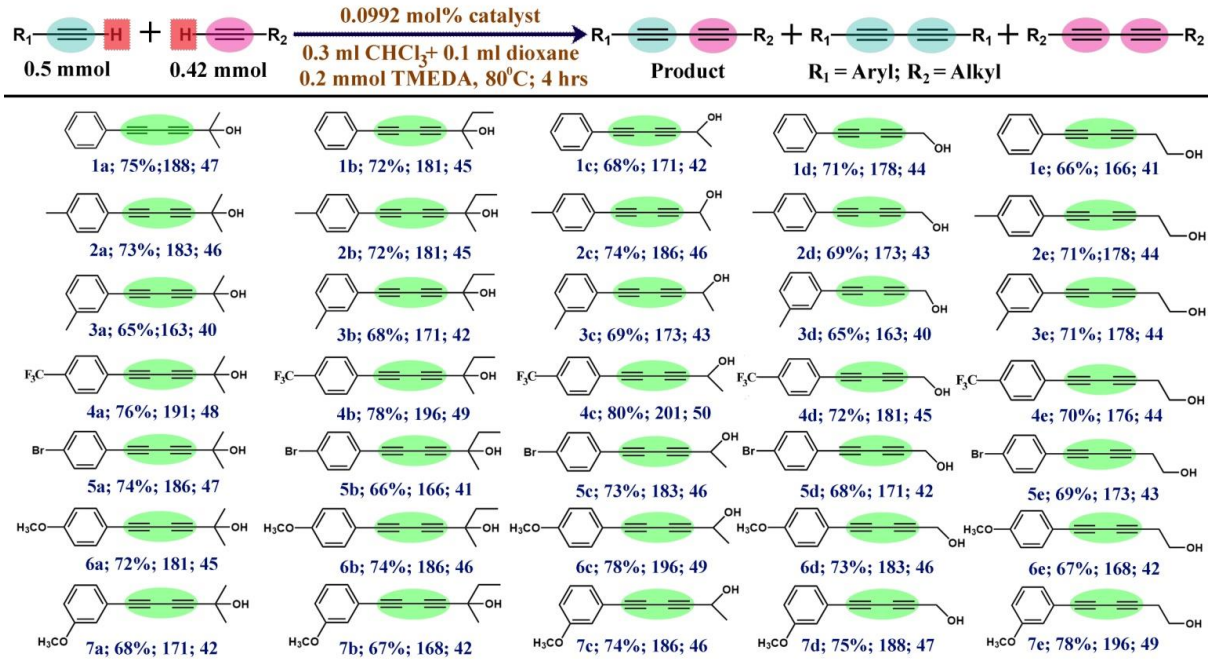

Figure 5.3. The details of the catalytic reaction and substrate scope by Cu@IISERP-COF9 composite. % yield, TON and TOF (h^{-1}) have been demonstrated. Color code: Pink and Cyan ellipses- alkyne bonds linked to different functional units. Green ellipse- alkyne bonds in the hetero-coupled products.

TON (>1000) could be due to the fact that catalytically active species are forming only on the exposed facets of the Cu/Cu_2O clusters. The atoms in the core of the clusters remain as non-participants, in other words, the nps do not fill the pores, rather plugs into the pore,[46] which lowers the active site/COF ratio and hence the TON. Reactivity can be improved if the nanoparticles of < 1 nm can be impregnated. The substrate scope has been studied extensively varying the functional groups on the substrates (Electron Withdrawing Groups (EWG) and Electron Donating Groups (EDG)). Different aliphatic alkynes with primary, secondary and tertiary propargyl alcohols have been used for catalytic conversion. Each of these combinations has produced the hetero-coupled product with good yields, selectivities, and significant TON, TOF (Figure 5.3).

Mechanistic studies:

Cyclic Voltammetry studies of neat COF and composite were employed to identify the different oxidation states implemented by the copper during these catalytic cycles. For this, the sample (Cu@COF) was coated on a Toray paper and used as the working electrode, while Pt and Ag/AgCl were used as the counter and reference electrodes, respectively. The electrolyte was

a saturated solution of tetrabutyl ammonium hexafluorophosphate in acetonitrile.[35] From the CV (Figures 5.4A and B), the prominent oxidation of Cu(0)/Cu(I) to Cu(II) and Cu(III) could be detected.[105,106] Access to such redox activity of copper is vital to achieving synergetic

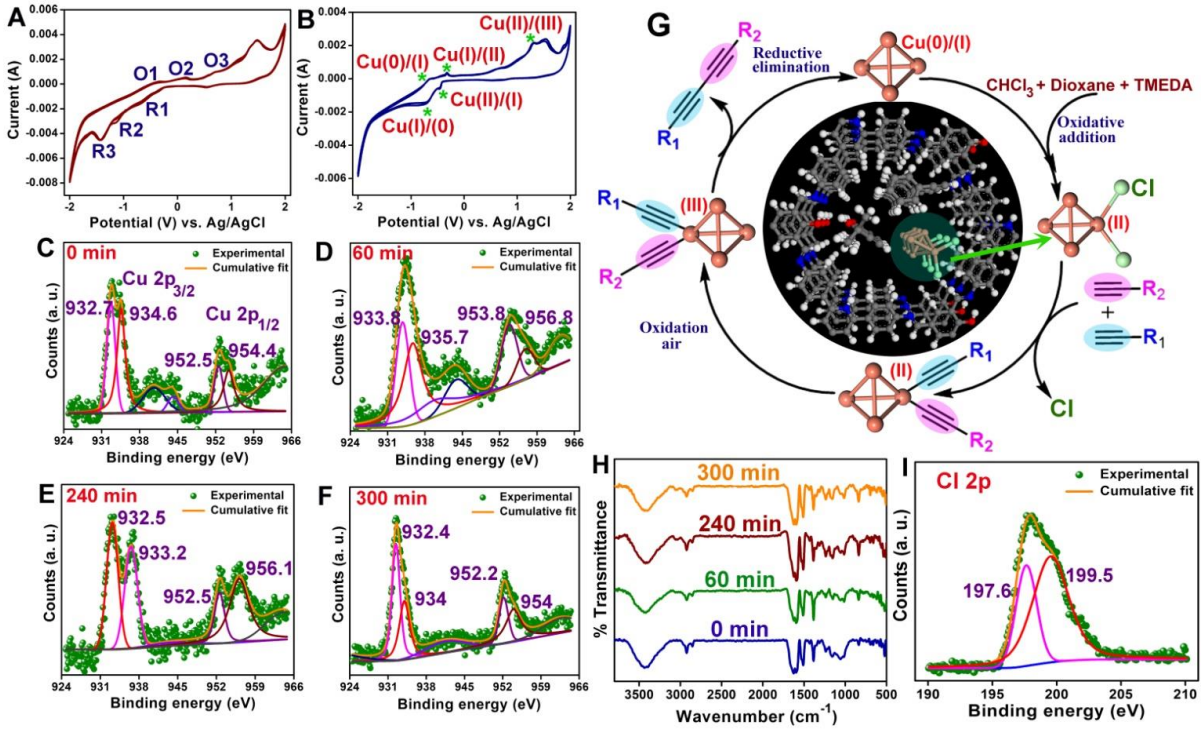

Figure 5.4. (A & B) Cyclic voltammogram of the COF vs. the Cu@COF showing the presence of redox activity in both. For neat COF the reversible redox peaks correspond to the imine bond (R1/O1), keto bond (R2/O2) and pyridyl ring (R3/O3). The CV plot of the Cu@COF displays the reversible formation of the Cu(0)-Cu(I)-Cu(II)-Cu(III)-Cu(0) species. (C-F) XPS spectra from Cu@COF frozen samples isolated at different intervals of the catalysis. (G) Schematic representation of the mechanism of the hetero coupling reaction on the copper cluster surface. (H) IR spectra of the catalyst's extracts from the arrested reactions showing no change in the functional groups of the COF. (I) Cl 2p XPS of the isolated sample during catalysis confirming the presence of Cu-Cl species.

effects during the catalysis.[68]Also, the COF is having a redox activity arising due to the presence of protonation[14] and other electronically active sites[107,108] such as keto-enol tautomerism at the phenol sites (see Figure 5.4). Notably, the redox potentials interrelated in the CV are distinctly different when the Cu is loaded into the sample. This points out that there are prominent synergistic interactions between the Cu nP and the COF which modulate the redox activity and influences the catalytic activity of the composite.

To further support the mechanism which involves the oxidation state change of Cu center, we have performed a detailed XPS study on the frozen aliquots isolated at different intervals of the reaction. The reaction mixture was frozen at different time intervals and the isolated solid was mounted onto the XPS sample holder inside the glove box and analyzed without exposing to air (Figure A.5.23) in order to prevent atmospheric perturbation. Initially, in the presence of

TMEDA and $CHCl_3$, the XPS spectrum of the sample contains shake-up peaks (940.5 and 944.5 eV Figure 5.4C-5.4F) which indicates that Cu is present in a higher oxidation state arising due to the oxidative addition at the Cu center and conversion of Cu(0)/Cu(I) to Cu(II). They undergo ligand exchange with two different alkynes to the Cu(II) centers forming a copper diacetylide complex (Figure 5.4G). Further, the Cu(II) species undergoes oxidation to Cu(III) in the presence of air as explained by Su et al.,[92] which is a critical transition state to assists the formation of hetero-coupled products. Finally, the Cu(III) readily undergoes reductive elimination and the desired hetero-coupled product forms (Figure 5.4G).[92] The XPS spectra of the intermediate specify an important feature of the shake-up peaks (Figures 5.4C-F). Beyond three hours of the reaction, no shake-up peak is observed which reveals the reduction of the Cu (III) species to 0 or +1 (Figure 5.4F). There is a shift of the Cu 2p binding energy with time (Figures 5.4C-5.4F). After 60 minutes into the reaction, the Cu $2p_{3/2}$ and Cu $2p_{½}$ appear at 933.8 and 953.8 eV. But after 300 minutes, the peaks are slightly red-shifted to 932.4 and 952.2 eV which again is a signature of the oxidation state change of Cu species encapsulated in the COF. The structural integrity is demonstrated by the IR spectra collected at these intermediate stages (Figure 5.4H). The confinement effect of the reactants and the Cu-cluster within the COF's functionalized nanopores provide a synergic nanoreactor favoring them to interact mutually.

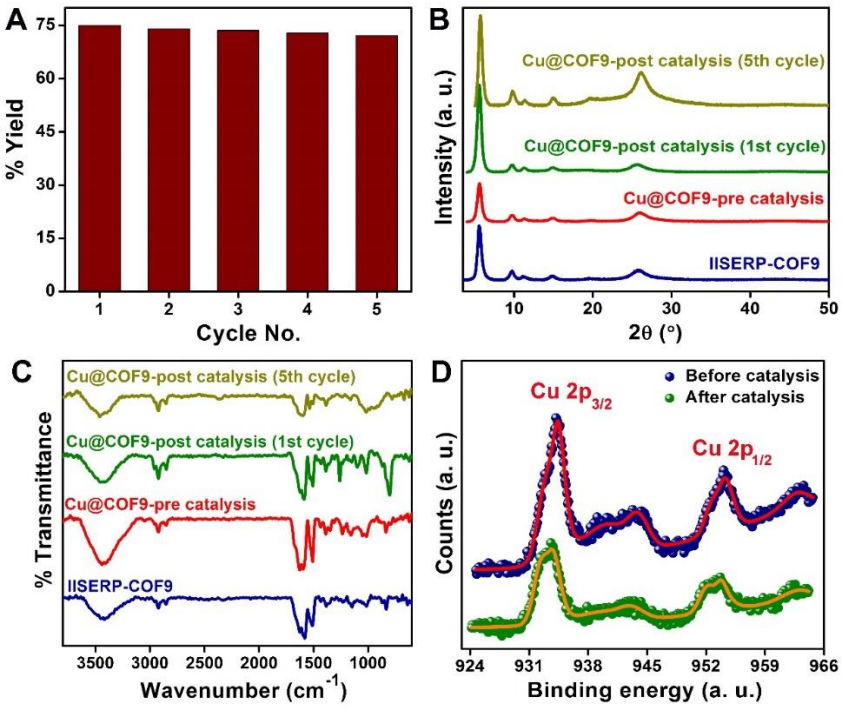

Figure 5.5. (A) The catalyst recyclability demonstrated over 5 cycles using the formation of 1a in Figure 3. Comparison of the (B) PXRD and (C) IR spectra of the spent catalysts with the as-made. (D) A

comparison of the XPS spectra of as-made Cu@COF with the post-catalysis Cu@COF sample showing the integrity of the catalyst.

Catalyst recyclability and spent-catalyst analysis:

The coupling reaction did not proceed when the supernatant extracted by centrifuge was employed as the catalyst-cum-solvent. ICP analysis of this supernatant revealed that no notable Cu was present. This approves the lack of leaching and indirectly the true heterogeneous nature of the catalysis. It is important to demonstrate the recyclability of the catalyst. The Cu@COF could be recycled for 5 cycles with retention of activity (Figure 5.5A) and the PXRD and IR confirmed the integrity of the catalyst (Figures 5.5B and 5.5C) while the XPS of the spent catalyst displays the recovery of the catalyst to its original form (Figure 5.5D, A.5.24-A.5.31).

Investigating favourability for hetero-coupling in the COF pores using DFT studies:

To rationalize the formation of hetero-coupled products and verify the ability of hydroxyl and pyridyl groups to act as the active sites, the substrates along with the catalytically active species (Cu cluster with halides as labile ligands on them (derived from ref.14)) are docked within the

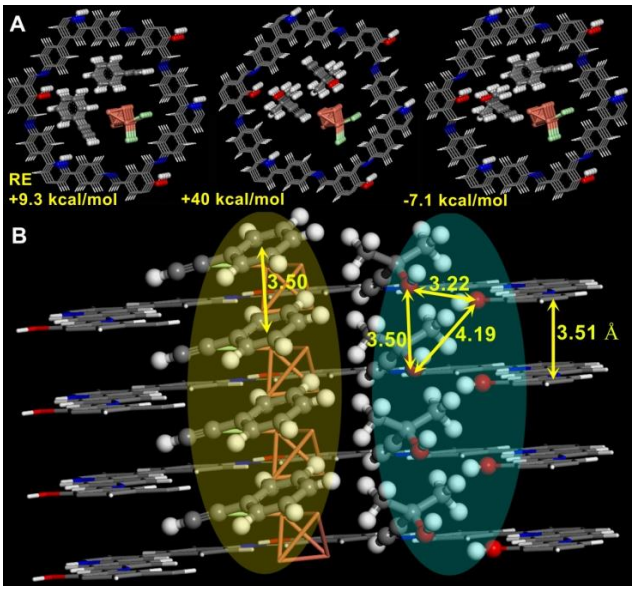

Figure 5.6. (A) Optimized geometries for the homo and hetero substrates with the associated relative energies. (B) A column of π-stacked alkynes and the column of the propargyl alkyne ordered by hydrogen-bonding between their hydroxyl groups with the phenolic groups lining the COF pores. The uniform arrangement of these two substrates confers the lowest energy configuration.

COF pores. The copper cluster employed was a 3 x 3 x 3 copper nanocluster derived from cubic copper lattice.[109]. The existence of the halide cluster has been determined through the EDX and XPS analysis (Figures 5.4H, A.5.31). A CASTEP routine is employed to the different configurations and geometry optimized (Figure 5.6A) which reveals that the co-existence of

hetero substrates with the catalyst in the pore has the lowest relative energy (relative energy: homo = +9.3 kcal/mol vs. hetero = -7.1 kcal/mol). As a control, we verified experimentally that the reaction proceeds even in the absence of TMEDA, but the Cu@COF had to be protonated using formic or acetic acid as it is not a strong enough base like TMEDA hence cannot abstract the proton from the reaction medium (i.e. $CHCl_3$). Removal of TMEDA and providing the required cation from the heterogeneous catalyst does bring extra atom efficiency and diminishes complexity. Most importantly it minimizes the steric crowding by the TMEDA within the limited space available within the Cu@COF nanopores. Besides, the role of the keto groups in the COF is monitored by a few control experiments. The homo-coupled product is predominant when the substrates are devoid of -OH groups. Further, A COF with no hydroxyl groups in the framework catalyzes the homo-product predominantly. In a nutshell, the hydroxyl, pyridyl and pore environment all play a crucial role in the hetero-coupling (Figure 5.6B).

5.5. Conclusion:

Coupling of two inactivated alkyne and to yield hetero-coupled products are challenging to be addressed. Here we have developed a resorcinol-pyridyl based COF that has H-bonding hydroxyl and pyridyl-lined pores. These functionalized pores, when loaded with small Cu/Cu_2O nanoparticles, cooperatively stabilize Cu-halide intermediates (derived from the chloroform solvent) to render an active catalytic nanoreactor. This composite is able to catalyze Glaser-Hay coupling which yielded predominantly hetero-coupled product. A series of control experiments are performed to map the role of COF with support from theoretical (DFT) studies. The abundance of protonation sites and the hydrogen bonding keto groups provide a favorable interaction to stabilize the intermediate. The CV studies suggest the electronic synergy between the COF and the redox-active copper sites. Our findings encourage the application of COF in the designed-development of recyclable heterogeneous catalysts for some crucial organic synthesis.

5.6. References:

1. M. S. Lohse, T. Bein, *Adv. Funct. Mater*. **2018**, *28*, 1705553-1705624.
2. N. Huang, P. Wang, D. Jiang, *Nat. Rev. Mats*. **2016**, *1*, 16068-16087.
3. S. Diercks, O. M. Yaghi, *Science* **2017**, *355*, 1585-1593.
4. S.-Y. Ding, W. Wang, *Chem. Soc. Rev*. **2013**, *42*, 548-568.
5. P. J. Waller, F. Gándara, O. M. Yaghi, *Acc. Chem. Res*. **2015**, *48*, 3053–3063.
6. S. Kandambeth, K. Dey, R. Banerjee, *J. Am. Chem. Soc*. **2019**, *141*, 1807–1822.

7. A. M. Evans, L. R. Parent, N. C. Flanders, R. P. Bisbey, E. Vitaku, M. S. Kirschner, R. D. Schaller, L. X. Chen, N. C. Gianneschi, W. R. Dichtel, *Science* **2018**, *361*, 52-57.
8. Y. Jin, Y. Hu, W. Zhang, *Nat. Rev. Chem*. **2017**, *1*, 0056-0067.
9. S. B. Kalidindi, R. A. Fischer, *Phys. Status Solidi B* **2013**, *250*, 1119–1127.
10. Y. Zeng, R. Zao, Y. Zhao, Y. *Adv. Mater*. **2016**, *28*, 2855–2873.
11. H. H. Fan, A. A. Mundstock, A. A. Feldhoff, A. A. Knebel, J. J. Gu, H. H. Meng, J. J. Caro, *J. Am. Chem. Soc*. **2018**, *140*, 10094–10098.
12. Q. Gao, X. Li, G.-H. Ning, K. Leng, B. Tian, C. Liu, W. Tang, H.-S. Xu, K. P. Loh, *Chem. Commun*. **2018**, *54*, 2349-2352.
13. L. Ascherl, E. W. Evans, M. Hennemann, D. D. Nuzzo, A. G. Hufnagel, M. Beetz, R. H. Friend, T. Clark, T. Bein, F. Auras, *Nat. Commun*. **2018**, *9*, 3802-3810.
14. M. R. Rao, Y. Fang, S. D. Feyter, D. F. Perepichka, *J. Am. Chem. Soc*. **2017**, *139*, 2421–2427.
15. Q. Sun, B. Aguila, L. D. Earl, C. W.Abney, L. Wojtas, P. K. Thallapally, S. Ma, *Adv. Mater*. **2018**, 1705479-1705488.
16. D. Mullangi, V. Dhavale, S. Shalini, S. Nandi, S. Collins, T. Woo, S. Kurungot, R. Vaidhyanathan, *Adv. Energy Mater*. **2016**, *6*, 1600110-1600118.
17. S. Haldar, K. Roy, S. Nandi, D. Chakraborty, D. Puthusseri, Y. Gawli, S. Ogale, R. Vaidhyanathan, *Adv. Energy Mater*. **2017**, *8*, 1702170-1702181.
18. S. Nandi, S. K. Singh, D. Mullangi, R. Illathvalappil, L. George, C. P. Vinod, S. Kurungot, R. Vaidhyanathan, *Adv. Energy Mater*. **2016**, *6*, 1601189-1601200.
19. S. Jin, M. Supur, M. Addicoat, K. Furukawa, L. Chen, T. Nakamura, S. Fukuzumi, S. Irle, D. Jiang, *J. Am. Chem. Soc*. **2015**, *137*, 7817–7827.
20. Q. Xu, S. Dalapati, D. Jiang, *ACS Cent. Sci*. **2016**, *2*, 586–587.
21. T. Banerjee, K. Gottschling, G. Savasci, C. Ochsenfeld, B. V. Lotsch, *ACS Energy Lett*. **2018**, *3*, 400–409.
22. J. Lv, X. Y. Tan, J. Xie, R. Yang, M. Yu, S. Sun, M. D. Li, D. Yuan; Y. Wang, *Angew. Chem. Int. Ed*. **2018**, *57*, 12716–12720
23. G. H. V. Bertrand, V. K. Michaelis, T.-C. Ong, R. G. Griffin, M. Dincă, *Proc. Nat. Ac. Sci*. **2013,** *110*, 4923-4928.
24. Z. Luo, L. Liu, J. Ning, K. Lei, Y. Lu, F. Li, J. A. Chen, *Angew. Chem. Int. Ed*. **2018**, *57*, 9443 – 9446
25. P. Bhanja, K. Bhunia, S. K. Das, D. Pradhan, R. Kimura, Y. Hijikata, S. Irle, A. Bhaumik, *ChemSusChem* **2017**, *10*, 921 – 929.
26. A. Khayum, V. Vijayakumar, S. Karak, S. Kandambeth, M. Bhadra, K. Suresh, N. Acharambath, S. Kurungot, R. Banerjee, *ACS Appl. Mater. Interfaces* **2018**, *10*, 28139–28146.
27. Y. Zhang, J. Duan, D. Ma, P. Li, S. Li, H. Li, J. Zhou, X. Ma, X. Feng, B. Wang, *Angew. Chem. Int. Ed*. **2017**, *56*, 16313 –16317.
28. Y. Du, H. Yang, J. M. Whiteley, S. Wan, Y. Jin, S.-H. Lee, W. Zhang, *Angew. Chem. Int. Ed*. **2016**, *55*, 1737 –1741.
29. Z. Meng, A. Aykanat, K. A. Mirica, *Chem. Mater*. **2019**, *31*, 819–825.
30. H. Ma, B. Liu, B. Li, L. Zhang, Y.-G. Li, H.-Q. Tan, H.-Y. Zang, G. Zhu, *J. Am. Chem. Soc*. **2016**, *138*, 5897–5903.
31. W. Kong, W. Jia, R. Wang, Y. Gong, C. Wang, P. Wu, J. Guo, *Chem. Commun*. **2019**, *55*, 75-78.
32. J. W. Crowe, L. A. Baldwin, P. L. McGrier, *J. Am. Chem. Soc*. **2016**, *138*, 10120-10123.
33. A. Bhunia, D. Esquivel, S. Dey, R. Fern´andez-Ter´an, Y. Goto, S. Inagaki, P. V. D. Voort, C. A. Janiak, *J. Mater. Chem. A* **2016**, *4*, 13450-13457.
34. S. Dalapati, E. Jin, M. Addicoat, T. Heine, D. Jiang, *J. Am. Chem. Soc.* **2016**, *138*, 5797−5800.

35. S. Haldar, D. Chakraborty, B. Roy, B.; S. B. Gangadhar, K. Rinku, D. Mullangi, P. Hazra, D. Kabra, R. Vaidhyanathan, *J. Am. Chem. Soc*. **2018**, *140*, 13367−13374.
36. P. Das, S. K. Mandal, *J. Mater. Chem. A* **2018**, *6*, 16246–16256.
37. G.-J. Chen, X.-B. Li, C.-C. Zhao, H.-C. Ma, J.-L. Kan, Y.-B. Xin, C.-X. Chen, Y.-B. Dong, *Inorg. Chem*. **2018**, *57*, 2678−2685.
38. X. Shi, Y. Yao, Y. Xu, K. Liu, G. Zhu, L. Chi, G. Lu, *ACS Appl. Mater. Interfaces* **2017**, *9*, 7481−7488.
39. M. Mu, Y. Wang, Y. Qin, X. Yan, Y. Li, L. Chen, *ACS Appl. Mater. Interfaces* **2017**, *9*, 22856−22863.
40. Y. Han, M. Zhang, Y.-Q. Zhang, Z.-H. Zhang, *Green Chem.* **2018**, *20*, 4891-4900.
41. S.-Y. Ding, J. Gao, J.; Q. Wang, Y. Zhang, W.-G. Song, C.-Y. Su, W. Wang, *J. Am. Chem. Soc*. **2011**, *133*, 19816–19822.
42. X. Wang, X. Han, J. Zhang, X. Wu, Y. Liu, Y. Cui, *J. Am. Chem. Soc*. **2016**, *138*, 12332−12335.
43. X. Han, Q. Xia, J. Huang, Y. Liu, C. Tan, Y. Cui, *J. Am. Chem. Soc*. **2017**, *139*, 8693−8697.
44. H. Li, Q. Pan, Y. Ma, X. Guan, M. Xue, Q. Fang, Y. Yan, V. Valtchev, S. Qiu, *J. Am. Chem. Soc.* **2016**, *138*, 14783−14788.
45. S. Lu, Y. Hu, S. Wan, R. McCaffrey, Y. Jin, H. Gu, W. Zhang, *J. Am. Chem. Soc*. **2017**, *139*, 17082−17088.
46. D. Mullangi, D. Chakraborty, A. Pradeep, V. Koshti, C. P. Vinod, S. Panja, S. Nair, R. Vaidhyanathan, *Small* **2018**, *14*, 1801233-1801241.
47. D. Mullangi, S. Nandi, S. Shalini, S. Sreedhala, C. P. Vinod, R. Vaidhyanathan, *Sci. Rep*. **2015,** *2*, 10876-10888.
48. D. Kaleeswaran, R. Antony, A. Sharma, A. Malani, R. Murugavel, *ChemPlusChem* **2017**, *82*, 1253-1265.
49. S. M. J. Rogge, A. Bavykina, J. Hajek, H. Garcia, A. Olivos-Suarez, A. Sepu´lveda-Escribano, A. Vimont, G. Clet, P. Bazin, F. Kapteijn, M. Daturi, *Chem. Soc. Rev*. **2017**, *46*, 3134-3184.
50. M. Yang, L. Wang, M. Li, T. Hou, Y. Li, *AIP Adv.* **2015**, *5*, 067136-067145.
51. X. Tian, X. Sun, Z. Jiang, Z.-J. Jiang, X. Hao, D. D. Shao, T. Maiyalagan, *ACS Appl. Energy Mater*. **2018**, *1*, 143−153.
52. J. Zhang, C. Zhao, N. Liu, H. Zhang, J. Liu, Y. Fu, B. Guo, Z. Wang, S. Lei, P. Hu, *Sci. Rep*. **2016**, *6*, 28330-28340.
53. W. Shi, A. Lei, **2014**, *55*, 2763-2772.
54. J. Liu, J. W. Y. Lam, B. Z. Tang, Chem. Rev. 2009, 109, 5799- 5867.
55. J.-N. Tisserant, R. Hany, E. Wimmer, A. Sanchez-Ferrer, J. Adamcik, G. Wicht, F. Nueesch, D. Rentsch, A. Borgschulte, R. Mezzenga, J. Heier, *Macromolecules* **2014**, *47*, 721-728.
56. S. Eisler, A. D. Slepkov, E. Elliott, T. Luu, R. McDonald, F. A. Hegmann, R. R. Tykwinski, *J. Am. Chem. Soc*. **2005**, *127*, 2666-2676.
57. B. Li, B. Gui, G. Hu, D. Yuan, C. Wang, *Inorg. Chem*. **2015**, *54*, 5139–5141.
58. M. A. Gotthardt, S. Grosjean, T. S. Brunner, J. Kotzel, A. M. Gänzler, S. Wolf, S. Bräse W. Kleist, *Dalton Trans*. **2015**, *44*, 16802-16809.
59. T. V. Zons, L. Brokmann, J. Lippke, T. Preuße, M. Hulsmann, A. Schaate, P. Behrens, A. Godt, *Inorg. Chem*. **2018**, *57*, 3348−3359.
60. P. Cadiot, W. Chodkiewicz, Marcel Dekker: New York, **1969**.
61. K. S. Sindhu, A. P. Thankachan, P. S. Sajitha, G. Anilkumar, *Org. Biomol. Chem*. **2015**, *13*, 6891-6905.
62. M. Yu, D. Pan, W. Jia, W. Chen, N. Jiao, *Tet. Lett*. **2010**, *51*, 1287-1290.
63. J. R. Suarez, D. Collado-Sanz, D. J. Cardenas, J. L. Chiara, *J. Org. Chem*. **2015**, *80*, 1098−1106
64. K. Balaraman, V. Kesavan, *Synthesis* **2010**, 3461-3466.

65. J. S. Lampkowski, C. E. Durham, M. S. Padilla, D. D. Young, *Org. Biomol. Chem*. **2015**, *13*, 424-427.
66. N. Devarajan, M. Karthik, P. Suresh, *Org. Biomol. Chem*. **2017**, *15*, 9191–9199.
67. F. Chen, K. Shen, J. Chen, X. Yang, J. Cui, Y. Li, *ACS Cent. Sci*. **2019**, *5*, 176–185.
68. R. Bai, G. Zhang, H. Yi, Z. Huang, X. Qi, C. Liu, J. T. Miller, A. J. Kropf, E. E. Bunel, Y. Lan, A. Lei, *J. Am. Chem. Soc*. **2014**, *136*, 16760−16763.
69. W. Yin, C. He, M. Chen, H. Zhang, A. Lei, *Org. Lett*. **2009**, *11*, 709–712.
70. K. S. Sindhu, G. Anilkumar, *RSC Adv*. **2014**, *4*, 27867-27887.
71. S. E. Allen, R. R. Walvoord, R. Padilla-Salinas, M. C. Kozlowski, *Chem. Rev*. **2013**, *113*, 6234–6458.
72. M. B. Gawande, A. Goswami, F.-X. Felpin, T. Asefa, X. Huang, R. Silva, X. Zou, R. Zboril, R. S. Varma, *Chem. Rev*. **2016**, *116*, 3722−3811.
73. K. D. Karlin, S.Itoh, *John Wiley & Sons, Inc.: Hoboken, NJ* **2011**.
74. G. Evano, N. Blanchard, *John Wiley & Sons, Inc.: Hoboken, NJ* **2014**.
75. P. Siemsen, R. C. Livingston, F. Diederich, *Angew. Chem. Int. Ed*. **2000**, *39*, 2632- 657.
76. X. Jia, K. Yin, C. Li, J. Li, H. Bian, *Green Chem*. **2011**, *13*, 2175-2178.
77. J. D. Crowley, S. M. Goldup, N. D. Gowans, D. A. Leigh, *J. Am. Chem. Soc*. **2010**, *132*, 6243-6248.
78. K. Kamata, S. Yamaguchi, M. Kotani, K. Yamaguchi, N. Mizuno, *Angew. Chem. Int. Ed*. **2008**, *47*, 2407-2410.
79. H.-Y. Gao, H. Wagner, D. Zhong, J.-H. Franke, A. Studer, H. Fuchs, *Angew. Chem., Int. Ed*. **2013**, *52*, 4024-4028.
80. S. Zhang, X. Liu, T. Wang, *Adv. Synth. Catal*. **2011**, *353*, 1463-1466.
81. G.-L. Lu, K.-H. Choi, Y.-H. J. Guo, *Organomet. Chem*. **2005**, *690*, 177-186.
82. B. S. Navale, R. G. Bhat, *RSC Adv*. **2013**, *3*, 5220–5226.
83. Y. Liu, C. Wang, X. Wang, J.-P. Wan, *Tetrahedron Lett*. **2013**, *54*, 3953-3955.
84. F. Alonso, M. Yus, *ACS Catal*. **2012**, *2*, 1441−1451.
85. V. T. Tripp, J. S. Lampkowski, R. Tyler, D. D. Young, *ACS Comb. Sci*. **2014**, *16*, 164–167.
86. R. Xiao, R. Yao, M. Cai, *Eur. J. Org. Chem*. **2012**, 4178–4184.
87. P. Kuhn, A. Alix, M. Kumarraja, B. Louis, P. Pale, J. Sommer, *Eur. J. Org. Chem*. **2009**, 423–429.
88. B. Lai, R. Bai, Y. Gu, *ACS Sustainable Chem. Eng*. **2018**, *6*, 17076−17086.
89. H. Xu, K. Wu, J. Tian, L. Zhu, X. Yao, *Green Chem*. **2018**, *20*, 793–797.
90. L. V. Gelderen, G. Rothenberg, V. R. Calderone, K. Wilson, N. R. Shiju, *Appl. Organomet. Chem*. **2013**, *27*, 23–27.
91. J. S. Lampkowski, D. M. Uthappa, J. F. Halonski, J. C. Maza, D. D. Young, *J. Org. Chem*. **2016**, *81*, 12520−12524.
92. L. Su, J. Dong, L. Liu, M. Sun, R. Qiu, Y. Zhou, S.-F. Yin, *J. Am. Chem. Soc*. **2016**, *138*, 12348−12351.
93. W. Chen, W. Yan, S. Wu, Z. Xu, K. W. K. Yeung, C. Yi, Macromol. Chem. Phys. 2010, 211, 1803–1813.
94. G.-H. Ning, Z. Chen, Q. Gao, W. Tang, Z. Chen, C. Liu, B. Tian, X. Li, K. P. Loh, *J. Am. Chem. Soc*. **2016**, *138*, 12348−12351.
95. S. Kandambeth, A. Mallick, B. Lukose, M. V. Mane, T. Heine, R. Banerjee, *J. Am. Chem. Soc*. **2012**, *134*, 19524−19527.
96. G. Dinda, D. Halder, C. Vazquez-Vazquez, M. A. Lopez-Quintela, A. Mitra, *J. Surface Sci. Technol*. **2015**, *31*, 117-122.
97. C. M. Phan, H. M. Nguyen, *J. Phys. Chem. A* **2017**, *121*, 3213−3219.
98. H. Xu, J.-X. Feng, Y.-X. Tong, G.-R. Li, *ACS Catal*. **2017**, *7*, 986−991.

99. P. Muthukumar, V. V. Kumar, G. R. K. Reddy, P. S. Kumar, S. P. Anthony, *Catal. Sci. Technol*. **2018**, *8*, 1414-1422.
100. M. Deo, S. Mujawar, O. Game, A. Yengantiwar, A. Banpurkar, S. Kulkarni, J. Jogd, S. Ogale, *Nanoscale* **2011**, *3*, 4706–4712.
101. H. Chen, T. Tu, M. Wen, *Dalton Trans*. **2015**, *44*, 15645–15652.
102. S. M. Pawar, J. Kim, A. I. Inamdar, H. Woo, Y. Jo, B. S. Pawar, S. Cho, H. Kim, H. Im, *Sci rep*. **2015**, *6*, 21310-21319.
103. D. A. Bulushev, A. L. Chuvilin, V. I. Sobolev, S. G. Stolyarova, Y. V. Shubin, I. P. Asanov, A. V. Ishchenko, G. Magnani, M. Ricc`o, A. V. Okotrub, L.G. Bulusheva, *J. Mater. Chem. A* **2017**, *5*, 10574–10583.
104. S. Bhunia, S. K. Das, R. Jana, S. C. Peter, S. Bhattacharya, M. Addicoat, A. Bhaumik, A. Pradhan, *ACS Appl. Mater. Interfaces* **2017**, *9*, 23843−23851.
105. H. H. Hassan, I. H. A. Badr, H. T. M. Abdel-Fatah, E. M. S. Elfeky, A. Mostafa, *Arabian Journal of Chemistry* **2015**, DOI 10.1016/j.arabjc.2015.07.001.
106. F. P. Bossu, K. L. Chellappa, D. W. Margerum, *J. Am. Chem. Soc*. **1977**, *99*, 2195-2203.
107. A. G. Peroff, E. Weitz, R. P. V. Duyne, *Phys. Chem. Chem. Phys*. **2016**, *18*, 1578-1586.
108. P. G. Siorski, K. S. Danel, M. Matusiewicz, T. Uchacz, W. Ku´znik, A. V. Kityk, *Fluoresc*. **2012**, *22*, 81–91.
109. R. W. G. Wyckoff, Crystal Structures 1, Second Edition. Interscience Publishers, New York. **1963**, 7-83.

Chapter 5 has been adopted form the reference "Chakraborty *et al*. *ACS Appl. Mater. Interfaces* **2019**, *11*, 15670−15679." With permission from the American Chemical Society.

5.7. Appendix of Chapter 5:

Table A.4.1. Atomic coordinates of the IISERP-COF9.

Space group: Pm; Crystal system: Monoclinic.

Unit cell parameters: a = 18.6612; b = 18.6612; c = 3.5144; β = 120°.

Atom	x	y	z
C1	0.26172	0.48924	0.02774
N2	0.18271	0.43832	0.02728
C3	0.64898	0.79977	0.02819
C4	0.28132	0.70114	0.02638
C5	0.36754	0.75186	0.02698
C6	0.19833	0.31381	0.02721
C7	0.16259	0.22765	0.02719
C8	0.07633	0.17681	0.02714
C9	0.02668	0.21379	0.02719
C10	0.06227	0.29971	0.02729
C11	0.03773	0.08566	0.02701
N12	0.08497	0.04861	0.02663
C13	0.5092	0.77455	0.02819
N14	0.56109	0.74757	0.02822
C15	0.20311	0.85192	0.02597
C16	0.29722	0.57952	0.02762
C17	0.24652	0.61514	0.02663
C18	0.68647	0.88629	0.0281
C19	0.77261	0.93518	0.02778
C20	0.82254	0.89853	0.02762
C21	0.78448	0.81194	0.02774
C22	0.69838	0.76304	0.02806
C23	0.91378	0.95043	0.02723
C24	0.95158	0.03663	0.02735
C25	0.22647	0.73646	0.02594
N26	0.25527	0.8158	0.02609
C27	0.14815	0.35034	0.02728
C28	0.41912	0.71747	0.02786
C29	0.38353	0.63056	0.02827
C30	0.11655	0.80274	0.02622
C31	0.06723	0.8395	0.02635
C32	0.10318	0.92599	0.02618
C33	0.18972	0.97501	0.02593
C34	0.23925	0.93817	0.02585
C35	0.05035	0.96445	0.0265
C36	0.96409	0.91464	0.0268
O37	0.43246	0.59497	0.03061

H38	0.30656	0.4645	0.02826
H39	0.39644	0.82203	0.02675
H40	0.26853	0.3549	0.02717
H41	0.20367	0.19853	0.02722
H42	0.04361	0.1735	0.02716
H43	0.02115	0.32879	0.02737
H44	0.53293	0.84395	0.02842
H45	0.17634	0.57392	0.02603
H46	0.64656	0.9167	0.02829
H47	0.80302	1.0055	0.02765
H48	0.82392	0.78101	0.02758
H49	0.668	0.69271	0.02821
H50	0.91194	0.06735	0.02774
H51	0.15679	0.69208	0.02545
H52	0.08654	0.73245	0.0263
H53	0.00306	0.79922	0.0266
H54	0.22022	1.04534	0.02578
H55	0.30954	0.97848	0.02567
H56	0.93452	0.84439	0.0267
H57	0.49133	0.63632	0.02771

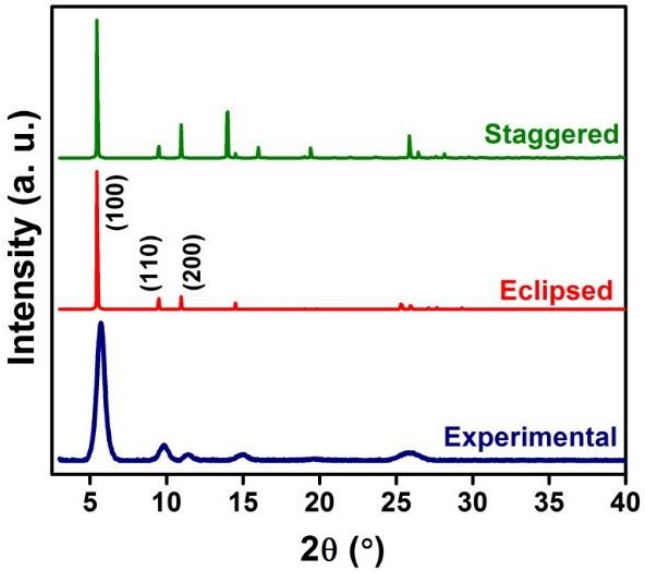

Figure A.5.1. Comparison of the PXRD patterns, simulated vs. experimental.

Thermo Gravimetric Analysis:

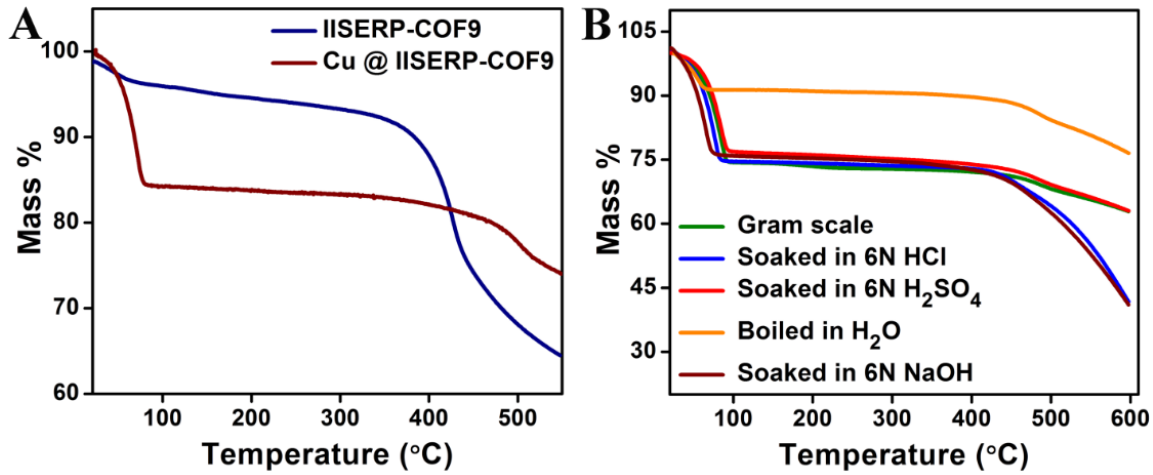

Figure A.5.2. (A) Thermo gravimetric analysis of IISERP-COF9 and Cu@IISERP-COF9. Note that the weight loss below 100°C for the Cu@IISERP-COF9 is due to occluded water molecules and not any adsorbed ascorbic acid (occluded ascorbic acid is known to leave at >200°C, (*J. Surface Sci. Technol.* **2015**, *31*, 117-122). (B) TGA of IISERP-COF9 treated with different chemicals.

Powder X-Ray Diffraction for chemical and thermal stability of COF:

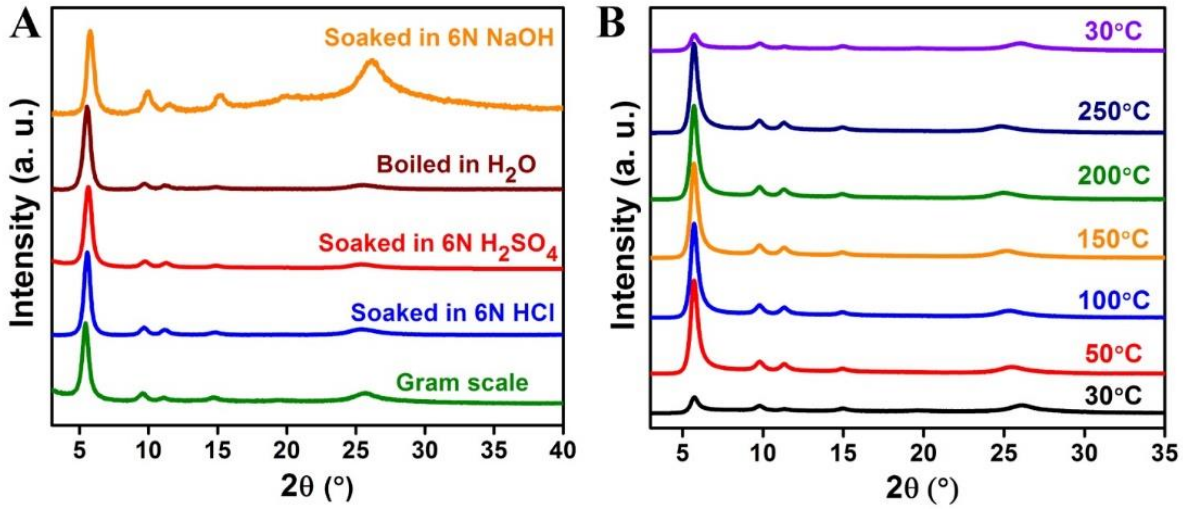

Figure A.5.3. (A) Powder X-ray diffraction patterns of IISERP-COF9 treated with different harsh chemicals. The COF retains its crystallinity even when exposed to acids and bases. (B) Variable Temperature (VT) PXRD of IISERP-COF9 showing the thermal stability of the COF.

Solid-State Nuclear Magnetic Resonance Spectroscopy (SSNMR):

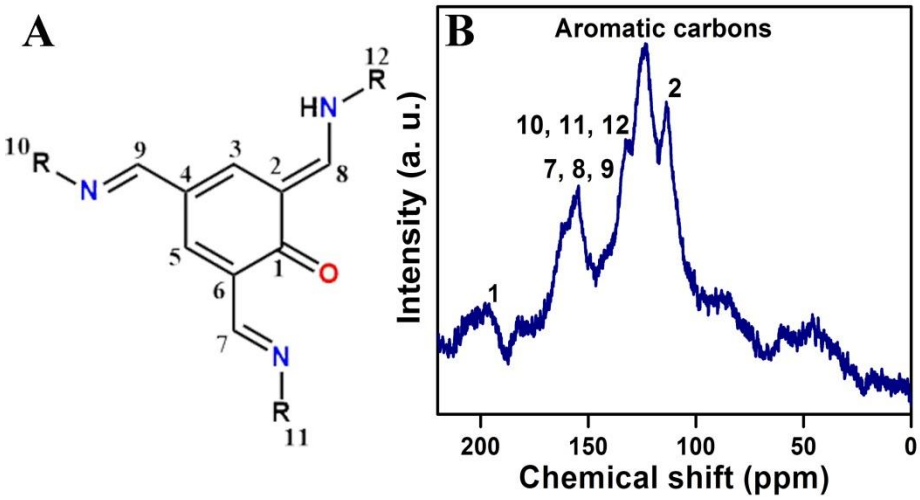

Figure A.5.4. Solid-state magic angle spinning NMR of IISERP-COF9.

Infra-Red analysis (IR):

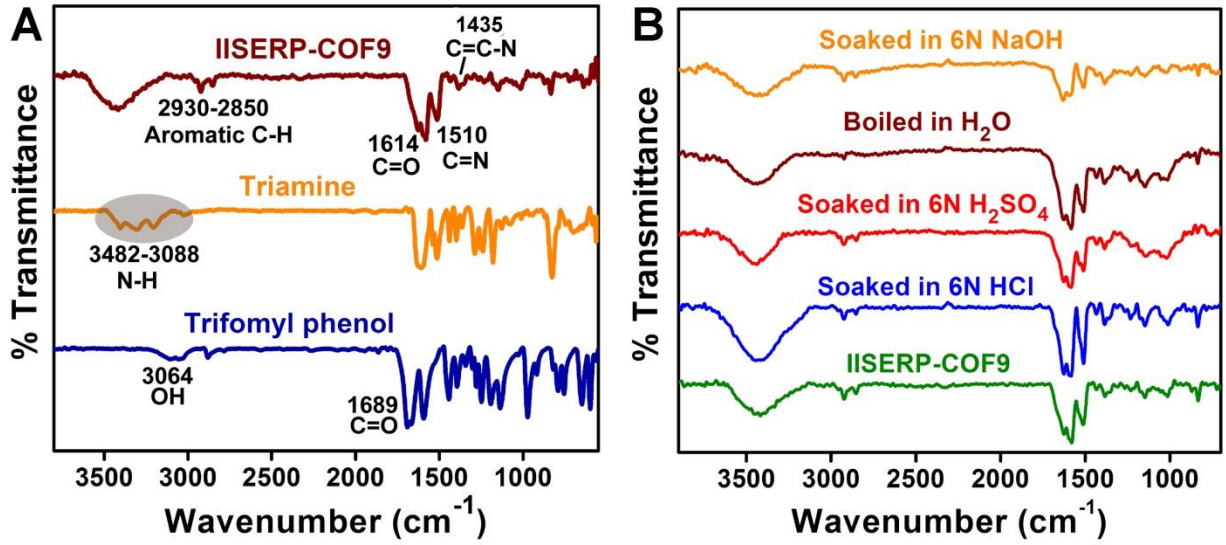

Figure A.5.5. (A) IR spectra of building blocks and IISERP-COF9. (B) Chemical stability demonstrated from IR spectra.

Discussion: The formation of COF is evidenced by the disappearance of N-H vibrational peaks at 3088 cm^{-1} to 3482 cm^{-1} and the presence of imine bond stretching at 1510 cm^{-1}. Carbonyl stretching frequency of the triformyl phenol (1689 cm^{-1}) shifts to the lower number 1614 cm^{-1} in COF. This is because the COF exists in keto form. The –OH stretching in triformyl phenol (3064 cm^{-1}) is absent in the COF. Moreover, the existence of -C=C-N bond vibration at 1435 cm^{-1} sows that the COF is in keto form a solid form. Aromatic –C-H vibration appears at ~2900 cm^{-1}. However, triformyl phenol-based COF exists as both enol and keto form in solution phase.[S2] (*Source: Infrared and Raman Spectra of Inorganic and Coordination Compounds, Part B, Applications in Coordination, Organometallic, and Bioinorganic Chemistry, 6th Edition, Kazuo Nakamoto*).

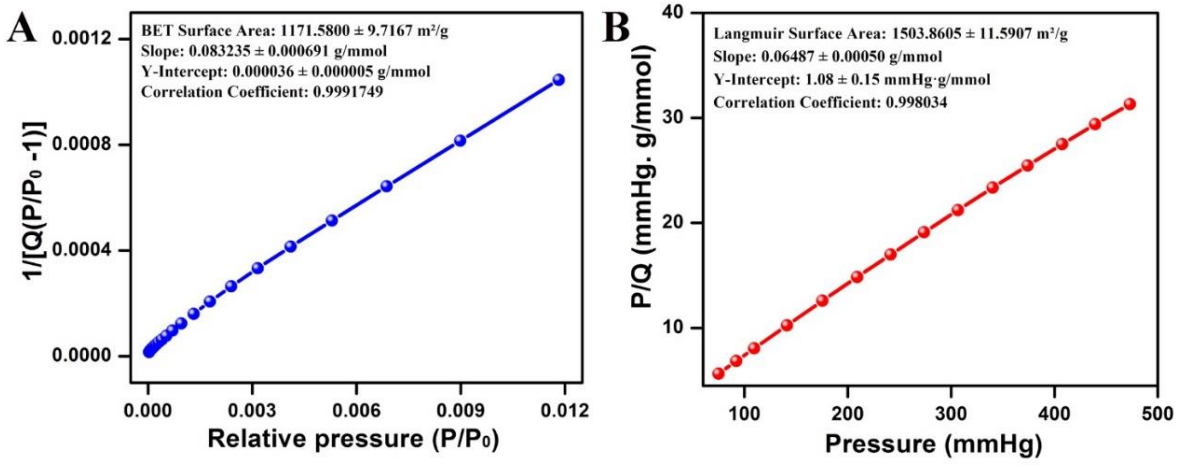

Figure A.5.6. (A) Brunauer–Emmett–Teller surface area plot for IISERP-COF9. (B) Langmuir surface area plot for IISERP-COF9.

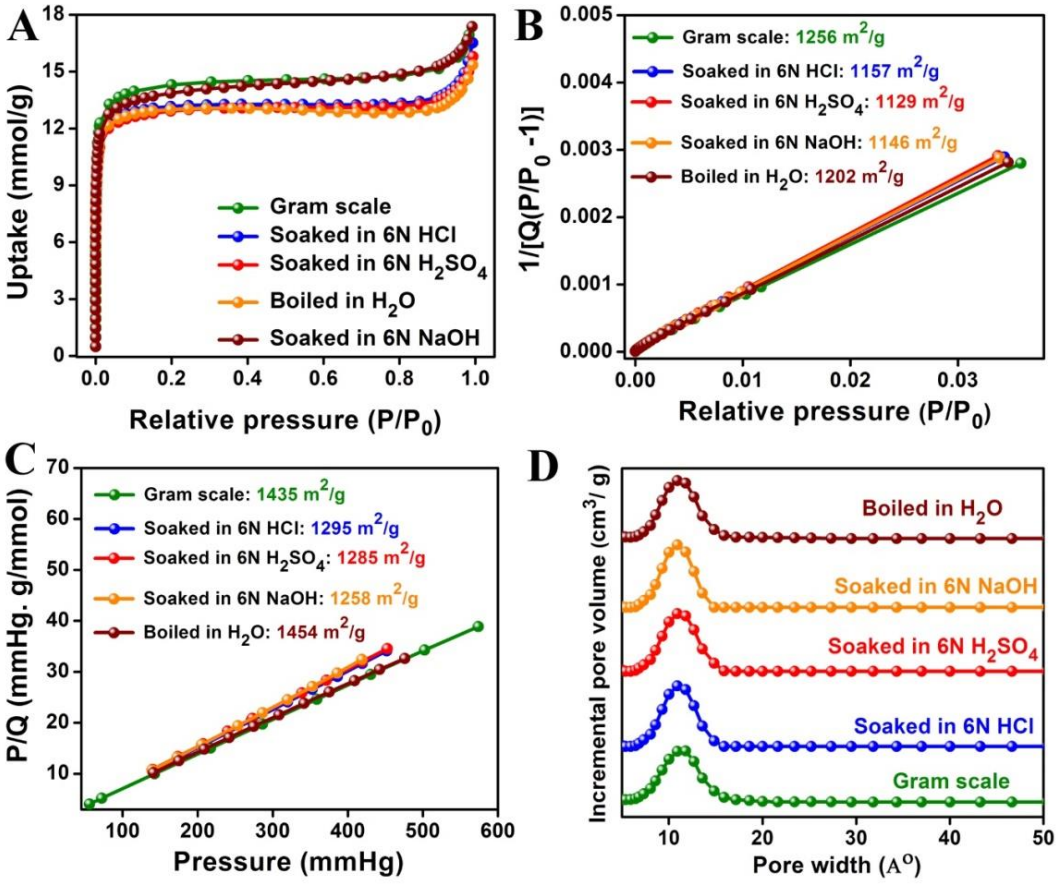

Figure A.5.7. (A) N_2 at 77 K isotherms of samples of IISERP-COF9 subjected to different chemical treatments. (B) BET surface area for samples of IISERP-COF9 subjected to different chemical treatments. (C) Langmuir surface area for samples of IISERP-COF9 exposed to harsh chemicals such as acids and bases. (D) The pore size distribution of samples of IISERP-COF9 subjected to different chemical treatments.

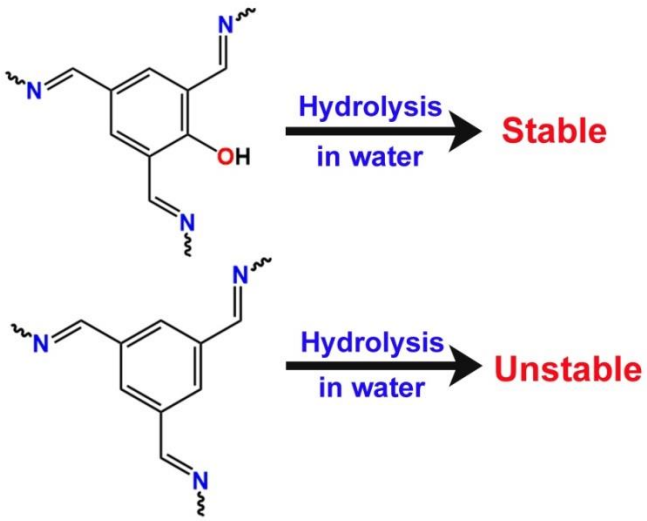

Figure A.5.8. Scheme showing that the presence of –OH group in the framework imparts stability through keto-enol tautomerism (triformyl phenol unit) whereas the benzene analogue is unstable to hydrolysis.

Microscopic studies:

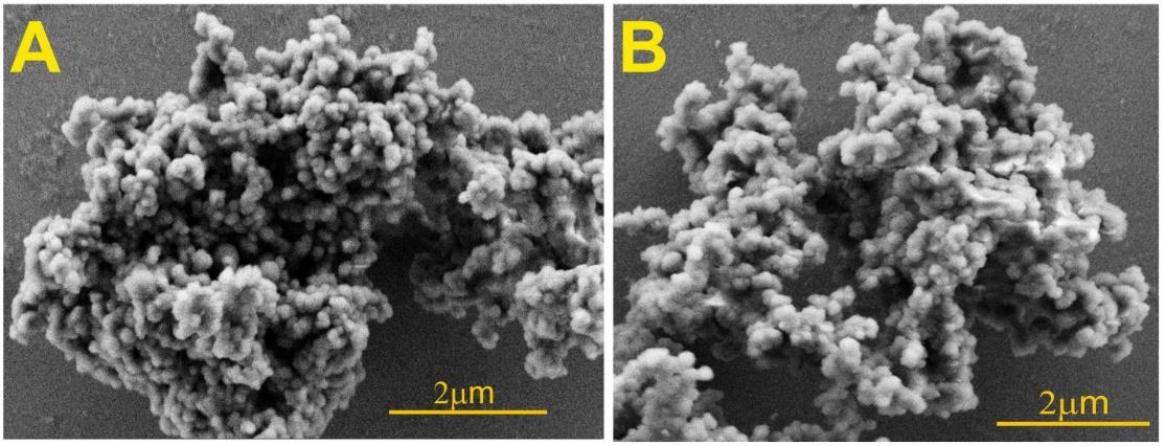

Figure A.5.9. (A, B) Scanning Electron Microscopic images of IISERP-COF9.

Element	Weight%	Atomic%
C K	64.43	69.83
N K	10.61	9.86
O K	24.95	20.30
Totals	100.00	

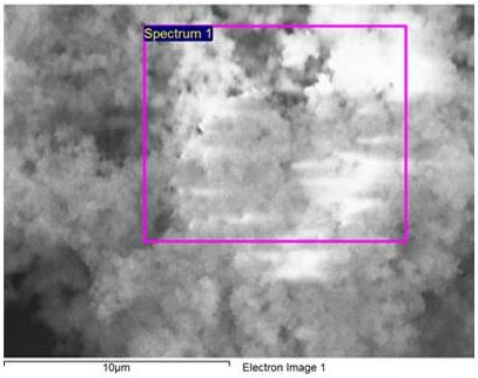

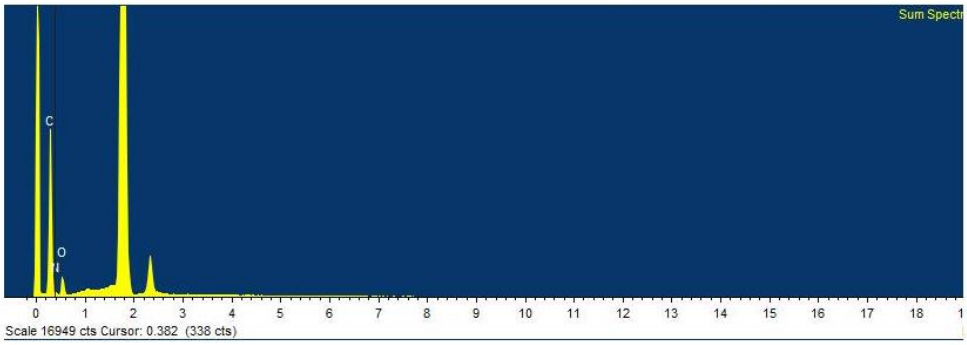

Figure A.5.10. Energy Dispersive X-Ray (EDX) images of IISERP-COF9.

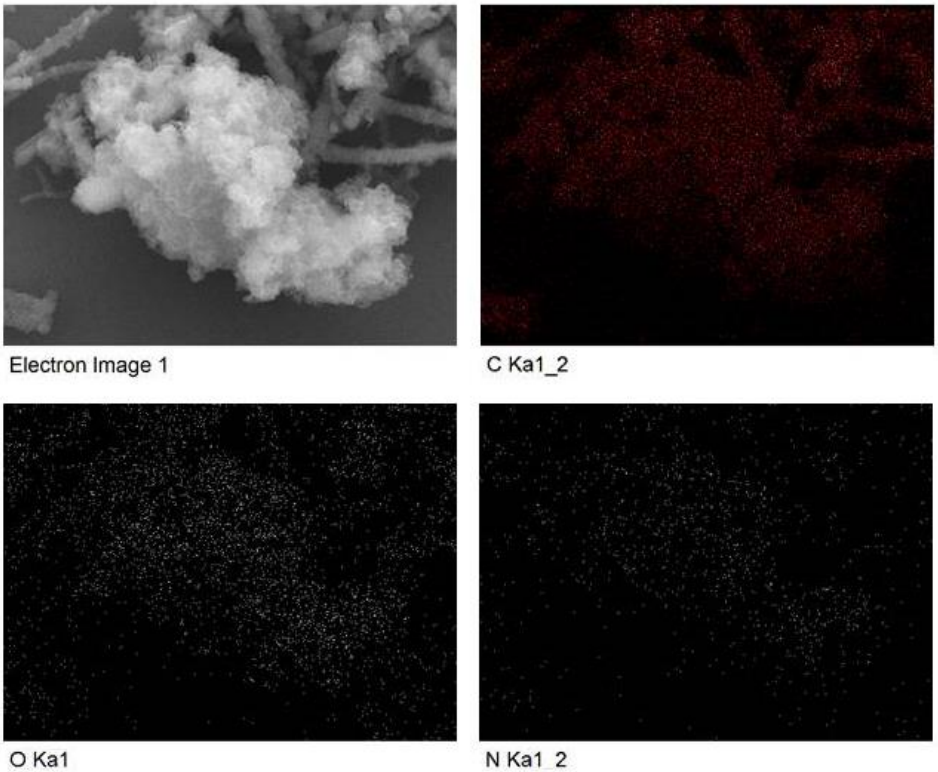

Figure A.5.11. Elemental mapping of IISERP-COF9.

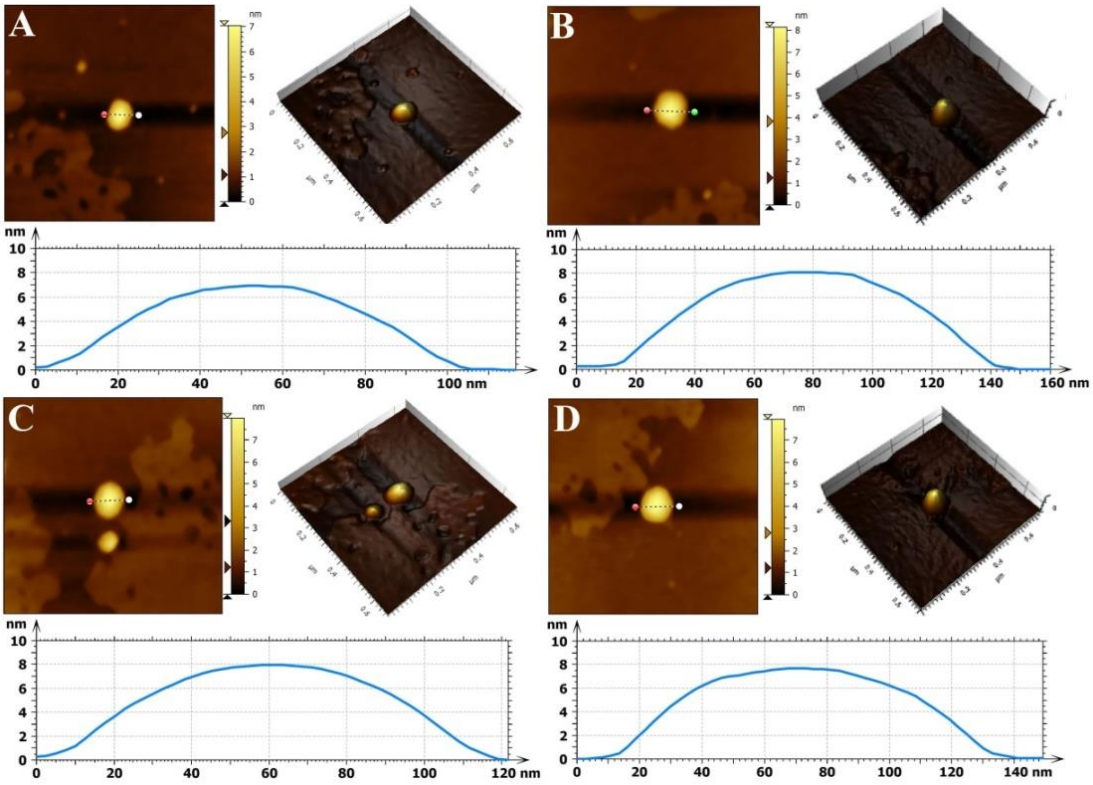

Figure A.5.12. Atomic Force Microscopic (AFM) images of IISERP-COF9.

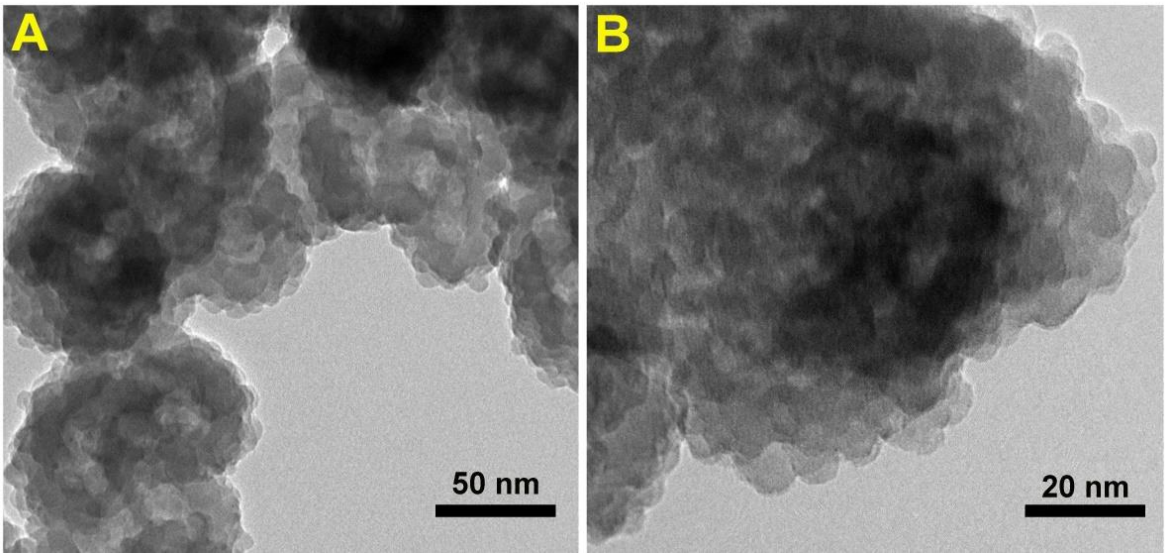

Figure A.5.13. Field Emission Transmission Electron Microscopic (FETEM) images of IISERP-COF9 at different magnifications showing that the spheres are made of aggregated COF flakes.

Characterizations of Cu@COF:

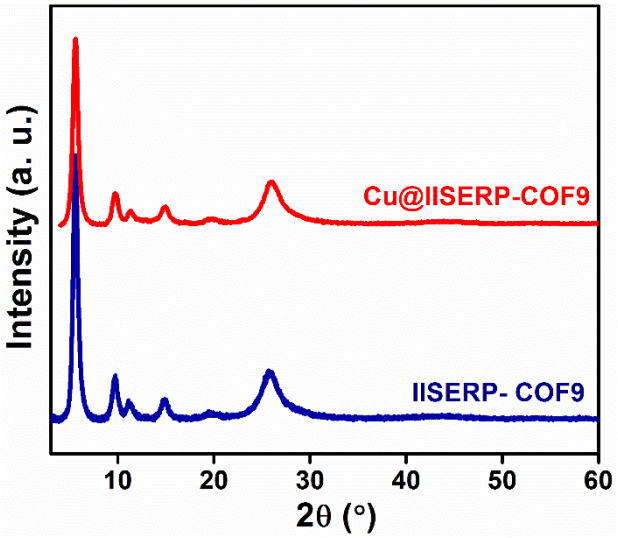

Figure A.5.14. Powder- X-Ray diffraction of IISERP-COF9 and Cu@IISERP-COF9. The PXRDs indicate that the COF retains its structural integrity after nanoparticle loading.

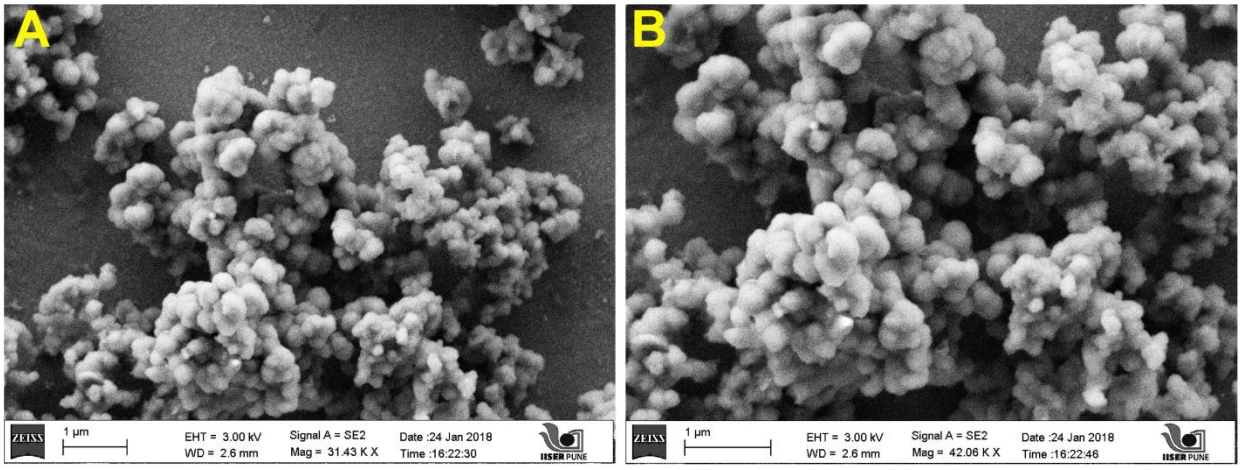

Figure A.5.15. (A, B) Scanning Electron Microscopic images of Cu@IISERP-COF9.

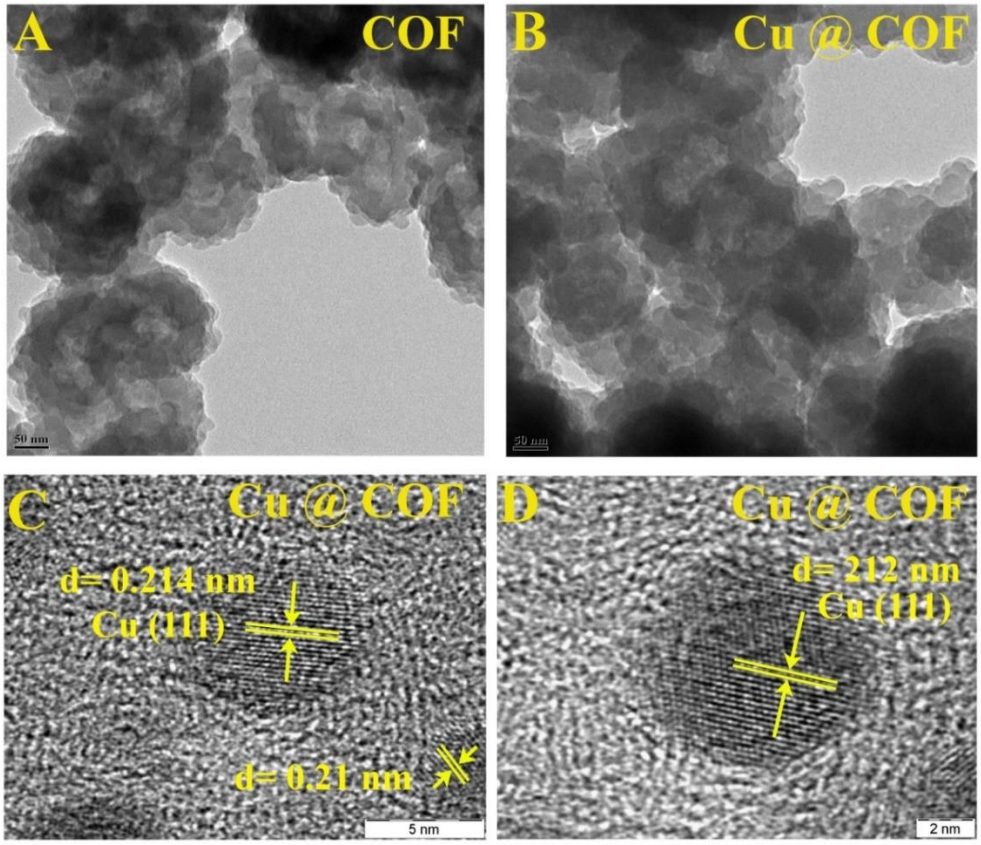

Figure A.5.16. (A, B) Field Emission Transmission Electron Microscopic (FETEM) images of COF and Cu@COF respectively. (B) High Resolution TEM (HRTEM) images of Cu@COF showing lattice fringes indexed to Cu nanoparticle.

Element	Weight%	Atomic%
C K	50.89	59.06
N K	18.13	18.04
O K	24.70	21.52
Cu K	6.29	1.38
Totals	100.00	

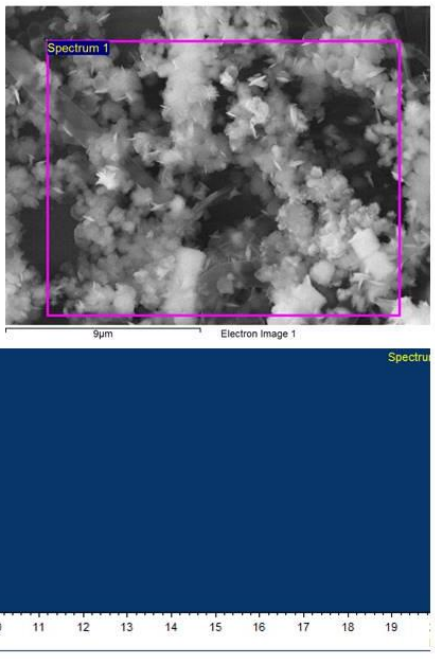

Figure A.5.17. Energy Dispersive X-Ray (EDX) images of Cu@IISERP-COF9 before catalysis.

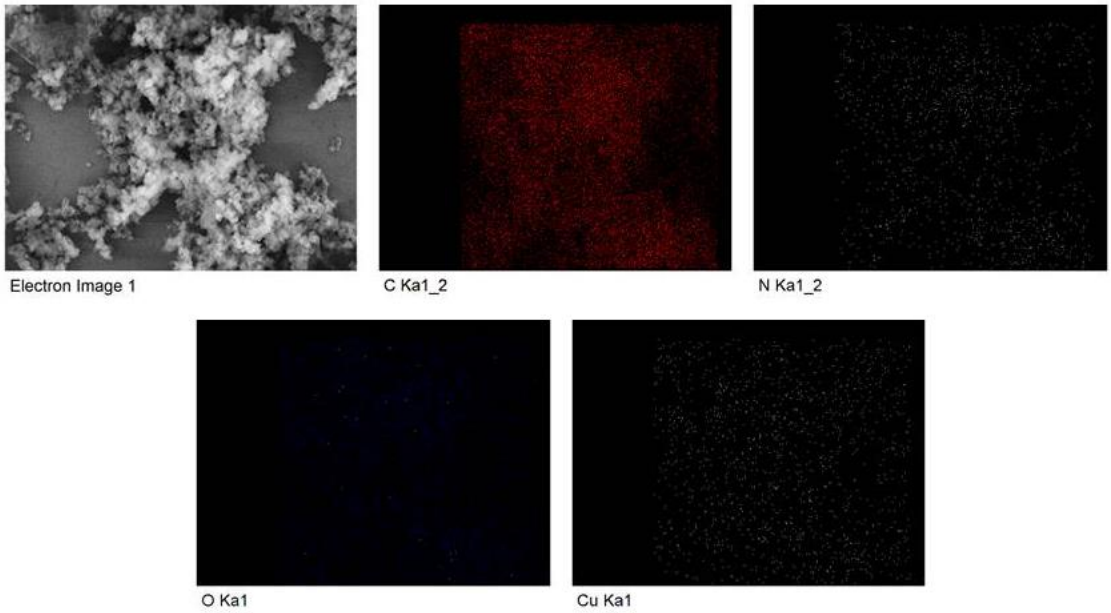

Figure A.5.18. Elemental mapping of Cu@IISERP-COF9.

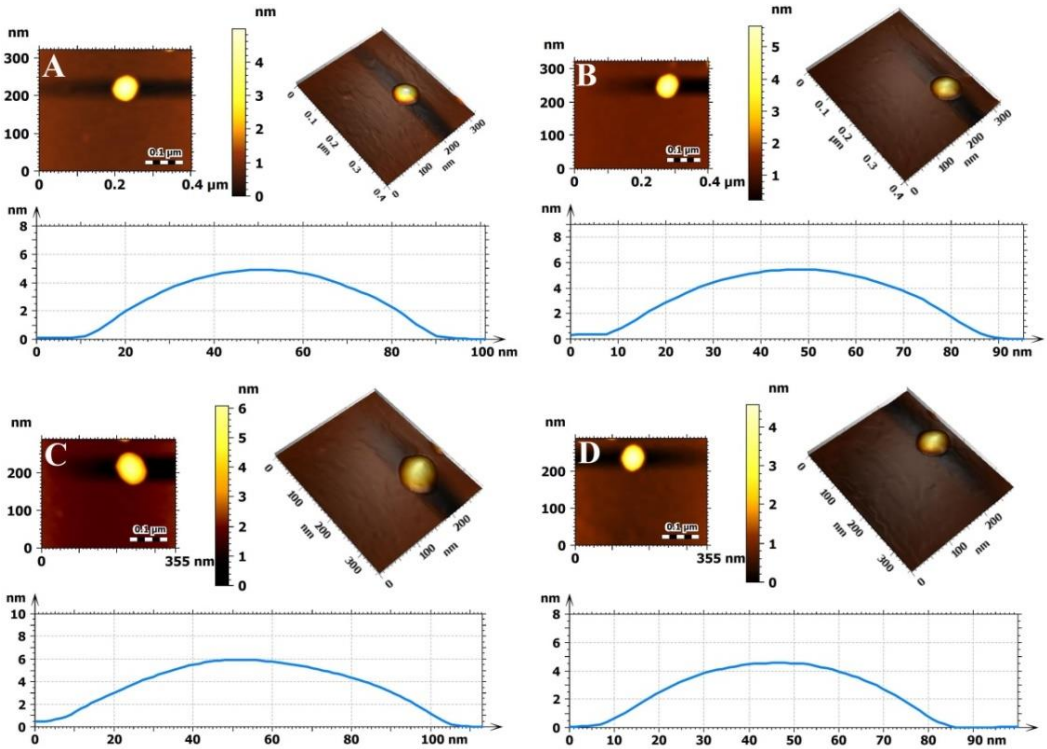

Figure A.5.19. AFM images of Cu@IISERP-COF9.

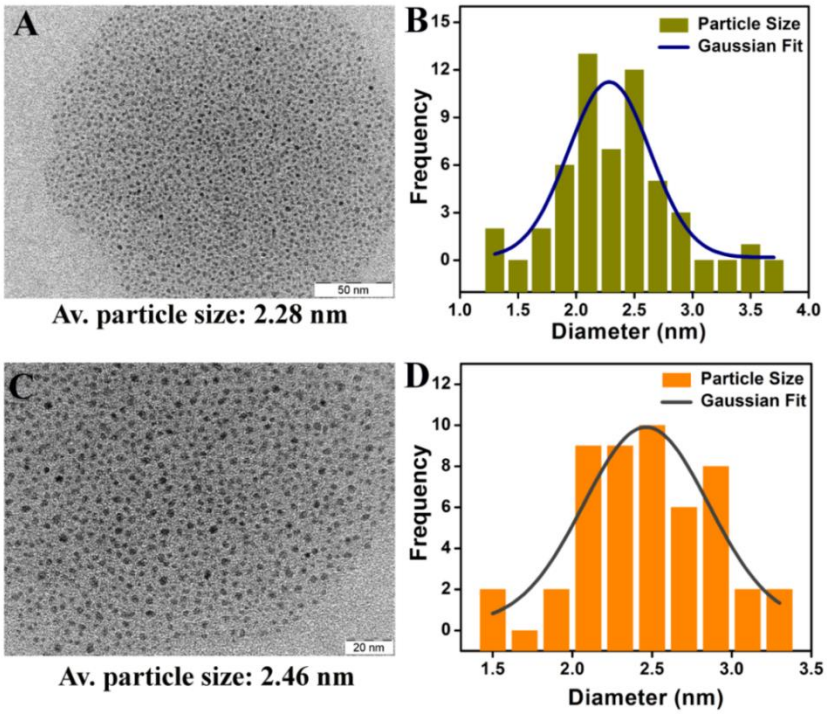

Figure A.5.20. The particle size distribution of Cu@IISERP-COF9 at two different magnifications.

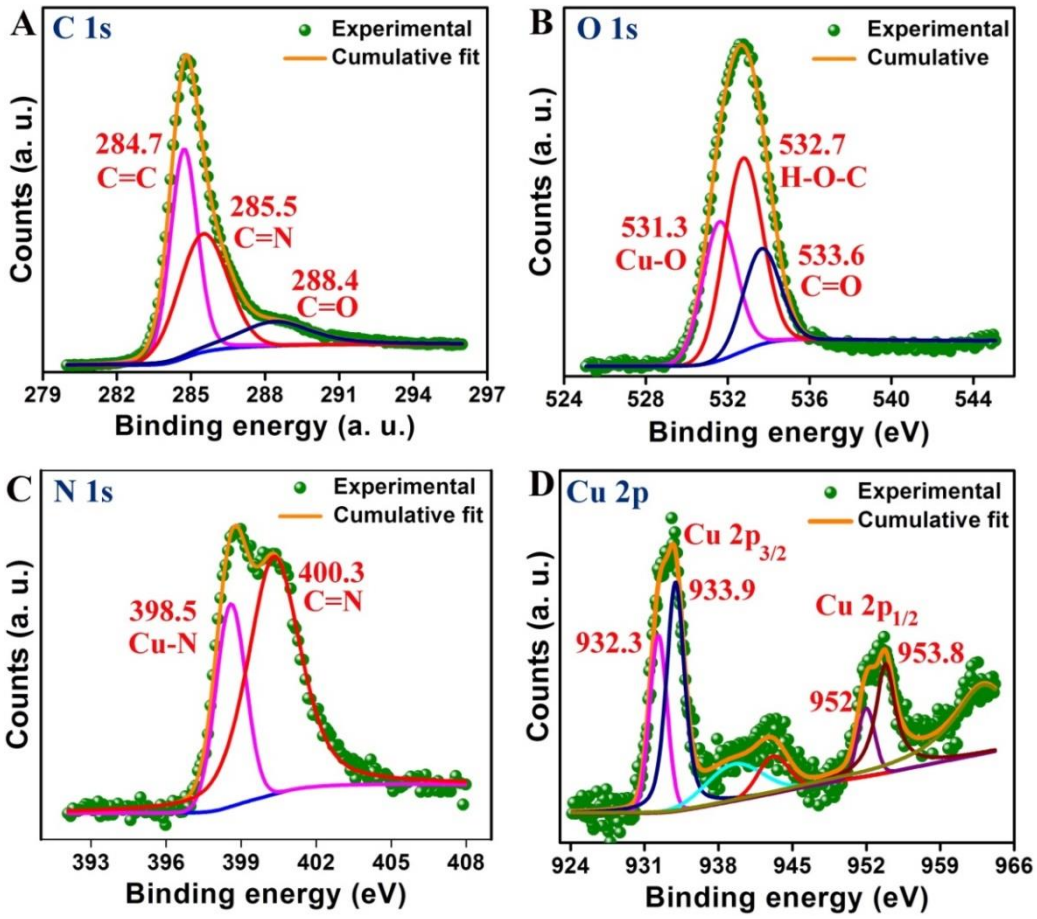

Figure A.5.21. XPS spectra of the as-synthesized Cu@COF.

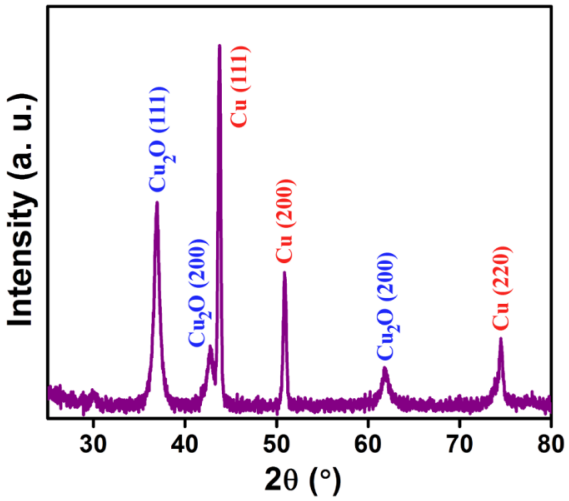

Figure A.5.22. PXRD of the composite pyrolyzed at 600°C under an inert atmosphere. This converts the COF into carbon. Characteristics peaks reveal the coexistence of Cu and Cu_2O nanoparticle in the composite. Face-center cubic Cu (JCPDF Card No.: 85-1326). Cubic phase Cu_2O (JCPDS card No.:75-1531).

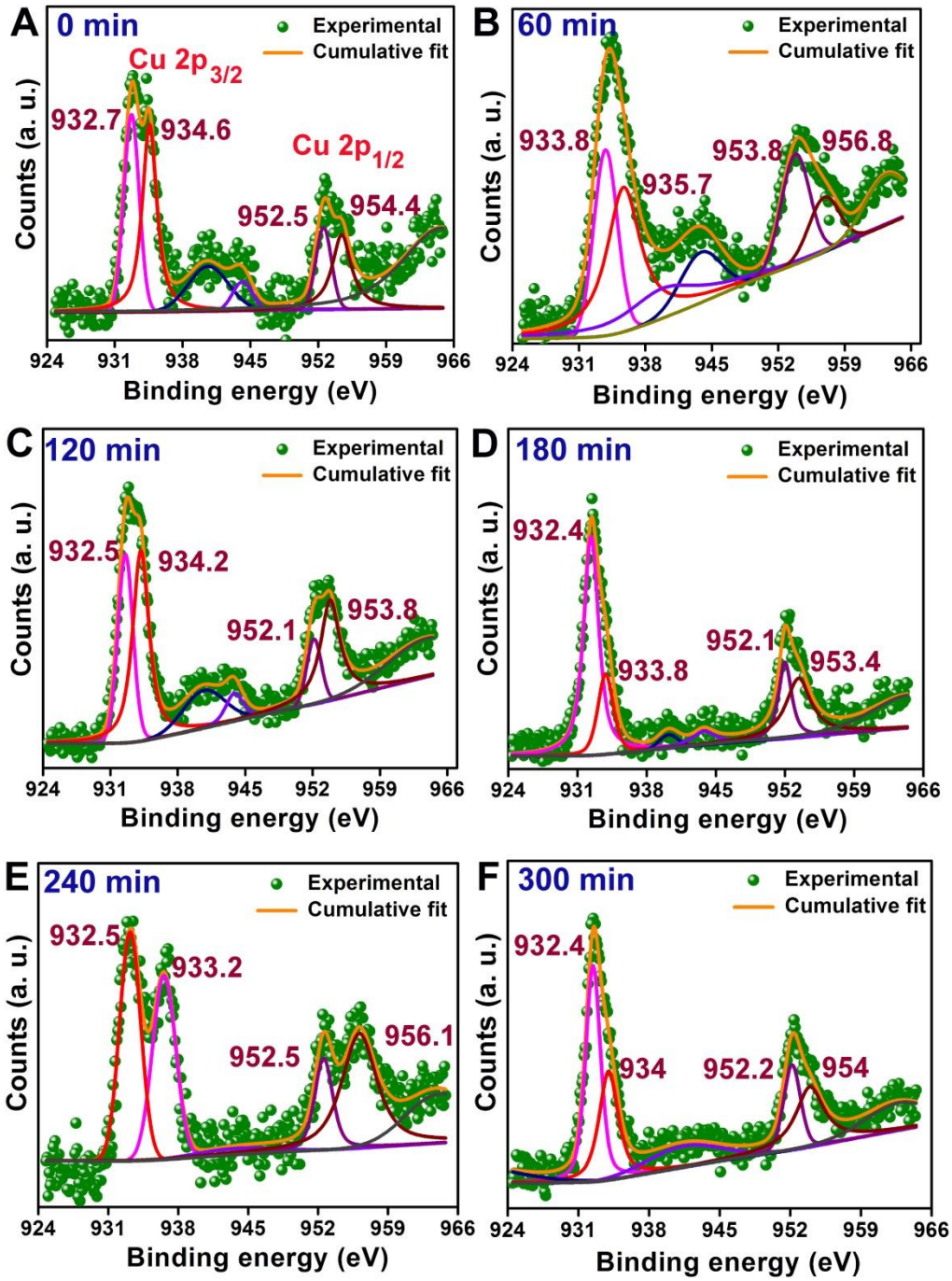

Figure A.5.23. XPS for the solid catalysts isolated at different time intervals during the catalytic process.

Characterizations of Cu @ COF after catalysis:

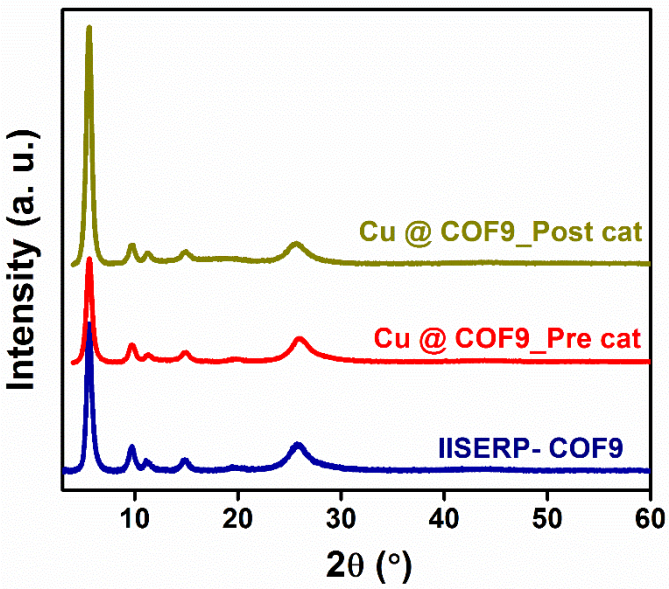

Figure A.5.24. Powder- X-Ray diffraction of IISERP-COF9 and Cu @ IISERP-COF9 before and after catalysis. The PXRDs indicate that the COF matrix and the catalyst retain their structural integrity after the catalytic process.

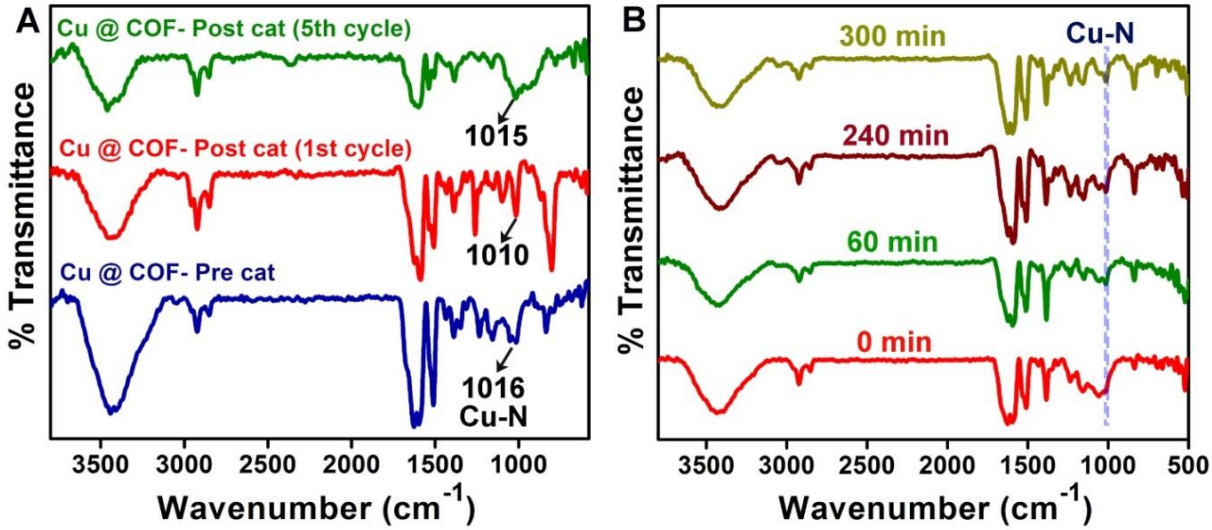

Figure A.5.25. (A) IR spectra of Cu loaded IISERP-COF9 before and after catalysis. (B) IR spectra of the solid samples frozen at different time intervals for mechanistic study. The Cu loaded COF shows a Cu-N stretching peak at 1016 cm^{-1} indicating that there is some interaction between the Cu and nitrogen from the framework.

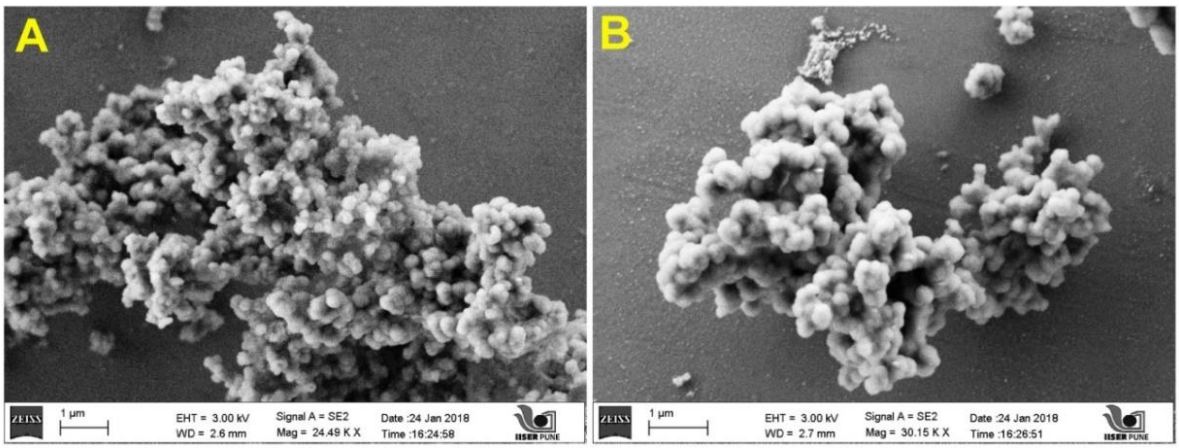

Figure A.5.26. (A, B) Scanning Electron Microscopic images of Cu@IISERP-COF9 after catalysis.

Element	Weight%	Atomic%
C K	61.81	68.83
N K	17.44	16.66
O K	15.23	13.57
Cu L	5.52	0.95
Totals	100.00	

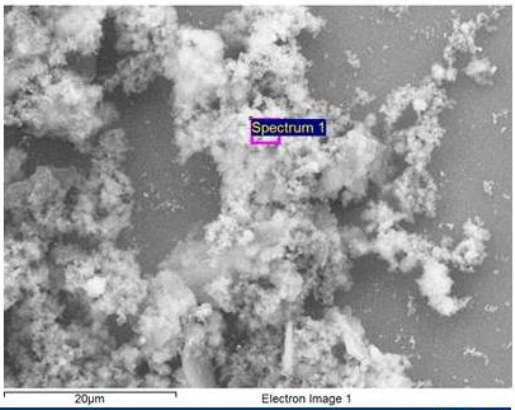

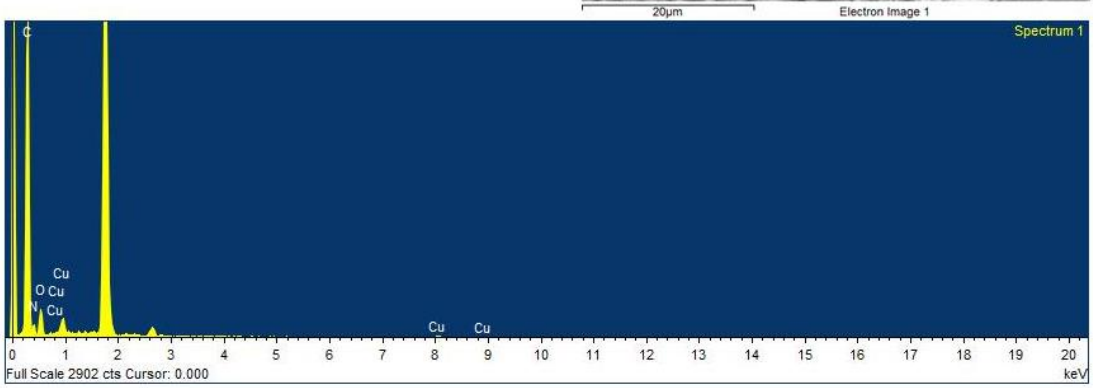

Figure A.5.27. Energy Dispersive X-Ray (EDX) images of Cu @ IISERP-COF9 after catalysis.

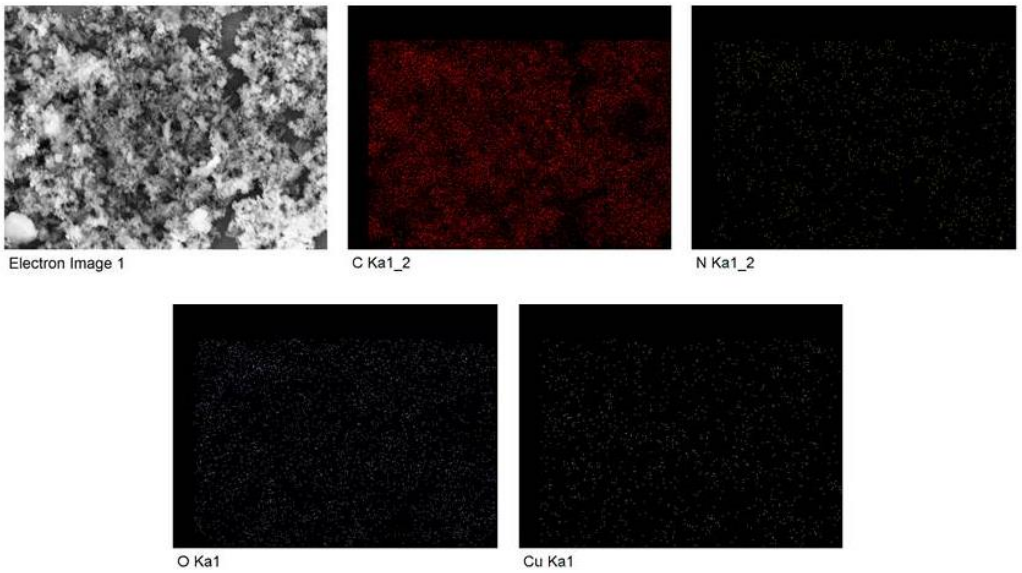

Figure A.5.28. Elemental mapping of Cu @ IISERP-COF9 after catalysis.

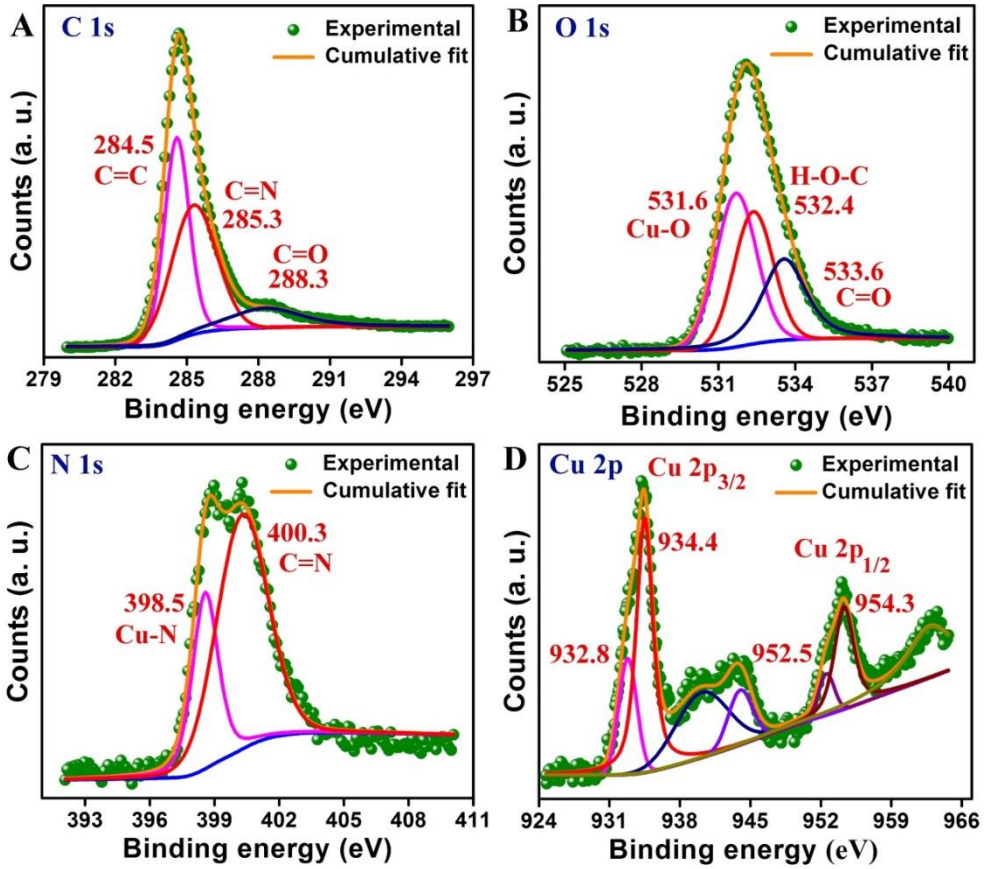

Figure A.5.29. XPS spectra for the composite after the catalytic process.

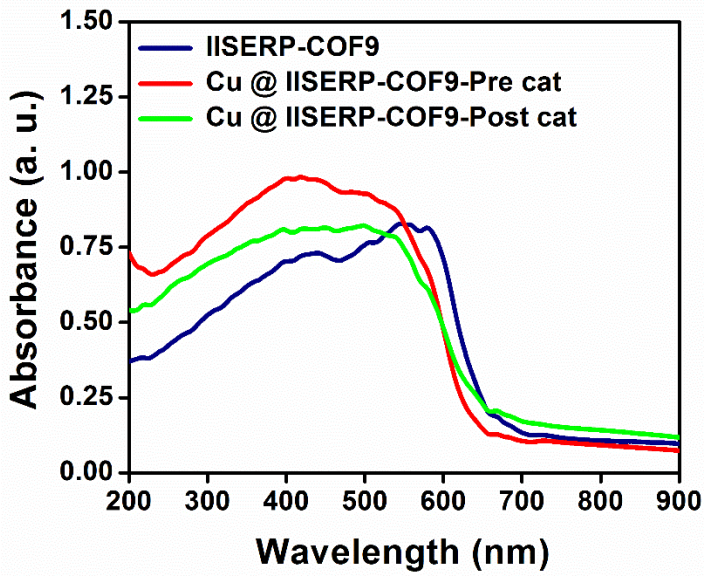

Figure A.5.30. Solid-state UV spectra of IISERP-COF9 and Cu nanoparticle doped COF.

Element	Weight%	Atomic%
C K	66.73	73.56
N K	11.73	11.09
O K	16.95	14.02
Cu K	2.32	0.48
Cl K	2.27	0.85
Totals	100.00	

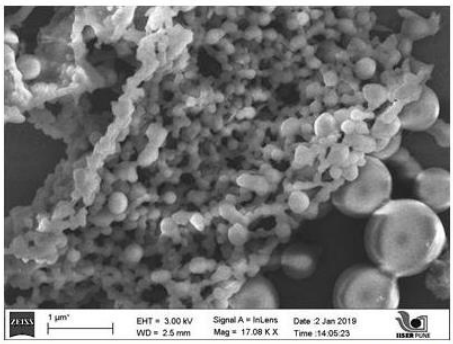

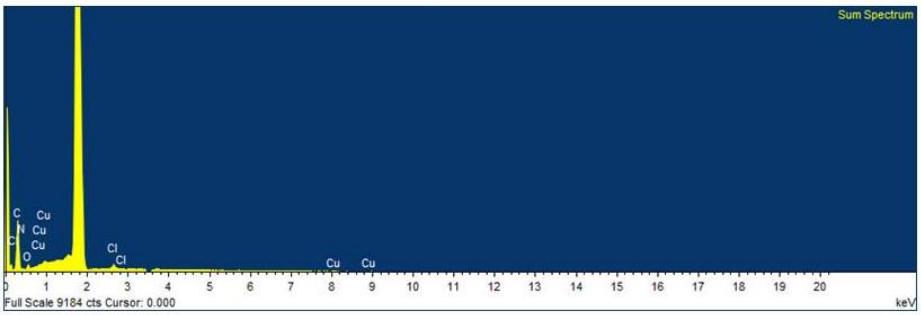

Figure A.5.31. EDX analysis of the catalyst recovered during the reaction showing presence of chlorine.

Nuclear Magnetic Resonance (NMR), High Resolution Mass Spectroscopy (HRMS) and Gas Chromatography (GC) data:

1a: 2-methyl-6-phenylhexa-3,5-diyn-2-ol:

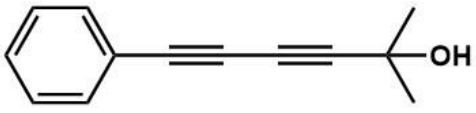

^{1}H NMR (400 MHz, $CDCl_3$): δ = 7.48 – 7.46 (m, 2H), 7.35 – 7.28 (m, 3H), 1.57 (s, 6H).
^{13}C NMR (101 MHz, $CDCl_3$): δ = 132.6, 129.3, 128.5, 121.6, 86.7, 78.9, 73.2, 67.1, 65.9, 31.2.
HRMS: calcd for $C_{13}H_{12}O$ $[M+H]^+$ 185.0924, found 185.0927.

1b: 3-methyl-7-phenylhepta-4,6-diyn-3-ol:

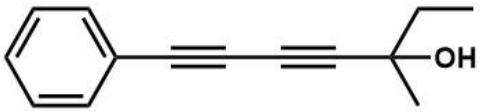

^{1}H NMR (400 MHz, $CDCl_3$): δ = 7.52 – 7.50 (m, 2H), 7.39 – 7.34 (m, 3H), 1.83 – 1.72 (m, 3H), 1.56 (s, 3H), 1.12 – 1.09 (t, J = 4 Hz, 3H).
^{13}C NMR (101 MHz, $CDCl_3$): δ = 132.5, 129.2, 128.4, 121.6, 85.9, 78.5, 73.2, 69.4, 68.1, 36.4, 29.0, 9.0.
HRMS: calcd for $C_{14}H_{14}O$ $[M+H]^+$ 198.1027, found 198.1030.

1c: 6-phenylhexa-3,5-diyn-2-ol:

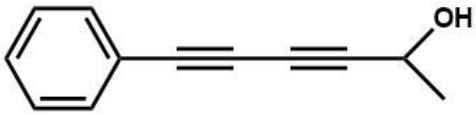

^{1}H NMR (400 MHz, $CDCl_3$): δ = 7.49 – 7.46 (m, 2H), 7.37 – 7.28 (m, 3H), 4.68 – 4.63 (m, 1H), 1.52 – 1.50 (d, J = 8 Hz, 3H).
^{13}C NMR (101 MHz, $CDCl_3$): δ = 132.7, 129.4, 128.5, 121.5, 84.1, 78.8, 73.2, 68.9, 59.0, 24.1.
HRMS: calcd for $C_{12}H_{10}O$ $[M+H]^+$ 170.0721, found 170.0722.

1d: 5-phenylpenta-2,4-diyn-1-ol:

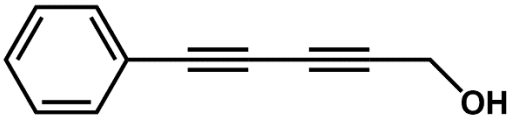

^{1}H NMR (400 MHz, $CDCl_3$): δ = 7.53 – 7.44 (m, 2H), 7.40 – 7.27 (m, 3H), 4.41 (s, 2H).
^{13}C NMR (101 MHz, $CDCl_3$): δ = 133.39, 129.36, 121.81, 80.84, 79.06, 73.58, 70.93, 52.15.
HRMS: calcd for $C_{11}H_8O$ $[M+H]^+$ 156.0618, found 156.0621.

1e: 6-phenylhexa-3,5-diyn-1-ol:

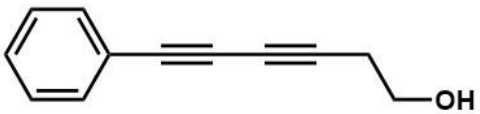

^{1}H NMR (400 MHz, $CDCl_3$) δ = 7.52 – 7.49 (m, 2H), 7.40 – 7.30 (m, 3H), 3.82 (t, J = 8 Hz, 2H), 2.67 (t, J = 8 Hz, 2H).
^{13}C NMR (101 MHz, $CDCl_3$) δ = 132.6, 129.1, 128.4, 121.7, 81.0, 75.4, 74.0, 66.9, 60.8, 24.0.

HRMS: calcd for $C_{11}H_8O$ $[M+H]^+$ 170.0722, found 170.0724.

2a: 2-methyl-6-(p-tolyl)hexa-3,5-diyn-2-ol:

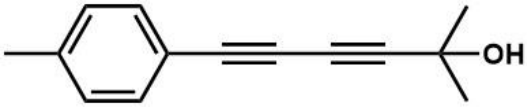

^{1}H NMR (400 MHz, $CDCl_3$): δ = 7.37 (d, J = 8 Hz, 2H), 7.11 (d, J = 8.0 Hz, 2H), 2.34 (s, 3H), 1.56 (s, 6H).
^{13}C NMR (101 MHz, $CDCl_3$): δ = 139.7, 132.5, 129.3, 118.5, 86.4, 79.2, 72.6, 67.3, 65.8, 31.2, 21.7.
HRMS: calcd for $C_{14}H_{14}O$ $[M+H]^+$ 198.1027, found 198.1030.

2b: 3-methyl-7-(p-tolyl)hepta-4,6-diyn-3-ol:

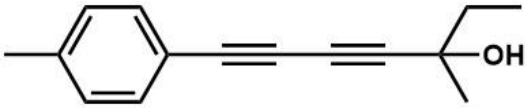

^{1}H NMR (400 MHz, $CDCl_3$): δ = 7.37 – 7.35 (m, 2H), 7.12 – 7.10 (m, 2H), 2.34 (s, 3H), 1.76 – 1.73 (m, 2H), 1.52 (s, 3H), 1.08 – 1.04 (t, J = 8 Hz, 3H).
^{13}C NMR (101 MHz, $CDCl_3$): δ = 139.7, 132.5, 129.3, 118.5, 85.6, 78.9, 72.7, 69.5, 68.3, 36.5, 29.1, 21.7, 9.1.
HRMS: calcd for $C_{15}H_{16}O$ $[M+H]^+$ 212.1229, found 212.1232.

2c: 6-(p-tolyl)hexa-3,5-diyn-2-ol:

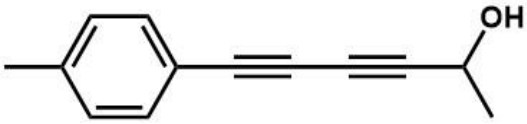

^{1}H NMR (400 MHz, $CDCl_3$) δ 7.36 (d, J = 8 Hz, 2H), 7.11 (d, J = 8 Hz, 2H), 4.67 – 4.63 (m, 1H), 2.34 (s, 3H), 1.50 (d, J = 4 Hz, 3H).
^{13}C NMR (101 MHz, $CDCl_3$): δ = 139.8, 132.6, 129.3, 118.4, 83.7, 79.1, 72.6, 69.0, 59.0, 24.1, 21.7.
HRMS: calcd for $C_{13}H_{12}O$ $[M+H]$+ 184.0924, found 184.0930.

2d: 5-(p-tolyl)penta-2,4-diyn-1-ol:

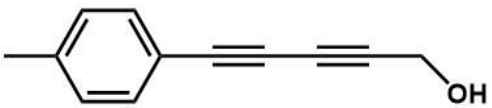

^{1}H NMR (400 MHz, $CDCl_3$): δ = 7.41 (d, J = 8 Hz, 2H), 7.15 (d, J = 8 Hz, 2H), 4.44 (s, 2H), 2.38 (s, 3H).

^{13}C NMR (101 MHz, $CDCl_3$): δ = 139.6, 132.3, 129.0, 127.9, 118.1, 79.9, 78.8, 72.4, 70.5, 51.5, 21.4.
HRMS: calcd for $C_{12}H_{10}O$ [M +H]+ 170.0721, found 170.0722.

2e: 6-(p-tolyl)hexa-3,5-diyn-1-ol:

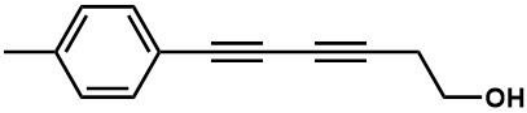

^{1}H NMR (400 MHz, $CDCl_3$): δ = 7.36 (d, J = 8 Hz, 2H), 7.11 – 7.09 (m, 2H), 3.78 (t, J = 6 Hz, 2H), 2.62 (t, J = 6Hz, 2H), 2.33 (s, 3H).
^{13}C NMR (101 MHz, $CDCl_3$): δ = 139.5, 132.5, 129.3, 118.7, 80.7, 75.7, 73.4, 67.1, 60.9, 24.1, 21.7.
HRMS: calcd for $C_{13}H_{12}O$ $[M+H]^+$ 184.0924, found 184.0928.

3a: 2-methyl-6-(m-tolyl)hexa-3,5-diyn-2-ol:

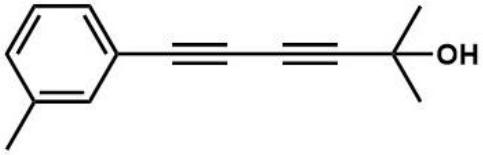

^{1}H NMR (400 MHz, $CDCl_3$): δ = 7.29 – 7.25 (m, 2H), 7.21 – 7.14 (m, J = 2H), 2.31 (s, 3H), 1.57 (s, 6H).
^{13}C NMR (101 MHz, $CDCl_3$): δ = 138.3, 133.1, 130.3, 129.8, 128.4, 121.4, 86.6, 79.2, 72.9, 67.3, 65.9, 31.3, 21.3.
HRMS: calcd for $C_{14}H_{14}O$ $[M+H]^+$ 198.1027, found 198.1030.

3b: 3-methyl-7-(m-tolyl)hepta-4,6-diyn-3-ol:

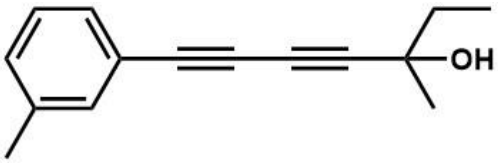

^{1}H NMR (400 MHz, $CDCl_3$) δ 7.33 – 7.31 (m, 2H), 7.25 – 7.18 (m, 2H), 2.35 (s, 3H), 1.81 – 1.75 (m, 1H), 1.56 (s, 3H), 1.10 (t, J = 8 Hz, 3H).
^{13}C NMR (101 MHz, $CDCl_3$): δ = 138.6, 133.5, 130.6, 130.1, 128.8, 121.8, 86.1, 79.2, 73.3, 69.8, 68.6, 36.9, 29.5, 21.6, 9.4.
HRMS: calcd for $C_{15}H_{16}O$ $[M+H]^+$ 212.1229, found 212.1235.

3c: 6-(m-tolyl)hexa-3,5-diyn-2-ol:

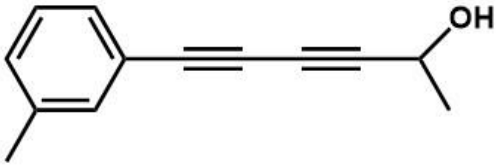

^{1}H NMR (400 MHz, $CDCl_3$): δ = 7.29 – 7.24 (m, 2H), 7.21 – 7.15 (m, 2H), 4.67 – 4.62 (m, 1H), 2.31 (s, 3H), 1.51 (d, J = 8 Hz, 3H).
^{13}C NMR (101 MHz, $CDCl_3$): δ = 138.0, 133.9, 132.9, 131.1, 130.1, 129.5, 128.5, 128.1, 121.6, 121.0, 83.6, 78.8, 72.5, 68.7, 58.7, 23.8, 21.0.
HRMS: calcd for $C_{13}H_{12}O$ $[M+H]^+$ 184.0924, found 184.0931.

3d: 5-(m-tolyl)penta-2,4-diyn-1-ol:

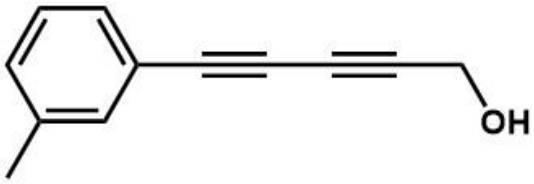

^{1}H NMR (400 MHz, $CDCl_3$): δ = 7.29 (d, J = 8 Hz, 2H), 7.21 – 7.15 (m, 2H), 4.41 (s, 2H), 2.31 (s, 3H).
^{13}C NMR (101 MHz, $CDCl_3$): δ = 138.0, 133.5, 132.9, 130.1, 129.5, 128.1, 121.0, 80.0, 78.7, 72.6, 70.4, 51.5, 21.0.
HRMS: calcd for $C_{12}H_{10}O$ $[M+H]^+$ 170.0721, found 170.0725.

3e: 6-(m-tolyl)hexa-3,5-diyn-1-ol:

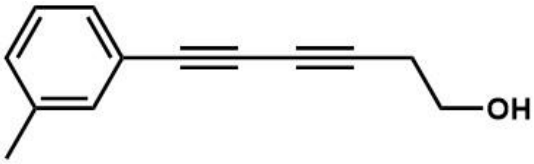

^{1}H NMR (400 MHz, $CDCl_3$) δ 7.28 – 7.25 (m, 2H), 7.20 – 7.13 (m, 2H), 3.78 (t, J = 8 Hz, 2H), 2.63 (t, J = 6 Hz, 2H), 2.31 (s, 3H).
^{13}C NMR (101 MHz, $CDCl_3$): δ = 137.9, 132.9, 129.8, 129.5, 128.1, 121.3, 80.5, 75.5, 73.4, 66.8, 60.6, 23.8, 21.0.
HRMS: calcd for $C_{13}H_{12}O$ $[M+H]^+$ 180.0924, found 180.0932.

4a: 2-methyl-6-(4-(trifluoromethyl)phenyl)hexa-3,5-diyn-2-ol:

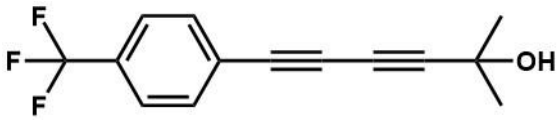

^{1}H NMR (400 MHz, $CDCl_3$): δ = 7.56 (s, 4H), 1.58 (s, 6H).
^{13}C NMR (101 MHz, $CDCl_3$): δ = 132.6, 125.3, 125.2, 125.2, 125.1, 87.8, 75.3, 66.5, 65.6, 30.9.
HRMS: calcd for $C_{14}H_{11}F_3O$ $[M+H]^+$ 252.0824, found 252.0829.

4b: 3-methyl-7-(4-(trifluoromethyl)phenyl)hepta-4,6-diyn-3-ol:

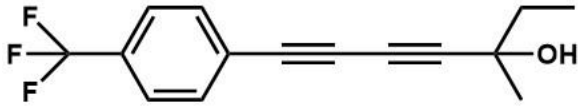

1H NMR (400 MHz, $CDCl_3$): δ = 7.61 (s, 4H), 1.82 – 1.76 (m, 2H), 1.57 (s, 3H), 1.11 (t, J = 8 Hz, 3H).
^{13}C NMR (101 MHz, $CDCl_3$): δ = 132.6, 125.2, 125.2, 87.1, 75.4, 69.2, 67.5, 36.2, 8.7.
HRMS: calcd for $C_{15}H_{13}F_3O$ $[M+H]^+$ 266.0926, found 266.0933.

4c: 6-(4-(trifluoromethyl)phenyl)hexa-3,5-diyn-2-ol:

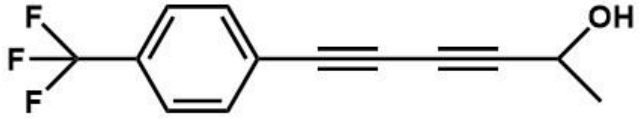

^{1}H NMR (400 MHz, $CDCl_3$): δ = 7.60 (s, 4H), 4.73 – 4.68 (m, 1H), 1.56 (d, J = 4 Hz, 3H).
^{13}C NMR (101 MHz, $CDCl_3$): δ = 132.6, 130.9, 130.6, 125.2, 125.2, 125.2, 125.1, 124.9, 122.2, 85.1, 75.2, 68.2, 58.7, 23.7.
HRMS: calcd for $C_{13}H_9F_3O$ $[M+H]^+$ 238.0621, found 238.0625.

4d: 5-(4-(trifluoromethyl)phenyl)penta-2,4-diyn-1-ol:

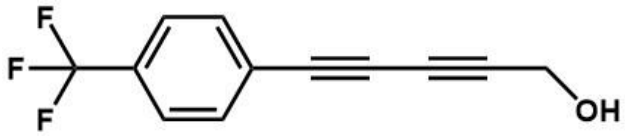

^{1}H NMR (400 MHz, $CDCl_3$): δ = 7.61 (s, 4H), 4.46 (s, 2H).
^{13}C NMR (101 MHz, $CDCl_3$): δ = 132.7, 125.2, 125.2, 81.5, 75.2, 69.8, 51.5.
HRMS: calcd for $C_{12}H_7F_3O$ $[M+H]^+$ 224.0418, found 224.0422.

4e: 6-(4-(trifluoromethyl)phenyl)hexa-3,5-diyn-1-ol:

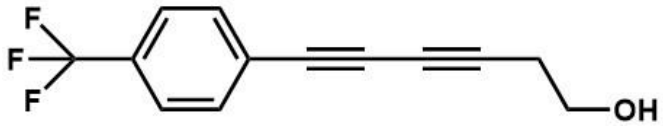

^{1}H NMR (400 MHz, $CDCl_3$): δ = 7.59 (s, 4H), 3.84 (t, J = 6 Hz, 2H), 2.68 (t, J = 6 Hz, 2H).
^{13}C NMR (101 MHz, $CDCl_3$): δ = 132.6, 130.9, 130.7, 130.3, 130.0, 125.5, 125.5, 125.2, 125.2, 125.1, 125.1, 122.2, 82.4, 76.1, 73.5, 66.3, 60.5, 23.8.
HRMS: calcd for $C_{13}H_9F_3O$ $[M+H]^+$ 238.0621, found 238.0629.

5a: 6-(4-bromophenyl)-2-methylhexa-3,5-diyn-2-ol:

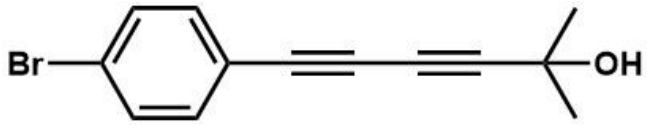

^{1}H NMR (400 MHz, $CDCl_3$): δ = 7.46 – 7.42 (m, 2H), 7.33 – 7.30 (m, 2H), 1.56 (s, 6H).
^{13}C NMR (101 MHz, $CDCl_3$): δ = 133.9, 131.8, 123.8, 120.6, 87.4, 77.7, 74.3, 66.9, 65.9, 31.1.
HRMS: calcd for $C_{13}H_{11}BrO$ $[M+H]^+$ 262.0013, found 262.0025.

5b: 7-(4-bromophenyl)-3-methylhepta-4,6-diyn-3-ol:

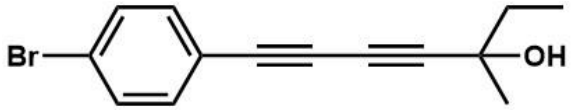

^{1}H NMR (400 MHz, $CDCl_3$): δ = 7.48 – 7.43 (m, 2H), 7.38 – 7.31 (m, 2H), 1.77 – 1.70 (m, 2H), 1.52 (s, 3H), 1.06 (t, J = 8 Hz, 3H).
^{13}C NMR (101 MHz, $CDCl_3$): δ = 133.0, 129.7, 128.9, 122.0, 86.3, 79.0, 73.7, 69.8, 68.6, 36.9, 29.5, 9.4.
HRMS: calcd for $C_{14}H_{13}BrO$ $[M+H]^+$ 276.0116, found 276.0122.

5c: 6-(4-bromophenyl)hexa-3,5-diyn-2-ol:

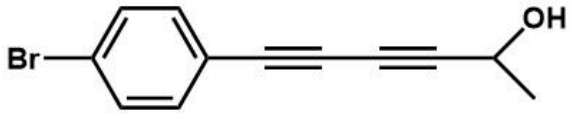

^{1}H NMR (400 MHz, $CDCl_3$): δ = 7.52 – 7.47 (m, 2H), 7.38 – 7.34 (m, 2H), 4.71 – 4.65 (m, 1H), 1.54 (d, J = 4 Hz, 3H).
^{13}C NMR (101 MHz, $CDCl_3$): δ = 133.7, 131.6, 123.6, 120.2, 84.4, 77.4, 74.1, 68.5, 58.7, 23.8.
HRMS: calcd for $C_{12}H_9BrO$ $[M+H]^+$ 247.9811, found 247.9813.

5d: 5-(4-bromophenyl)penta-2,4-diyn-1-ol:

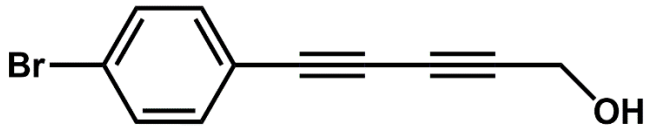

^{1}H NMR (400 MHz, $CDCl_3$): δ = 7.57 – 7.41 (m, 2H), 7.39 – 7.29 (m, 2H), 4.40 (s, 2H).
^{13}C NMR (101 MHz, $CDCl_3$): δ = 132.02, 131.86, 81.10, 74.3, 51.77.
HRMS: calcd for $C_{11}H_7BrO$ $[M+H]^+$ 233.9708, found 233.9715.

5e: 6-(4-bromophenyl)hexa-3,5-diyn-1-ol:

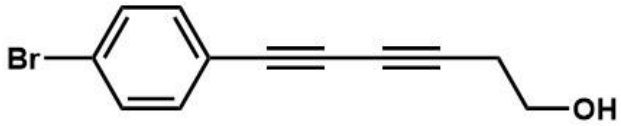

^{1}H NMR (400 MHz, $CDCl_3$): δ = 7.49 – 7.45 (m, 2H), 7.37 – 7.33 (m, 2H), 3.82 (t, J = 6 Hz, 2H), 2.66 (t, J = 6 Hz, 2H).
^{13}C NMR (101 MHz, $CDCl_3$): δ = 133.7, 131.5, 123.3, 120.5, 81.6, 74.9, 74.0, 66.5, 60.5, 23.8.
HRMS: calcd for $C_{12}H_9BrO$ $[M+H]^+$ 247.9811, found 247.9820.

6a: 6-(4-methoxyphenyl)-2-methylhexa-3,5-diyn-2-ol:

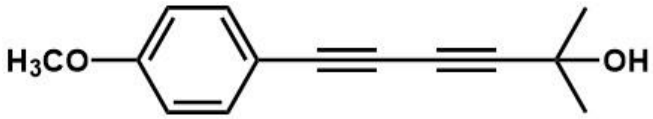

^{1}H NMR (400 MHz, $CDCl_3$): δ = 7.50 – 7.38 (m, 2H), 6.92 – 6.80 (m, 2H), 3.83 (s, 3H), 1.60 (s, 6H).
^{13}C NMR (101 MHz, $CDCl_3$): δ = 160.2, 133.9, 113.9, 113.3, 86.0, 78.8, 71.8, 67.1, 65.6, 55.1, 31.0.
HRMS: calcd for $C_{14}H_{14}O_2$ $[M+H]^+$ 214.1026, found 214.1029.

6b: 7-(4-methoxyphenyl)-3-methylhepta-4,6-diyn-3-ol:

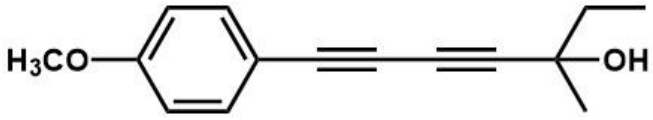

^{1}H NMR (400 MHz, $CDCl_3$): δ = 7.47 – 7.43 (m, 2H), 6.88 – 6.84 (m, 2H), 3.84 (s, 3H), 1.82 – 1.71 (m, 2H), 1.55 (s, 3H), 1.10 (t, J = 8 Hz, 3H).
^{13}C NMR (101 MHz, $CDCl_3$): δ = 160.2, 134.0, 114.0, 113.3, 85.1, 78.6, 71.9, 69.2, 68.2, 55.2, 36.3, 28.9, 8.8.
HRMS: calcd for $C_{15}H_{16}O_2$ $[M+H]^+$ 228.1229, found 228.1236.

6c: 6-(4-methoxyphenyl)hexa-3,5-diyn-2-ol:

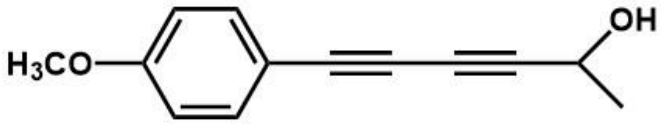

^{1}H NMR (400 MHz, $CDCl_3$): δ = 7.43 – 7.39 (m, 2H), 6.84 – 6.80 (m, 2H), 4.67 – 4.62 (m, 1H), 3.80 (s, 3H), 1.50 (d, J = 4 Hz, 3H).
^{13}C NMR (101 MHz, $CDCl_3$): δ = 160.5, 134.3, 114.2, 113.4, 83.5, 79.0, 72.0, 69.1, 59.0, 55.4, 28.4, 24.1.
HRMS: calcd for $C_{13}H_{12}O_2$ $[M+H]^+$ 200.0824, found 200.0826.

6d: 5-(4-methoxyphenyl)penta-2,4-diyn-1-ol:

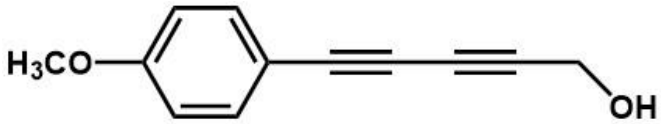

^{1}H NMR (400 MHz, $CDCl_3$): δ = 7.44 – 7.40 (m, 2H), 6.84 – 6.81 (m, 2H), 4.40 (s, 2H), 3.80 (s, 3H).
^{13}C NMR (101 MHz, $CDCl_3$): δ = 160.3, 134.1, 114.0, 113.1, 79.7, 78.7, 71.8, 70.5, 55.2, 51.5.
HRMS: calcd for $C_{12}H_{10}O_2$ $[M+H]^+$ 186.0721, found 186.0722.

6e: 6-(4-methoxyphenyl)hexa-3,5-diyn-1-ol:

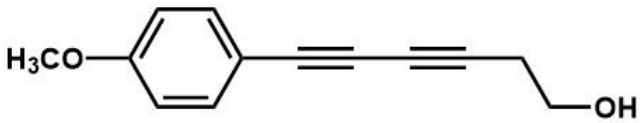

^{1}H NMR (400 MHz, $CDCl_3$): δ = 7.46 – 7.42 (m, 2H), 6.87 – 6.84 (m, 2H), 3.83 – 3.80 (m, 5H), 2.66 (t, J = 6 Hz, 2H).
^{13}C NMR (101 MHz, $CDCl_3$): δ = 160.0, 134.0, 113.9, 113.5, 80.1, 75.4, 72.5, 66.9, 60.7, 55.1, 23.9.
HRMS: calcd for $C_{13}H_{12}O_2$ $[M+H]^+$ 200.0824, found 200.0825.

7a: 6-(3-methoxyphenyl)-2-methylhexa-3,5-diyn-2-ol:

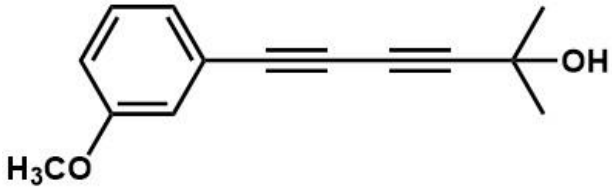

^{1}H NMR (400 MHz, $CDCl_3$): δ = 7.28 – 7.22 (m, 1H), 7.11 – 7.09 (m, 1H), 7.02 (m, 1H), 6.95 – 6.92 (m, 1H), 3.81 (s, 3H), 1.60 (s, 6H).

^{13}C NMR (101 MHz, $CDCl_3$): δ = 159.1, 129.3, 124.9, 122.3, 117.0, 115.8, 86.5, 78.5, 72.7, 66.8, 65.6, 55.1, 30.9.
HRMS: calcd for $C_{14}H_{14}O_2$ $[M+H]^+$ 214.1026, found 214.1032.

7b: 6-(3-methoxyphenyl)-2,2-dimethylhexa-3,5-diyn-1-ol:

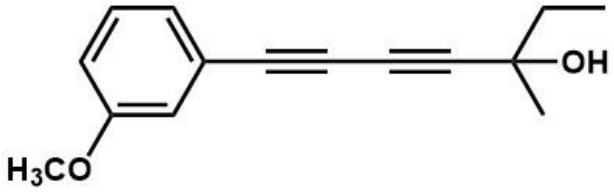

^{1}H NMR (400 MHz, $CDCl_3$): δ = 7.28 – 7.22 (m, 1H), 7.12 – 7.09 (m, 1H), 7.03 – 7.02 (m, 1H), 6.95 – 6.92 (m, 1H), 3.81 (s, 2H), 1.85 – 1.71 (m, 2H), 1.55 (s, 3H), 1.10 (t, J = 8 Hz, 3H).
^{13}C NMR (101 MHz, $CDCl_3$): δ = 159.1, 129.3, 124.9, 122.3, 117.0, 115.8, 85.8, 78.2, 72.8, 69.2, 67.9, 55.1, 36.2, 28.8, 8.8.
HRMS: calcd for $C_{15}H_{16}O_2$ $[M+H]^+$ 228.1229, found 228.1231.

7c: 6-(3-methoxyphenyl)hexa-3,5-diyn-2-ol:

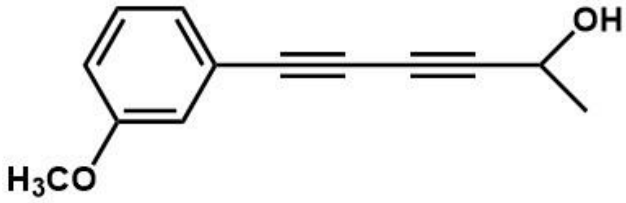

^{1}H NMR (400 MHz, $CDCl_3$): δ = 7.28 – 7.23 (m, 1H), 7.12 – 7.09 (m, 1H), 7.03 – 7.02 (m, 1H), 6.99 – 6.93 (m, 1H), 4.71 – 4.66 (m, 1H), 3.81 (s, 3H), 1.54 (d, J = 8 Hz, 3H).
^{13}C NMR (101 MHz, $CDCl_3$): δ = 159.1, 129.3, 124.9, 122.2, 117.0, 115.9, 83.8, 78.5, 72.7, 68.6, 58.7, 55.1, 23.8.
HRMS: calcd for $C_{13}H_{12}O_2$ $[M+H]^+$ 200.0824, found 200.0829.

7d: 5-(3-methoxyphenyl)penta-2,4-diyn-1-ol:

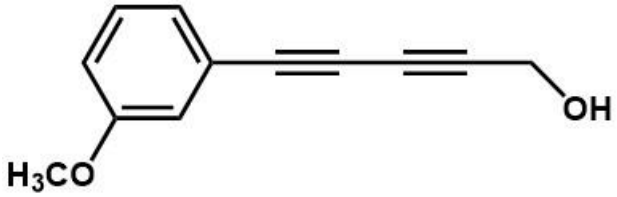

^{1}H NMR (400 MHz, $CDCl_3$): δ = 7.25 – 7.19 (m, 1H), 7.09 – 7.07 (m, 1H), 7.00 – 6.99 (m, 1H), 6.93 – 6.90 (m 1H), 4.41 (s, 2H), 3.78 (s, 3H).
^{13}C NMR (101 MHz, $CDCl_3$): δ = 159.1, 129.4, 125.0, 122.1, 117.0, 116.0, 80.3, 78.3, 72.7, 70.3, 55.1, 51.5.

HRMS: calcd for $C_{12}H_{10}O_2$ $[M+H]^+$ 186.0721, found 186.0733.

7e: 6-(3-methoxyphenyl)hexa-3,5-diyn-1-ol:

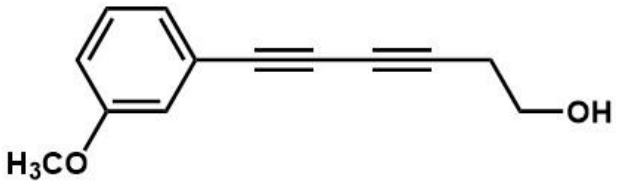

^{1}H NMR (400 MHz, $CDCl_3$): δ = 7.25 – 7.18 (m, 1H), 7.07 – 7.05 (m, 1H), 6.98 (s, 1H), 6.90 – 6.88 (m, 1H), 3.80 – 3.77 (m, 5H), 2.63 (t, J = 6.2 Hz, 2H).
^{13}C NMR (101 MHz, $CDCl_3$): δ = 159.0, 129.3, 124.9, 122.5, 117.0, 115.6, 80.9, 75.1, 73.5, 66.6, 60.6, 55.1, 23.8.
HRMS: calcd for $C_{13}H_{12}O_2$ $[M+H]^+$ 200.0824, found 200.0828.

Summary

Porous materials are the new generation materials which have diverse applications. Tuning the porous structure, one can achieve favorable host-guest interaction leading to unique properties. The thesis deals with the synthesis and characterizations of the different porous materials. The thesis is divided into two parts. In part-1, gaseous guest adsorption has been studied and in the second part, the guest is an active nanoparticle that catalyzes challenging organic reactions.

Part 1 consists of two chapters. In chapter 2, selective adsorption of Xe (noble gas) has been studied using stable porous polymers. It is very important to capture Xe from the off-gas stream of a nuclear power plant. The present technology (cryogenic separation) doesn't provide energy efficiency during Xe extraction from the air. In order to demonstrate the ability of porous materials as a potential alternate for noble gas capture, we have chosen stable, easily synthesizable, stable, porous polymers. The polymers were able to separate Xe over Kr at different temperatures at 1 bar pressure. The IAST selectivities revealed that the polymers are selective towards Xe over other gases such as Kr, N_2, and CO_2. Further, dynamic breakthrough analysis exhibited higher retention time for Xe compared to the other gases. The thermal and chemical stability of the polymers is an important feature for the application in harsh conditions. Although, the high Xe capacity, selectivity, and molecular confinements are the potential points to be addressed. However, here we have presented porous polymers for Xe capture for the first time.

In chapter 3, we have adopted an ultra-microporous MOF having uniform pore to demonstrate the high capacity, selectivity and confinement effect. The MOF (Ni-PyC) had high Xe uptake at 298K, 1 bar which saturated at low pressure. The heat of adsorption and selectivity studies revealed the preferential adsorption of Xe over other gases. We compared our material to the recently reported benchmark MOF (SBMOF-1) and cage (CC3) and found that the MOF possessed the highest uptake and selectivities over these materials. To understand the interaction within the pore, we took help from theoretical calculations. The DFT studies revealed that in Ni-PyC Xe had a slightly greater interaction with the framework compared to the SBMOF-1. Further ^{129}Xe NMR spectroscopy was performed to demonstrate the molecular confinement effect. It has been validated that the ultra-microporous materials and high surface area contribute to the better adsorption of noble gases.

Part 2 deals with the covalent organic frameworks supported active nanoparticles for catalysis. In chapter 4, a microporous, stable COF has been prepared by Schiff base condensation. The stability was attributed to the microporosity, keto-enol tautomerism, and interplanar hydrogen

bonding. CO_2 adsorption studies were performed and the COF exhibited selective CO_2 adsorption over N_2 and CH_4. The breakthrough separation studies were performed and the COF had greater retention time for CO_2 indicating selective nature under dynamic conditions. Ag has been an important metal to fix CO_2 into value-added products. In this chapter. Ag nanoparticles are loaded into the COF and the CO_2 fixation was studied using the propargyl alcohol. The reaction produced cyclic carbonates with high yield, turn over number and turn over frequency. The ability of the COF to host active Ag nps and selective CO_2 capacity synergistically contribute to the high degree of CO_2 fixation reaction.

In chapter 5, Cu nanoparticle loaded COF has been studied for challenging Glaser-Hay coupling. Glaser-Hay coupling leads to the C-C bond formation between two terminal alkynes. Here we are able to catalyze the reaction in heterogeneous fashion using Cu@COF. A detailed mechanistic study revealed that the reaction proceeded via the anionic pathway. The XPS studies of the frozen sample at different time intervals exhibited significant peaks shifts and alternation in the Cu 2p satellites. Thus, this indicated the oxidative addition and reductive elimination involved in the catalytic cycles. We performed DFT and control reactions to show the role of the COF. The hydrogen bonding sites present in the COF pore directed the formation of hetero-coupled product in the reaction. The recyclability and the post-catalysis stability studies had proven the robustness of the Cu@COF catalyst.

In this thesis, we have covered a wide range of porous materials and discussed the applications based on the pore architecture and different functionalities present in the frameworks. Three distinct porous materials are used here, namely MOF, POF, and COF. Among these three candidates, MOFs have metal nodes coordinated by organic linkers. MOFs display a high degree of crystallinity and tuneability. However, the presence of metal-ligand co-ordinate bonds destabilizes the system and the MOFs are hydrolyzable in the presence of moisture, acids, and bases. On the other hand, porous polymers (POFs) contain covalent bonds (C-C, C-N, C=N, etc.) which are remarkably stable. The polymers exhibit exceptional stability towards acids, bases, organic solvents, and humidity. But the organic porous polymers are amorphous in nature and they are often non-reproducible during synthesis. It becomes difficult to study the structure- property relationship of a porous organic framework due to the lack of crystallinity. Covalent Organic Frameworks (COFs) are the crystalline organic polymers that are formed by covalent linking of the organic building blocks. This brings in the additional advantage of crystallinity to the framework. The rational choice of building blocks results in

different porous architecture, surface area, and functionalities. Still, several disadvantages are associated with COFs, particularly the stability of Schiff bonds in case of imine bonded COFs. But, the introduction of electronically active groups (electron-donating/withdrawing groups), hydrogen bonding moieties, etc. render stability into the framework.

The importance of porous supports for different applications has been demonstrated in the thesis. An ultra-microporous (POFs and MOFs) network favors selective gas adsorption, while the high degree of interaction sites present in the pore (COFs) prepares an optimal nanoreactor through the inclusion of nanoparticles. Our experimental and theoretical approach validates the advantages of porous solids for gas separation and catalytic processes.

Copyright Clearance Center Marketplace™

Order Confirmation

Thank you, your order has been placed. An email confirmation has been sent to you.

This is not an invoice. Please go to manage account to access your order history and invoices.

CUSTOMER INFORMATION

Payment by invoice: You can cancel your order until the invoice is generated by contacting customer service.

Billing Address

Debanjan Chakraborty
Dr. Homi Bhabha Road
Pashan
Pune
Pune, 411008
India

+91 8408890544
debanjan.chakraborty@students.iiserpune.ac.in

Customer Location

Debanjan Chakraborty
Dr. Homi Bhabha Road
Pashan
Pune
Pune, 411008
India

PO Number (optional)

N/A

Payment options

Invoice

ORDER CONFIRMATION

Total Due: 0.00 USD

Confirmation Number: 1016263

Order Date: 03-Feb-2020

1. Journal of materials chemistry. A, Materials for energy and sustainability

0.00 USD

Order license ID	1016263-1
ISSN	2050-7496
Type of Use	Republish in a thesis/dissertation
Publisher	Royal Society of Chemistry
Portion	Image/photo/illustration

LICENSED CONTENT

Publication Title	Journal of materials chemistry. A, Materials for energy and sustainability	**Country**	United Kingdom of Great Britain and Northern Ireland
Author/Editor	Royal Society of Chemistry (Great Britain)	**Rightsholder**	Royal Society of Chemistry
Date	01/01/2013	**Publication Type**	e-Journal
Language	English	**URL**	http://pubs.rsc.org/en/journals/journalissues/ta

REQUEST DETAILS

Portion Type	Image/photo/illustration	**Distribution**	Worldwide
Number of images / photos / illustrations	1	**Translation**	Original language of publication
Format (select all that apply)	Electronic	**Copies for the disabled?**	No
Who will republish the content?	Academic institution	**Minor editing privileges?**	No
Duration of Use	Current edition and up to 5 years	**Incidental promotional use?**	No
Lifetime Unit Quantity	Up to 499	**Currency**	USD
Rights Requested	Main product		

NEW WORK DETAILS

Title	Porous Materials for Gas Separation and Catalysis	**Institution name**	Indian Institute of Science Education and Research
Instructor name	Debanjan Chakraborty	**Expected presentation date**	2020-04-15

ADDITIONAL DETAILS

Order reference number	N/A	**The requesting person / organization to appear on the license**	Debanjan Chakraborty

REUSE CONTENT DETAILS

Title, description or numeric reference of the portion(s)	143	**Title of the article/chapter the portion is from**	N/A
Editor of portion(s)	N/A	**Author of portion(s)**	Royal Society of Chemistry (Great Britain)
Volume of serial or monograph	N/A	**Issue, if republishing an article from a serial**	N/A
Page or page range of portion	10	**Publication date of portion**	2013-01-01

Order Total: 0.00 USD

Total Items: 1 **Total Due: 0.00 USD**

Accepted: All Publisher and CCC Terms and Conditions

Copyright Clearance Center Marketplace™

Order Confirmation

Thank you, your order has been placed. An email confirmation has been sent to you. Your order license details and printable licenses will be available within 24 hours. Please access Manage Account for final order details.

This is not an invoice. Please go to manage account to access your order history and invoices.

CUSTOMER INFORMATION

Payment by invoice: You can cancel your order until the invoice is generated by contacting customer service.

Billing Address

Debanjan Chakraborty
Dr. Homi Bhabha Road
Pashan
Pune
Pune, 411008
India

+91 8408890544
debanjan.chakraborty@students.iiserpune.ac.in

Customer Location

Debanjan Chakraborty
Dr. Homi Bhabha Road
Pashan
Pune
Pune, 411008
India

PO Number (optional)

N/A

Payment options

Invoice

PENDING ORDER CONFIRMATION

Total Due: 0.00 USD

Confirmation Number: Pending

Order Date: 03-Feb-2020

1. Journal of materials chemistry. A, Materials for energy and sustainability

0.00 USD

Order license ID	Pending
ISSN	2050-7496
Type of Use	Republish in a thesis/dissertation
Publisher	Royal Society of Chemistry

Portion	Image/photo/illustration

LICENSED CONTENT

Publication Title	Journal of materials chemistry. A, Materials for energy and sustainability	**Country**	United Kingdom of Great Britain and Northern Ireland
Author/Editor	Royal Society of Chemistry (Great Britain)	**Rightsholder**	Royal Society of Chemistry
Date	01/01/2013	**Publication Type**	e-Journal
Language	English	**URL**	http://pubs.rsc.org/en/journals/journalissues/ta

REQUEST DETAILS

Portion Type	Image/photo/illustration	**Distribution**	Worldwide
Number of images / photos / illustrations	1	**Translation**	Original language of publication
Format (select all that apply)	Electronic	**Copies for the disabled?**	No
Who will republish the content?	Academic institution	**Minor editing privileges?**	No
Duration of Use	Current edition and up to 5 years	**Incidental promotional use?**	No
Lifetime Unit Quantity	Up to 499	**Currency**	USD
Rights Requested	Main product		

NEW WORK DETAILS

Title	Porous Materials for Gas Separation and Catalysis	**Institution name**	Indian Institute of Science Education and Research
Instructor name	Debanjan Chakraborty	**Expected presentation date**	2020-04-15

ADDITIONAL DETAILS

Order reference number	N/A	**The requesting person / organization to appear on the license**	Debanjan Chakraborty

REUSE CONTENT DETAILS

Title, description or numeric reference of the portion(s)	144	**Title of the article/chapter the portion is from**	N/A
Editor of portion(s)	N/A	**Author of portion(s)**	Royal Society of Chemistry (Great Britain)
Volume of serial or monograph	N/A	**Issue, if republishing an article from a serial**	N/A

Page or page range of portion	11	**Publication date of portion**	2013-01-01

Order Total: 0.00 USD

Total Items: 1

Total Due: 0.00 USD

Accepted: All Publisher and CCC Terms and Conditions

Novel Nitrogen and Sulfur Rich Hyper-Cross-Linked Microporous Poly-Triazine-Thiophene Copolymer for Superior CO2 Capture

Author: Sudipta K. Kundu, Asim Bhaumik

Publication: ACS Sustainable Chemistry & Engineering

Publisher: American Chemical Society

Date: Jul 1, 2016

PERMISSION/LICENSE IS GRANTED FOR YOUR ORDER AT NO CHARGE

This type of permission/license, instead of the standard Terms & Conditions, is sent to you because no fee is being charged for your order. Please note the following:

- Permission is granted for your request in both print and electronic formats, and translations.
- If figures and/or tables were requested, they may be adapted or used in part.
- Please print this page for your records and send a copy of it to your publisher/graduate school.
- Appropriate credit for the requested material should be given as follows: "Reprinted (adapted) with permission from (COMPLETE REFERENCE CITATION). Copyright (YEAR) American Chemical Society." Insert appropriate information in place of the capitalized words.
- One-time permission is granted only for the use specified in your request. No additional uses are granted (such as derivative works or other editions). For any other uses, please submit a new request.

If credit is given to another source for the material you requested, permission must be obtained from that source.

BACK CLOSE WINDOW

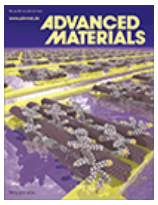

Microporous Organic Polymers for Methane Storage

Author: Colin D. Wood, Bien Tan, Abbie Trewin, et al
Publication: Advanced Materials
Publisher: John Wiley and Sons
Date: May 26, 2008

Order Completed

Thank you for your order.

This Agreement between Indian Institute of Science Education and Research Pune ("You") and John Wiley and Sons ("John Wiley and Sons") consists of your license details and the terms and conditions provided by John Wiley and Sons and Copyright Clearance Center.

Your confirmation email will contain your order number for future reference.

License Number	4761120834398
License date	Feb 02, 2020

Printable Details

Licensed Content

Licensed Content Publisher	John Wiley and Sons
Licensed Content Publication	Advanced Materials
Licensed Content Title	Microporous Organic Polymers for Methane Storage
Licensed Content Author	Colin D. Wood, Bien Tan, Abbie Trewin, et al
Licensed Content Date	May 26, 2008
Licensed Content Volume	20
Licensed Content Issue	10
Licensed Content Pages	6

Order Details

Type of use	Dissertation/Thesis
Requestor type	University/Academic
Format	Print and electronic
Portion	Figure/table
Number of figures/tables	1
Will you be translating?	No

About Your Work

Title of your thesis / dissertation	Porous Framework Materials for Gas Separation and Catalysis
Expected completion date	May 2020
Expected size (number of pages)	200

Additional Data

Original Wiley figure/table number(s)	Figure 2

Requestor Location

Requestor Location	Indian Institute of Science Education and Research Pune Dr. Homi Bhabha Road Pashan Pune Pune, 411008 India Attn: Indian Institute of Science Education and Research Pune

Tax Details

Publisher Tax ID	EU826007151

Price

Total	0.00 USD

Would you like to purchase the full text of this article? If so, please continue on to the content ordering system located here: Purchase PDF
If you click on the buttons below or close this window, you will not be able to return to the content ordering system.

Total: 0.00 USD

CLOSE WINDOW ORDER MORE

Copyright Clearance Center Marketplace™

Order Confirmation

Thank you, your order has been placed. An email confirmation has been sent to you. Your order license details and printable licenses will be available within 24 hours. Please access Manage Account for final order details.

This is not an invoice. Please go to manage account to access your order history and invoices.

CUSTOMER INFORMATION

Payment by invoice: You can cancel your order until the invoice is generated by contacting customer service.

Billing Address

Debanjan Chakraborty
Dr. Homi Bhabha Road
Pashan
Pune
Pune, 411008
India

+91 8408890544
debanjan.chakraborty@students.iiserpune.ac.in

Customer Location

Debanjan Chakraborty
Dr. Homi Bhabha Road
Pashan
Pune
Pune, 411008
India

PO Number (optional)

N/A

Payment options

Invoice

PENDING ORDER CONFIRMATION

Total Due: 0.00 USD

Confirmation Number: Pending

Order Date: 03-Feb-2020

1. Chemical communications

0.00 USD

Order license ID	Pending
ISSN	1364-548X
Type of Use	Republish in a thesis/dissertation
Publisher	ROYAL SOCIETY OF CHEMISTRY
Portion	Image/photo/illustration

LICENSED CONTENT

Publication Title	Chemical communications	**Country**	United Kingdom of Great Britain and Northern Ireland
Author/Editor	Royal Society of Chemistry (Great Britain)	**Rightsholder**	Royal Society of Chemistry
Date	01/01/1996	**Publication Type**	e-Journal
Language	English		

REQUEST DETAILS

Portion Type	Image/photo/illustration	**Distribution**	Worldwide
Number of images / photos / illustrations	1	**Translation**	Original language of publication
Format (select all that apply)	Electronic	**Copies for the disabled?**	No
Who will republish the content?	Academic institution	**Minor editing privileges?**	No
Duration of Use	Current edition and up to 5 years	**Incidental promotional use?**	No
Lifetime Unit Quantity	Up to 499	**Currency**	USD
Rights Requested	Main product		

NEW WORK DETAILS

Title	Porous Materials for Gas Separation and Catalysis	**Institution name**	Indian Institute of Science Education and Research Pune
Instructor name	Debanjan Chakraborty	**Expected presentation date**	2020-04-15

ADDITIONAL DETAILS

Order reference number	N/A	**The requesting person / organization to appear on the license**	Debanjan Chakraborty

REUSE CONTENT DETAILS

Title, description or numeric reference of the portion(s)	155	**Title of the article/chapter the portion is from**	N/A
Editor of portion(s)	N/A	**Author of portion(s)**	Royal Society of Chemistry (Great Britain)
Volume of serial or monograph	N/A	**Issue, if republishing an article from a serial**	N/A
Page or page range of portion	15	**Publication date of portion**	1996-01-01

Order Total: 0.00 USD

Total Items: 1 **Total Due: 0.00 USD**

Accepted: All Publisher and CCC Terms and Conditions

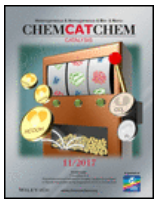

Pd Nanoparticles Decorated on Hypercrosslinked Microporous Polymer: A Highly Efficient Catalyst for the Formylation of Amines through Carbon Dioxide Fixation

Author: Sk Manirul Islam, Asim Bhaumik, Sk Safikul Islam, et al

Publication: ChemCatChem

Publisher: John Wiley and Sons

Date: May 16, 2017

Order Completed

Thank you for your order.

This Agreement between Indian Institute of Science Education and Research Pune ("You") and John Wiley and Sons ("John Wiley and Sons") consists of your license details and the terms and conditions provided by John Wiley and Sons and Copyright Clearance Center.

Your confirmation email will contain your order number for future reference.

License Number	4761121393709
License date	Feb 02, 2020

Printable Details

Licensed Content

Licensed Content Publisher	John Wiley and Sons
Licensed Content Publication	ChemCatChem
Licensed Content Title	Pd Nanoparticles Decorated on Hypercrosslinked Microporous Polymer: A Highly Efficient Catalyst for the Formylation of Amines through Carbon Dioxide Fixation
Licensed Content Author	Sk Manirul Islam, Asim Bhaumik, Sk Safikul Islam, et al
Licensed Content Date	May 16, 2017
Licensed Content Volume	9
Licensed Content Issue	11
Licensed Content Pages	8

Order Details

Type of use	Dissertation/Thesis
Requestor type	University/Academic
Format	Print and electronic
Portion	Figure/table
Number of figures/tables	1
Will you be translating?	No

About Your Work

Title of your thesis / dissertation	Porous Framework Materials for Gas Separation and Catalysis
Expected completion date	May 2020
Expected size (number of pages)	200

Additional Data

Original Wiley figure/table number(s)	Figure 3

Requestor Location

Requestor Location	Indian Institute of Science Education and Research Pune Dr. Homi Bhabha Road Pashan Pune Pune, 411008 India Attn: Indian Institute of Science Education and Research Pune

Tax Details

Publisher Tax ID	EU826007151

Price

Total	0.00 USD

Would you like to purchase the full text of this article? If so, please continue on to the content ordering system located here: Purchase PDF
If you click on the buttons below or close this window, you will not be able to return to the content ordering system.

Total: 0.00 USD

CLOSE WINDOW ORDER MORE

High-Throughput Synthesis of Zeolitic Imidazolate Frameworks and Application to CO_2 Capture

Author:
Rahul Banerjee,Anh Phan,Bo Wang,Carolyn Knobler,Hiroyasu Furukawa,Michael O'Keeffe,Omar M. Yaghi

Publication: Science

Publisher: The American Association for the Advancement of Science

Date: Feb 15, 2008

Order Completed

Thank you for your order.

This Agreement between Indian Institute of Science Education and Research Pune ("You") and The American Association for the Advancement of Science ("The American Association for the Advancement of Science") consists of your license details and the terms and conditions provided by The American Association for the Advancement of Science and Copyright Clearance Center.

Your confirmation email will contain your order number for future reference.

License Number	4761130035760
License date	Feb 02, 2020

Printable Details

Licensed Content

Licensed Content Publisher	The American Association for the Advancement of Science
Licensed Content Publication	Science
Licensed Content Title	High-Throughput Synthesis of Zeolitic Imidazolate Frameworks and Application to CO_2 Capture
Licensed Content Author	Rahul Banerjee,Anh Phan,Bo Wang,Carolyn Knobler,Hiroyasu Furukawa,Michael O'Keeffe,Omar M. Yaghi
Licensed Content Date	Feb 15, 2008
Licensed Content Volume	319
Licensed Content Issue	5865

Order Details

Type of Use	Thesis / Dissertation
Requestor type	Scientist/individual at a research institution
Format	Print and electronic
Portion	Figure
Number of figures/tables	1

About Your Work

Title	Porous Framework Materials for Gas Separation and Catalysis
Institution name	n/a
Expected presentation date	May 2020

Additional Data

Order reference number	160
Portions	Figure 1

Requestor Location

Requestor Location	Indian Institute of Science Education and Research Pune Dr. Homi Bhabha Road Pashan Pune Pune, 411008 India Attn: Indian Institute of Science Education and Research Pune

Tax Details

Price

Total	0.00 USD

Total: 0.00 USD

CLOSE WINDOW ORDER MORE

Direct Observation and Quantification of CO_2 Binding Within an Amine-Functionalized Nanoporous Solid

Author:
Ramanathan Vaidhyanathan,Simon S. Iremonger,George K. H. Shimizu,Peter G. Boyd,Saman Alavi,Tom K. Woo

Publication: Science

Publisher: The American Association for the Advancement of Science

Date: Oct 29, 2010

Order Completed

Thank you for your order.

This Agreement between Indian Institute of Science Education and Research Pune ("You") and The American Association for the Advancement of Science ("The American Association for the Advancement of Science") consists of your license details and the terms and conditions provided by The American Association for the Advancement of Science and Copyright Clearance Center.

Your confirmation email will contain your order number for future reference.

License Number	4761130119876
License date	Feb 02, 2020

Printable Details

Licensed Content

Licensed Content Publisher	The American Association for the Advancement of Science
Licensed Content Publication	Science
Licensed Content Title	Direct Observation and Quantification of CO_2 Binding Within an Amine-Functionalized Nanoporous Solid
Licensed Content Author	Ramanathan Vaidhyanathan,Simon S. Iremonger,George K. H. Shimizu,Peter G. Boyd,Saman Alavi,Tom K. Woo
Licensed Content Date	Oct 29, 2010
Licensed Content Volume	330
Licensed Content Issue	6004

Order Details

Type of Use	Thesis / Dissertation
Requestor type	Scientist/individual at a research institution
Format	Print and electronic
Portion	Figure
Number of figures/tables	1

About Your Work

Title	Porous Framework Materials for Gas Separation and Catalysis
Institution name	n/a
Expected presentation date	May 2020

Additional Data

Order reference number	176
Portions	Figure 2

Requestor Location

Requestor Location	Indian Institute of Science Education and Research Pune Dr. Homi Bhabha Road Pashan Pune Pune, 411008 India Attn: Indian Institute of Science Education and Research Pune

Tax Details

Price

Total	0.00 USD

Total: 0.00 USD

CLOSE WINDOW ORDER MORE

Porous materials with optimal adsorption thermodynamics and kinetics for CO2 separation

Author: Patrick Nugent et al

Publication: Nature

Publisher: Springer Nature

Date: Feb 27, 2013

Order Completed

Thank you for your order.

This Agreement between Indian Institute of Science Education and Research Pune ("You") and Springer Nature ("Springer Nature") consists of your license details and the terms and conditions provided by Springer Nature and Copyright Clearance Center.

Your confirmation email will contain your order number for future reference.

License Number	4761130383145
License date	Feb 02, 2020

Printable Details

Licensed Content

Licensed Content Publisher	Springer Nature
Licensed Content Publication	Nature
Licensed Content Title	Porous materials with optimal adsorption thermodynamics and kinetics for CO2 separation
Licensed Content Author	Patrick Nugent et al
Licensed Content Date	Feb 27, 2013

Order Details

Type of Use	Thesis/Dissertation
Requestor type	academic/university or research institute
Format	print and electronic
Portion	figures/tables/illustrations
Number of figures/tables/illustrations	1
High-res required	no
Will you be translating?	no
Circulation/distribution	1 - 29
Author of this Springer Nature content	no

About Your Work

Title	Porous Framework Materials for Gas Separation and Catalysis
Institution name	n/a
Expected presentation date	May 2020

Additional Data

Order reference number	177
Portions	Figure 3

Requestor Location

Requestor Location	Indian Institute of Science Education and Research Pune Dr. Homi Bhabha Road Pashan Pune Pune, 411008 India Attn: Indian Institute of Science Education and Research Pune

Tax Details

Price

Total	0.00 USD

Total: 0.00 USD

CLOSE WINDOW ORDER MORE

A Fine-Tuned Fluorinated MOF Addresses the Needs for Trace CO2 Removal and Air Capture Using Physisorption

Author: Prashant M. Bhatt, Youssef Belmabkhout, Amandine Cadiau, et al

Publication: Journal of the American Chemical Society

Publisher: American Chemical Society

Date: Jul 1, 2016

PERMISSION/LICENSE IS GRANTED FOR YOUR ORDER AT NO CHARGE

This type of permission/license, instead of the standard Terms & Conditions, is sent to you because no fee is being charged for your order. Please note the following:

- Permission is granted for your request in both print and electronic formats, and translations.
- If figures and/or tables were requested, they may be adapted or used in part.
- Please print this page for your records and send a copy of it to your publisher/graduate school.
- Appropriate credit for the requested material should be given as follows: "Reprinted (adapted) with permission from (COMPLETE REFERENCE CITATION). Copyright (YEAR) American Chemical Society." Insert appropriate information in place of the capitalized words.
- One-time permission is granted only for the use specified in your request. No additional uses are granted (such as derivative works or other editions). For any other uses, please submit a new request.

If credit is given to another source for the material you requested, permission must be obtained from that source.

BACK CLOSE WINDOW

This page is available in the following languages:

Creative Commons License De

Attribution 4.0 International (CC BY 4.0)

This is a human-readable summary of (and not a substitute for) the license.

You are free to:

Share — copy and redistribute the material in any medium or format

Adapt — remix, transform, and build upon the material

for any purpose, even commercially.

The licensor cannot revoke these freedoms as long as you follow the license terms.

Under the following terms:

Attribution — You must give appropriate credit, provide a link to the license, and indicate if changes were made. You may do so in any reasonable manner, but not in any way that suggests the licensor endorses you or your use.

No additional restrictions — You may not apply legal terms or technological measures that legally restrict others from doing anything the license permits.

Notices:

You do not have to comply with the license for elements of the material in the public domain or where your use is permitted by an applicable exception or limitation.

No warranties are given. The license may not give you all of the permissions necessary for your intended use. For example, other rights such as publicity, privacy, or moral rights may limit how you use the material.

Separation of rare gases and chiral molecules by selective binding in porous organic cages

Author: Linjiang Chen et al
Publication: Nature Materials
Publisher: Springer Nature
Date: Jul 20, 2014

Order Completed

Thank you for your order.

This Agreement between Indian Institute of Science Education and Research Pune ("You") and Springer Nature ("Springer Nature") consists of your license details and the terms and conditions provided by Springer Nature and Copyright Clearance Center.

Your confirmation email will contain your order number for future reference.

License Number	4761130678765
License date	Feb 02, 2020

Printable Details

Licensed Content

Licensed Content Publisher	Springer Nature
Licensed Content Publication	Nature Materials
Licensed Content Title	Separation of rare gases and chiral molecules by selective binding in porous organic cages
Licensed Content Author	Linjiang Chen et al
Licensed Content Date	Jul 20, 2014

Order Details

Type of Use	Thesis/Dissertation
Requestor type	academic/university or research institute
Format	print and electronic
Portion	figures/tables/illustrations
Number of figures/tables/illustrations	1
High-res required	no
Will you be translating?	no
Circulation/distribution	1 - 29
Author of this Springer Nature content	no

About Your Work

Title	Porous Framework Materials for Gas Separation and Catalysis
Institution name	n/a
Expected presentation date	May 2020

Additional Data

Order reference number	182
Portions	Figure 2

Requestor Location

Requestor Location	Indian Institute of Science Education and Research Pune Dr. Homi Bhabha Road Pashan Pune Pune, 411008 India Attn: Indian Institute of Science Education and Research Pune

Tax Details

Price

Total	0.00 USD

Total: 0.00 USD

CLOSE WINDOW ORDER MORE

Copyright Clearance Center Marketplace™

Order Confirmation

Thank you, your order has been placed. An email confirmation has been sent to you. Your order license details and printable licenses will be available within 24 hours. Please access Manage Account for final order details.

This is not an invoice. Please go to manage account to access your order history and invoices.

CUSTOMER INFORMATION

Payment by invoice: You can cancel your order until the invoice is generated by contacting customer service.

Billing Address

Debanjan Chakraborty
Dr. Homi Bhabha Road
Pashan
Pune
Pune, 411008
India

+91 8408890544
debanjan.chakraborty@students.iiserpune.ac.in

Customer Location

Debanjan Chakraborty
Dr. Homi Bhabha Road
Pashan
Pune
Pune, 411008
India

PO Number (optional)

N/A

Payment options

Invoice

PENDING ORDER CONFIRMATION

Total Due: 0.00 USD

Confirmation Number: Pending

Order Date: 03-Feb-2020

1. Chemical Society reviews

0.00 USD

Order license ID	Pending
ISSN	1460-4744
Type of Use	Republish in a thesis/dissertation
Publisher	ROYAL SOCIETY OF CHEMISTRY
Portion	Image/photo/illustration

LICENSED CONTENT

Publication Title	Chemical Society reviews	**Country**	United Kingdom of Great Britain and Northern Ireland
Author/Editor	Royal Society of Chemistry (Great Britain)	**Rightsholder**	Royal Society of Chemistry
Date	01/01/1972	**Publication Type**	e-Journal
Language	English	**URL**	http://www.rsc.org/csr

REQUEST DETAILS

Portion Type	Image/photo/illustration	**Distribution**	Worldwide
Number of images / photos / illustrations	1	**Translation**	Original language of publication
Format (select all that apply)	Electronic	**Copies for the disabled?**	No
Who will republish the content?	Academic institution	**Minor editing privileges?**	No
Duration of Use	Current edition and up to 5 years	**Incidental promotional use?**	No
Lifetime Unit Quantity	Up to 499	**Currency**	USD
Rights Requested	Main product		

NEW WORK DETAILS

Title	Porous Framework Materials for Gas Separation and Catalysis	**Institution name**	Indian Institute of Science Education and Research Pune
Instructor name	Debanjan Chakraborty	**Expected presentation date**	2020-04-15

ADDITIONAL DETAILS

Order reference number	N/A	**The requesting person / organization to appear on the license**	Debanjan CHakraborty

REUSE CONTENT DETAILS

Title, description or numeric reference of the portion(s)	191	**Title of the article/chapter the portion is from**	N/A
Editor of portion(s)	N/A	**Author of portion(s)**	Royal Society of Chemistry (Great Britain)
Volume of serial or monograph	N/A	**Issue, if republishing an article from a serial**	N/A
Page or page range of portion	54	**Publication date of portion**	1972-01-01

Order Total: 0.00 USD

Total Items: 1 **Total Due: 0.00 USD**

Accepted: All Publisher and CCC Terms and Conditions

Copyright Clearance Center Marketplace™

Order Confirmation

Thank you, your order has been placed. An email confirmation has been sent to you. Your order license details and printable licenses will be available within 24 hours. Please access Manage Account for final order details.

This is not an invoice. Please go to manage account to access your order history and invoices.

CUSTOMER INFORMATION

Payment by invoice: You can cancel your order until the invoice is generated by contacting customer service.

Billing Address

Debanjan Chakraborty
Dr. Homi Bhabha Road
Pashan
Pune
Pune, 411008
India

+91 8408890544
debanjan.chakraborty@students.iiserpune.ac.in

Customer Location

Debanjan Chakraborty
Dr. Homi Bhabha Road
Pashan
Pune
Pune, 411008
India

PO Number (optional)

N/A

Payment options

Invoice

PENDING ORDER CONFIRMATION

Total Due: 0.00 USD

Confirmation Number: Pending

Order Date: 03-Feb-2020

1. Chemical communications

0.00 USD

Order license ID	Pending
ISSN	1364-548X
Type of Use	Republish in a thesis/dissertation
Publisher	ROYAL SOCIETY OF CHEMISTRY
Portion	Image/photo/illustration

LICENSED CONTENT

Publication Title	Chemical communications	**Country**	United Kingdom of Great Britain and Northern Ireland
Author/Editor	Royal Society of Chemistry (Great Britain)	**Rightsholder**	Royal Society of Chemistry
Date	01/01/1996	**Publication Type**	e-Journal
Language	English		

REQUEST DETAILS

Portion Type	Image/photo/illustration	**Distribution**	Worldwide
Number of images / photos / illustrations	1	**Translation**	Original language of publication
Format (select all that apply)	Electronic	**Copies for the disabled?**	No
Who will republish the content?	Academic institution	**Minor editing privileges?**	No
Duration of Use	Current edition and up to 5 years	**Incidental promotional use?**	No
Lifetime Unit Quantity	Up to 499	**Currency**	USD
Rights Requested	Main product		

NEW WORK DETAILS

Title	Porous Materials for Gas Separation and Catalysis	**Institution name**	Indian Institute of Science Education and Research Pune
Instructor name	Debanjan Chakraborty	**Expected presentation date**	2020-04-15

ADDITIONAL DETAILS

Order reference number	N/A	**The requesting person / organization to appear on the license**	Debanjan Chakraborty

REUSE CONTENT DETAILS

Title, description or numeric reference of the portion(s)	194	**Title of the article/chapter the portion is from**	N/A
Editor of portion(s)	N/A	**Author of portion(s)**	Royal Society of Chemistry (Great Britain)
Volume of serial or monograph	N/A	**Issue, if republishing an article from a serial**	N/A
Page or page range of portion	55	**Publication date of portion**	1996-01-01

Order Total: 0.00 USD

Total Items: 1 **Total Due: 0.00 USD**

Accepted: All Publisher and CCC Terms and Conditions

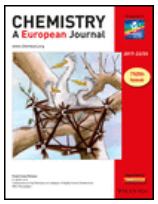

A 2D Mesoporous Imine-Linked Covalent Organic Framework for High Pressure Gas Storage Applications

Author: Hani M. El-Kaderi, Ransheng Ding, Thomas E. Reich, et al

Publication: Chemistry - A European Journal

Publisher: John Wiley and Sons

Date: Feb 5, 2013

Order Completed

Thank you for your order.

This Agreement between Indian Institute of Science Education and Research Pune ("You") and John Wiley and Sons ("John Wiley and Sons") consists of your license details and the terms and conditions provided by John Wiley and Sons and Copyright Clearance Center.

Your confirmation email will contain your order number for future reference.

License Number	4761140636584
License date	Feb 03, 2020

Printable Details

Licensed Content

Licensed Content Publisher	John Wiley and Sons
Licensed Content Publication	Chemistry - A European Journal
Licensed Content Title	A 2D Mesoporous Imine-Linked Covalent Organic Framework for High Pressure Gas Storage Applications
Licensed Content Author	Hani M. El-Kaderi, Ransheng Ding, Thomas E. Reich, et al
Licensed Content Date	Feb 5, 2013
Licensed Content Volume	19
Licensed Content Issue	10
Licensed Content Pages	5

Order Details

Type of use	Dissertation/Thesis
Requestor type	University/Academic
Format	Print and electronic
Portion	Figure/table
Number of figures/tables	1
Will you be translating?	No

About Your Work

Title of your thesis / dissertation	Porous Framework Materials for Gas Separation and Catalysis
Expected completion date	May 2020
Expected size (number of pages)	200

Additional Data

Original Wiley figure/table number(s)	Figure 2

Requestor Location

Requestor Location	Indian Institute of Science Education and Research Pune Dr. Homi Bhabha Road Pashan Pune Pune, 411008 India Attn: Indian Institute of Science Education and Research Pune

Tax Details

Publisher Tax ID	EU826007151

Price

Total	0.00 USD

Would you like to purchase the full text of this article? If so, please continue on to the content ordering system located here: Purchase PDF
If you click on the buttons below or close this window, you will not be able to return to the content ordering system.

Total: 0.00 USD

CLOSE WINDOW ORDER MORE

Copyright Clearance Center Marketplace™

Order Confirmation

Thank you, your order has been placed. An email confirmation has been sent to you. Your order license details and printable licenses will be available within 24 hours. Please access Manage Account for final order details.

This is not an invoice. Please go to manage account to access your order history and invoices.

CUSTOMER INFORMATION

Payment by invoice: You can cancel your order until the invoice is generated by contacting customer service.

Billing Address

Debanjan Chakraborty
Dr. Homi Bhabha Road
Pashan
Pune
Pune, 411008
India

+91 8408890544
debanjan.chakraborty@students.iiserpune.ac.in

Customer Location

Debanjan Chakraborty
Dr. Homi Bhabha Road
Pashan
Pune
Pune, 411008
India

PO Number (optional)

N/A

Payment options

Invoice

PENDING ORDER CONFIRMATION

Total Due: 0.00 USD

Confirmation Number: Pending

Order Date: 03-Feb-2020

1. Journal of materials chemistry. A, Materials for energy and sustainability

0.00 USD

Order license ID	Pending
ISSN	2050-7496
Type of Use	Republish in a thesis/dissertation
Publisher	Royal Society of Chemistry

Portion	Image/photo/illustration

LICENSED CONTENT

Publication Title	Journal of materials chemistry. A, Materials for energy and sustainability	**Country**	United Kingdom of Great Britain and Northern Ireland
Author/Editor	Royal Society of Chemistry (Great Britain)	**Rightsholder**	Royal Society of Chemistry
Date	01/01/2013	**Publication Type**	e-Journal
Language	English	**URL**	http://pubs.rsc.org/en/journals/journalissues/ta

REQUEST DETAILS

Portion Type	Image/photo/illustration	**Distribution**	Worldwide
Number of images / photos / illustrations	1	**Translation**	Original language of publication
Format (select all that apply)	Electronic	**Copies for the disabled?**	No
Who will republish the content?	Academic institution	**Minor editing privileges?**	No
Duration of Use	Current edition and up to 5 years	**Incidental promotional use?**	No
Lifetime Unit Quantity	Up to 499	**Currency**	USD
Rights Requested	Main product		

NEW WORK DETAILS

Title	Porous Materials for Gas Separation and Catalysis	**Institution name**	Indian Institute of Science Education and Research
Instructor name	Debanjan Chakraborty	**Expected presentation date**	2020-04-15

ADDITIONAL DETAILS

Order reference number	N/A	**The requesting person / organization to appear on the license**	Debanjan Chakraborty

REUSE CONTENT DETAILS

Title, description or numeric reference of the portion(s)	198	**Title of the article/chapter the portion is from**	N/A
Editor of portion(s)	N/A	**Author of portion(s)**	Royal Society of Chemistry (Great Britain)
Volume of serial or monograph	N/A	**Issue, if republishing an article from a serial**	N/A

Page or page range of portion	44	**Publication date of portion**	2013-01-01

Order Total: 0.00 USD

Total Items: 1

Total Due: 0.00 USD

Accepted: All Publisher and CCC Terms and Conditions

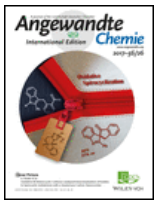

Two-Dimensional Covalent Organic Frameworks for Carbon Dioxide Capture through Channel-Wall Functionalization

Author: Donglin Jiang, Rajamani Krishna, Xiong Chen, et al

Publication: Angewandte Chemie International Edition

Publisher: John Wiley and Sons

Date: Jan 22, 2015

Order Completed

Thank you for your order.

This Agreement between Indian Institute of Science Education and Research Pune ("You") and John Wiley and Sons ("John Wiley and Sons") consists of your license details and the terms and conditions provided by John Wiley and Sons and Copyright Clearance Center.

Your confirmation email will contain your order number for future reference.

License Number	4761140888632
License date	Feb 03, 2020

Printable Details

Licensed Content

Licensed Content Publisher	John Wiley and Sons
Licensed Content Publication	Angewandte Chemie International Edition
Licensed Content Title	Two-Dimensional Covalent Organic Frameworks for Carbon Dioxide Capture through Channel-Wall Functionalization
Licensed Content Author	Donglin Jiang, Rajamani Krishna, Xiong Chen, et al
Licensed Content Date	Jan 22, 2015
Licensed Content Volume	54
Licensed Content Issue	10
Licensed Content Pages	5

Order Details

Type of use	Dissertation/Thesis
Requestor type	University/Academic
Format	Print and electronic
Portion	Figure/table
Number of figures/tables	1
Will you be translating?	No

About Your Work

Title of your thesis / dissertation	Porous Framework Materials for Gas Separation and Catalysis
Expected completion date	May 2020
Expected size (number of pages)	200

Additional Data

Original Wiley figure/table number(s)	Figure 2

Requestor Location

Requestor Location	Indian Institute of Science Education and Research Pune Dr. Homi Bhabha Road Pashan Pune Pune, 411008 India Attn: Indian Institute of Science Education and Research Pune

Tax Details

Publisher Tax ID	EU826007151

Price

Total	0.00 USD

Would you like to purchase the full text of this article? If so, please continue on to the content ordering system located here: Purchase PDF
If you click on the buttons below or close this window, you will not be able to return to the content ordering system.

Total: 0.00 USD

CLOSE WINDOW ORDER MORE

Covalent Organic Framework with Frustrated Bonding Network for Enhanced Carbon Dioxide Storage

Author: Qiang Gao, Xing Li, Guo-Hong Ning, et al

Publication: Chemistry of Materials

Publisher: American Chemical Society

Date: Mar 1, 2018

PERMISSION/LICENSE IS GRANTED FOR YOUR ORDER AT NO CHARGE

This type of permission/license, instead of the standard Terms & Conditions, is sent to you because no fee is being charged for your order. Please note the following:

- Permission is granted for your request in both print and electronic formats, and translations.
- If figures and/or tables were requested, they may be adapted or used in part.
- Please print this page for your records and send a copy of it to your publisher/graduate school.
- Appropriate credit for the requested material should be given as follows: "Reprinted (adapted) with permission from (COMPLETE REFERENCE CITATION). Copyright (YEAR) American Chemical Society." Insert appropriate information in place of the capitalized words.
- One-time permission is granted only for the use specified in your request. No additional uses are granted (such as derivative works or other editions). For any other uses, please submit a new request.

If credit is given to another source for the material you requested, permission must be obtained from that source.

BACK CLOSE WINDOW

In-Depth Experimental and Computational Investigations for Remarkable Gas/Vapor Sorption, Selectivity, and Affinity by a Porous Nitrogen-Rich Covalent Organic Framework

Author: Prasenjit Das, Sanjay K. Mandal
Publication: Chemistry of Materials
Publisher: American Chemical Society
Date: Mar 1, 2019

PERMISSION/LICENSE IS GRANTED FOR YOUR ORDER AT NO CHARGE

This type of permission/license, instead of the standard Terms & Conditions, is sent to you because no fee is being charged for your order. Please note the following:

- Permission is granted for your request in both print and electronic formats, and translations.
- If figures and/or tables were requested, they may be adapted or used in part.
- Please print this page for your records and send a copy of it to your publisher/graduate school.
- Appropriate credit for the requested material should be given as follows: "Reprinted (adapted) with permission from (COMPLETE REFERENCE CITATION). Copyright (YEAR) American Chemical Society." Insert appropriate information in place of the capitalized words.
- One-time permission is granted only for the use specified in your request. No additional uses are granted (such as derivative works or other editions). For any other uses, please submit a new request.

If credit is given to another source for the material you requested, permission must be obtained from that source.

Construction of Covalent Organic Framework for Catalysis: Pd/COF-LZU1 in Suzuki–Miyaura Coupling Reaction

Author: San-Yuan Ding, Jia Gao, Qiong Wang, et al
Publication: Journal of the American Chemical Society
Publisher: American Chemical Society
Date: Dec 1, 2011

PERMISSION/LICENSE IS GRANTED FOR YOUR ORDER AT NO CHARGE

This type of permission/license, instead of the standard Terms & Conditions, is sent to you because no fee is being charged for your order. Please note the following:

- Permission is granted for your request in both print and electronic formats, and translations.
- If figures and/or tables were requested, they may be adapted or used in part.
- Please print this page for your records and send a copy of it to your publisher/graduate school.
- Appropriate credit for the requested material should be given as follows: "Reprinted (adapted) with permission from (COMPLETE REFERENCE CITATION). Copyright (YEAR) American Chemical Society." Insert appropriate information in place of the capitalized words.
- One-time permission is granted only for the use specified in your request. No additional uses are granted (such as derivative works or other editions). For any other uses, please submit a new request.

If credit is given to another source for the material you requested, permission must be obtained from that source.

BACK CLOSE WINDOW

Catalysis and CO2 Capture by Palladium-Incorporated Covalent Organic Frameworks

Author: Ramaswamy Murugavel, Ateeque Malani, Abhishek Sharma, et al

Publication: CHEMPLUSCHEM

Publisher: John Wiley and Sons

Date: Oct 9, 2017

Order Completed

Thank you for your order.

This Agreement between Indian Institute of Science Education and Research Pune ("You") and John Wiley and Sons ("John Wiley and Sons") consists of your license details and the terms and conditions provided by John Wiley and Sons and Copyright Clearance Center.

Your confirmation email will contain your order number for future reference.

License Number	4761141146154
License date	Feb 03, 2020

Printable Details

Licensed Content

Licensed Content Publisher	John Wiley and Sons
Licensed Content Publication	CHEMPLUSCHEM
Licensed Content Title	Catalysis and CO2 Capture by Palladium-Incorporated Covalent Organic Frameworks
Licensed Content Author	Ramaswamy Murugavel, Ateeque Malani, Abhishek Sharma, et al
Licensed Content Date	Oct 9, 2017
Licensed Content Volume	82
Licensed Content Issue	10
Licensed Content Pages	13

Order Details

Type of use	Dissertation/Thesis
Requestor type	University/Academic
Format	Print and electronic
Portion	Figure/table
Number of figures/tables	2
Will you be translating?	No

About Your Work

Title of your thesis / dissertation	Porous Framework Materials for Gas Separation and Catalysis
Expected completion date	May 2020
Expected size (number of pages)	200

Additional Data

Original Wiley figure/table number(s)	Figure 3

Requestor Location

Requestor Location	Indian Institute of Science Education and Research Pune Dr. Homi Bhabha Road Pashan Pune Pune, 411008 India Attn: Indian Institute of Science Education and Research Pune

Tax Details

Publisher Tax ID	EU826007151

Price

Total	0.00 USD

Would you like to purchase the full text of this article? If so, please continue on to the content ordering system located here: Purchase PDF
If you click on the buttons below or close this window, you will not be able to return to the content ordering system.

Total: 0.00 USD

CLOSE WINDOW ORDER MORE

Synthesis of Ultrafine and Highly Dispersed Metal Nanoparticles Confined in a Thioether-Containing Covalent Organic Framework and Their Catalytic Applications

Author: Shuanglong Lu, Yiming Hu, Shun Wan, et al
Publication: Journal of the American Chemical Society
Publisher: American Chemical Society
Date: Nov 1, 2017

PERMISSION/LICENSE IS GRANTED FOR YOUR ORDER AT NO CHARGE

This type of permission/license, instead of the standard Terms & Conditions, is sent to you because no fee is being charged for your order. Please note the following:

- Permission is granted for your request in both print and electronic formats, and translations.
- If figures and/or tables were requested, they may be adapted or used in part.
- Please print this page for your records and send a copy of it to your publisher/graduate school.
- Appropriate credit for the requested material should be given as follows: "Reprinted (adapted) with permission from (COMPLETE REFERENCE CITATION). Copyright (YEAR) American Chemical Society." Insert appropriate information in place of the capitalized words.
- One-time permission is granted only for the use specified in your request. No additional uses are granted (such as derivative works or other editions). For any other uses, please submit a new request.

If credit is given to another source for the material you requested, permission must be obtained from that source.

BACK CLOSE WINDOW

Imparting Catalytic Activity to a Covalent Organic Framework Material by Nanoparticle Encapsulation

Author: Xiaofei Shi, Youjin Yao, Yulong Xu, et al

Publication: Applied Materials

Publisher: American Chemical Society

Date: Mar 1, 2017

PERMISSION/LICENSE IS GRANTED FOR YOUR ORDER AT NO CHARGE

This type of permission/license, instead of the standard Terms & Conditions, is sent to you because no fee is being charged for your order. Please note the following:

- Permission is granted for your request in both print and electronic formats, and translations.
- If figures and/or tables were requested, they may be adapted or used in part.
- Please print this page for your records and send a copy of it to your publisher/graduate school.
- Appropriate credit for the requested material should be given as follows: "Reprinted (adapted) with permission from (COMPLETE REFERENCE CITATION). Copyright (YEAR) American Chemical Society." Insert appropriate information in place of the capitalized words.
- One-time permission is granted only for the use specified in your request. No additional uses are granted (such as derivative works or other editions). For any other uses, please submit a new request.

If credit is given to another source for the material you requested, permission must be obtained from that source.

BACK CLOSE WINDOW

Highly Stable COF-Supported Co/Co(OH)2 Nanoparticles Heterogeneous Catalyst for Reduction of Nitrile/Nitro Compounds under Mild Conditions

Author: Ramanathan Vaidhyanathan, Sunil Nair, Soumendranath Panja, et al

Publication: Small

Publisher: John Wiley and Sons

Date: Jul 30, 2018

Order Completed

Thank you for your order.

This Agreement between Indian Institute of Science Education and Research Pune ("You") and John Wiley and Sons ("John Wiley and Sons") consists of your license details and the terms and conditions provided by John Wiley and Sons and Copyright Clearance Center.

Your confirmation email will contain your order number for future reference.

License Number	4761141323802
License date	Feb 03, 2020

Printable Details

Licensed Content

Licensed Content Publisher	John Wiley and Sons
Licensed Content Publication	Small
Licensed Content Title	Highly Stable COF-Supported Co/Co(OH)2 Nanoparticles Heterogeneous Catalyst for Reduction of Nitrile/Nitro Compounds under Mild Conditions
Licensed Content Author	Ramanathan Vaidhyanathan, Sunil Nair, Soumendranath Panja, et al
Licensed Content Date	Jul 30, 2018
Licensed Content Volume	14
Licensed Content Issue	37
Licensed Content Pages	8

Order Details

Type of use	Dissertation/Thesis
Requestor type	Author of this Wiley article
Format	Print and electronic
Portion	Figure/table
Number of figures/tables	1
Will you be translating?	No

About Your Work

Title of your thesis / dissertation	Porous Framework Materials for Gas Separation and Catalysis
Expected completion date	May 2020
Expected size (number of pages)	200

Additional Data

Original Wiley figure/table number(s)	1

Requestor Location

Requestor Location	Indian Institute of Science Education and Research Pune Dr. Homi Bhabha Road Pashan Pune Pune, 411008 India Attn: Indian Institute of Science Education and Research Pune

Tax Details

Publisher Tax ID	EU826007151

Price

Total	0.00 USD

Would you like to purchase the full text of this article? If so, please continue on to the content ordering system located here: Purchase PDF
If you click on the buttons below or close this window, you will not be able to return to the content ordering system.

Total: 0.00 USD

CLOSE WINDOW ORDER MORE

Cu/Cu2O Nanoparticles Supported on a Phenol–Pyridyl COF as a Heterogeneous Catalyst for the Synthesis of Unsymmetrical Diynes via Glaser–Hay Coupling

Author: Debanjan Chakraborty, Shyamapada Nandi, Dinesh Mullangi, et al

Publication: Applied Materials

Publisher: American Chemical Society

Date: May 1, 2019

PERMISSION/LICENSE IS GRANTED FOR YOUR ORDER AT NO CHARGE

This type of permission/license, instead of the standard Terms & Conditions, is sent to you because no fee is being charged for your order. Please note the following:

- Permission is granted for your request in both print and electronic formats, and translations.
- If figures and/or tables were requested, they may be adapted or used in part.
- Please print this page for your records and send a copy of it to your publisher/graduate school.
- Appropriate credit for the requested material should be given as follows: "Reprinted (adapted) with permission from (COMPLETE REFERENCE CITATION). Copyright (YEAR) American Chemical Society." Insert appropriate information in place of the capitalized words.
- One-time permission is granted only for the use specified in your request. No additional uses are granted (such as derivative works or other editions). For any other uses, please submit a new request.

BACK CLOSE WINDOW

Hyper-Cross-linked Porous Organic Frameworks with Ultramicropores for Selective Xenon Capture

Author: Debanjan Chakraborty, Shyamapada Nandi, Michael A. Sinnwell, et al

Publication: Applied Materials

Publisher: American Chemical Society

Date: Apr 1, 2019

PERMISSION/LICENSE IS GRANTED FOR YOUR ORDER AT NO CHARGE

This type of permission/license, instead of the standard Terms & Conditions, is sent to you because no fee is being charged for your order. Please note the following:

- Permission is granted for your request in both print and electronic formats, and translations.
- If figures and/or tables were requested, they may be adapted or used in part.
- Please print this page for your records and send a copy of it to your publisher/graduate school.
- Appropriate credit for the requested material should be given as follows: "Reprinted (adapted) with permission from (COMPLETE REFERENCE CITATION). Copyright (YEAR) American Chemical Society." Insert appropriate information in place of the capitalized words.
- One-time permission is granted only for the use specified in your request. No additional uses are granted (such as derivative works or other editions). For any other uses, please submit a new request.

Ag Nanoparticles Supported on a Resorcinol-Phenylenediamine-Based Covalent Organic Framework for Chemical Fixation of CO2

Author: Debanjan Chakraborty, Pragalbh Shekhar, Himan Dev Singh, et al

Publication: Chemistry - An Asian Journal

Publisher: John Wiley and Sons

Date: Oct 17, 2019

Order Completed

Thank you for your order.

This Agreement between Indian Institute of Science Education and Research Pune ("You") and John Wiley and Sons ("John Wiley and Sons") consists of your license details and the terms and conditions provided by John Wiley and Sons and Copyright Clearance Center.

Your confirmation email will contain your order number for future reference.

License Number	4757040573313
License date	Jan 27, 2020

Printable Details

Licensed Content

Licensed Content Publisher	John Wiley and Sons
Licensed Content Publication	Chemistry - An Asian Journal
Licensed Content Title	Ag Nanoparticles Supported on a Resorcinol-Phenylenediamine-Based Covalent Organic Framework for Chemical Fixation of CO2
Licensed Content Author	Debanjan Chakraborty, Pragalbh Shekhar, Himan Dev Singh, et al
Licensed Content Date	Oct 17, 2019
Licensed Content Volume	14
Licensed Content Issue	24
Licensed Content Pages	7

Order Details

Type of use	Dissertation/Thesis
Requestor type	Author of this Wiley article
Format	Print and electronic
Portion	Full article
Will you be translating?	No

About Your Work

Title of your thesis / dissertation	Porous Framework Materials for Gas Separation and Catalysis
Expected completion date	May 2020
Expected size (number of pages)	200

Additional Data

Requestor Location

Requestor Location	Indian Institute of Science Education and Research Pune Dr. Homi Bhabha Road Pashan Pune Pune, 411008 India Attn: Indian Institute of Science Education and Research Pune

Tax Details

Publisher Tax ID	EU826007151

Price

Total	0.00 USD

Would you like to purchase the full text of this article? If so, please continue on to the content ordering system located here: Purchase PDF
If you click on the buttons below or close this window, you will not be able to return to the content ordering system.

Total: 0.00 USD

CLOSE WINDOW ORDER MORE

Copyright Clearance Center Marketplace™

Order Confirmation

Thank you, your order has been placed. An email confirmation has been sent to you. Your order license details and printable licenses will be available within 24 hours. Please access Manage Account for final order details.

This is not an invoice. Please go to manage account to access your order history and invoices.

CUSTOMER INFORMATION

Payment by invoice: You can cancel your order until the invoice is generated by contacting customer service.

Billing Address

Debanjan Chakraborty
Dr. Homi Bhabha Road
Pashan
Pune
Pune, 411008
India

+91 8408890544
debanjan.chakraborty@students.iiserpune.ac.in

Customer Location

Debanjan Chakraborty
Dr. Homi Bhabha Road
Pashan
Pune
Pune, 411008
India

PO Number (optional)

N/A

Payment options

Invoice

PENDING ORDER CONFIRMATION

Total Due: 0.00 USD

Confirmation Number: Pending

Order Date: 05-Feb-2020

1. Journal of materials chemistry. A, Materials for energy and sustainability

0.00 USD

Order license ID	Pending
ISSN	2050-7496
Type of Use	Republish in a thesis/dissertation
Publisher	Royal Society of Chemistry
Portion	Image/photo/illustration

LICENSED CONTENT

Publication Title	Journal of materials chemistry. A, Materials for energy and sustainability	**Country**	United Kingdom of Great Britain and Northern Ireland
Author/Editor	Royal Society of Chemistry (Great Britain)	**Rightsholder**	Royal Society of Chemistry
Date	01/01/2013	**Publication Type**	e-Journal
Language	English	**URL**	http://pubs.rsc.org/en/journals/journalissues/ta

REQUEST DETAILS

Portion Type	Image/photo/illustration	**Distribution**	Worldwide
Number of images / photos / illustrations	1	**Translation**	Original language of publication
Format (select all that apply)	Electronic	**Copies for the disabled?**	No
Who will republish the content?	Academic institution	**Minor editing privileges?**	No
Duration of Use	Current edition and up to 5 years	**Incidental promotional use?**	No
Lifetime Unit Quantity	Up to 499	**Currency**	USD
Rights Requested	Main product		

NEW WORK DETAILS

Title	Porous Materials for Gas Separation and Catalysis	**Institution name**	Indian Institute of Science Education and Research
Instructor name	Debanjan Chakraborty	**Expected presentation date**	2020-04-15

ADDITIONAL DETAILS

Order reference number	N/A	**The requesting person / organization to appear on the license**	Debanjan Chakraborty

REUSE CONTENT DETAILS

Title, description or numeric reference of the portion(s)	198	**Title of the article/chapter the portion is from**	N/A
Editor of portion(s)	N/A	**Author of portion(s)**	Royal Society of Chemistry (Great Britain)
Volume of serial or monograph	N/A	**Issue, if republishing an article from a serial**	N/A
Page or page range of portion	44	**Publication date of portion**	2013-01-01

2. Journal of materials chemistry. A, Materials for energy and sustainability

0.00 USD

Order license ID	Pending
ISSN	2050-7496
Type of Use	Republish in a thesis/dissertation
Publisher	Royal Society of Chemistry
Portion	Image/photo/illustration

LICENSED CONTENT

Publication Title	Journal of materials chemistry. A, Materials for energy and sustainability	Country	United Kingdom of Great Britain and Northern Ireland
Author/Editor	Royal Society of Chemistry (Great Britain)	Rightsholder	Royal Society of Chemistry
Date	01/01/2013	Publication Type	e-Journal
Language	English	URL	http://pubs.rsc.org/en/journals/journalissues/ta

REQUEST DETAILS

Portion Type	Image/photo/illustration	Distribution	Worldwide
Number of images / photos / illustrations	1	Translation	Original language of publication
Format (select all that apply)	Electronic	Copies for the disabled?	No
Who will republish the content?	Academic institution	Minor editing privileges?	No
Duration of Use	Current edition and up to 5 years	Incidental promotional use?	No
Lifetime Unit Quantity	Up to 499	Currency	USD
Rights Requested	Main product		

NEW WORK DETAILS

Title	Porous Materials for Gas Separation and Catalysis	Institution name	Indian Institute of Science Education and Research Pune
Instructor name	Debanjan Chakraborty	Expected presentation date	2020-04-15

ADDITIONAL DETAILS

Order reference number	N/A	The requesting person / organization to appear on the license	Debanjan Chakraborty

REUSE CONTENT DETAILS

Title, description or numeric reference of the portion(s)	182	**Title of the article/chapter the portion is from**	N/A
Editor of portion(s)	N/A	**Author of portion(s)**	Royal Society of Chemistry (Great Britain)
Volume of serial or monograph	N/A	**Issue, if republishing an article from a serial**	N/A
Page or page range of portion	45	**Publication date of portion**	2013-01-01

Order Total: 0.00 USD

Total Items: 2 **Total Due: 0.00 USD**

Accepted: All Publisher and CCC Terms and Conditions